MRR 2009-2

New Nouveau Brunswick

Natural Resources
Minerals, Policy and Planning

Mineral Resource Report

Geological Investigations in New Brunswick for 2008

Gwen L. Martin, editor

2009

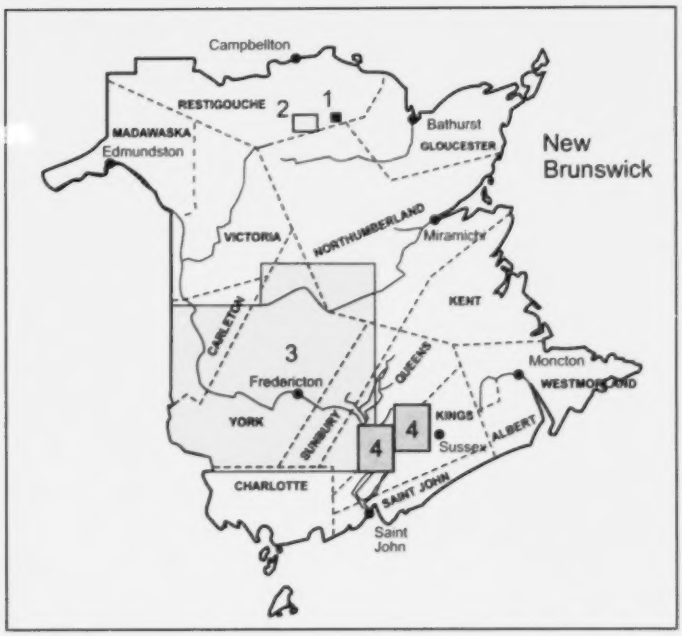

Mineral Resource Report 2009-2

GEOLOGICAL INVESTIGATIONS IN NEW BRUNSWICK FOR 2008

Print Edition
ISBN 978-1-55471-018-8
ISSN 0548-4014

Online Edition
ISBN 978-1-55471-019-5
ISSN 1717-1237

CD-ROM Edition
ISBN 978-1-55471-020-1
ISSN 1911-7582

Numbers on location map refer to the papers in this volume (see ***Table of Contents*** on facing page).

Cover illustration Sandstone of the Grant Brook Formation, exposed along the southern part of Taylors Brook in Kings County, New Brunswick.

Photograph courtesy of Kathleen Thorne, New Brunswick Department of Natural Resources.

Figure preparation Terry Leonard, Gwen L. Martin

Editing, design, layout Gwen L. Martin

Translation Le Bureau de traduction, Ministère de l'Approvisionnement et des Services du Nouveau-Brunswick (Translation Bureau, New Brunswick Department of Supply and Services)

Recommended citation Martin, G.L. (editor). 2009. Geological investigations in New Brunswick for 2008. New Brunswick Department of Natural Resources; Minerals, Policy and Planning Division, Mineral Resource Report 2009-2, 218 p.

This report has been prepared by:

Minerals, Policy and Planning Division
New Brunswick Department of Natural Resources

Hon. Wally Stiles
Minister of Natural Resources

December 2009

TABLE OF CONTENTS

PAGES

1 **Trace-Element Contents of Base Metal Concentrates from the Caribou Mine, Bathurst Mining Camp, New Brunswick: Implications for the Recovery of Indium from Mill Products** 1–27

SEAN H. MCCLENAGHAN [1], JAMES A. WALKER [1], AND DAVID R. LENTZ [2]

[1] Geological Surveys Branch, New Brunswick Department of Natural Resources

[2] Department of Geology, University of New Brunswick, Fredericton, New Brunswick

2 **Copper–Cobalt–Gold Mineralization in the Ramsay Brook Area, Tobique–Chaleurs Zone, Northern New Brunswick: A Possible Iron-Oxide–Copper–Gold (IOCG) System** 28–65

JAMES A. WALKER [1] AND DOUGLAS CLARK [2]

[1] Geological Surveys Branch, New Brunswick Department of Natural Resources

[2] Consulting Geologist, Bathurst, New Brunswick

3 **The Appalachian Glacier Complex, and the Middle–Late Pleistocene History of West-Central New Brunswick, Canada** 66–140

ALLEN A. SEAMAN [1]

[1] Geological Surveys Branch, New Brunswick Department of Natural Resources

4 **Stratigraphy, Geochemistry, and Geochronology of the Annidale and New River Belts, and the Development of the Penobscot Arc in Southern New Brunswick** 141–218

SUSAN C. JOHNSON [1], MALCOLM J. MACLEOD [1], LESLIE R. FYFFE [1], AND GREGORY R. DUNNING [2]

[1] Geological Surveys Branch, New Brunswick Department of Natural Resources

[2] Department of Earth Sciences, Memorial University, St. John's, Newfoundland

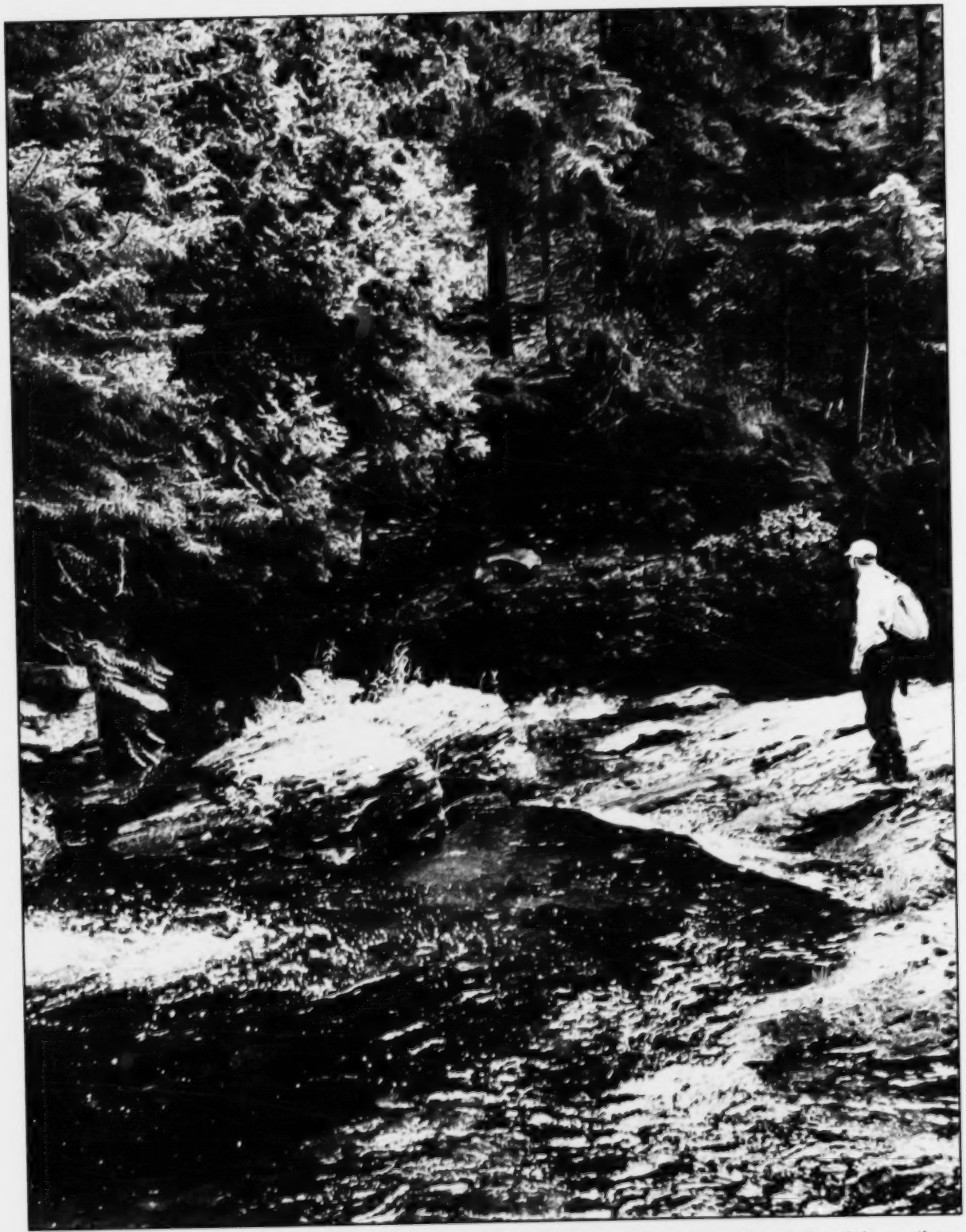

Frontispiece. Schistose rocks of the Lawson Brook Formation, exposed along O'Neill Brook in southern New Brunswick. *Photograph courtesy of Kathleen Thorne, New Brunswick Department of Natural Resources.*

TRACE-ELEMENT CONTENTS OF BASE METAL CONCENTRATES FROM THE CARIBOU MINE, BATHURST MINING CAMP, NEW BRUNSWICK: IMPLICATIONS FOR THE RECOVERY OF INDIUM FROM MILL PRODUCTS

SEAN H. MCCLENAGHAN [1], JAMES A. WALKER [1], AND DAVID R. LENTZ [2]

[1] Geological Surveys Branch, New Brunswick Department of Natural Resources,
P.O. Box 50, Bathurst, New Brunswick, CANADA E2A 3Z1 *(Sean.McClenaghan@gnb.ca)*

[2] Department of Geology, University of New Brunswick,
P.O. Box 4400, Fredericton, New Brunswick, CANADA E3B 5A3

McClenaghan, S.H., Walker, J.A., and Lentz, D.R. 2009. Trace-element contents of base metal concentrates from the Caribou mine, Bathurst Mining Camp, New Brunswick: implications for the recovery of indium from mill products. *In* Geological Investigations in New Brunswick for 2008. *Edited by* G.L. Martin. New Brunswick Department of Natural Resources; Minerals, Policy and Planning Division, Mineral Resource Report 2009–2, p. 1–27.

The Caribou volcanogenic massive sulphide deposit in northern New Brunswick is the second-largest deposit in the Bathurst Mining Camp, with a historical geological resource of 70 Mt grading 4.3% Zn, 1.6% Pb, 0.5% Cu, 51.3 g/t Ag, and 1.7 g/t Au. To date, the deposit has produced 1.73 Mt of massive sulphides grading 6.3% Zn and 3.0% Pb, and holds additional resources of 3.72 Mt grading 6.5% Zn, 2.8% Pb, and 87 g/t Ag. Zinc concentrates from the Caribou mill average 49.9% Zn, 2.18% Pb, 0.52% Cu, and 120 g/t Ag; they also contain Cd (1043 ppm), In (57.6 ppm), and Sn (273 ppm). Positive Spearman rank correlations between Cd, In, Sn, Bi, and Zn for historical massive sulphide analyses indicate the concentration, and mutual presence of, these elements in sphalerite. Microanalyses of sphalerite grains from massive sulphides and concentrates to some extent corroborate the bulk correlations. However, levels of indium in sphalerite are below the detection capabilities of the electron microprobe. Although indium is partitioned into zinc concentrate from the Caribou mill, it is present in such low levels as to not significantly increase the value of the Caribou ore.

Le gisement de sulfures massifs volcanogènes de la mine Caribou, dans le nord du Nouveau-Brunswick, est le deuxième gisement en importance du Camp minier de Bathurst. On y a déjà découvert 70 tonnes métriques de ressources minérales, d'une teneur de 4,3 % Zn, 1,6 % Pb, 0,5 % Cu, 51,3 g/t Ag et 1,7 g/t Au. Le gisement a produit jusqu'à maintenant 1,73 tonne métrique de sulfures massifs d'une teneur de 6,3 % Zn et de 3,0 % Pb, tandis que 3,72 tonnes métriques d'autres ressources minérales avaient une teneur de 2,8 % Pb, de 6,5 % Zn et de 87 g/t Ag. Le concentré de zinc produit à l'usine de la mine Caribou a une teneur moyenne de 49,9% Zn, de 2,18 % Pb, et de 0,52 % Cu, et il a une teneur moyenne en argent de 120 g/t. Le concentré de zinc contient également du cadmium (1043 ppm), de l'indium (57,6 ppm), et de l'étain (273 ppm). Des corrélations inter-éléments positives établies par la méthode Spearman et ayant porté sur les éléments Cd, In, Sn, Bi et Zn dans les analyses de sulfures massifs déjà réalisées, indiquent une concentration de ces éléments dans la sphalérite. Une microanalyse des grains de sphalérite dans les sulfures massifs et les concentrés corrobore dans une certaine mesure les corrélations de minéralisation en masse. Par ailleurs, la teneur en indium dans la sphalérite se situe en deçà des possibilités de détection par une microsonde électronique. Même si le concentré de zinc de l'usine de la mine Caribou contient des traces d'indium, sa teneur est si faible qu'elle ne pourrait accroître de manière importante la valeur du minerai extrait de la mine Caribou.

INTRODUCTION

The Caribou mine is situated in northern New Brunswick, 56 km west of Bathurst (Fig. 1) in the northwestern part of the Bathurst Mining Camp (Bathurst Camp or BMC). This Zn–Pb–Cu–Ag-type volcanogenic massive sulphide (VMS) deposit is the second largest in the Bathurst Camp after the Brunswick No. 12 deposit (Goodfellow and McCutcheon 2003; McClenaghan et al. 2009a, 2009b), with geological resources historically estimated at 70 Mt grading 4.3% Zn, 1.6% Pb, 0.5% Cu, 51.3 g/t Ag, and 1.7 g/t Au (Cavelero 1993).

The Caribou deposit represents one of the most significant base metal resources remaining in the Bathurst Camp and contains the highest reported gold grades associated with any VMS mineralization in northern New Brunswick (Goodfellow 2003; McClenaghan et al. 2003). Furthermore, the deposit remains open at depth and along strike, giving it the greatest potential for further discovery and expansion of base metal resources in the Bathurst Camp. Yet despite its large size and economic grade, the Caribou mine has experienced a challenging production history (Cavelero 1993) and undergone numerous suspensions of mining operations (see ***Historical Overview***), due chiefly to poor metal recoveries and low commodity values.

Base metal production from the Bathurst Camp has consisted mainly of zinc, lead, and copper and at one time accounted for 25% and 30% of Canada's zinc and lead production, respectively. In addition to these primary metal commodities, the BMC has produced byproduct Au, Ag, Sb, Sn, Bi, Co, and In. Documenting the contents of these latter elements in the massive sulphides and resulting mill products is important from an economic standpoint, as the value of these elements at the smelting stage can increase value of the ore in the form of metal credits. The credits can offset smelter penalties for deleterious elements such as Cd, As, and Se, which also occur in mill concentrates.

The occurrence of discrete indium minerals (roquesite, indite, laforetite) in hydrothermal systems is generally rare; thus, their incorporation in common base metal sulphide minerals is unlikely to account for indium enrichment in VMS deposits. However, indium does occur widely as a trace-element substitution in the mineral structures of sphalerite, chalcopyrite, stannite, and cassiterite (Schwarz-Schampera and Herzig 2002). The abundance of these minerals, sphalerite in particular, makes large VMS deposits such as Kidd Creek, Neves Corvo, and Brunswick No. 12 an important source of byproduct indium.

This report focuses on the elevated contents of indium (up to 0.11% In) reported in sphalerite from massive sulphides of the Caribou deposit (Goodfellow 2003). Given the current high price of indium (US$500–550/kg, as reported in *The Northern Miner*, December 2009), determining the indium content of Caribou concentrates could increase the value of the mine. The current report also aims to evaluate the potential recovery of indium from Caribou ore by quantifying and characterizing indium in mill products from the mine.

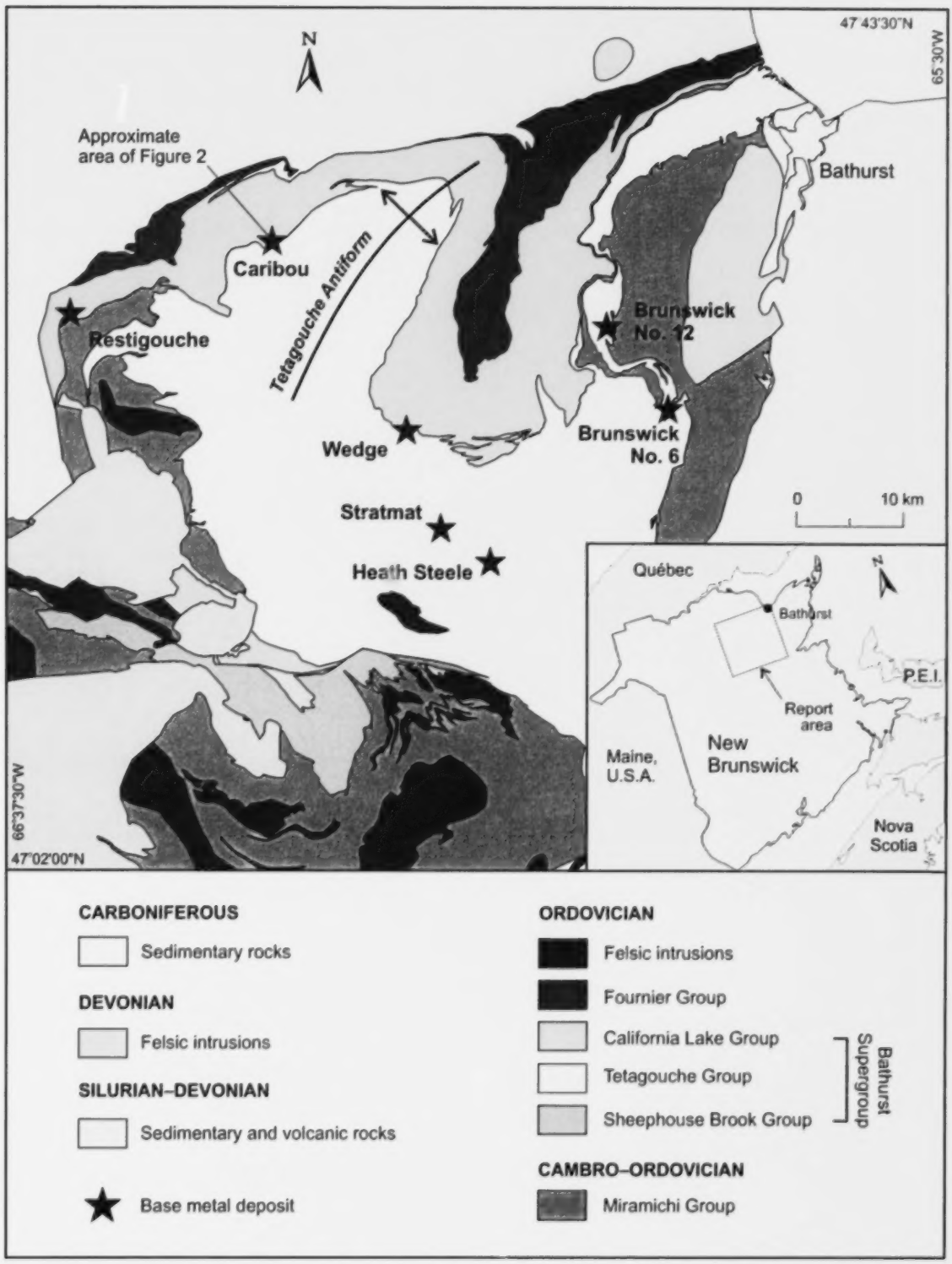

Figure 1. Simplified geology map of the Bathurst Mining Camp, northeastern New Brunswick, showing location of the Caribou deposit relative to formerly and currently producing base metal deposits.

HISTORICAL OVERVIEW

1955 to 1985

Anaconda Company Ltd. discovered the Caribou deposit in 1955 following an airborne electromagnetic survey that was flown over the northwestern part of the Bathurst Mining Camp (Cavelero 1993). Subsequent mapping and recognition of strong ground electromagnetic anomalies delineated the 'Caribou Synform' (Fig. 2; Roscoe 1971), a favourable target for the concentration of massive sulphides along the northern limb of the Tetagouche Antiform (Fig. 1). Anomalous base metal values in stream silt and water samples collected from nearby Forty Mile Brook and from seeps along the synform reinforced the high potential for discovery in the area. Anaconda began diamond drilling in 1955. The first hole on the east limb of the synform intersected greater than 15 m of massive sulphides containing notable base metal contents (Cheriton 1958). Subsequent drilling defined further resources, and an underground exploration adit was developed in 1959 to retrieve a bulk sample of massive sulphides for metallurgical testing.

Underground work resumed in 1965 and continued until 1967. The work included developing a ramp to the 100 m exploration level and excavating a drift that extended along the entire known length of the deposit. In 1966, a gossanous zone capping the deposit and a copper-rich supergene zone were discovered during emplacement of a ventilation raise. Anaconda commenced open-pit mining of the enriched cap in 1970 in a joint venture with Cominco, but the material was mineralogically untreatable by flotation techniques of the day. The enriched cap was exploited again during the early 1980s through another Anaconda–Cominco joint venture, this time by a heap-leach method (Cavelero 1993).

1986 to 2008

East West Minerals Ltd. purchased the Caribou mine from Anaconda in 1986 and built a base metal concentrator on site. Underground production commenced in 1988 but was suspended the following year. Breakwater Resources Ltd. acquired the mine in February 1990 and briefly restarted production before suspending operations in October 1990. The mine resumed production in 1997 under CanZinco Ltd., a division of Breakwater Resources Ltd., until operations ceased again in 1998 due to depressed metal prices (McCutcheon et al. 2005).

Massive sulphide production before 2000 included 1.34 Mt grading 6.8% Zn, 3.2% Pb, 0.32% Cu, and 97 g/t Ag. Supplemental production from supergene zones comprised

- 337,000 t of supergene sulphides grading 3.66% Cu and mined by open pit between 1970 and 1974, and
- 61,500 t of stockpiled gossan that was heap-leached between 1982 and 1983, producing 110,000 oz Ag and 8,300 oz Au.

In 2005, Blue Note Metals Inc. acquired a 100% interest in the Caribou mine through its

subsidiary, Blue Note Mining Ltd., and commenced mine refurbishing. The work included reconstructing a 3000 t/d mill and concentrator using an IsaMill™ (Lyne Coté, pers. comm., 2009). The proprietary IsaMill technology, developed by Xstrata, is a horizontal grinding and high-velocity stirring system that can achieve ultrafine (millimetre-size) particle sizes and hence more selective mineral liberation and higher recovery of base metals than a conventional ball-milling process (Coté and Adante 2009).

Mining operations at Caribou resumed in autumn 2007 with an outlined NI 43-101-compliant resource of 3.72 Mt of massive sulphides grading 6.5% Zn, 2.8% Pb, and 87 g/t Ag (McCutcheon et al. 2003). Production in 2007 and 2008 totalled 0.39 Mt grading 4.8% Zn and 2.3% Pb (McCutcheon and Walker 2009), with recoveries of 83.6% Zn and 72.2% Pb. Declining commodity prices led to the mine's closure in late 2008.

Regional Geology

The VMS deposits of the Bathurst Mining Camp occur within an Ordovician bimodal volcanic and sedimentary sequence in northern New Brunswick (Fig. 1). Volcanic rocks in the BMC formed within a continental to transitional oceanic back-arc basin (similar to the Japan Sea back-arc basin), situated above a southeast-directed subduction zone (van Staal et al. 2003).

The volcanic rocks represent ensialic to ensimatic portions of the Tetagouche–Exploits back-arc basin, formed as a result of rifting of the Popelogan arc between 475 Ma and 455 Ma. Subsequent closure of the Tetagouche–Exploits basin through northwest-directed subduction from the Late Ordovician (Caradocian) to Silurian (Ludlovian) resulted in the development of an accretionary wedge referred to as the Brunswick Subduction Complex (van Staal 1994). Several allochthonous to para-autocthonous thrust sheets (nappes) can be recognized within the imbricated accretionary wedge on the basis of their distinctive stratigraphic sequences. These nappes underwent intense polyphase deformation and associated lower- to upper-greenschist facies metamorphism (van Staal and Williams 1984; van Staal et al. 1988). They subsequently were folded into shallow and steep structures (van Staal et al. 2003).

The oldest rocks in the Bathurst Mining Camp belong to the Miramichi Group (Fig. 1). They consist of a continentally derived turbidite sequence of quartz wacke, quartzite, siltstone, and black shale of Cambrian to Early Ordovician age (ca 490–478 Ma; Sullivan and van Staal 1990). The Miramichi Group is conformably to disconformably overlain by Ordovician felsic and mafic volcanic rocks and associated sedimentary rocks of the coeval Sheephouse Brook, Tetagouche, and California Lake groups, collectively referred to as the Bathurst Supergroup (Fig. 1; van Staal et al. 2003).

In the northern part of the Bathurst Camp, VMS deposits are associated predominantly with rocks of the California Lake Group. The group is divided into four formations that, in ascending stratigraphic order, are the Spruce Lake, Mount Brittain, Canoe Landing Lake, and Boucher Brook formations. The two dominantly felsic volcanic units—those being the Spruce Lake (host to the Caribou VMS deposit) and Mount Brittain formations (Fig. 2)—formed from

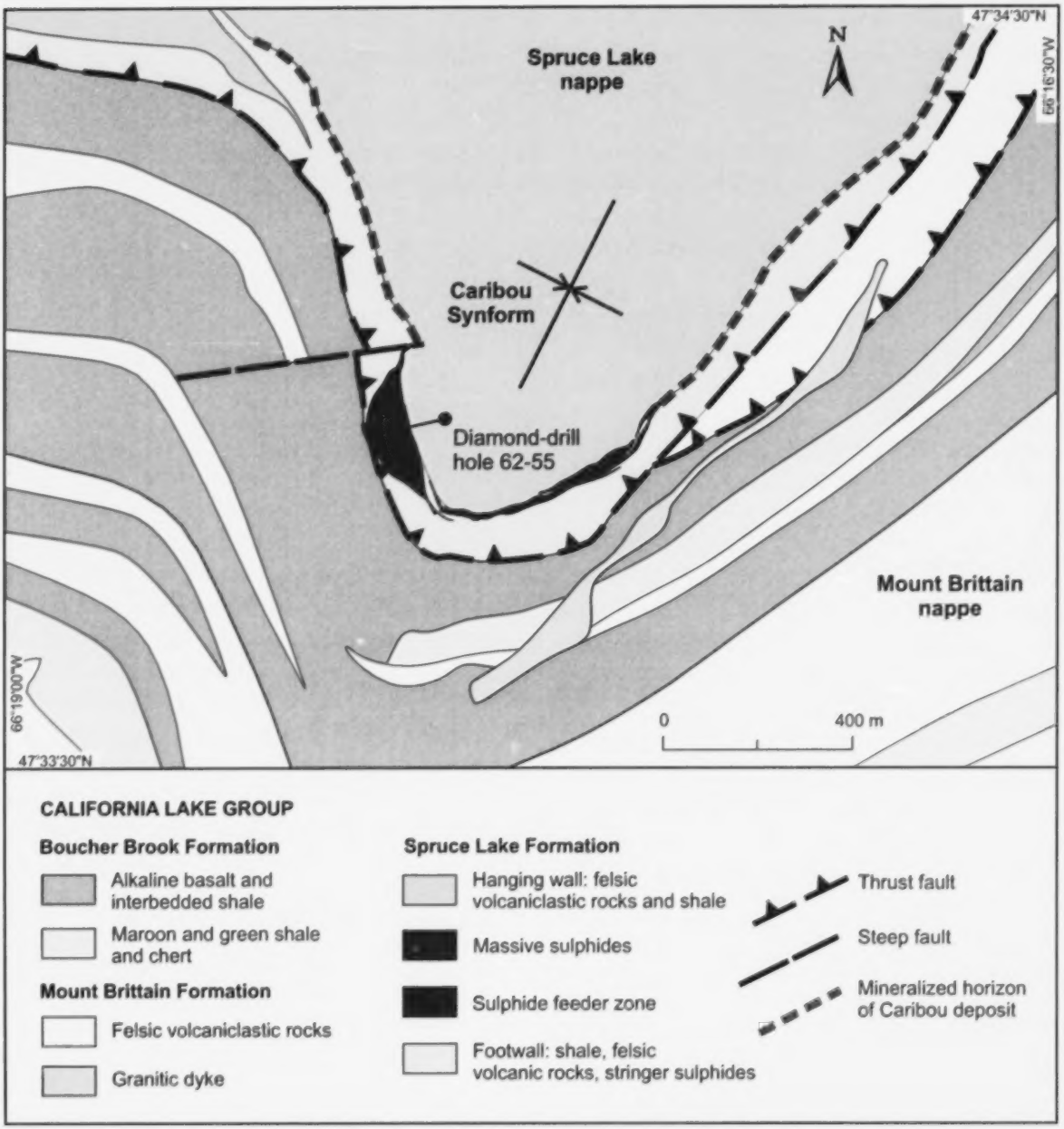

Figure 2. Surface geology of the Caribou volcanogenic massive sulphide deposit, Bathurst Mining Camp, northeastern New Brunswick (modified from Goodfellow 2003).

high-temperature partial melts of a crustal block (Lentz 1999; Rogers et al. 2003). Further extension within the back-arc basin led to the eruption of material that subsequently became mafic volcanic rocks of the Boucher Brook Formation.

The California Lake Group is structurally overlain by an oceanic crustal sequence of tholeiitic basalt, lithic wacke, limestone, and shale. These rocks are assigned to the Fournier Group (Fig. 1), which represents an extension in ensimatic portions of the Tetagouche–Exploits back-arc basin (van Staal et al. 2003).

DEPOSIT GEOLOGY

The Caribou VMS deposit has been described by several workers (Cheriton 1958; Roscoe 1971; Davis 1972; Helmstaedt 1973; Rankin 1982; Cavelero 1993). The most recent description of its geology and genesis is provided by Goodfellow (2003).

The Spruce Lake nappe is structurally bounded by the Mount Brittain nappe to the south (Fig. 2) and the Canoe Landing Lake nappe to the north (the latter is situated about 2.5 km northwest of the mine site, outside the area of Fig. 2). Within the Spruce Lake nappe, massive sulphides are hosted in sedimentary and felsic volcaniclastic rocks of the Spruce Lake Formation. Footwall rocks consist of laminated to thin-bedded black to dark grey shale, interbedded with feldspathic sandstone and light grey siltstone. These rocks are hydrothermally altered and cut by a sulphide feeder zone that is best preserved in the western end of the deposit (Fig. 2). The feeder zone is directly overlain by a stratiform massive sulphide unit, which consists of a copper-rich vent complex and a zinc–lead-rich bedded sulphide facies (Goodfellow 2003). Massive sulphides form a very sharp contact with the hanging-wall rocks of feldspar–phyric crystal tuff and ash tuff (Goodfellow 2003).

The Caribou deposit consists of six en echelon, massive sulphide lenses (Fig. 2), extending for 1.5 km around the Caribou Synform (Roscoe 1971; Cavelero 1993). The largest lens has a strike length of 305 m and contains massive sulphides that reach from surface to a depth of at least 1200 m. The massive sulphide lenses are composed primarily of pyrite, sphalerite, galena, and chalcopyrite with minor tetrahedrite, marcasite, arsenopyrite, electrum, and bournonite. Non-sulphide gangue minerals include quartz, siderite, magnetite, chlorite, muscovite, and stilpnomelane.

At least four phases of deformation have affected rocks at the Caribou deposit (van Staal et al. 1990, 2003). Early D_1 and D_2 events gave rise to isoclinal folds and a strong penetrative axial planar schistosity that ranges from a slatey cleavage in sedimentary rocks to a spaced cleavage in felsic volcanic rocks. Three sets of kink folds postdate the schistosity; they were formed before and during creation of the Caribou Synform. The F_4 Caribou Synform (Fig. 2; Roscoe 1971) formed as a large-scale, dextral kink on the northwest limb of the Tetagouche Antiform. The west limb of the synform is vertical, and the east limb dips 80° to 95°NW. The axial plane strikes 25°, dips 75° to 80°W, and plunges 75° to the northwest (Cavelero 1993).

ANALYTICAL PROTOCOL

Introduction

A total of 12 samples of mill products consisting of mill feed, zinc concentrate, lead concentrate, and plant tailings were collected for three consecutive 24-hour mill-run periods between August 13 and 15, 2008. Ore processed during these three periods was derived solely from the Caribou deposit and did not include material from the nearby Restigouche mine (Fig. 1), which had been used periodically to supplement the Caribou mill feed.

Sample pulps were submitted to analytical facilities at the Caribou mine to determine the Zn, Pb, Cu, Fe, and Ag contents (Table 1; Appendix 1) by fire-assay atomic absorption spectrometry (FAAS). Samples with base metal contents that exceeded 10% were subsequently titrated and re-analyzed. Sample splits were also forwarded to Activation Laboratories Ltd. (Actlabs) in Ancaster, Ontario. The Actlabs assessment consisted of 1) multi-element geochemical analyses for elements including indium (Table 2; Appendix 2), and 2) analyses for indium only. The multi-element analyses (Ultratrace 2 package) were conducted by inductively coupled plasma–mass spectrometry (ICP–MS); the indium-only analyses were performing using instrumental neutron activation analysis (INAA).

Table 1. Bulk assays of Caribou mill-run products by fire-assay atomic absorption spectrometry (FAAS).

	Mill Feed (n = 3)	Concentrates		Plant Tailings (n = 3)
		Zinc (n = 3)	Lead (n = 3)	
Zn	6.11	49.9	5.23	0.91
Pb	2.78	2.18	43.2	0.82
Cu	0.23	0.52	0.39	0.20
Fe	29.9	11.0	18.9	32.2
Ag	69.7	120	531	38.7

Notes: 1. All analyses except Ag are measured in %; Ag is measured in ppm (g/t).
2. n = number of analyses.

ICP–MS Analyses

Samples analyzed by ICP–MS were prepared using two independent digestion methods. Samples were analyzed separately as a check on the efficiency of various digestions on mineral phases resistant to chemical attack. The classic aqua regia digestion (used on all samples) employs a combination of concentrated hydrochloric (HCl) and nitric (HNO_3) acids. Aqua regia leaches sulphides but can be less effective in dissolving some oxides and silicates. A second, more aggressive, technique (used on zinc concentrates only) involves a fusion of sodium peroxide (Na_2O_2) and the sample, wherein the resulting molten bead is quickly digested in a weak HNO_3 solution. This Na_2O_2 fusion technique ensures that rare-earth elements and high-field-strength elements in resistant phases are properly dissolved.

Precision (standard deviation and coefficient of variation) and accuracy (% error values) for each element as determined by a particular analytical technique (Table 2) were estimated by analyzing a standard reference material, namely the massive sulphide standard MS-1 (see Lentz 1995). Results of these determinations were as follows.

- Samples subjected to the ICP–MS (Na_2O_2 fusion) technique yielded error values of less than 10% for S, Ag, As, Ba, Cd, Co, Cs, Cu, In, Sb, Tl, W, and Eu.

- Higher error values (>10%) were encountered for Si, Al, Fe, Mg, Ca, Ga, Mo, Sn, U, V, and Y.
- Values for K, P, Be, Cr, Hf, Mo, Nb, Pb, Rb, Sr, Ta, Th, Zn, La, Ce, Pr, Nd, Sm, Gd, Tb, Dy, Ho, Er, Tm, Yb, and Lu generally lay outside the detection range of the instrument for the standard reference material analyzed.
- Obtaining accuracy estimates for analyses of Mn, B, Bi, Hf, Ge, Ni, Sc, Se, Li, Re, and Te was not feasible, due to a lack of high-precision data for the standard MS-1.

The Ultratrace 2 analytical package of Actlabs, using aqua regia digestion, provided lower detection limits than did similar ICP–MS analyses using fusion methods. However, it also exhibited less overall accuracy and showed higher levels of error. Specifically,

- analyses of As, Cd, Co, Cu, Ga, In, Sb, Tl, U, W, and Ce by ICP–MS yielded error values of less than 10%;
- analyses of Al, Fe, Mg, Ca, Na, P, S, Ba, Be, Cr, Cs, Mo, Nb, Rb, Sn, Sr, Th, V, Y, Zr, Nd, and Eu showed higher error values; and
- analyses of standard reference material indicated that values for Ti, K, Au, Ag, B, Hf, Pb, Re, Sc, Ta, Te, Zn, La, Pr, Sm, Gd, Tb, Dy, Ho, Er, Tm, Yb, and Lu generally lay outside the detection range of the instrument.

INAA Analyses

Instrumental neutron activation analysis (INAA) is a non-destructive trace-element technique capable of measuring up to 35 elements at ppb and per cent levels of detection. The method involves irradiating encapsulated samples and standards for several days near the core of the neutron source. Interaction between the neutron flux and constituent elements in samples results in a process of neutron capture, which creates several short-lived isotopes of a specific element. As the newly formed isotope decays back to the stable ground state, gamma rays with a characteristic energy are emitted and subsequently measured (Hoffman 1992).

Quantification by gamma-ray spectrometry takes place over several weeks to accommodate isotopes with longer half-lives. In addition, a select suite of elements—including indium—can be analyzed by use of their short-lived isotopes. This process requires a separate procedure, as the presence of aluminium and manganese can induce radioactivity in the sample (Hoffman 1992).

Due to its reliance on direct measurement of pulverized samples, and hence its lack of dilution that typically accompanies chemical digestion, INAA is especially useful for detecting trace elements with low concentrations in geological samples. These elements include gold, platinum-group elements, and several other trace elements, including indium (Hannington and Gorton 1991; Hoffman 1992). The use of INAA also circumvents issues arising from the residence of trace elements in mineral phases such as cassiterite, zircon, monazite, and barite that are resistant to dissolution by conventional acid digestions.

Table 2. Bulk analyses of mill-run products from the Caribou deposit (and standard reference material, MS-1) by ICP–MS.

	Aqua Regia Digestion ICP–MS									Na_2O_2 Fusion Digestion ICP–MS					
	Mill Feed n = 3	Concentrates		Plant Tailings n = 3	Standard (MS-1)					Zinc Concn'te n = 3	Standard (MS-1)				
		Zinc n = 3	Lead n = 3		Precision				Accuracy		Precision				Accuracy
					DL	Mean	SD	CV	% Error		DL	Mean	SD	CV	% Error
SiO_2 (%)	–	–	–	–	–	–	–	–	–	0.1	0.01	2.70	0.03	0.01	58.9
Al_2O_3	0.3	0.02	0.01	0.3	0.01	0.11	–	–	62.1	0.03	0.01	0.05	–	–	27.4
Fe_2O_3	13.5	5.9	10.2	13.0	0.01	9.7	3.588	0.37	50.1	7.7	0.05	19.6	0.08	0.004	25.9
TiO_2	<0.01	<0.01	<0.01	<0.01	0.01	<0.01	–	–	–	<0.01	0.01	<0.01	–	–	–
MgO	0.3	0.01	0.008	0.3	0.01	0.11	–	–	67.1	0.02	0.01	0.03	–	–	48.8
MnO	0.19	0.04	0.02	0.21	0.0001	0.09	0.1076	1.19	–	0.05	0.0003	460	8.5	0.02	–
CaO	0.2	0.05	0.01	0.3	0.01	0.11	–	–	55.9	0.03	0.01	0.01	0.004	0.35	86.5
Na_2O	0.01	0.008	0.007	0.01	0.001	0.009	0.0029	0.33	86.7	–	–	–	–	–	–
K_2O	0.03	<0.01	<0.01	0.04	0.01	<0.01	–	–	–	<0.1	0.1	<0.1	–	–	–
P_2O_5	0.009	0.001	0.002	0.01	0.001	0.005	0.0049	1.03	78.1	<0.005	0.005	<0.005	–	–	–
S	14.0	12.2	14.5	13.0	0.001	13.2	1.16	0.09	39.3	35.6	0.01	37.4	0.38	0.01	0.28
Au (ppb)	<0.5	32.9	203	<0.5	0.5	<0.5	–	–	–	–	–	–	–	–	–
Ag (ppm)	53.6	>100	>100	33.5	0.002	>100	–	–	–	140	10	153	5.77	0.04	1.02
As	4320	2513	5080	4567	0.1	492	55	0.11	6.39	3010	5	698	12.5	0.02	0.56
B	<1	<1	<1	<1	1	<1	–	–	–	<10	10	<10	–	–	–
Ba	2.60	1.70	<0.5	2.53	0.5	1.83	0.40	0.22	99.0	<3	3	317	6.51	0.02	0.89
Be	0.27	0.13	0.15	0.37	0.1	0.13	0.06	0.43	54.7	<3	3	<3	–	–	–
Bi	17.5	12.9	107	19.0	0.02	3.00	0.20	0.07	–	10.7	2	<2	–	–	–
Cd	108	947	116	17.8	0.01	180	2.00	0.01	0.96	1043	2	191	3.21	0.02	2.80
Co	25.9	7.23	13.1	25.2	0.1	6.97	0.15	0.02	1.69	8.33	0.2	7.90	0.17	0.02	0.05
Cr	35.0	29.3	14.6	57.7	0.5	2.27	0.06	0.03	29.9	50.0	30	<30	–	–	–
Cs	0.47	0.10	0.10	0.57	0.02	0.10	–	–	19.8	<0.1	0.1	0.20	–	–	1.23
Cu	1637	5090	3480	1633	0.01	194	4.51	0.02	0.11	7370	2	229	21.5	0.09	2.92
Ga	6.07	3.14	0.69	6.92	0.02	6.54	0.05	0.01	0.43	3.50	0.2	16.3	0.06	0.004	178
Ge	0.17	0.37	0.50	0.13	0.1	0.30	0.17	0.58	–	1.13	0.7	8.47	0.15	0.02	–
Hf	0.27	0.10	0.30	0.47	0.1	<0.1	–	–	–	<10	10	<10	–	–	–
In	6.77	54.8	4.96	2.02	0.02	31.6	0.42	0.01	0.52	57.6	0.2	34.3	1.07	0.03	0.07
Li	3.5	0.23	0.27	4.27	0.1	1.10	0.95	0.87	–	<3	3	<3	–	–	–
Mo	4.30	8.77	24.8	3.65	0.01	2.06	0.15	0.07	45.3	9.33	1	3.00	–	–	27.4
Nb	0.13	<0.1	<0.1	0.13	0.1	0.1	0.00	0.00	47.3	<2.4	2.4	<2.4	–	–	–
Ni	10.9	5.43	11.0	13.8	0.1	5.10	0.20	0.04	–	<10	10	<10	–	–	–
Pb	>10000	5660	>10000	6663	0.01	>10000	–	–	–	>5000	0.8	>5000	–	–	–
Rb	2.83	0.33	0.37	3.30	0.1	0.40	0.10	0.25	41.0	0.47	0.4	1.10	0.10	0.25	41.0

	Aqua Regia Digestion ICP–MS									Na_2O_2 Fusion Digestion ICP–MS					
	Mill Feed n = 3	Concentrates		Plant Tailings n = 3	Standard (MS-1)					Zinc Concn'te n = 3	Standard (MS-1)				
		Zinc n = 3	Lead n = 3		Precision				Accuracy		Precision				Accuracy
					DL	Mean	SD	CV	% Error		DL	Mean	SD	CV	% Error
Re	0.003	0.006	0.01	0.002	0.001	<0.001	–	–	–	–	–	–	–	–	–
Sb	291	266	>500	280	0.02	296	10.41	0.04	3.18	292	2	415	13.3	0.03	2.40
Sc	1.30	<0.1	<0.1	1.47	0.1	<0.1	–	–	–	–	–	–	–	–	–
Se	2.43	23.3	85.1	1.97	0.1	3.80	0.26	0.07	–	31.4	0.8	1.50	–	–	–
Sn	10.9	27.7	10.9	8.63	0.05	24.9	0.53	0.02	90.9	273	0.5	821	16.8	0.02	29.6
Sr	15.5	2.57	1.40	19.7	0.5	2.53	0.35	0.14	55.8	<3	3	<3	–	–	–
Ta	<0.05	<0.05	<0.05	<0.05	0.05	<0.05	–	–	–	<0.2	0.2	<0.2	–	–	–
Te	0.17	0.11	0.64	0.20	0.02	<0.02	–	–	–	<6	6	<6	–	–	–
Th	3.63	0.53	0.67	3.73	0.1	0.20	0.10	0.50	329	0.20	0.1	<0.1	–	–	–
Tl	29.4	12.0	45.6	26.1	0.02	63.9	10.36	0.16	6.76	10.6	0.1	84.0	1.33	0.02	0.02
U	3.50	2.83	2.73	3.87	0.1	0.40	0.00	0.00	1.23	1.90	0.1	0.27	0.06	0.22	17.7
V	13.3	<1	<1	16.3	1	1.00	0.00	0.00	25.0	38.0	5	34.3	2.31	0.07	26225
W	2.30	0.37	0.97	0.60	0.1	73.0	2.93	0.04	4.68	<0.7	0.7	91.3	0.91	0.01	0.04
Y	4.86	0.99	3.28	7.76	0.01	0.24	0.01	0.02	17.7	1.47	0.1	0.73	0.23	0.31	75.8
Zn	>5000	>5000	>5000	>5000	0.1	>5000	–	–	–	>5000	30	>5000	–	–	–
Zr	15.9	7.93	21.6	24.2	0.1	2.17	0.25	0.12	140	–	–	–	–	–	–
La	2.13	<0.5	<0.5	2.93	0.5	<0.5	–	–	–	0.80	0.4	1.15	–	–	–
Ce	6.86	1.40	1.56	8.48	0.01	0.92	–	–	2.32	<0.8	0.8	2.70	–	–	–
Pr	0.83	0.10	0.10	1.00	0.1	<0.1	–	–	–	0.13	0.1	0.30	–	–	–
Nd	3.27	0.41	0.44	4.09	0.02	0.17	–	–	19.8	<0.4	0.4	1.80	–	–	–
Sm	0.90	0.10	0.10	1.07	0.1	<0.1	–	–		0.13	0.1	0.30	–	–	–
Eu	0.37	0.10	0.10	0.40	0.1	0.10	–	–	19.8	<0.1	0.1	0.20	–	–	1.23
Gd	1.07	0.10	0.10	1.33	0.1	<0.1	–	–	–	0.13	0.1	0.30	–	–	–
Tb	0.20	<0.1	<0.1	0.20	0.1	<0.1	–	–	–	<0.1	0.1	<0.1	–	–	–
Dy	1.07	0.10	0.10	1.30	0.001	<0.001	–	–	–	<0.3	0.3	<0.3	–	–	–
Ho	0.20	<0.1	<0.1	0.23	0.1	<0.1	–	–	–	<0.2	0.2	<0.2	–	–	–
Er	0.53	0.10	0.10	0.67	0.1	<0.1	–	–	–	<0.1	0.1	<0.1	–	–	–
Tm	0.10	<0.1	<0.1	0.10	0.1	<0.1	–	–	–	<0.1	0.1	<0.1	–	–	–
Yb	0.40	0.10	0.10	0.57	0.1	<0.1	–	–	–	<0.1	0.1	<0.1	–	–	–
Lu	0.10	<0.1	<0.1	0.10	0.1	<0.1	–	–	–	–	–	–	–	–	–

Notes: 1. Whole-rock analyses are measured in %. All trace-element analyses except Au are measured in ppm. Au is measured in ppb.

2. n = number of analyses.

3. **DL** = detection limit. **SD** = standard deviation. **CV** = coefficient of variation, calculated as follows: [Std Dev / Mean] x 100. Accuracy is estimated by % error, calculated as follows: $[MS\text{-}1_{measured} - MS\text{-}1_{actual}]^2 / [MS\text{-}1_{actual}]^2$.

For the current study, samples of mill products and standard reference materials were analyzed for indium by INAA as a check on analyses requiring digestions. Analyses of indium by INAA were highly precise, showing a variation coefficient of 2.3%, based on replicate analyses (n = 3) of the massive sulphide standard (MS-1; Lentz 1995). The INAA analyses, which were accurate to within error values that averaged 2.9%, slightly underestimated the indium content of the massive sulphide standard (MS-1).

Microprobe Analyses

Sample pulps from the mill-run material were also submitted to the thin section and rock preparation laboratory at the Department of Geology, University of New Brunswick, where polished petrographic sections were prepared to a thickness of 120 µm. In addition, a polished section of massive sulphide was selected for microanalysis to compare with the concentrate sections. The polished section was obtained from a representative segment of the bedded zinc–lead sulphide facies in core from diamond-drill hole 62-55 at the western end of the Caribou deposit (Fig. 2; McClenaghan 2002).

Examination of polished sections was carried out using conventional reflective light microscopy. Quantitative compositional analyses of S, Mn, Fe, Co, Cu, Zn, As, Se, Cd, In, and Sn in sphalerite were conducted using a JEOL JXA-733 Superprobe with a PGT Prism 2000 energy dispersive spectrometer and a PGT Spirit X-ray analysis system (Table 3; Appendix 3). The microprobe system operated at a 15 kV accelerating voltage and a 200 nA beam current; it scanned over a rastered 5 μm^2 area with a peak counting time of 200 seconds. Standards consisted of pure metals, with the exception of troilite for Fe and S, and sphalerite for Zn.

Table 3. Electron microprobe analyses of sphalerite grains in zinc concentrate and massive sulphides, Caribou deposit, Bathurst Mining Camp, northeastern New Brunswick.

	Mean Detection Limit (mdl)	All Sphalerite n = 16	Zinc Concentrates			Massive Sulphides
			08-SHM-CAR-4 n = 4	08-SHM-CAR-9 n = 4	08-SHM-CAR-14 n = 4	97-SHM-62-55 n = 4
S	0.011	33.3	33.3	33.4	33.2	33.2
Mn	0.033	0.03	0.02	0.04	0.04	0.01
Fe	0.031	4.57	3.44	4.70	4.46	5.66
Co	0.037	0.01	0.01	0.005	0.01	0.01
Cu	0.046	0.44	1.10	0.06	0.03	0.56
Zn	0.053	61.4	61.4	62.0	62.0	60.0
As	0.030	<mdl	<mdl	<mdl	<mdl	<mdl
Se	0.012	0.01	0.008	0.006	0.007	0.006
Cd	0.041	0.17	0.15	0.16	0.18	0.17
In	0.011	<mdl	<mdl	<mdl	<mdl	<mdl
Sn	0.044	0.21	0.030	<mdl	0.39	<mdl
Total	–	99.9	99.4	100.3	100.0	99.7
Zn/Cd	–	412	555	382	345	364

Notes: 1. All values are shown in %.
2. n = number of analyses.

RESULTS AND DISCUSSION

Mill feed for the three sampled intervals averages 6.11% Zn, 2.78% Pb, 0.23% Cu, and 69.7 g/t Ag (Table 1). This is consistent with historical grades for the Caribou deposit and typical of the bedded zinc–lead sulphide facies, which contains most of the ore resources of the Caribou mine.

Mineralogically, pyrite, sphalerite, galena, and chalcopyrite account for nearly all Fe, Zn, Pb, and Cu contents in the massive sulphides. These minerals are also responsible for the broad suite of trace elements revealed in the analyses reported herein and in Goodfellow (2003). Trace-element analyses show As, Bi, Cd, Co, Cu, Ga, In, Mo, Sb, Se, Sn, and Tl in the massive sulphides and mill products (Table 2).

Overall, Zn in the massive sulphides exhibits a positive Spearman rank correlation with Pb, Ag, Hg, Cd, Ga, Sb, Sn, and In (Fig. 3; Goodfellow 2003). Goodfellow shows the indium content averaging 13.8 ppm in 88 samples from the bedded zinc–lead facies, sometimes reaching as high as 92 ppm.

Zinc concentrates for the three mill-run periods average 49.9% Zn, 2.18% Pb, 0.52% Cu, and 120 g/t Ag (Table 1). They also show enrichment in Cd, In, Sn, Mo, Sb, and Se (Table 2). Indium content as determined by ICP–MS (aqua regia) averages 54.8 ppm. This is corroborated by ICP–MS (Na_2O_2 fusion) and INAA data that show average indium contents of 57.6 ppm (Table 2) and 52.7 ppm, respectively—a near tenfold increase in concentration from the mill feed (avg. 6.77 ppm).

Plant tailings average 2.02 ppm In, indicating an approximate 70.2% recovery of the metal from the mill feed. The strong affinity exhibited by Cd, Sn, In, and Se for zinc concentrate suggests that their concentration in sphalerite is as a crystal-bound refractory phase. Earlier work by Petruk and Schnarr (1981) supports this assumption; they demonstrated a strong association of indium with zinc concentrates of the Brunswick No. 12 mine, in which approximately 74% of all assayed In was attributed to a solid solution in sphalerite.

Sphalerite in massive sulphide sections consists largely of anhedral, crimson red to brown masses. It forms intimate mixtures with galena, chalcopyrite, and sulphosalts. Sphalerite and galena are fine grained and interlayered with massive pyrite, giving the ore a banded appearance. Sphalerite grains in concentrate samples exhibit a bimodal distribution, comprising large anhedral masses up to 500 µm in size, surrounded by very fine-grained sphalerite and pyrite, with trace amounts of galena and chalcopyrite.

Goodfellow (2003) reported a mean of 0.037% In within sphalerite grains from the Caribou deposit, with indium content as high as 0.107%. However, electron microprobe analyses of sphalerite grains conducted during the present study (Table 3) yielded indium levels below the instrumental detection limit (0.011%); consequently, these analyses are inconclusive as to confirming the residence of indium. This discrepancy in results between Goodfellow (2003)

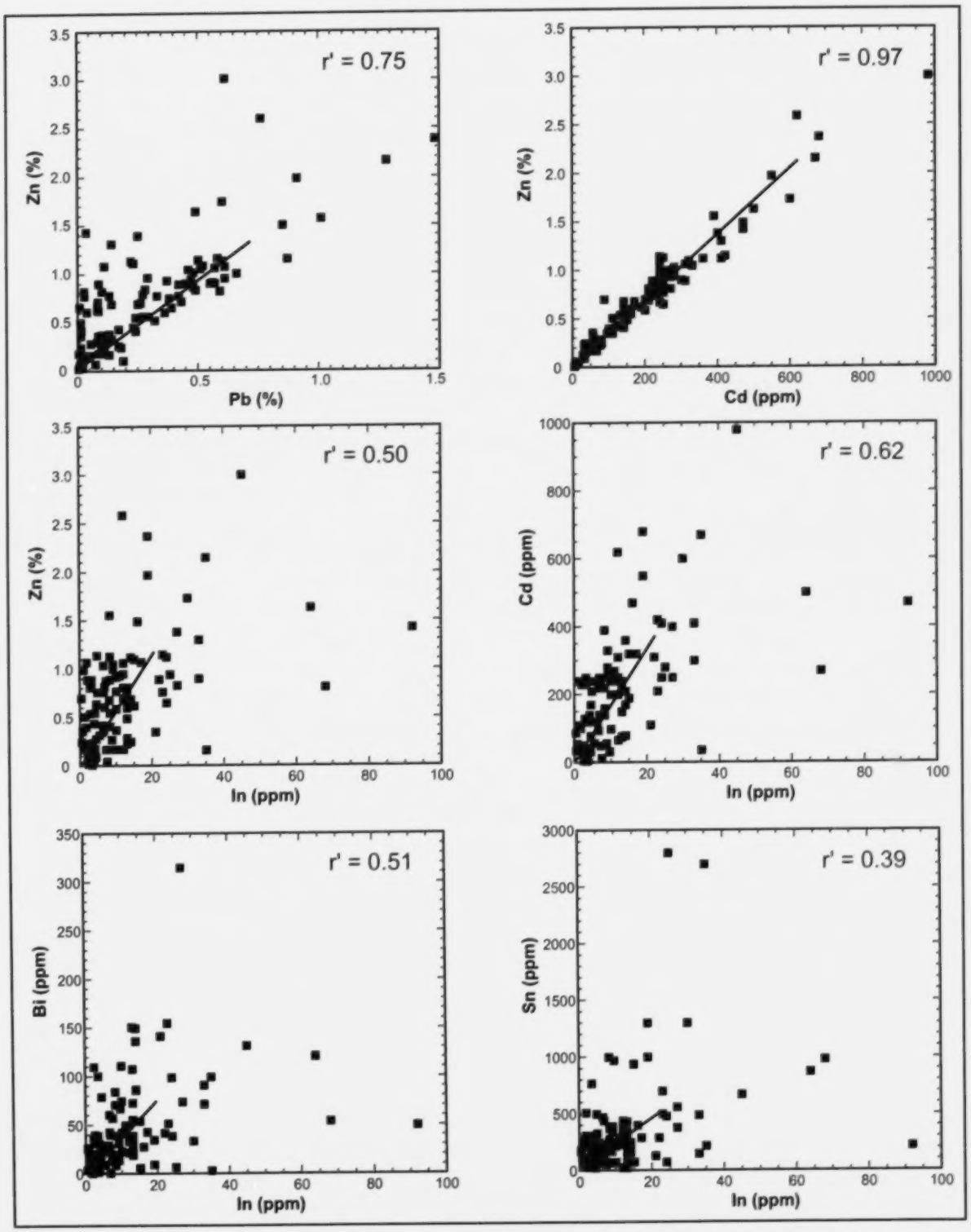

Figure 3. Binary plots of selected trace and major elements as determined by bulk ICP–MS analyses of 88 samples from the bedded massive sulphide facies of the Caribou deposit. Data are from Goodfellow (2003). Spearman rank correlation coefficients (r') are displayed with each plot (99% confidence interval, r' = >0.15). Positive correlations between Zn, Cd, In, and Bi suggest their mutual presence in sphalerite.

and the current report can be attributed to the generally low concentration of indium in the analyzed sphalerite and to the practical detection limits of the conventional electron microprobe. Nevertheless, a positive correlation does exist between zinc and indium in the Caribou deposit (Fig. 3). As well, numerous microanalytical studies of sphalerite grains from elsewhere in the Bathurst Mining Camp have attributed the mineralogical balance of indium to sphalerite (e.g., Sutherland and Halls 1969; van Staal 1985; Lentz 2002; McClenaghan et al. 2009a).

Aside from the incorporation of discrete inclusions of indium-rich mineral phases such as roquesite, cassiterite, and stannite within sphalerite, the most likely mechanism for indium enrichment is the coupled substitution of In into the sphalerite mineral structure through the following exchange:

$$Cu^{+} + In^{3+} = 2Zn^{2+}$$

This substitution is further enhanced by structural similarities between the mineral roquesite ($CuInS_2$) and sphalerite (ZnS), which result in a binary solid solution series (discontinuous).

Electron microprobe analyses of sphalerite reveal a highly varied copper content that ranges from 0.05% Cu (the detection limit) to 4.23% Cu (Appendix 3). Elevated contents are due in part to fine inclusions of chalcopyrite ($CuFeS_2$), often referred to as chalcopyrite disease (Barton 1978; Pisutha-Arnond and Ohmoto 1983; Barton and Bethke 1987; Eldridge et al. 1988). These inclusions likely represent an exhalative sulphide facies that has undergone hydrothermal recrystallization (zone refining) by late copper-bearing hydrothermal fluids (Powe 2008; McClenaghan et al. 2009b) and experienced further metamorphic enhancement through diffusion-induced segregation. Although diseased sphalerite masses are not widespread within massive sulphides in the Caribou deposit, their occurrence accounts for some of the elevated copper content (7370 ppm) in the zinc concentrates (Table 2).

In general, sphalerite compositions from a broad range of hydrothermal vein and exhalative deposits worldwide exhibit correlative behavior between indium and copper. In fact, data show a strong association between the two elements, with chalcopyrite disease textures forming as a precursor to indium diffusion fronts in experimentally grown sphalerite grains (Schwarz-Schampera and Herzig 2002). As with sphalerite, chalcopyrite is isostructural with roquesite and can accommodate indium as a straight substitution for iron. Notable indium contents have been reported in chalcopyrite from the Kidd Creek VMS deposit (up to 750 ppm In: Cabri et al. 1985) and some Australian deposits (up to 100 ppm: Huston et al. 1995). The sporadic occurrence of diseased sphalerite grains in massive sulphides and concentrates for the Caribou deposit may account for the discrepancy between indium contents reported herein and in Goodfellow (2003).

Electron microprobe analyses of sphalerite (Table 3) also show significant contents of Cd (avg. 0.17%) and Fe (avg. 4.57%). Cd commonly occurs as a substitution for Zn in the

sphalerite structure, wherein Zn/Cd averages 412. This ratio is similar to contents reported elsewhere in the Bathurst Camp (Lentz 2002; Goodfellow 2003; McClenaghan et al. 2009a), as well as in some other Canadian VMS deposits (avg. Zn/Cd = 377: Jonasson and Sangster 1978). Theoretically, sphalerite can accommodate up to 12.2% Fe (Boorman 1967), in which the iron content is strongly controlled by iron diffusion during dynamic metamorphism (see Barton and Toulmin 1966; Scott and Barnes 1971).

Contents of Co, As, Mn, Se, and Sn are generally below detection limits for the electron microprobe (Table 3). However, the bulk geochemical analyses yield highly varied results for Sn in zinc concentrates (Table 2), ranging from an average of 27.7 ppm for samples analyzed by ICP–MS (aqua regia) to 273 ppm with ICP–MS (Na_2O_2 fusion). Furthermore, analysis of the standard reference material (MS-1) by both methods exhibits a similar phenomenon. The Na_2O_2 fusion method displays a greater degree of accuracy, a consequence of the limitations of aqua regia digestion of cassiterite relative to the more robust Na_2O_2 fusion.

Cassiterite, identified in sphalerite-rich massive sulphide sections at Caribou, generally occurs as a trace accessory phase in the zinc–lead sulphide facies of VMS deposits in the Bathurst Mining Camp. Cassiterite is an important source of tin in massive sulphides and, in conjunction with chalcopyrite, accounts for most of the tin budget. Analyses of cassiterite from Brunswick No. 12 (McClenaghan et al. 2009a) show a significant indium content (avg. 328 ppm). A positive correlation between tin and indium is evident in bulk geochemical data for the Caribou massive sulphides (Goodfellow 2003). However, ICP–MS (Na_2O_2 fusion) analyses of the zinc concentrate show only a modest increase in indium content (Table 2), indicating minor contributions from cassiterite to the overall indium budget.

Lead concentrates for the three mill-run periods average 5.23% Zn, 43.2% Pb, 0.39% Cu, and 531 g/t Ag (Table 1). They also contain Sb (>500 ppm), Bi (107 ppm), Mo (24.8 ppm), Se (85.1 ppm), and Tl (45.6 ppm) (Table 2). Results are consistent with compositions of galena from elsewhere in the Bathurst Camp. Galena in the BMC is widely known to be a significant carrier of silver (Boorman 1968; Jambor and Laflamme 1978; Chen and Petruk 1980; McClenaghan et al. 2009a) and accounts for 34.7% of the Ag in the mill feed at Brunswick No. 12 (Petruk and Schnarr 1981). Jambor and Laflamme (1978) also recognized that galena contains the bulk of the Ag in the Caribou deposit, where it occurs as a trace-element substitution for Pb and/or as fine-grained (submicroscopic) argentiferous inclusions in galena.

The Bi content in galena is also elevated, consistent with coupled Ag substitution for Pb in the galena structure (Craig 1967). This is in keeping with an earlier report (Jambor and Laflamme 1978) of galena from the Caribou deposit containing as much as 1.58% Bi. Indium in lead concentrates as determined by ICP–MS (aqua regia) averages 4.96 ppm (Table 2), a decrease in concentration from the mill feed (avg. 6.77 ppm) and consistent with the selective partitioning of indium into the zinc concentrate.

Plant tailings for the three mill-run periods average 0.91% Zn, 0.82% Pb, 0.20% Cu, and

38.7 g/t Ag (Table 1). These levels are due to residual sphalerite, galena, and chalcopyrite that are too fine grained to be extracted economically. Similarities in copper grades for the mill feed and plant tailings attest to the affinity of chalcopyrite for iron sulphides and are consistent with the concentration of copper in the vent complex facies at the Caribou deposit (Goodfellow 2003). Plant tailings exhibit slight enrichments in As (avg. 4567 ppm) and Ni (13.8 ppm) and only minor variations in Co (25.2 ppm) (Table 2). This is consistent with their concentration in pyrite and arsenopyrite, which would have increased in modal abundance due to the selective extraction of sphalerite and galena from the mill feed. The Sb content (avg. 280 ppm) in the tailings is also similar to that in the mill feed, due to elevated Sb content in arsenopyrite as a structural substitution for As (McClenaghan et al. 2004), and in galena.

Conclusions and Recommendations

Analyses of mill products from the Caribou mine show that indium content is not at sufficient levels to significantly increase the value of Caribou ore. Three independent analytical methods confirm that indium has an affinity for the zinc concentrate, which averages 57.6 ppm In; indium in the lead concentrate is lower, averaging 4.96 ppm In. Analyses of mill feed and plant tailings indicate a roughly tenfold enrichment factor in the zinc concentrate, with approximately 70% recovery of indium, overall.

Microanalytical work was conducted to determine the indium content in sphalerite, but indium levels lay below detection capabilities of the electron microprobe. Thus, the mineral balance of indium remains undetermined. However, bulk correlations among Zn, Sn, In, and Cd, as well as the enrichment of indium in the zinc concentrate, suggest that indium is concentrated in sphalerite and to a lesser degree in cassiterite.

Although the Caribou ore mill feed exhibits a low indium content (avg. 6.77 ppm), higher contents are reported for bedded zinc–lead sulphides from the deposit (Goodfellow 2003). Caution should be exercised in interpreting the potential of indium recovery from the Caribou mine based solely on results of the present report. A detailed study is recommended—one that includes bulk sampling of massive sulphides as well as extended mill-run periods for the collection of mill products—to rigorously assess indium content and distribution within the ore zones and associated ore concentrates.

Acknowledgements

The authors thank Lyne Coté and Benoit Drolet of Blue Note Mining Ltd. for providing samples and assays of mill products from the Caribou mine. Electron microprobe analyses were carried out at the University of New Brunswick with the help of Douglas Hall. The manuscript benefitted from a critical review by Kathleen Thorne and the editorial comments of Les Fyffe, both with the Geological Surveys Branch, New Brunswick Department of Natural Resources.

REFERENCES

Barton, P.B. Jr. 1978. Ore textures involving sphalerite from the Furutobe mine, Akita Prefecture, Japan. Mining Geology, **28**, p. 293–300.

Barton, P.B. Jr., and Bethke, P.M. 1987. Chalcopyrite disease in sphalerite: pathology and epidemiology. American Mineralogist, **72**, p. 451–467.

Barton, P.B. Jr., and Toulmin P. III. 1966. Phase relations involving sphalerite in the Fe–Zn–S system. Economic Geology, **61**, p. 815–849.

Boorman, R.S. 1967. Sub-solidus studies in the ZnS–FeS–FeS_2 system. Economic Geology, **62**, p. 614–631.

Boorman, R.S. 1968. Silver in some New Brunswick galenas. New Brunswick Research and Productivity Council, Research Note 11, 22 p.

Cabri, L.J., Campbell, J.L., Laflamme, J.H.G., Leigh, R.G., Maxwell, J.A., and Scott, J.D. 1985. Proton-microprobe analysis of trace elements in sulfides from some massive sulfide deposits. Canadian Mineralogist, **23**, p. 133–148.

Cavelero, R.A. 1993. The Caribou massive-sulfide deposit, Bathurst Camp, New Brunswick. *In* Guidebook to the Metallogeny of the Bathurst Camp. *Edited by* S.R. McCutcheon and D.R. Lentz. 3rd Annual Field Conference, Geological Society of CIM, p. 115–134.

Chen, T.T., and Petruk, W. 1980. Mineralogy and characteristics that affect recoveries of metals and trace-elements from the ore at Heath Steele Mines, New Brunswick. The Canadian Mining and Metallurgical Bulletin, **73**, p. 167–179.

Cheriton, C.G. 1958. The structure of the Caribou sulphide body of the Anaconda Company (Canada), Limited, Bathurst District, N.B. Canadian Institute of Mining and Metallurgy Bulletin, **51**, p. 178–179.

Coté, L., and Adante, J. 2009. Design, start-up and optimization of Pb & Zn flotation circuits utilizing ultra-fine grinding technology. *In* Proceedings of the 41st Annual Canadian Mineral Processors Conference, Ottawa, Ontario, p. 3–27.

Craig, J.R. 1967. Phase relations and mineral assemblages in the Ag–Bi–Pb–S system. Mineralium Deposita, **1**, p. 278–305.

Davis, G.H. 1972. Deformational history of the Caribou strata-bound sulfide deposit, Bathurst, New Brunswick, Canada. Economic Geology, **67**, p. 634–655.

Eldridge, C.S., Bourcier, W.L., Ohmoto, H., and Barnes, H.L. 1988. Hydrothermal inoculation and incubation of the chalcopyrite disease in sphalerite. Economic Geology, **83**, p. 978–989.

Goodfellow, W.D. 2003. Geology and genesis of the Caribou deposit, Bathurst Mining Camp, New Brunswick, Canada. *In* Massive Sulfide Deposits in the Bathurst Mining Camp, New Brunswick and Northern Maine. *Edited by* W.D. Goodfellow, S.R. McCutcheon, and J.M. Peter. Economic Geology, Monograph 11, p. 327–360.

Goodfellow, W.D., and McCutcheon, S.R. 2003. Geologic and genetic attributes of volcanic sediment-hosted massive sulfide deposits of the Bathurst Mining Camp, northern New Brunswick—a synthesis. *In* Massive Sulfide Deposits in the Bathurst Mining Camp, New Brunswick and Northern Maine. *Edited by* W.D. Goodfellow, S.R. McCutcheon, and J.M. Peter. Economic Geology, Monograph 11, p. 245–301.

Hannington, M.D., and Gorton, M.P. 1991. Analysis of sulfides for gold and associated trace metals by direct neutron activation with a low-flux reactor. Geostandards Newsletter, **15**, p. 145–154.

Helmstaedt, H. 1973. Discussion: deformational history of the Caribou strata-bound deposits, Bathurst, New Brunswick, Canada. Economic Geology, **68**, p. 571–572.

Hoffman, E.L. 1992. Instrumental neutron activation in geoanalysis. Journal of Geochemical Exploration, **44**, p. 297–319.

Huston D.L., Sie S.H., Suter G.F., Cooke D.R., and Both, R.A. 1995. Trace elements in sulfide minerals

from eastern Australian volcanic hosted massive sulfide deposits. Part I–Proton microprobe analyses of pyrite, chalcopyrite, and sphalerite. Part II–Selenium levels in pyrite: comparison with ^{34}S values and implications for the source of sulfur in volcanogenic hydrothermal systems. Economic Geology, **90**, p. 1167–1196.

Jambor, J.L., and Laflamme, G.H.G. 1978. The mineral sources of silver and their distribution in the Caribou massive sulfide deposit, Bathurst area, New Brunswick. Energy, Mines and Resources Canada, CANMET Report 78-14, 26 p.

Jonasson, I.R., and Sangster, D.F. 1978. Zn:Cd ratios for sphalerites separated from some Canadian sulphide ore samples. Geological Survey of Canada, Current Research 1978-1B, p. 195–201.

Lentz, D.R. 1995. Preliminary evaluation of six in-house rock geochemical standards from the Bathurst Camp, New Brunswick. *In* Current Research 1994. *Edited by* S.A.A. Merlini. New Brunswick Department of Natural Resources and Energy; Minerals, Policy and Planning Division, Miscellaneous Report 18, p. 81–89.

Lentz, D.R. 1999. Petrology, geochemistry, and oxygen isotope interpretation of felsic volcanic and related rocks hosting the Brunswick 6 and 12 massive sulfide deposits (Brunswick Belt), Bathurst Mining Camp, New Brunswick, Canada. Economic Geology, **94**, p. 57–86.

Lentz, D.R. 2002. Sphalerite and arsenopyrite at the Brunswick No. 12 massive sulfide deposit, Bathurst Camp, New Brunswick: constraints on P-T evolution. Canadian Mineralogist, **40**, p. 19–31.

McClenaghan, S.H. 2002. Gold in massive sulphide deposits, Bathurst Mining Camp, New Brunswick: form, distribution and genesis. Unpublished M.Sc. thesis, University of Ottawa, 371 p.

McClenaghan, S.H., Goodfellow, W.D., and Lentz, D.R. 2003. Gold in massive sulfide deposits, Bathurst Mining Camp: distribution and genesis. *In* Massive Sulfide Deposits in the Bathurst Mining Camp, New Brunswick and Northern Maine. *Edited by* W.D. Goodfellow, S.R. McCutcheon, and J.M. Peter. Economic Geology, Monograph 11, p. 303–326.

McClenaghan, S.H., Lentz, D.R., and Cabri, L.J. 2004. Abundance and speciation of gold in massive sulfides of the Bathurst Mining Camp, New Brunswick, Canada. Canadian Mineralogist, **42**, p. 851–871.

McClenaghan, S.H., Lentz, D.R., Martin, J., and Diegor, W.G. 2009a. Gold in the Brunswick No. 12 volcanogenic massive sulfide deposit, Bathurst Mining Camp, Canada: evidence from bulk ore analysis and laser ablation ICP–MS data on sulfide phases. Mineralium Deposita, **44**, p. 523–557.

McClenaghan, S.H., Lentz, D.R., and Powe, E.M. 2009b. Distribution of Cu-rich massive sulfides at the Brunswick No. 12 deposit, Bathurst Mining Camp, New Brunswick. *In* Proceedings of the 24th International Applied Geochemistry Symposium, Fredericton, New Brunswick, Canada. *Edited by* D.R. Lentz, K.G. Thorne, and K.-L. Beal. Association of Applied Geochemists, **1**, p. 507–510.

McCutcheon, S.R., and Walker, J. 2009. Stratigraphic setting of base-metal deposits in the Bathurst Mining Camp (BMC), New Brunswick. 24th International Applied Geochemistry Symposium, Fredericton, New Brunswick, Canada. Association of Applied Geochemists, Field Trip Guidebook, 95 p.

McCutcheon, S.R., Luff, W.M., and Boyle, R.W. 2003. The Bathurst Mining Camp, New Brunswick, Canada: history of discovery and evolution of geologic models. *In* Massive Sulfide Deposits in the Bathurst Mining Camp, New Brunswick and Northern Maine. *Edited by* W.D. Goodfellow, S.R. McCutcheon, and J.M. Peter. Economic Geology, Monograph 11, p. 17–35.

McCutcheon, S.R., Walker, J., Bernard, P., Lentz, D., Downey, W., and McClenaghan, S. 2005. Stratigraphic setting of base-metal deposits in the Bathurst Mining Camp, New Brunswick. Geological Association of Canada/Mineralogical Association of Canada Annual Meeting Halifax, Nova Scotia, Field Trip B4 Guidebook, 105 p.

Petruk, W., and Schnarr, J.R. 1981. An evaluation of the recovery of free and unliberated mineral grains, metals and trace elements in the concentrator of Brunswick Mining and Smelting Limited. The Canadian Mining and Metallurgical Bulletin, **74**, p. 132–159.

Pisutha-Arnond, V., and Ohmoto, H. 1983. Thermal history, and chemical and isotopic compositions of the ore-forming fluids responsible for the Kuroko massive sulfide deposits in the Hokuroku District of Japan. *In* The Kuroko and Related Volcanogenic Massive Sulfide deposits. *Edited by* H. Ohmoto and B.J. Skinner. Economic Geology, Monograph 5, p. 523–558.

Powe, E.M. 2008. Petrology, geochemistry and distribution of the copper zones at the Brunswick No. 12 volcanogenic massive sulfide deposit, Bathurst Mining Camp, New Brunswick. Unpublished B.Sc. thesis, University of New Brunswick, 91 p.

Rankin, L.D. 1982. The geology of the Portage Lakes–Caribou area, northern New Brunswick. Unpublished M.Sc. thesis, University of New Brunswick, 220 p.

Rogers, N., van Staal, C.R., McNicoll, V., and Theriault, R. 2003. Volcanology and tectonic setting of the northern Bathurst Mining Camp: part 1—extension and rifting of the Popelogan Arc. *In* Massive Sulfide Deposits in the Bathurst Mining Camp, New Brunswick and Northern Maine. *Edited by* W.D. Goodfellow, S.R. McCutcheon, and J.M. Peter. Economic Geology, Monograph 11, p. 157–180.

Roscoe, W.E. 1971. Geology of the Caribou deposit, Bathurst, N.B. Canadian Journal of Earth Sciences, **8**, p. 1125–1136.

Schwarz-Schampera, U., and Herzig, P.M. 2002. Indium: Geology, Mineralogy, and Economics. Springer, Heidelberg, 257 p.

Scott, S.D., and Barnes, H.L. 1971. Sphalerite geothermometry and geobarometry. Economic Geology, **66**, p. 653–669.

Sullivan, R.W., and van Staal, C.R. 1990. Age of metarhyolite from the Tetagouche Group, Bathurst, New Brunswick, from U–Pb isochron analyses of zircons enriched in common lead. Geological Survey of Canada, Current Research, Radiogenic Age and Isotopic Studies 89-2, p. 109–117.

Sutherland, J.K., and Halls, C. 1969. Composition of some New Brunswick sphalerites. New Brunswick Research and Productivity Council, Research Note 21, 33 p.

van Staal, C.R. 1985. Structure and metamorphism of the Brunswick Mines area, Bathurst, New Brunswick, Canada. Unpublished Ph.D. thesis, University of New Brunswick, 484 p.

van Staal, C.R. 1994. Brunswick subduction complex in the Canadian Appalachians: record of the Late Ordovician to Late Silurian collision between Laurentia and the Gander margin of Avalon. Tectonics, **13**, p. 946–962.

van Staal, C.R., and Williams, P.F. 1984. Structure, origin and concentration of the Brunswick 12 and 6 orebodies. Economic Geology, **79**, p. 1669–1692.

van Staal, C.R., Winchester, J., and Cullen, R. 1988. Evidence for D_1-related thrusting and folding in the Bathurst–Millstream river area, New Brunswick. Geological Survey of Canada, Current Research 1988-1B, p. 135–148.

van Staal, C.R., Ravenhurst, C.E., Winchester, J.A., Roddick, J.C., and Langton, J.P. 1990. Evidence for a post-Taconic blueschist suture in northern New Brunswick, Canada. Geology, **18**, p. 1073–1077.

van Staal, C.R., Wilson, R.A., Rogers, N., Fyffe, L.R., Langton, J.P., McCutcheon, S.R., McNicoll, V., and Ravenhurst, C.E. 2003. Geology and tectonic history of the Bathurst Supergroup, Bathurst Mining Camp, and its relationships to coeval rocks in southwestern New Brunswick and adjacent Maine—a synthesis. *In* Massive Sulfide Deposits in the Bathurst Mining Camp, New Brunswick and Northern Maine. *Edited by* W.D. Goodfellow, S.R. McCutcheon, and J.M. Peter. Economic Geology, Monograph 11, p. 37–6.

Appendix 1. Bulk analyses of mill-run products from the Caribou deposit by fire-assay atomic absorption spectrometry (FAAS).

Notes: 1. All analyses except Ag are measured in %. Ag is measured in ppm.
2. Complete sample numbers are 08-SHM-CAR-1, 08-SHM-CAR-2, etc.
3. All dates are in the year 2008.

Sample #	CAR-1	CAR-2	CAR-3	CAR-4
Source	Mill Feed	Pb Concentrate	Plant Tailings	Zn Concentrate
Date	Aug. 13	Aug. 13	Aug. 13	Aug. 13
Zn (%)	6.36	5.26	0.89	49.3
Pb	3.16	42.1	0.91	2.21
Cu	0.22	0.39	0.18	0.50
Fe	29.2	19.4	31.1	11.7
Ag (ppm)	79	531	45	127
Sample #	CAR-6	CAR-7	CAR-8	CAR-9
Source	Mill Feed	Pb Concentrate	Plant Tailings	Zn Concentrate
Date	Aug. 14	Aug. 14	Aug. 14	Aug. 14
Zn (%)	6.08	5.15	0.93	49.7
Pb	2.61	46.4	0.77	2.32
Cu	0.22	0.37	0.20	0.52
Fe	30.1	17.6	32.9	10.8
Ag (ppm)	56	522	27	104
Sample #	CAR-11	CAR-12	CAR-13	CAR-14
Source	Mill Feed	Pb Concentrate	Plant Tailings	Zn Concentrate
Date	Aug. 15	Aug. 15	Aug. 15	Aug. 15
Zn (%)	5.89	5.29	0.92	50.9
Pb	2.56	41.2	0.78	2.02
Cu	0.24	0.41	0.21	0.55
Fe	30.4	19.8	32.6	10.4
Ag (ppm)	74	541	44	128

Appendix 2. Bulk analyses of mill-run products from the Caribou deposit (and standard reference material) by inductively coupled plasma–mass spectrometry (ICP–MS).

Notes: 1. Whole-rock analyses are measured in %. All trace-element analyses except Au are measured in ppm. Au is measured in ppb.
2. Complete sample numbers are 08-SHM-CAR-1, 08-SHM-CAR-2, etc.
3. All sampling dates are in the year 2008.

Sample #	CAR-1	CAR-2	CAR-3	CAR-4	CAR-5	CAR-6	CAR-7	CAR-8	CAR-9	CAR-10
Source	Mill Feed	Pb Concen'te	Plant Tailings	Zn Concen'te	Standard MS-1	Mill Feed	Pb Concen'te	Plant Tailings	Zn Concen'te	Standard MS-1
Date	Aug. 13	Aug. 13	Aug. 13	Aug. 13		Aug. 14	Aug. 14	Aug. 14	Aug. 14	
Digestion	Aqua Regia	Aqua Regia	Aqua Regia	Aqua Regia	Aqua Regia	Aqua Regia	Aqua Regia	Aqua Regia	Aqua Regia	Aqua Regia
Si (%)	–	–	–	–	–	–	–	–	–	–
Al	0.45	0.02	0.54	0.03	0.04	0.46	0.02	0.55	0.03	0.04
Fe	18.9	15	18.9	9.19	16.3	17.7	14.5	18.2	8.17	18
Ti	<0.01	<0.01	0.01	<0.01	<0.01	<0.01	<0.01	<0.01	<0.01	<0.01
Mg	0.47	0.02	0.65	0.03	0.03	0.35	0.01	0.42	0.02	0.03
Mn	0.251	0.0226	0.275	0.0556	0.0451	0.238	0.0235	0.284	0.0545	0.0471
Ca	0.34	0.02	0.61	0.08	0.06	0.16	0.01	0.25	0.06	0.06
Na	0.016	0.008	0.016	0.01	0.007	0.016	0.009	0.015	0.011	0.009
K	0.03	<0.01	0.04	<0.01	<0.01	0.03	<0.01	0.04	<0.01	<0.01
P	0.019	0.005	0.024	0.003	0.003	0.021	0.006	0.023	0.003	0.003
S	13.54	14.69	13.03	12.77	14.88	13.35	14.36	13.01	11.65	15.25
Au (ppb)	<0.5	291	<0.5	24.1	<0.5	<0.5	308	<0.5	49	<0.5
Ag (ppm)	58.5	>100	35.6	>100	>100	53.2	>100	33	>100	>100
As	4970	6380	5440	3090	437	4090	4470	4260	2330	547
B	<1	<1	<1	<1	<1	<1	<1	<1	<1	<1
Ba	2.7	2.2	2.1	1.7	2.2	2	1.2	2.9	1.6	1.9
Be	0.2	0.1	0.3	0.1	0.1	0.3	<0.1	0.4	0.1	0.1
Bi	14.5	79.3	13.9	12	2.77	16.7	124	23.4	14.9	3.14
Cd	108	107	17.5	921	178	113	121	18.8	973	182
Co	21.8	11.8	21.1	7.3	6.8	25.3	13.4	27.1	7.5	7
Cr	34.2	13.2	62.6	32.9	2.3	35.6	14.5	53	28.1	2.2
Cs	0.4	0.1	0.5	0.1	0.1	0.5	0.1	0.6	0.1	0.1
Cu	1600	3010	1620	4980	194	1650	3610	1650	5100	199
Ga	5.99	0.65	6.7	3.45	6.49	6.14	0.68	6.85	3.08	6.55
Ge	0.2	0.6	0.1	0.4	0.2	0.1	0.8	0.2	0.3	0.2
Hf	0.2	0.3	0.5	0.1	<0.1	0.3	0.3	0.4	0.1	<0.1
In	6.16	4.03	1.64	48.7	31.1	7.49	5.46	2.27	59.5	31.9
Li	3.4	0.5	4.2	0.2	0.5	3.3	0.1	4	0.2	0.6
Mo	4.02	22.9	3.59	10.6	2.23	3.97	32.9	3.89	7.44	2.01
Nb	0.2	<0.1	0.2	<0.1	0.1	0.1	<0.1	0.1	<0.1	0.1

Sample #	CAR-1	CAR-2	CAR-3	CAR-4	CAR-5	CAR-6	CAR-7	CAR-8	CAR-9	CAR-10
Source	Mill Feed	Pb Concen'te	Plant Tailings	Zn Concen'te	Standard MS-1	Mill Feed	Pb Concen'te	Plant Tailings	Zn Concen'te	Standard MS-1
Date	Aug. 13	Aug. 13	Aug. 13	Aug. 13		Aug. 14	Aug. 14	Aug. 14	Aug. 14	
Digestion	Aqua Regia	Aqua Regia	Aqua Regia	Aqua Regia	Aqua Regia	Aqua Regia	Aqua Regia	Aqua Regia	Aqua Regia	Aqua Regia
Ni	11.4	10.9	13.9	6	5.1	10.5	11.5	13.9	5.5	5.3
Pb	>10000	>10000	7310	6440	>10000	>10000	>10000	6290	5780	>10000
Rb	2.9	0.4	3.3	0.4	0.5	2.3	0.3	3.1	0.3	0.3
Re	0.005	0.01	0.002	0.006	0.001	0.003	0.012	0.003	0.006	<0.001
Sb	295	>500	273	272	293	307	>500	292	276	308
Sc	1.7	0.1	1.7	0.1	<0.1	1.1	<0.1	1.3	<0.1	<0.1
Se	2.6	88.4	2.2	23.5	4.1	2.3	162	2.7	22.2	3.7
Sn	9.32	10.2	7.7	27.1	24.5	11.9	11.1	8.63	26.7	25.5
Sr	18.8	1.3	24.8	3.1	2.2	14.8	1.4	17.9	2.4	2.5
Ta	<0.05	<0.05	<0.05	<0.05	<0.05	<0.05	<0.05	<0.05	<0.05	<0.05
Te	0.19	1.03	0.28	0.23	0.08	0.15	0.49	0.15	0.07	<0.02
Th	4.7	1	3.7	0.6	0.3	3.2	0.5	3.7	0.5	0.2
Tl	31.5	41.5	26.9	12.7	60	28.7	51.3	27.4	12.3	75.6
U	3.4	2.5	3.8	3.1	0.4	3.6	2.8	3.8	2.7	0.4
V	13	<1	16	<1	1	14	<1	16	1	1
W	1.1	0.7	0.5	0.4	73.5	2.9	1.2	0.7	0.4	75.7
Y	4.85	2.83	8	0.99	0.24	5.06	3.22	7.39	0.95	0.25
Zn	>5000	>5000	>5000	>5000	>5000	>5000	>5000	>5000	>5000	>5000
Zr	15.8	22.1	26.6	9.1	1.9	15.9	21.1	22.1	7.2	2.2
La	2.2	<0.5	3.1	<0.5	<0.5	2.2	<0.5	2.9	<0.5	<0.5
Ce	6.78	1.67	9	1.44	0.95	7.29	1.5	8.39	1.4	0.91
Pr	0.8	0.1	1.1	0.1	<0.1	0.9	0.1	1	0.1	<0.1
Nd	3.26	0.51	4.27	0.44	0.16	3.48	0.39	4.06	0.39	0.17
Sm	0.9	0.1	1.1	0.1	<0.1	1	0.1	1.1	0.1	0.1
Eu	0.4	0.1	0.4	0.1	0.1	0.4	0.1	0.4	0.1	0.1
Gd	1.1	0.1	1.4	0.1	0.1	1.1	0.1	1.3	0.1	0.1
Tb	0.2	<0.1	0.2	<0.1	<0.1	0.2	<0.1	0.2	<0.1	<0.1
Dy	1.1	0.1	1.3	0.1	<0.001	1.1	0.1	1.3	0.1	<0.001
Ho	0.2	<0.1	0.2	<0.1	<0.1	0.2	<0.1	0.2	<0.1	<0.1
Er	0.5	0.1	0.7	0.1	<0.1	0.6	0.1	0.6	0.1	<0.1
Tm	0.1	<0.1	0.1	<0.1	<0.1	0.1	<0.1	0.1	<0.1	<0.1
Yb	0.4	0.1	0.6	0.1	<0.1	0.4	0.1	0.5	0.1	<0.1
Lu	0.1	<0.1	0.1	<0.1	<0.1	0.1	<0.1	0.1	<0.1	<0.1

Sample #	CAR-11	CAR-12	CAR-13	CAR-14	CAR-15	CAR-4	CAR-5	CAR-9	CAR-10	CAR-14	CAR-15
Source	Mill Feed	Pb Concen'te	Plant Tailings	Zn Concen'te	Standard MS-1	Zn Concen'te	Standard MS-1	Zn Concen'te	Standard MS-1	Zn Concen'te	Standard MS-1
Date	Aug. 15	Aug. 15	Aug. 15	Aug. 15		Aug. 13		Aug. 14		Aug. 15	
Digestion	Aqua Regia	Aqua Regia	Aqua Regia	Aqua Regia	Aqua Regia	Na_2O_2 Fusion	Na_2O_2 Fusion	Na_2O_2 Fusion	Na_2O_2 Fusion	Na_2O_2 Fusion	Na_2O_2 Fusion
Si (%)	–	–	–	–	–	0.32	5.79	0.23	5.69	0.21	5.82
Al	0.51	0.02	0.65	0.03	0.04	0.06	0.09	0.05	0.09	0.05	0.09
Fe	21.5	14.3	18.6	7.81	15.9	11.6	28	10.9	28	10.7	28.2
Ti	<0.01	<0.01	<0.01	<0.01	<0.01	<0.01	<0.01	<0.01	<0.01	<0.01	<0.01
Mg	0.43	0.01	0.53	0.02	0.03	0.04	0.05	0.03	0.05	0.03	0.05
Mn	0.236	0.0223	0.27	0.043	0.0462	669	587	650	606	552	587
Ca	0.2	0.01	0.29	0.07	0.06	0.02	0.01	0.04	0.02	0.05	0.02
Na	0.016	0.01	0.018	0.01	0.009	–	–	–	–	–	–
K	0.04	<0.01	0.05	<0.01	<0.01	<0.1	<0.1	<0.1	<0.1	<0.1	<0.1
P	0.02	0.006	0.025	0.004	0.002	<0.005	<0 005	<0.005	<0.005	<0.005	<0.005
S	15.13	14.3	12.85	12.06	14.11	35.5	37	35.7	37.6	35.6	37.7
Au (ppb)	<0.5	9.8	<0.5	25.7	<0.5	–	–	–	–	–	–
Ag (ppm)	49	>100	31.8	>100	>100	140	150	140	150	140	160
As	3900	4390	4000	2120	492	3540	710	2800	698	2690	685
B	<1	<1	<1	<1	<1	10	<10	<10	<10	<10	<10
Ba	3.1	<0.5	2.6	1.8	1.4	<3	311	<3	317	<3	324
Be	0.3	0.2	0.4	0.2	0.2	<3	<3	<3	<3	<3	<3
Bi	21.3	117	19.7	11.8	3.08	8	<2	13	<2	11	<2
Cd	103	121	17.2	946	180	1020	190	1010	189	1100	195
Co	30.6	14.1	27.5	6.9	7.1	7.8	8	8.8	8	8.4	7.7
Cr	35.1	16	57.5	27	2.3	60	<30	50	<30	40	<30
Cs	0.5	0.1	0.6	0.1	0.1	<0.1	0.2	<0.1	0.2	<0.1	0.2
Cu	1660	3820	1630	5190	190	6780	211	7260	224	8070	253
Ga	6.07	0.74	7.21	2.9	6.58	3.6	16.4	3.5	16.3	3.4	16.3
Ge	0.2	0.1	0.1	0.4	0.5	1.1	8.6	1.3	8.5	1	8.3
Hf	0.3	0.3	0.5	0.1	<0.1	<10	<10	<10	<10	<10	<10
In	6.66	5.39	2.14	56.3	31.7	51.4	33.1	59	34.5	62.5	35.2
Li	3.9	0.2	4.6	0.3	2.2	<3	<3	<3	<3	<3	<3
Mo	4.92	18.7	3.46	8.28	1.94	9	3	10	3	9	3
Nb	0.1	<0.1	0.1	<0.1	0.1	<2.4	<2.4	<2.4	<2.4	<2.4	<2.4
Ni	10.9	10.5	13.6	4.8	4.9	<10	<10	<10	<10	<10	<10
Pb	>10000	>10000	6390	4760	>10000	>5000	>5000	>5000	>5000	>5000	>5000
Rb	3.3	0.4	3.5	0.3	0.4	0.5	1.1	0.5	1.1	0.4	1.1
Re	0.002	0.008	0.002	0.006	<0.001	–	–	–	–	–	–

Sample #	CAR-11	CAR-12	CAR-13	CAR-14	CAR-15	CAR-4	CAR-5	CAR-9	CAR-10	CAR-14	CAR-15
Source	Mill Feed	Pb Concen'te	Plant Tailings	Zn Concen'te	Standard MS-1	Zn Concen'te	Standard MS-1	Zn Concen'te	Standard MS-1	Zn Concen'te	Standard MS-1
Date	Aug. 15	Aug. 15	Aug. 15	Aug. 15		Aug. 13		Aug. 14		Aug. 15	
Digestion	Aqua Regia	Aqua Regia	Aqua Regia	Aqua Regia	Aqua Regia	Na_2O_2 Fusion	Na_2O_2 Fusion	Na_2O_2 Fusion	Na_2O_2 Fusion	Na_2O_2 Fusion	Na_2O_2 Fusion
Sb	272	>500	276	251	288	298	400	295	418	282	426
Sc	1.1	<0.1	1.4	<0.1	<0.1	–	–	–	–	–	–
Se	2.4	5	1	24.1	3.6	35	1.5	28.2	<0.8	30.9	<0.8
Sn	11.6	11.5	9.55	29.2	24.7	276	802	274	827	269	834
Sr	13	1.5	16.3	2.2	2.9	<3	<3	<3	3	<3	<3
Ta	<0.05	<0.05	<0.05	<0.05	<0.05	<0.2	<0.2	<0.2	<0.2	<0.2	<0.2
Te	0.18	0.41	0.17	0.03	<0.02	<6	<6	<6	<6	<6	<6
Th	3	0.5	3.8	0.5	0.1	0.2	0.2	0.2	<0.1	0.2	<0.1
Tl	27.9	44	24.1	11	56	10.8	84.7	11	82.5	9.9	84.9
U	3.5	2.9	4	2.7	0.4	2	0.3	1.8	0.2	1.9	0.3
V	13	<1	17	<1	1	38	33	34	33	42	37
W	2.9	1	0.6	0.3	69.9	<0.7	91.4	<0.7	90.3	<0.7	92.1
Y	4.66	3.78	7.9	1.04	0.24	1.4	1	1.4	0.6	1.6	0.6
Zn	>5000	>5000	>5000	>5000	>5000	>5000	>5000	>5000	>5000	>5000	>5000
Zr	15.9	21.6	24	7.5	2.4	–	–	–	–	–	–
La	2	<0.5	2.8	<0.5	<0.5	0.8	1.7	0.7	0.6	0.9	<0.4
Ce	6.51	1.52	8.06	1.37	0.9	<0.8	2.7	<0.8	<0.8	1.5	<0.8
Pr	0.8	0.1	0.9	0.1	<0.1	0.1	0.3	0.1	<0.1	0.2	<0.1
Nd	3.06	0.42	3.93	0.41	0.17	<0.4	1.8	<0.4	<0.4	0.6	<0.4
Sm	0.8	0.1	1	0.1	0.1	0.1	0.3	0.1	<0.1	0.2	<0.1
Eu	0.3	0.1	0.4	0.1	0.1	<0.1	0.2	0.1	0.2	<0.1	0.2
Gd	1	0.1	1.3	0.1	<0.1	0.1	0.3	0.2	<0.1	0.1	<0.1
Tb	0.2	<0.1	0.2	<0.1	<0.1	<0.1	<0.1	<0.1	<0.1	<0.1	<0.1
Dy	1	0.1	1.3	0.1	<0.001	<0.3	<0.3	<0.3	<0.3	<0.3	<0.3
Ho	0.2	<0.1	0.3	<0.1	<0.1	<0.2	<0.2	<0.2	<0.2	<0.2	<0.2
Er	0.5	0.1	0.7	0.1	<0.1	<0.1	<0.1	<0.1	<0.1	<0.1	<0.1
Tm	0.1	<0.1	0.1	<0.1	<0.1	<0.1	<0.1	<0.1	<0.1	<0.1	<0.1
Yb	0.4	0.1	0.6	0.1	<0.1	<0.1	<0.1	<0.1	<0.1	<0.1	<0.1
Lu	0.1	<0.1	0.1	<0.1	<0.1	–	–	–	–	–	–

Appendix 3. Electron microprobe analyses of sphalerite grains in zinc concentrate and massive sulphides from the Caribou deposit.

Notes: 1. All values are quoted in %.
2. All dates are in the year 2008. * = date of sampling; § = date of analysis.
3. mdl = mean detection limit.

Sample #	Mean Detection Limit	08-SHM-CAR-4	08-SHM-CAR-4	08-SHM-CAR-4	08-SHM-CAR-4
Source		Zn Concentrate	Zn Concentrate	Zn Concentrate	Zn Concentrate
Date *		Aug. 13	Aug. 13	Aug. 13	Aug. 13
S (%)	0.0114	33.36	33.18	33.3	33.21
Mn	0.0334	0.0031	0.0124	0.0545	0.01
Fe	0.0312	5.12	0.3928	4	4.26
Co	0.0366	<mdl	0.0029	0.0194	<mdl
Cu	0.0457	0.0643	0.0759	0.0472	4.23
Zn	0.0525	60.1	66.25	62.11	57.21
As	0.0299	<mdl	<mdl	<mdl	<mdl
Se	0.0115	0.0113	<mdl	0.0045	–
Cd	0.0405	0.1771	0.061	0.11	0.2486
In	0.0105	<mdl	<mdl	<mdl	<mdl
Sn	0.0435	<mdl	0.0295	<mdl	<mdl
Total	–	98.83	100	99.64	99.18
Zn/Cd	–	339	1086	565	230
Point #	–	2	3	4	5
X (mm)	–	24.8621	25.7099	25.7306	24.2114
Y (mm)	–	7.4905	6.64	6.2728	5.3143
Date §	–	Oct. 14	Oct. 14	Oct. 14	Oct. 14
Time	–	02:47:08PM	03:00:19PM	03:25:55PM	03:37:22PM
Sample #		08-SHM-CAR-9	08-SHM-CAR-9	08-SHM-CAR-9	08-SHM-CAR-9
Source		Zn Concentrate	Zn Concentrate	Zn Concentrate	Zn Concentrate
Date *		Aug. 14	Aug. 14	Aug. 14	Aug. 14
S (%)	–	33.36	33.18	33.82	33.08
Mn	–	0.0409	0.0353	0.0206	0.055
Fe	–	5.72	3.07	6.52	3.48
Co	–	0.0096	<mdl	<mdl	0.0012
Cu	–	0.0038	0.0369	0.0556	0.1481
Zn	–	60.79	64.02	59.65	63.4
As	–	<mdl	<mdl	<mdl	<mdl
Se	–	0.0089	0.0015	0.002	0.012
Cd	–	0.1679	0.1466	0.1477	0.1937
In	–	<mdl	<mdl	<mdl	<mdl
Sn	–	<mdl	<mdl	<mdl	<mdl
Total	–	100.1	100.49	100.22	100.37
Zn/Cd	–	362	437	404	327
Point #	–	6	7	8	9
X (mm)	–	38.6046	37.9424	36.1691	35.2796
Y (mm)	–	28.4365	28.5698	28.4823	31.01
Date §	–	Oct. 14	Oct. 14	Oct. 14	Oct. 14
Time	–	03:49:07PM	04:00:25PM	04:29:16PM	04:40:40PM

Sample #		08-SHM-CAR-14	08-SHM-CAR-14	08-SHM-CAR-14	08-SHM-CAR-14
Source		Zn Concentrate	Zn Concentrate	Zn Concentrate	Zn Concentrate
Date *		Aug. 15	Aug. 15	Aug. 15	Aug. 15
S (%)	–	33.15	33.22	33.19	33.33
Mn	–	0.0487	0.0485	0.0277	0.0435
Fe	–	6.71	3.58	3.95	3.6
Co	–	0.0068	0.0098	<mdl	0.0143
Cu	–	0.0418	0.0182	0.0194	0.0424
Zn	–	59.07	63.62	62.82	62.48
As	–	<mdl	<mdl	<mdl	<mdl
Se	–	0.0074	<mdl	<mdl	<mdl
Cd	–	0.1715	0.1816	0.2049	0.1656
In	–	<mdl	<mdl	<mdl	<mdl
Sn	–	<mdl	<mdl	0.3898	<mdl
Total	–	99.21	100.68	100.6	99.68
Zn/Cd	–	344	350	307	377
Point #	–	10	11	12	13
X (mm)	–	33.4891	28.7924	29.8624	28.3624
Y (mm)	–	59.377	60.0678	63.219	64.7565
Date §	–	Oct. 14	Oct. 14	Oct. 14	Oct. 14
Time	–	04:52:23PM	05:06:53PM	05:19:52PM	05:31:42PM
Sample #		97-SHM-62-55	97-SHM-62-55	97-SHM-62-55	97-SHM-62-55
Source		Massive	Massive Sulphides	Massive	Massive
Section #		206	206	152	152
S (%)	–	33.16	33.07	33.33	33.23
Mn	–	<mdl	0.0109	0.0154	0.0148
Fe	–	4.31	4.41	7.05	6.87
Co	–	0.0085	<mdl	0.023	0.0077
Cu	–	0.6173	1.54	0.0657	0.0267
Zn	–	61.34	60.16	59.36	59.31
As	–	<mdl	<mdl	<mdl	<mdl
Se	–	0.014	0.0021	<mdl	0.0015
Cd	–	0.1314	0.2106	0.1539	0.187
In	–	<mdl	<mdl	<mdl	<mdl
Sn	–	<mdl	<mdl	<mdl	<mdl
Total	–	99.59	99.41	100	99.66
Zn/Cd	–	467	286	386	317
Point #	–	14	15	16	17
X (mm)	–	18.3521	22.2676	24.0646	13.6871
Y (mm)	–	10.736	10.7148	31.667	39.7523
Date §	–	Oct. 15	Oct. 15	Oct. 15	Oct. 15
Time	–	10:26:22AM	10:38:21AM	10:52:38AM	11:06:06AM

COPPER–COBALT–GOLD MINERALIZATION IN THE RAMSAY BROOK AREA, TOBIQUE–CHALEURS ZONE, NORTHERN NEW BRUNSWICK: A POSSIBLE IRON-OXIDE–COPPER–GOLD (IOCG) SYSTEM

JAMES A. WALKER [1] AND DOUGLAS CLARK [2]

[1] Geological Surveys Branch, New Brunswick Department of Natural Resources, P.O. Box 50, Bathurst, New Brunswick, CANADA E2A 3Z1 *(jim.walker@gnb.ca)*

[2] Consulting Geologist, 1010 Winton Crescent, Bathurst, New Brunswick, CANADA E2A 4G7

Walker, J.A., and Clark, D. 2009. Copper–cobalt–gold mineralization in the Ramsay Brook area, Tobique–Chaleurs Zone, northern New Brunswick: a possible iron-oxide–copper–gold (IOCG) system. *In* Geological Investigations in New Brunswick for 2008. *Edited by* G.L. Martin. New Brunswick Department of Natural Resources; Minerals, Policy and Planning Division, Mineral Resource Report 2009-2, p. 28–65.

In the Ramsay Brook area located approximately 75 km west-southwest of Bathurst, New Brunswick, copper–cobalt–gold mineralization appears in two prospects known as the Ramsay–Pitre and Malachite occurrences. The two occurrences, separated by a distance of 800 m, are similar in terms of their mineralization and style of alteration and may be part of the same hydrothermal system. The host rocks are red to greyish green siltstone and fine-grained sandstone of the Early Devonian Greys Gulch Formation (Tobique Group). The Greys Gulch rocks are intruded by several, typically narrow (2–≤30 m thick), fine- to medium-grained gabbroic dykes that are compositionally similar to the larger Ramsay Brook Gabbro situated about 3 km to the northeast.

Although the dykes are generally unaltered, their margins and some narrow zones within the dykes are bleached. The host sedimentary rocks are affected by a pervasive sodic–calcic metasomatism that has resulted in albitization and carbonate development extending well beyond the dykes. This alteration appears to be controlled by primary physicochemical characteristics of individual beds: some beds have concentrations of calcite porphyroblasts that account for 20% of the rock volume, whereas adjacent beds may be devoid of porphyroblasts.

Mineralization has been intersected by trenching and drilling over a strike length of 1 km and extends from surface to a depth of at least 70 m. Two types of mineralization have been recognized: 1) proximal sulphide veins and veinlets dominated by pyrite with minor chalcopyrite, cobaltite, gersdorffite, arsenopyrite and sphalerite, which are prominent in the carbonate-altered sedimentary rocks adjacent to, and locally within, the gabbroic dykes, and 2) distal disseminated blebs of chalcopyrite, cobaltite, arsenopyrite, pyrite and iron oxides restricted to the sedimentary rocks. Assay data reveal that, within the alteration zone, sedimentary rocks are elevated in Cu, Co, and Au, the highest values occurring in association with elevated concentrations of sulphide veining. The highest Cu grade reported is 3.03% over 0.5 m, and the best Co grade is 8860 ppm over 1 m. The Au content is commonly above the detection limit (5 ppb) and locally is up to 440 ppb. Values for Bi, As, and Zn are also elevated.

Although the grades and widths reported thus far from the Ramsay–Pitre and Malachite occurrences are subeconomic, assay results indicate that grades become higher toward

the northeast. Furthermore, geophysical anomalies related to the presence of gabbroic dykes intensify to the northeast. Combined, these two observations indicate the possibility of higher grade mineralization in that direction. The style of copper–cobalt–gold mineralization and alteration in the Ramsay Brook area shares many attributes of an iron-oxide–copper–gold (IOCG) system. These attributes include the Cu–Co–Au–Fe-oxide association, widespread sodic–calcic metasomatism, continental rift setting, and proximity of major faults.

Dans la région du ruisseau Ramsay, à environ 75 km à l'ouest et au sud-ouest de Bathurst, au Nouveau-Brunswick, deux minéralisations de cuivre-cobalt-or semblent présentes dans deux gîtes d'intérêt. Ce sont les minéralisations connues sous le nom de Ramsay–Pitre et Malachite. Une distance de 800 m sépare les deux minéralisations d'apparence semblable du point de vue de l'altération et de la minéralisation et il semblerait qu'elles soient issues du même complexe hydrothermal. Les roches encaissantes se composent de siltite rouge à vert-gris et de grès à grain fin de la formation Greys Gulch du Dévonien précoce (Groupe de Tobique). Les roches de la formation Greys Gulch présentent une intrusion de plusieurs dykes de gabbro généralement étroites (d'une épaisseur comprise entre 2 et plus ou moins de 30 m), à grain fin à moyen, et dont la composition s'apparente aux roches de gabbro de plus grande taille du ruisseau Ramsay, observées à environ 3 km au nord-est.

Même si les dykes ne présentent généralement pas d'altération, leurs bordures et certaines bandes étroites à l'intérieur paraissent avoir subi un lessivage. Les roches sédimentaires encaissantes ont subi un métasomatisme sodocalcique envahissant qui s'est traduit par l'albitisation et l'accumulation de carbonate dont on observe la présence au-delà des dykes. Cette altération semble avoir été déterminée par les caractéristiques physico-chimiques primaires des strates concernées : certaines strates ont des concentrations de porphyroblastes calcitiques qui composent 20 % du volume des roches, tandis que les strates adjacentes pourraient être exemptes de porphyroblastes.

La minéralisation a été interceptée par l'excavation de tranchées et des forages dans l'axe de la direction, sur une distance d'un kilomètre, et elle s'enfonce à partir de la surface jusqu'à une profondeur d'au moins 70 m. La présence de deux genres de minéralisations a été établie : 1) des filons et des filonnets de sulfures en milieu proximal, dominés par de la pyrite et de faibles quantités de chalcopyrite, de cobaltite, de gersdorffite, d'arsénopyrite et de sphalérite, ces minéraux étant surtout présents dans les roches sédimentaires ayant subi une altération de carbonate situées en bordure de dykes de gabbro, et à l'occasion dans les dykes; and 2) des inclusions diffuses situées à distance de chalcopyrite, de cobaltite, d'arsénopyrite, d'oxyde de pyrite et de fer, dont la présence se limite aux roches sédimentaires. Les données de titrage révèlent que dans la zone d'altération, les roches sédimentaires renferment une forte proportion de cuivre, de cobalt et d'or, les plus grandes teneurs étant observées dans les concentrations de filons de sulfures. La plus grande teneur de cuivre est d'une masse atomique de 3,03 % sur une distance de 0,5 m, tandis que la plus forte teneur de cobalt est de 8 860 ppm sur 1 m. La teneur en or est généralement au-dessus de la limite de détection (5 $pp10^9$), alors qu'à certains endroits, elle peut atteindre 440 $pp10^9$. Les teneurs en bismuth, en arsenic et en zinc sont également élevées.

Même si les teneurs et les largeurs signalées jusqu'ici dans les minéralisations Ramsay–Pitre et Malachite sont d'une qualité ne justifiant pas leur exploitation économique, les résultats de titrage indiquent que la teneur augmente vers le nord-est des minéralisations. En outre, les anomalies géophysiques associées à la présence de dykes de gabbro se font plus nombreuses au nord-est. Ces deux observations indiquent la possibilité d'une minéralisation de plus forte teneur dans cette direction. Le genre de minéralisation cuivre-cobalt-or et d'altération connexe dans le secteur du ruisseau Ramsay présente un grand nombre de similitudes avec un système de fer-oxyde-cuivre-or. Ces propriétés sont caractéristiques de la mise en place du rift continental, d'un métasomatisme sodocalcique à grande échelle et d'une association Cu–Co–Au–Fe-oxyde.

INTRODUCTION

The Ramsay Brook area is located approximately 75 km west-southwest of Bathurst in northern New Brunswick and is accessible by Highway 180 and a series of logging roads (Fig. 1). The area is largely underlain by Silurian–Early Devonian rocks of the Tobique–Chaleurs Zone (Fig. 1) and contains several gold ± base metal occurrences that were identified in the mid-1980s (Ruitenberg et al. 1989). Many of the occurrences are associated with iron-carbonate alteration zones adjacent to mafic intrusions that were emplaced along, or proximal to, major structural breaks such as the McCormack Brook Fault (Fig. 1).

Two such prospects are the Ramsay–Pitre occurrence (New Brunswick Department of Natural Resources (NBDNR) Unique Reference Number (URN) 1139) and the Malachite occurrence (URN 1339), both of which contain significant copper–cobalt–gold mineralization (Fig. 2). The present report documents the mineralization and style of alteration at these two occurrences. As well, it formulates a possible geological model to explain the genesis of, and possible links between, the two showings.

REGIONAL GEOLOGY

The Ramsay Brook area lies within the Tobique–Chaleurs Zone (Fig. 1, inset), the youngest of several tectonostratigraphic zones that strike north-northeast to south-southwest across northern New Brunswick. Volcanic and sedimentary rocks of the Tobique–Chaleurs Zone are interpreted to have formed in a continental-margin rift, generated by transpression during oblique accretion of the Miramichi Zone (Fig. 1, inset) onto the Laurentian margin during the Acadian Orogeny (Dostal et al. 1989; van Staal and De Roo 1995). For a description of regional stratigraphy and facies relationships in the northern part of the Tobique–Chaleurs Zone, see Walker and McCutcheon (1995) and Wilson and Kamo (2008).

A number of New Brunswick government-sponsored mapping projects (Fyffe 1971, 1974; Walker and McCutcheon 1990; Wilson 2003, 2005; Wilson and Kamo 2008) have been conducted in the Ramsay Brook area and have resulted in the delineation of two sequences of rocks: the Silurian Chaleurs Group and Early Devonian Tobique Group. The Chaleurs Group is in unconformable contact with Middle Ordovician rocks of the Miramichi Zone (Fig. 1). The Chaleurs Group in the report area consists of three formations that, in ascending stratigraphic

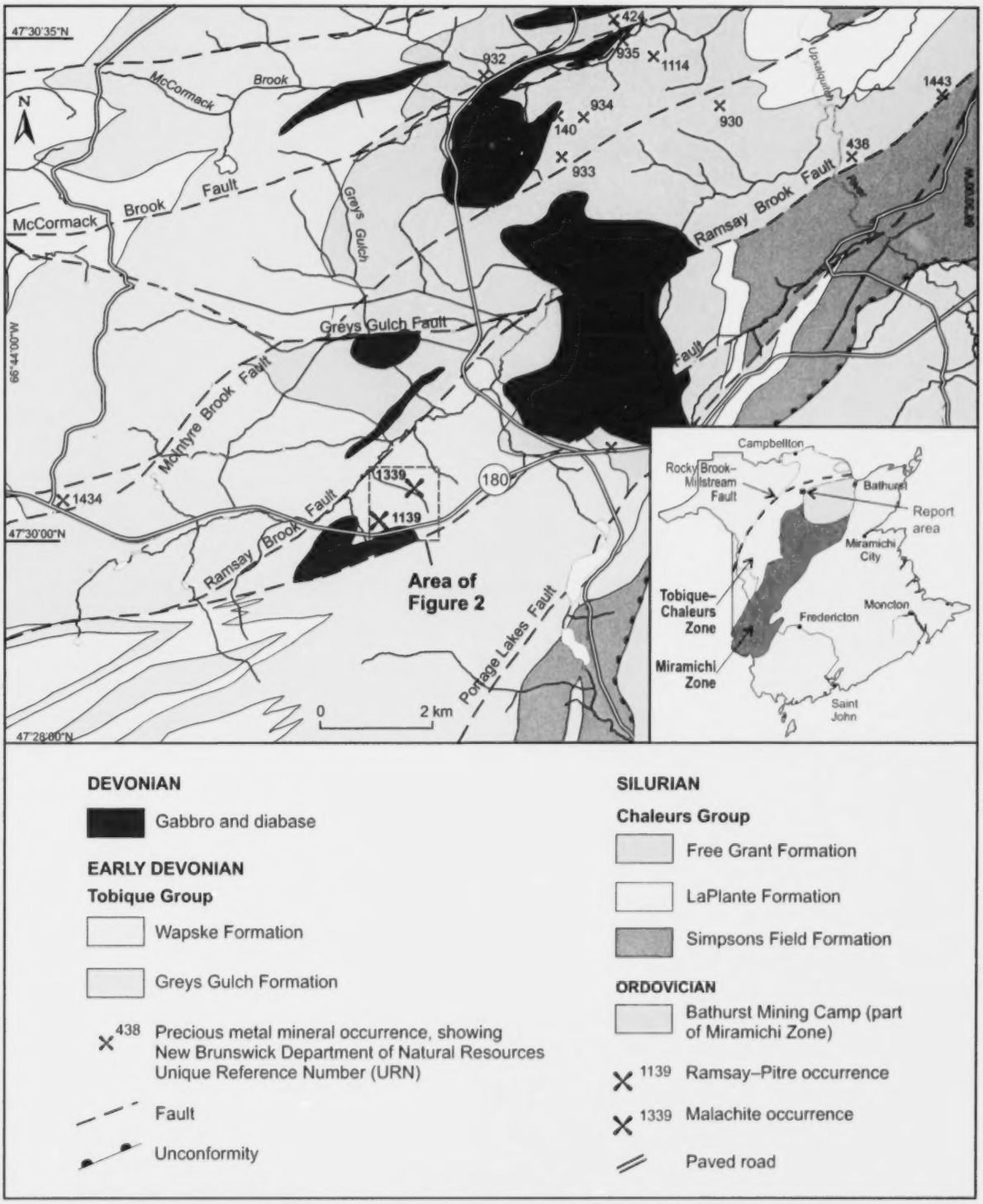

Figure 1. Simplified geology map of the Ramsay Brook area, located in the southeastern corner of the Upsalquitch Forks map area (NTS 21 O/10) and northeastern part of the Nepisiquit Lakes map area (NTS 21 O/07). Geology is modified from Wilson (2003, 2005).

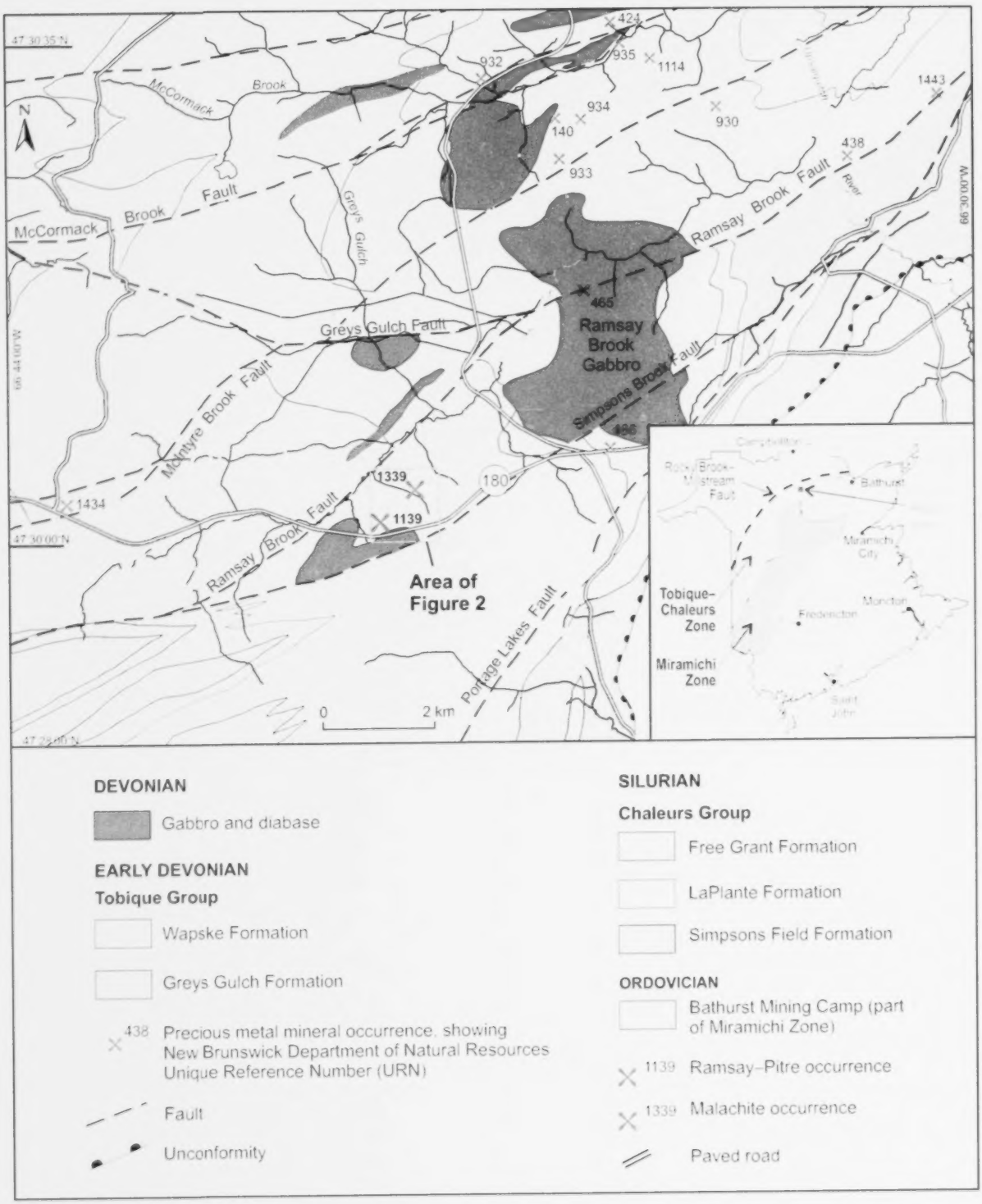

Figure 1. Simplified geology map of the Ramsay Brook area, located in the southeastern corner of the Upsalquitch Forks map area (NTS 21 O/10) and northeastern part of the Nepisiquit Lakes map area (NTS 21 O/07). Geology is modified from Wilson (2003, 2005).

order, are the Simpsons Field, LaPlante, and Free Grant formations. The Simpsons Field Formation consists mainly of thick-bedded red to grey conglomerate, coarse-grained sandstone, and minor siltstone. The LaPlante Formation comprises buff to light grey limestone and calcareous siltstone. The Free Grant Formation consists of grey, thin- to medium-bedded, fine- to medium-grained, locally calcareous quartzose sandstone and siltstone.

The Chaleurs Group is disconformably overlain by the Tobique Group that, in the report area, includes the Greys Gulch Formation and overlying Wapske Formation (Walker and McCutcheon 1995; Wilson 2003, 2005; Wilson and Kamo 2008). The Greys Gulch Formation is dominated by fine-grained, red to greyish red and greyish green, micaceous feldspathic sandstone, siltstone, and mudstone that are the host rocks to both the Malachite and Ramsay–Pitre occurrences (Fig. 2).

The Greys Gulch Formation was originally included in the upper part of the Chaleurs Group (Walker and McCutcheon 1995) but has recently been reassigned to the lower part of the Tobique Group (Wilson 2005; Wilson and Kamo 2008). Mafic and felsic volcanic rocks occur in the upper part of the Greys Gulch Formation but not in the immediate vicinity of the Ramsay–Pitre and Malachite occurrences (Fig. 1). The Wapske Formation gradationally overlies the Greys Gulch Formation to the southwest of the Ramsay–Pitre and Malachite occurrences. It consists predominantly of grey to greyish green siltstone and micaceous quartzose to locally feldspathic sandstone.

EXPLORATION HISTORY

Discovery

The Ramsay Brook area was first staked for its copper potential in 1989 by Mr. Norman Pitre of Lone Pine Exploration Services Ltd., following his discovery of chalcopyrite mineralization in rubble along an old bush road approximately 100 m to the north of Highway 180 (Pitre 1991). The name 'Ramsay–Pitre occurrence' (URN 1139, Fig. 2) refers in part to this particular site of 'discovery outcrop.' Pitre (1991) reported up to 8560 ppm Cu in samples of carbonate–silica–altered 'rhyolite' along the bush road. A limited VLF electromagnetic survey on part of the property showed that both the mineralized zone and adjacent gabbroic dykes had a positive EM response (Pitre 1992). Pitre (1992) also reported that a sample containing malachite and azurite taken along the south side of Highway 180 west of the initial discovery returned 5.77% Cu.

The next phase of exploration consisted of induced polarization and Max-Min surveys, soil sampling (copper only), and trenching. This work revealed that the mineralized zone dipped toward the south (Pitre 1993). Subsequently, a small gravity survey indicated a local anomaly toward the northeast, one that was attributed to a mafic intrusion (Pitre 1995).

The Ramsay–Pitre occurrence was restaked in 1997 by Log House Construction Ltd. under the name 'Malachite Group', following the discovery of black gossanous material on the

property by Mr. Rufus Smith (Mersereau 1998; Smith 1999a). The sampled material assayed 29% Cu but contained no visible chalcopyrite; the copper content thus was attributed to secondary oxides (Smith 2002).

In a report on prospecting and trenching conducted for Log House Construction, Mersereau (1998) noted that grab samples assayed up to 3% Cu and 2620 ppb Au. He suggested that sulphides (pyrite–pyrrhotite–arsenopyrite–chalcopyrite) and magnetite were associated with 'felsic dykes' that intruded the gabbro. Follow-up activities consisting of trenching, backpack-drilling, and soil and rock sampling were conducted on the property (Smith 1999a, 2001). The trenching uncovered narrow (<10 m), relatively unaltered, fine-grained mafic intrusions as well as orange-weathering rocks with pyrite–chalcopyrite mineralization. The highest reported assays ranged from 0.2% to 8.0% Cu (Smith 2001). Like previous authors (Pitre 1992, 1993; Mersereau 1998), Smith (2001) identified the sulphide-bearing rocks as weathered and altered 'aphyric to sparsely feldspar–phyric rhyolite flows.' However, petrographic work contracted by Phelps Dodge (and reported in Smith 1999a), and conclusions based on examination of drill core during the current study (see below), both have shown these rocks to be carbonate–albite-altered sedimentary rocks.

The association of cobalt with mineralization at the Ramsay–Pitre occurrence was recognized in 2001 when samples excavated from trenches began to form a pink-weathering crust of erytherite ($Co_3(AsO_4)_2 \cdot 8H_2O$), also known as 'cobalt bloom', on freshly exposed surfaces. The erytherite formed after approximately one year of exposure to the atmosphere. Lithogeochemical analyses of grab samples conducted by Hudson Bay Mining at the request of the property owner, Rufus Smith, corroborated the presence of cobalt in these rocks (Clark 2002). Smith (2002) reported additional assay results that returned copper grades similar to those previously reported, as well as high Cu/S values and cobalt values up to 5925 ppm.

Montoro Resources Inc. subsequently optioned the Ramsay–Pitre property, conducting soil geochemistry, magnetic and VLF surveys, trenching (Clark 2002), and two phases of diamond drilling (Clark 2004, 2005). The first drilling phase consisted of four holes totalling 446.5 m, three of which (M04-01, -02, and -03) were drilled in the area of early trenching located about 350 m north of the original Ramsay–Pitre discovery outcrop (Clark 2004). These three drillholes, together with the pre-2002 activities described above, are included as part of the Ramsay–Pitre occurrence and its record of work (URN 1139; Fig. 2).

The second drilling phase conducted by Montoro Resources consisted of five holes totalling 677 m (Clark 2005). A total of five drillholes—four from the second drilling phase (M04-05, -06, -07, and -09) and one from the first drilling phase (M04-04)—were drilled about 500 m north of the first Ramsay–Pitre drilling site. These five holes intersected mineralization that is referred to as the 'Malachite occurrence' (URN 1339; Fig. 2). The drill cores acquired during the two Montoro Resources drill programs are stored at the New Brunswick Department of Natural Resources core storage facility in Madran. These cores are the source of all sampled material on which the current study is based.

GEOLOGY OF THE RAMSAY–PITRE AND MALACHITE OCCURRENCES

Introduction

Outcrop at the Ramsay–Pitre and Malachite occurrences is all but absent. The rock type descriptions presented below are based primarily on observations made of drill core and of exposures revealed during trenching. Likewise, the spatial relationships among the gabbroic dykes and host sedimentary rocks (Fig. 2) are interpreted on the basis of correlations drawn using data from drill-core logs and trenched contacts.

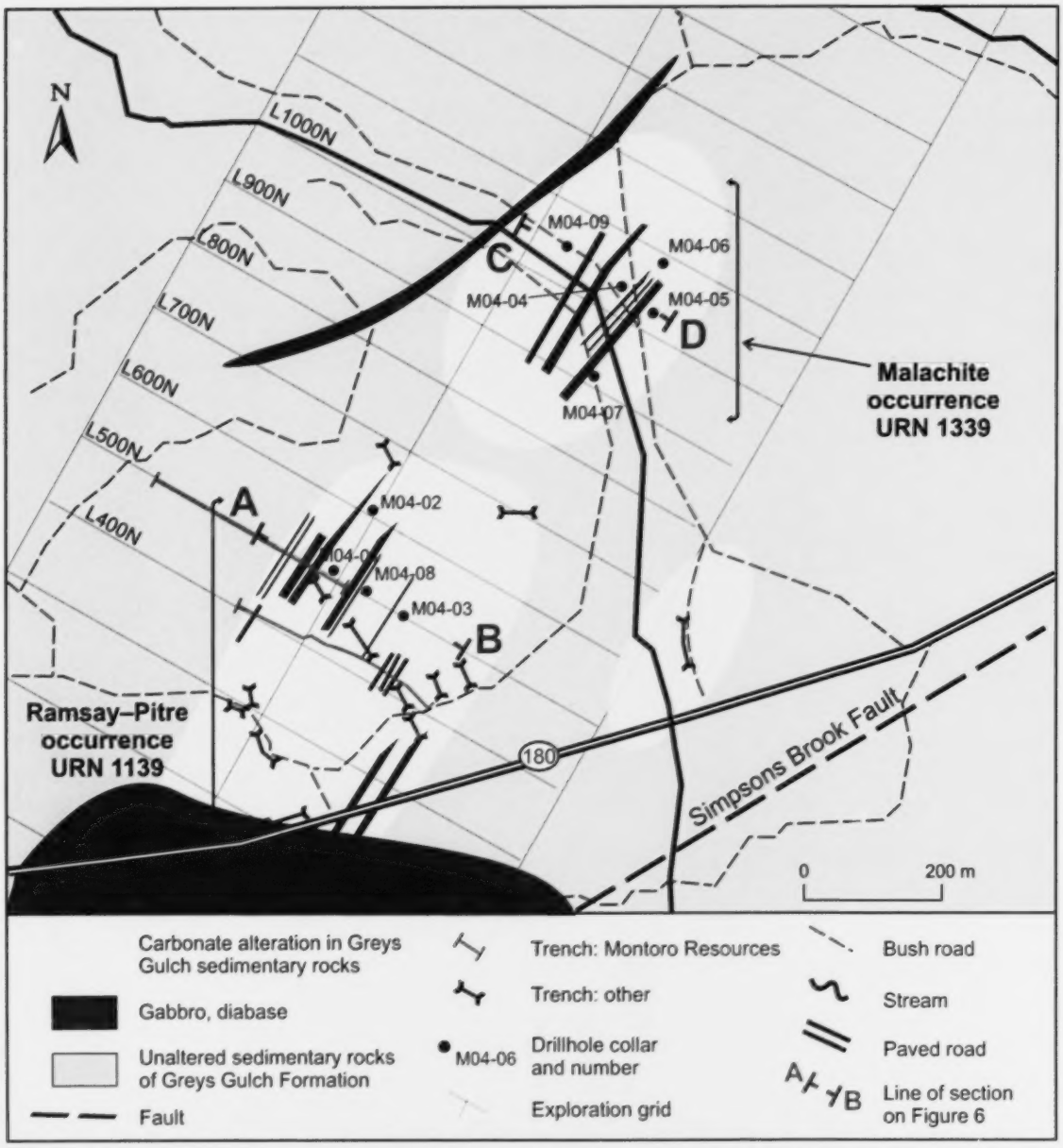

Figure 2. Geology of Ramsay–Pitre and Malachite occurrences, northern New Brunswick, compiled and modified from Wilson (2003, 2005) and Clark (2004, 2005). Figure 1 shows area of Figure 2.

Sedimentary Rocks

All sedimentary rocks in the vicinity of the Ramsay–Pitre and Malachite occurrences (Fig. 2) are assigned to the Greys Gulch Formation. Although they are not exposed at surface, they have been uncovered by trenching and are intersected in all of the exploration drillholes (Clark 2004, 2005) over a strike length that exceeds 1 km (Fig. 2).

In the drill cores examined, the sedimentary rocks consist of siltstone and fine-grained sandstone that are dominantly orange or greyish orange, but that are red in less altered sections (Fig. 3a). They are very thin- to thin-bedded; bed thickness averages 1 cm to 5 cm, with some beds reaching up to 10 cm (Fig. 3a, 3b, 4a, 4b). The sandstone consists of subrounded to well-rounded quartz with subordinate feldspar and rock fragments.

In most respects, these rocks are similar to others in the Greys Gulch Formation. However, Greys Gulch rocks are more typically greyish green to greyish red instead of orange. As well, sedimentary rocks of the Ramsay–Pitre and Malachite occurrences are quite calcareous: almost all of the cores effervesce with hydrochloric acid. The carbonate content is so high that primary layering is commonly obscured. Petrographic examination shows carbonate minerals (calcite and minor siderite) as irregular anastamosing layer-parallel masses and porphyroblastic growths at both occurrences. Although carbonate alteration affects all sedimentary rocks proximal to the dykes and mineralization (Fig. 3a, 3b, 4a), it is better developed in coarser grained beds in distal parts of the alteration zone (Fig. 4b). This tendency likely reflects the higher permeability of sandstones relative to siltstones. Although the anhedral to euhedral calcite porphyroblasts are better developed in some beds than in others, they do not appear to have a preferred orientation. This suggests they grew after the last tectonic deformation—that is, in the absence of an asymmetrical stress field. Some porphyroblasts have a thin, distinct rim of calcite with a slightly different extinction angle, implying at least two generations of carbonate growth (Fig. 4b).

Many thin sections of Greys Gulch rocks from other areas show some carbonate, but in none of them does the carbonate content come close to the amount seen in rocks of the Ramsay–Pitre and Malachite occurrences. Furthermore, calcite porphyroblasts are not evident in thin sections from outside the mineralized zone in the Ramsay Brook area. These observations suggest that most of the carbonate in these rocks, in particular the porphyroblastic calcite, was introduced after lithification.

Mafic Intrusions

The largest of the several mafic intrusions in the Ramsay Brook area is the Ramsay Brook Gabbro, which lies approximately 2.5 km northeast of the Malachite occurrence (Fig. 1). Hornblende from the Ramsay Brook Gabbro yields a Late Devonian $^{40}Ar/^{39}Ar$ age of 374 ± 6 Ma (Murphy 1989). Other, smaller (<2 km in the long direction) mafic plutons tend to occur in proximity to faults and commonly have spatially associated iron-carbonate alteration ± gold mineralization (Fig. 1).

Figure 3a. Sedimentary rocks of the Greys Gulch Formation, showing altered orange and greyish orange siltstone interlayered with relatively unaltered red siltstone. Core is from drillhole M04-01 (125–128 m) at the Ramsay–Pitre occurrence. Core diameter is ~4.7 cm.

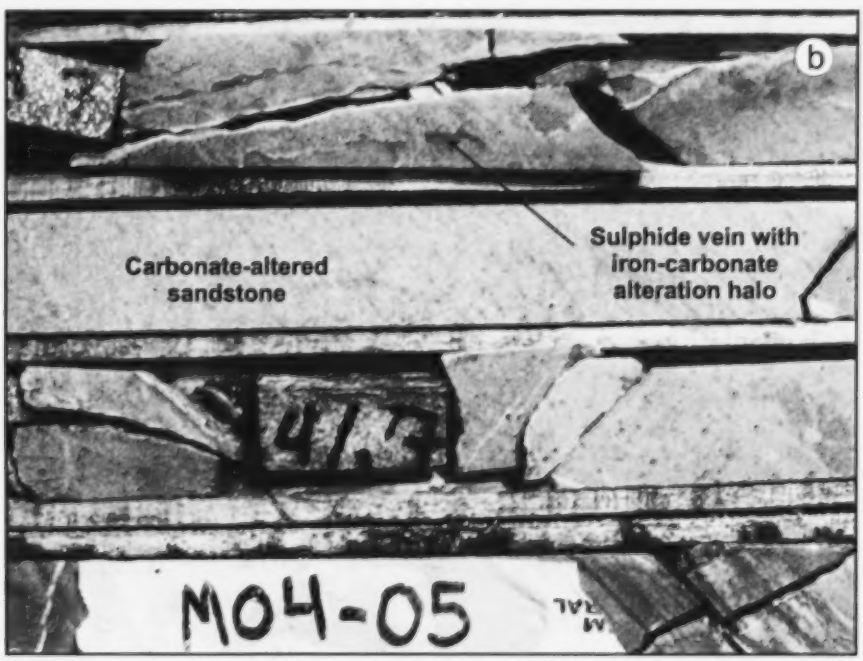

Figure 3b. Sedimentary rocks of the Greys Gulch Formation, showing orange carbonate-altered sandstone with a blotchy appearance that is due to porphyroblastic growth. Core is from drillhole M04-05 (41.7 m) at the Malachite occurrence. Note the sulphide vein (grey), intense carbonate alteration, and fine lamination in bottom right of photograph. Core diameter is ~4.7 cm.

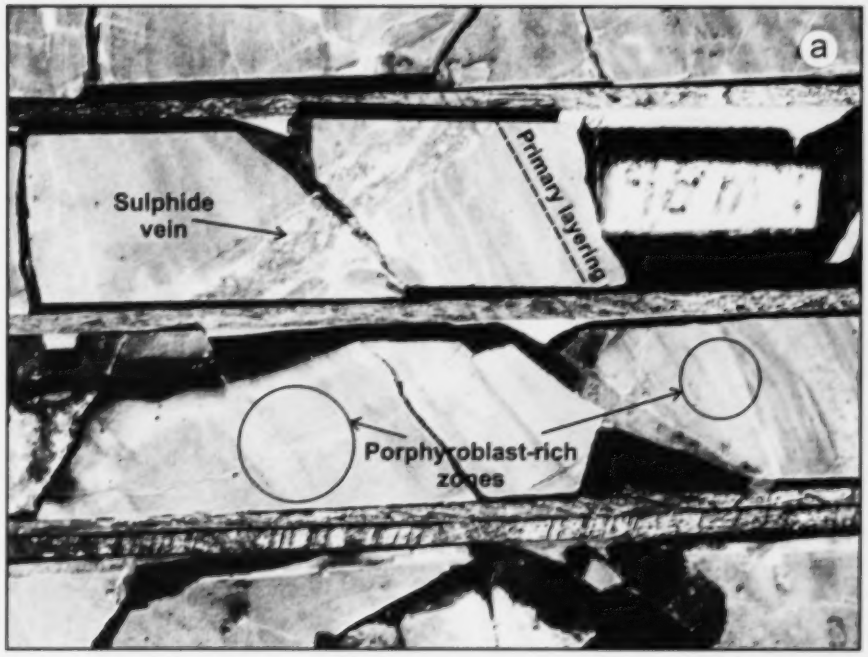

Figure 4a. Sedimentary rocks of the Greys Gulch Formation, showing thin-bedded, carbonate-altered siltstone with zones of carbonate porphyroblasts. Core is from drillhole M04-05 at the Malachite occurrence. A sulphide vein that cuts bedding at a high angle also apparently cross-cuts carbonate alteration at this location (48 m). Core diameter is ~4.7 cm.

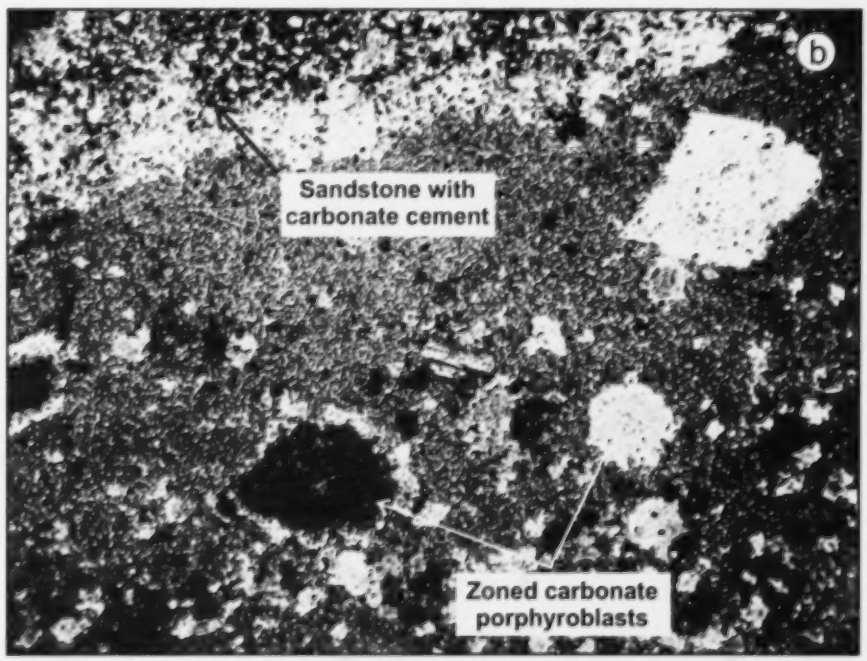

Figure 4b. Photomicrograph of carbonate-altered sedimentary rocks in core from drillhole M04-01 (79.4 m) at the Ramsay–Pitre occurrence. Image shows subhedral to anhedral porphyroblasts developed in siltstone bed, and irregular carbonate in fine-grained sandstone bed (upper left). Field of view is ~5 mm. Photographed under crossed polarizers.

Most exploration holes drilled at the Ramsay–Pitre and Malachite occurrences intersected gabbroic dykes cutting sedimentary rocks of the Greys Gulch Formation (Fig. 2, 5a–5c, 6a, 6b). Drilling results suggest that the dykes are subvertical and varied in width, with drill intersections ranging between 2 m and 30 m. At the macroscale, the dykes seem to be generally unaltered (Fig. 5a). However, they locally are cut by narrow bleached zones that rarely exceed 1 m wide and that commonly coincide with carbonate veining (Fig. 5b).

In thin section, the gabbro from the bleached zones is affected by pervasive carbonate alteration, and the plagioclase crystals are variously saussuritized (Fig. 5c). Sulphide veinlets, which rarely exceed 1 cm in width, also locally coincide with the bleached zones. In contrast with the narrow bleached zones within the gabbroic dykes, dyke margins commonly have well-developed carbonate alteration zones that are up to 2 m wide and contain locally abundant sulphide veins. Individually, these sulphide veins may exceed 5 cm in thickness. Detailed descriptions of the sulphide veins and altered zones appear below under ***Mineralization*** and ***Alteration***.

LITHOGEOCHEMISTRY

Lithogeochemical data presented in this report were obtained from two sources.

1. The larger dataset comprises 508 samples (425 sedimentary rocks and 83 gabbroic rocks) collected from core during the Montoro Resources exploration program and analyzed at SGS Mineral Services in Lakefield, Ontario. The analyses, documented in Clark (2004, 2005), were conducted for 1) multi-elements using inductively coupled plasma–mass spectrometry (ICP–MS), and 2) gold by fire assay (FA).

2. The smaller dataset consists of eight core samples collected specifically for the present study to obtain a complete set of major oxides and to better document the extent of hydrothermal alteration. These core samples comprise the following material.

   - Three core samples were taken at the Ramsay–Pitre occurrence from drillhole M04-01 at depths 79.4, 80.9, and 97.9 m. The samples are numbered M04-01-79.4 (siltstone), M04-01-80.9 (siltstone), and M04-01-97.9 (siltstone).

   - Five core samples were taken at the Malachite occurrence from drillhole M04-05 at depths 20.5, 20.6, 28.0, 76.0, and 176.6 m. The samples are numbered M0-05-20.5 (gabbro), M0-05-20.6 (gabbro), M0-05-28.0 (gabbro), M0-05-76.0 (siltstone), and M0-05-176.6 (siltstone).

Analyses for this smaller dataset were conducted at Activation Laboratories Ltd. in Ancaster, Ontario, and are summarized in Table 1.

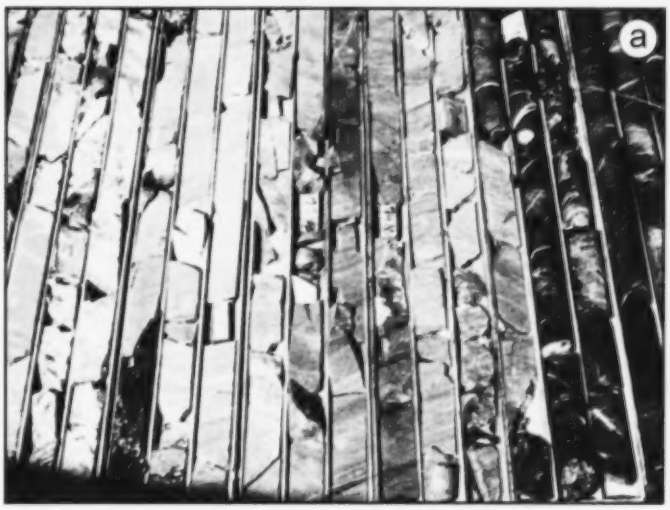

Figure 5a. Relatively unaltered gabbroic dyke with minor bleaching (on right), and orange, carbonate-altered sedimentary rocks of the Greys Gulch Formation (on left). Core is from drillhole M04-01 (65–94 m) at the Ramsay–Pitre occurrence; top of hole is to the right. Core diameter is ~4.7 cm.

Figure 5b. Variously altered gabbroic dyke, showing unaltered gabbro cut by zones of orange carbonate alteration. Core is from drillhole M04-05 (122 m) at the Malachite occurrence. Note that later calcite veins (white) are both conformable with, and cross-cut, the earlier alteration. Core diameter is ~4.7 cm.

Figure 5c. Photomicrograph of altered gabbro, showing sausseritized plagioclase in core from drillhole M04-01 (62.8 m) at the Ramsay–Pitre occurrence. Field of view is ~2.5 mm. Photographed under crossed polarizers.

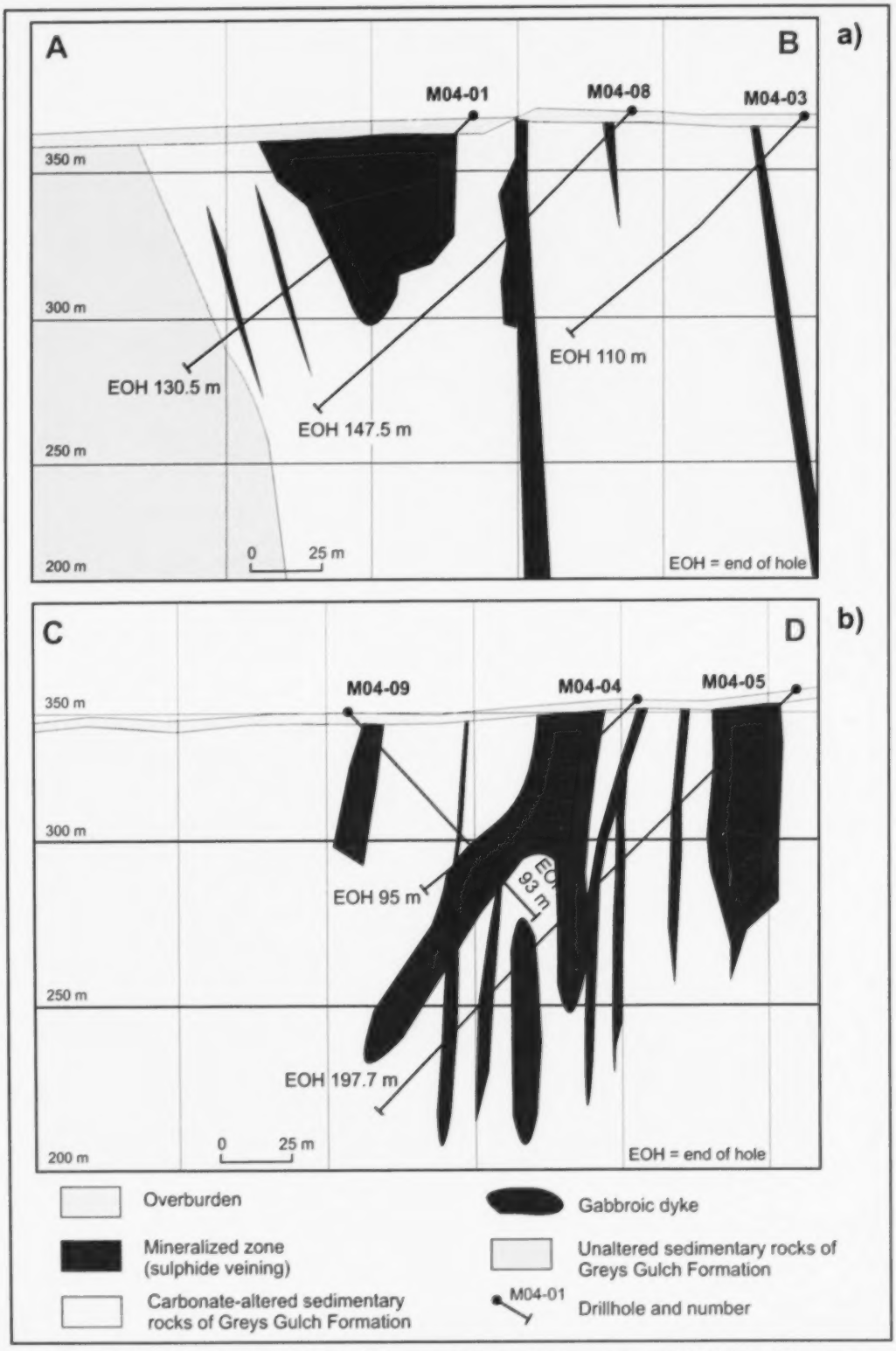

Figure 6. Geological cross-sections of a) Ramsay–Pitre occurrence, and b) Malachite occurrence. Both sections are modified from Clark (2005). Figure 2 shows location of section lines A–B and C–D.

Table 1. Lithogeochemical data for Ramsay–Pitre and Malachite occurrences, obtained for the present study.

Symbol	Unit Symbol	Detection Limit	Analysis Method	M04-05-20.6	M04-05-20.5	M04-05-28.0	M04-01-79.4	M04-01-80.9	M04-01-97.9	M04-05-76.0	M04-05-176.6
				Gabbro	Gabbro	Gabbro	Siltstone	Siltstone	Siltstone	Siltstone	Siltstone
SiO_2	%	0.01	FUS-ICP	41.39	45.73	45.57	60.94	61.66	55.29	57.59	60.82
Al_2O_3	%	0.01	FUS-ICP	8.68	17.05	16.82	15.21	14.7	12.47	13.36	14.34
Fe_2O_3(t)	%	0.01	FUS-ICP	23.49	8.87	8.61	1.8	1.82	3.54	3.85	2.2
MnO	%	0.001	FUS-ICP	0.081	0.054	0.033	0.045	0.051	0.112	0.068	0.061
MgO	%	0.01	FUS-ICP	1.68	7.6	7.9	2.13	2.25	2.97	2.49	2.13
CaO	%	0.01	FUS-ICP	3.82	9.31	8.7	4.29	4.34	7.27	5.37	4.53
Na_2O	%	0.01	FUS-ICP	4.36	2.58	2.83	8.21	7.52	6.82	7.07	8
K_2O	%	0.01	FUS-ICP	0.21	2.28	1.48	0.32	0.44	0.15	0.33	0.17
TiO_2	%	0.001	FUS-ICP	0.498	1.224	1.259	0.84	0.855	0.676	0.743	0.801
P_2O_5	%	0.01	FUS-ICP	0.1	0.1	0.11	0.16	0.16	0.14	0.13	0.15
LOI	%		FUS-ICP	16.38	4.27	6.81	6.3	6.43	10.09	8.05	6.39
Total	%	0.01	FUS-ICP	100.7	99.06	100.1	100.3	100.2	99.53	99.05	99.59
Au	ppb	1	INAA	<1	<1	<1	<1	2	<1	<1	3
Ag	ppm	0.5	INAA/TD-ICP	1.7	<0.5	<0.5	<0.5	<0.5	<0.5	<0.5	<0.5
As	ppm	1	INAA	293	2	3	24	11	8	218	15
Ba	ppm	1	FUS-ICP	13	109	79	13	16	24	21	9
Be	ppm	1	FUS-ICP	2	1	1	2	2	2	2	1
Bi	ppm	0.1	FUS-MS	708	3.8	2.7	2.2	0.9	1.2	16	2.8
Br	ppm	0.5	INAA	<0.5	<0.5	<0.5	<0.5	<0.5	<0.5	<0.5	<0.5
Cd	ppm	0.5	TD-ICP	4.3	0.9	0.8	<0.5	<0.5	0.5	<0.5	<0.5
Co	ppm	0.1	INAA	243	38	30	2	1	2	26	7
Cr	ppm	0.5	INAA	61	219	235	106	103	74	92	84
Cs	ppm	0.1	FUS-MS	0.1	10.7	8	0.1	0.2	<0.1	0.1	<0.1
Cu	ppm	1	TD-ICP	1370	35	3	4	6	18	14	9
Ga	ppm	1	FUS-MS	14	17	18	26	20	21	18	18
Ge	ppm	0.5	FUS-MS	1.4	1.5	2	1.8	1.9	1.6	1.4	1.4
Hf	ppm	0.1	FUS-MS	3.6	2.1	2.2	5.6	5.4	4.7	6	5.3
Hg	ppm	1	INAA	<1	<1	<1	<1	<1	<1	<1	<1
Mo	ppm	2	FUS-MS	3	<2	<2	22	<2	<2	<2	<2
Nb	ppm	0.2	FUS-MS	7.8	3.3	5.5	13.4	13.5	10.2	11.7	12.7
Ni	ppm	1	TD-ICP	1140	56	60	34	23	194	164	23
Pb	ppm	5	TD-ICP	195	<5	<5	<5	<5	<5	<5	<5
Rb	ppm	2	FUS-MS	7	165	88	11	15	3	9	3
S	%	0.001	TD-ICP	17.6	0.047	0.077	0.01	0.009	0.049	1.15	0.162
Sb	ppm	0.1	INAA	19.4	1.4	1.4	1.8	2	3.7	3.3	1
Sc	ppm	0.01	INAA	9.3	31.4	35.6	14.8	14.5	11.4	10.7	11.2
Se	ppm	0.5	INAA	<0.5	<0.5	<0.5	<0.5	<0.5	<0.5	<0.5	<0.5
Sn	ppm	1	FUS-MS	4	<1	2	3	4	5	3	3
Sr	ppm	2	FUS-ICP	85	329	278	116	130	152	105	81
Ta	ppm	0.1	FUS-MS	0.6	0.2	0.2	1	1	0.8	0.9	0.9
Th	ppm	0.05	FUS-MS	5.77	0.85	0.86	10	10.1	7.29	8.02	10.6
U	ppm	0.05	FUS-MS	2.42	0.27	0.33	4.22	4.93	2.35	2.36	3.61
V	ppm	5	FUS-ICP	170	230	250	108	131	124	83	75
W	ppm	1	INAA	<1	<1	<1	<1	<1	<1	<1	<1
Y	ppm	1	FUS-ICP	20	21	24	35	30	26	15	35
Zn	ppm	1	INAA/TD-ICP	649	14	11	5	5	14	4	4
Zr	ppm	1	FUS-MS	139	80	81	219	209	187	246	212
La	ppm	0.05	FUS-MS	7.46	4.71	5.84	21.4	24.9	12.8	6.37	46.8
Ce	ppm	0.1	FUS-MS	23.4	13.4	15.3	70	78.8	40.6	20.3	93.3
Pr	ppm	0.02	FUS-MS	3.45	2	2.23	9.64	10.5	5.69	3.07	11
Nd	ppm	0.05	FUS-MS	13.1	9.08	10.5	33.2	35.5	20.9	11.3	35.6
Sm	ppm	0.01	FUS-MS	3.36	2.59	3.01	6.91	7.1	4.91	2.71	6.86
Eu	ppm	0.005	FUS-MS	0.861	1.13	1.36	1.73	2.13	1.33	0.931	2.4
Gd	ppm	0.02	FUS-MS	3.49	3.17	3.7	6.24	6.17	4.54	2.68	6.1
Tb	ppm	0.01	FUS-MS	0.67	0.63	0.73	1.11	1.04	0.84	0.5	1.13
Dy	ppm	0.02	FUS-MS	4.23	4.09	4.77	6.77	6.04	5.27	3.11	6.96
Ho	ppm	0.01	FUS-MS	0.85	0.79	0.93	1.29	1.12	1.02	0.62	1.31
Er	ppm	0.01	FUS-MS	2.55	2.3	2.66	3.64	3.2	3	1.81	3.65
Tl	ppm	0.05	FUS-MS	<0.05	0.47	0.23	0.05	<0.05	<0.05	0.06	<0.05
Tm	ppm	0.005	FUS-MS	0.388	0.342	0.395	0.535	0.464	0.449	0.277	0.523
Yb	ppm	0.01	FUS-MS	2.65	2.12	2.47	3.34	2.97	2.99	1.79	3.21
Lu	ppm	0.002	FUS-MS	0.426	0.297	0.346	0.482	0.455	0.449	0.273	0.438

Notes: **FUS–MS** = lithium metaborate/tetraborate fusion–mass spectrometry. **FUS–ICP** = fused disk–inductively coupled plasma. **INAA** = instrumental neutron activation. **TD–ICP** = total digestion–inductively coupled plasma mass spectrometry.

Sedimentary Rocks

Lithogeochemical characteristics of the sedimentary rocks sampled and analyzed as part of this investigation (Table 1) are, for the most part, typical of clastic sedimentary rocks. Analytical values that lie within the normal range include those for SiO_2 (55–62%) and for trace and minor elements such as Cr (74–106 ppm), Ni (23–194 ppm), Ti (4050–5135 ppm), and Mn (348–867 ppm). However, the rocks are atypical in regard to the more mobile alkali elements: Na_2O contents are high (6.8–8.2%), K_2O contents are very low (0.15–0.44%), and CaO contents, although varied, are commonly elevated (4.3–7.3%).

Contents of Ca and Mn for the sedimentary samples (n = 425) reported in Clark (2004, 2005) range from 0.26% to 8.12% and from 12 ppm to 1540 ppm, respectively. These numbers show a strong correlation between Ca and Mn, such that the Pearson correlation coefficient is 0.787. This correlation is likely a function of Mn incorporation into the calcite and/or the development of minor amounts of rhodochrosite or siderite. The significance of these atypical alkali-element contents is discussed below under ***Alteration***.

Gabbro

Two drillhole samples (M04-05-20.5 and -28) of generally unaltered (hereafter referred to as unaltered) gabbro and one sample (M04-05-20.6) of altered and mineralized gabbro were analyzed during the present investigation (Table 1). For comparison, analyses of rock from the Ramsay Brook Gabbro, from near the Ramsay–Pitre and Malachite occurrences, and from similar dykes situated about 4 km west of the Malachite occurrence were compiled from Murphy (1989) and are included on the lithogeochemical discrimination diagrams (Fig. 7a–7d).

The two unaltered samples plot in the basalt field on the SiO_2 vs total alkalis diagram (Fig. 7a), whereas they fall in the monzogabbro field on the K–(Na+Ca) vs Si/3–(K+Na+2Ca/3) diagram (Fig. 7b). The close grouping of the altered and unaltered samples on these diagrams appears to reflect limited mobility of these elements during alteration of the gabbros. However, the atypically high ($CaO+Na_2O$) and low K_2O in the adjacent sedimentary rocks described above suggest that the alkali elements were somewhat mobile. This conclusion is supported by variations in the contents of immobile elements (see below).

In terms of their immobile-element chemistry (specifically their Zr:Ti and Nb:Y ratios), the unaltered gabbro samples plot in the andesite/basalt field near the boundary with the subalkaline basalt field. Conversely, the altered, mineralized samples plot toward higher Zr/TiO_2, with one sample from Murphy (1989) falling in the andesite field and sample M04-05-20.6 falling on the boundary between the andesite and rhyodacite/dacite fields (Fig. 7c).

The variation between altered (higher Zr/Ti) and unaltered (lower Zr/Ti) samples may be a function of Ti depletion due to leaching of Fe–Ti phases by oxidizing–alkaline fluids (see ***Discussion***, below). Chondrite-normalized data for the unaltered gabbro samples from this study differ from those of dykes from near the Ramsay–Pitre and Malachite occurrences

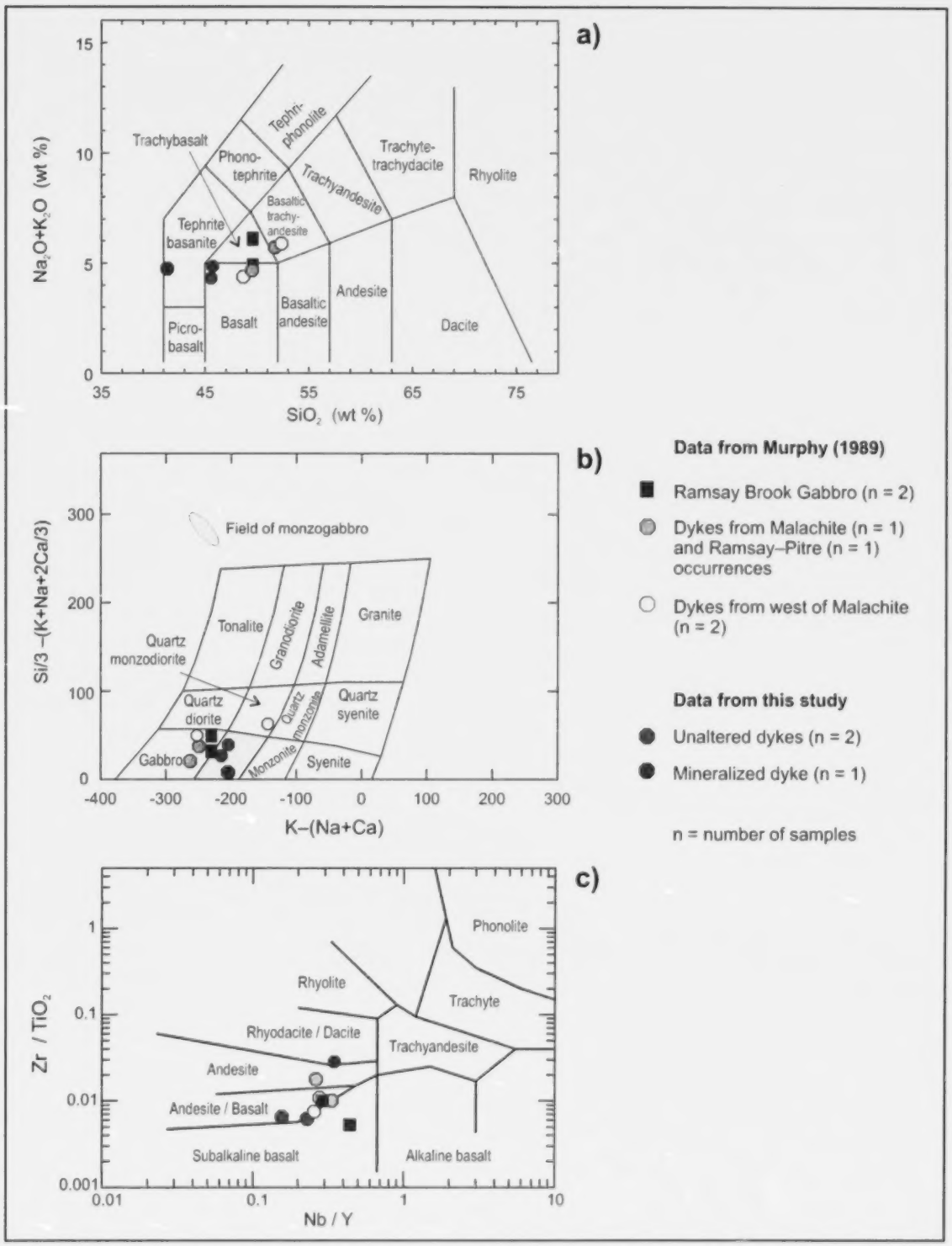

Figure 7. Discrimination diagrams comparing data from three gabbro samples analyzed for this study with additional data from Murphy (1989). See text for details. a) SiO_2 vs Na_2O+K_2O diagram, field boundaries from Le Maitre et al. (1989). b) K–(Na+Ca) vs Si/3–(K+Na+2Ca/3) diagram, after Debon and Le Fort (1983). c) Nb/Y vs Zr/TiO_2 diagram, field boundaries from Winchester and Floyd (1977).

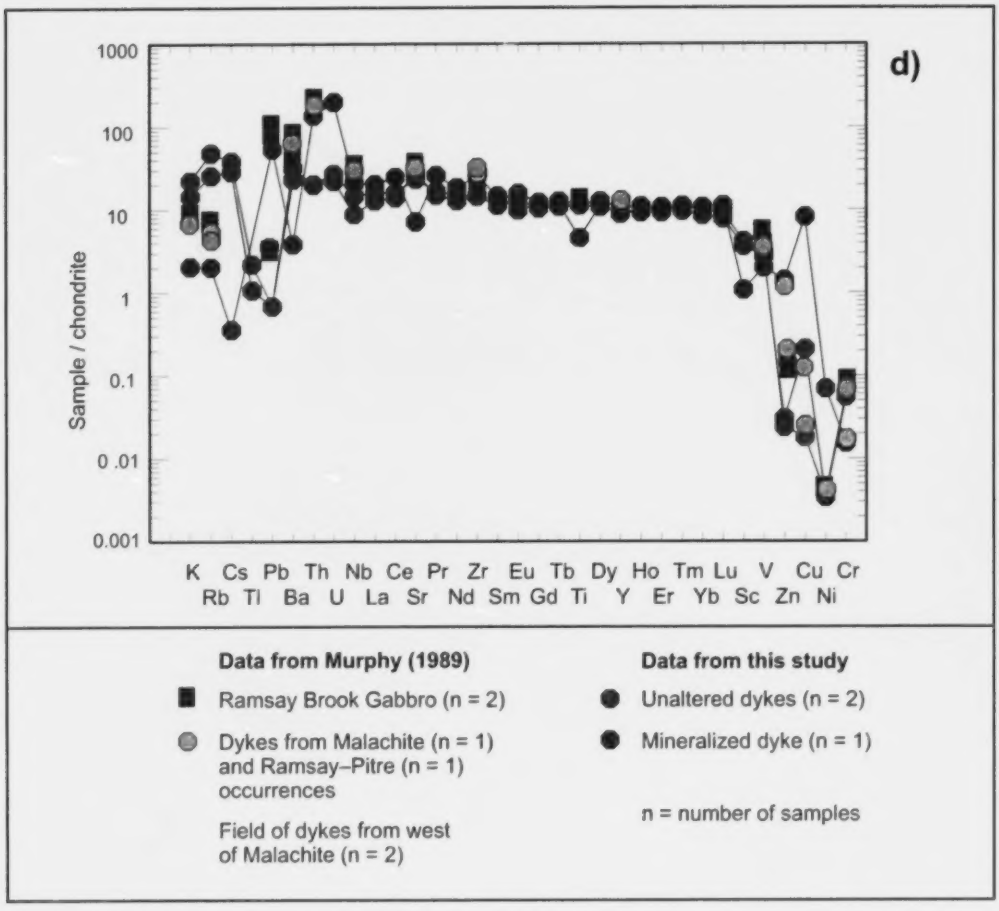
d)
1000
100
10
1
0.1
0 .01
0.001
Sample / chondrite
K Cs Pb Th Nb Ce Pr Zr Eu Tb Dy Ho Tm Lu V Cu Cr
Rb Tl Ba U La Sr Nd Sm Gd Ti Y Er Yb Sc Zn Ni
Data from Murphy (1989)
Ramsay Brook Gabbro (n = 2)
Dykes from Malachite (n = 1) and Ramsay–Pitre (n = 1) occurrences
Field of dykes from west of Malachite (n = 2)
Data from this study
Unaltered dykes (n = 2)
Mineralized dyke (n = 1)
n = number of samples

Figure 7d. Chondrite-normalized extended-element spider diagram, comparing data from three gabbro samples analyzed for this study with data from Murphy (1989); see text for details. Normalization factors are from Taylor and McLennan (1985).

analyzed by Murphy (1989). Specifically, the latter samples have lower K and Rb; slightly higher Sr and Zr; and higher Pb, Ba, Th, Cu and Zn than the former samples (Fig. 7d). The sample of altered, mineralized gabbro (M04-05-20.6) analyzed during this study is strongly depleted in K, Rb, Cs, Ba; slightly depleted in Sr, Ti and Sc; and enriched in Ni, Cu, Zn, Th and U relative to the two unaltered gabbro samples (Fig. 7d).

MINERALIZATION

The zone of mineralization and alteration at the Ramsay–Pitre and Malachite occurrences has been traced by drilling and trenching over a strike length that exceeds 1 km. The zone reaches from surface to a depth of 70 m and remains open both along strike and at depth (Fig. 2, 6a, 6b). Two types of mineralization have been recognized: Type 1 consists of massive sulphide veins that occur proximal to and within mafic dykes (Fig. 8a, 8b), and Type 2 consists of more distal disseminated sulphide and iron-oxide mineralization that occurs in surrounding sedimentary rocks (Fig. 8c).

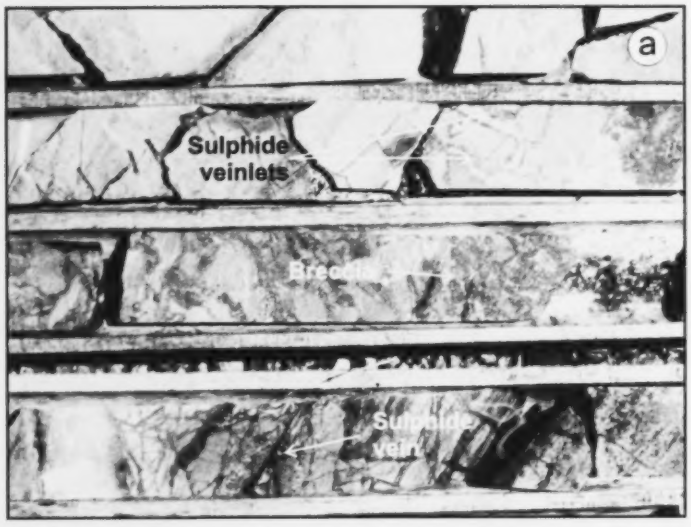

Figure 8a. Sulphide veinlets, quartz-cemented breccia (33 m), and a sulphide vein cutting carbonate-altered siltstone. Core is from drillhole M04-05 at the Malachite occurrence. Core diameter is ~4.7 cm.

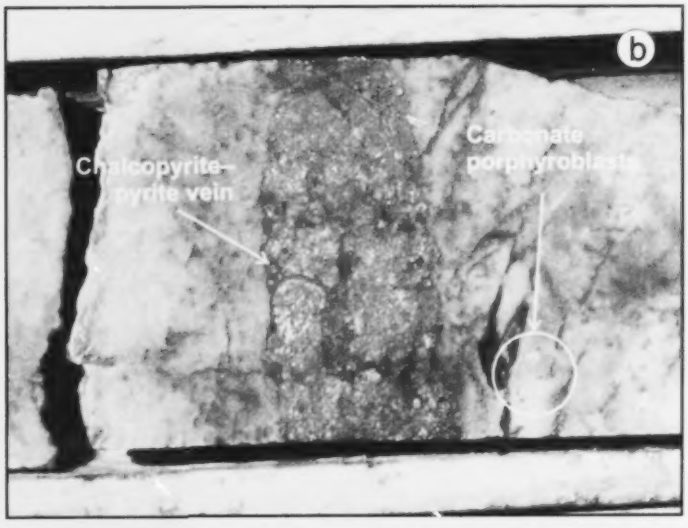

Figure 8b. Chalcopyrite–pyrite vein cutting carbonate-altered sedimentary rocks adjacent to a gabbroic dyke. Core is from drillhole M04-04 (26 m) at the Malachite occurrence. Core diameter is ~4.7 cm.

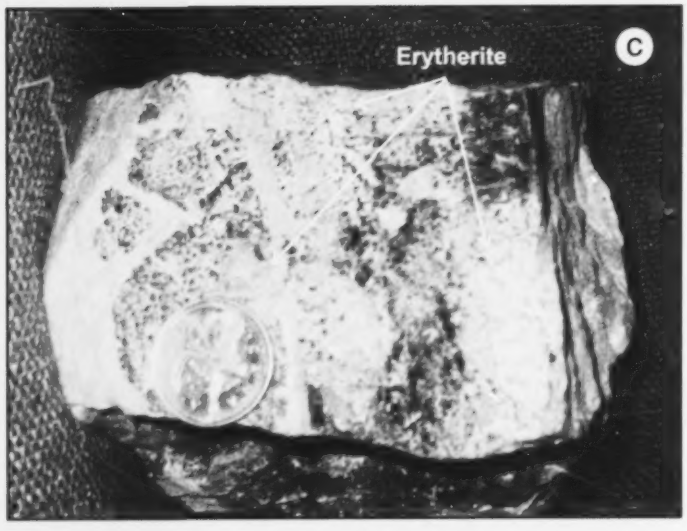

Figure 8c. Surface sample showing erytherite ($Co_3(AsO_4)_2 \cdot 8H_2O$) or 'cobalt bloom.' Sample was collected from a trench at the Ramsay–Pitre occurrence. Coin diameter is 2.4 cm.

Microprobe analyses were conducted on selected sulphide phases to address ambiguity in the optical identification of some mineral species and to help determine the paragenetic relationships and trace-element zoning. Microprobe analysis was conducted using a JEOL-733 system operating at a 15 kV accelerating voltage and a 30 nA beam current, with count times of 100 seconds.

The detection limit for most elements analyzed under these conditions is 0.08%. Photomicrographs of the probed samples appear on Figures 9a to 9c and Figures 10a to 10c; analytical results are given in Appendix 1.

Type 1 Mineralization

Vein mineralization consists of sulphide veins and veinlets that vary in width between 0.5 mm and 5 cm (Fig. 8a, 8b). These veins are best developed in sedimentary rocks immediately adjacent to the gabbroic dykes and, to a lesser extent, within the dykes. At the hand-sample scale, sulphides in these veins appear to be of one generation; however, earlier sulphide-only and later sulphide–iron-oxide–sericite veins can be distinguished under the microscope. The sulphide veins are dominated by pyrite (FeS_2); subordinate chalcopyrite ($CuFeS_2$) and cobaltite ((Co,Fe)AsS); and minor arsenopyrite (FeAsS), gersdorffite (NiAsS) and sphalerite (ZnS).

Microscopically, pyrite in sulphide-only veins can be divided into an earlier generation of large equant grains and a later generation of anhedral, spongy pyrite (Fig. 9a). In some thin sections, the earlier pyrite is overgrown by thin rims of gersdorffite (Fig. 9b). In one thin section, a sulphide–iron-oxide–sericite vein terminates an earlier sulphide-only vein (Fig. 10a). Thin rims of unidentified iron oxides mantle some chalcopyrite grains in the later veins of Type 1 mineralization (Fig. 10b). These relationships are described more fully below under ***Paragenetic Relationships***.

Type 2 Mineralization

Disseminated mineralization is more widely developed than vein mineralization. It consists of zones of irregularly shaped, fine-grained (≤1 mm diameter) disseminated sulphides and iron oxides (Fig. 9c, 11a, 11b), the latter of which mantle the chalcopyrite grains in most analyzed thin sections. Attempts to analyze these iron-oxide rims (Fig. 9c–point 30; Fig. 10b–points 28, 29; Appendix 1), were unsuccessful because they are too small (5–10 μ) to probe. Disseminated mineralization occurs throughout the zone of orange, carbonate-bearing sedimentary rocks for some distance (>30 m) from the gabbroic dykes and is cut by Type 1 vein mineralization adjacent to the dykes. Cobalt bloom (erytherite) appears in weathered surface samples of sedimentary rocks containing Type 2 mineralization (Fig. 8c).

The iron-oxide rims described above likely represent a late-stage hydrothermal overprint on earlier deposited Type 1 and Type 2 chalcopyrite, rather than a recent weathering event. This interpretation is based on two observations. First, in the thin sections examined, no other

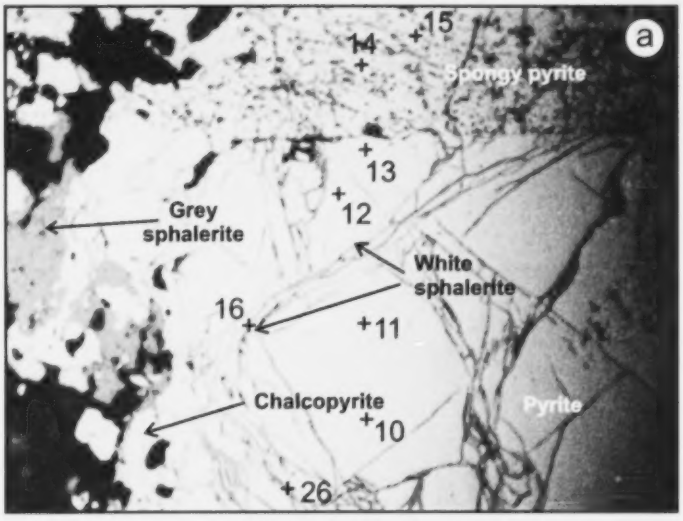

Figure 9a. Photomicrograph showing large pyrite grain with curvilinear fractures filled by white (low-iron) sphalerite (analyzed at points 16, 26, 27**) and rimmed by spongy pyrite in a matrix of grey sphalerite and chalcopyrite. Sample is from sulphide-only vein in core from drillhole M04-01 (97.9 m) at the Ramsay–Pitre occurrence.

Photographed in reflected light. Field of view is ~1.3 mm.

** *Point 27 lies in a small sphalerite grain to the lower left of point 26, just below the edge of this photograph.*

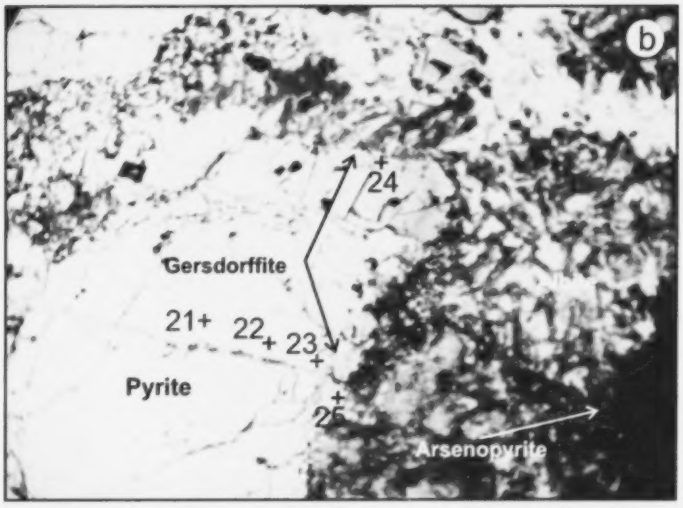

Figure 9b. Photomicrograph showing large pyrite grain with gersdorffite rim in sulphide-only vein that is hosted by albitized sedimentary rock containing minor arsenopyrite veinlet. Sample is from core of drillhole M04-05 (32.5 m) at the Malachite occurrence.

Photographed under combined plane-polarized and reflected light. Field of view is ~1.3 mm.

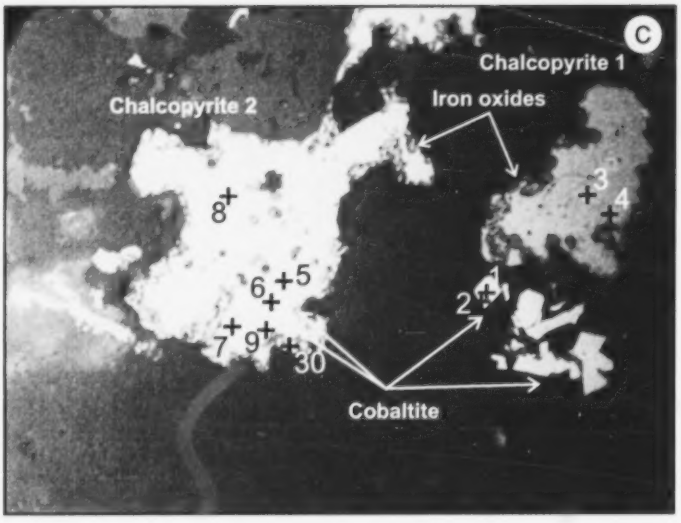

Figure 9c. Photomicrograph showing carbonate-altered siltstone containing disseminated cobaltite, and cobaltite overgrown by chalcopyrite, the latter rimmed by iron oxides. Sample is from a surface grab sample collected at the Malachite occurrence.

Photographed under reflected light. Field of view is ~0.32 mm.

Note for Figures 9a–9c: Numbered crosses mark microprobe sample points (see Appendix 1).

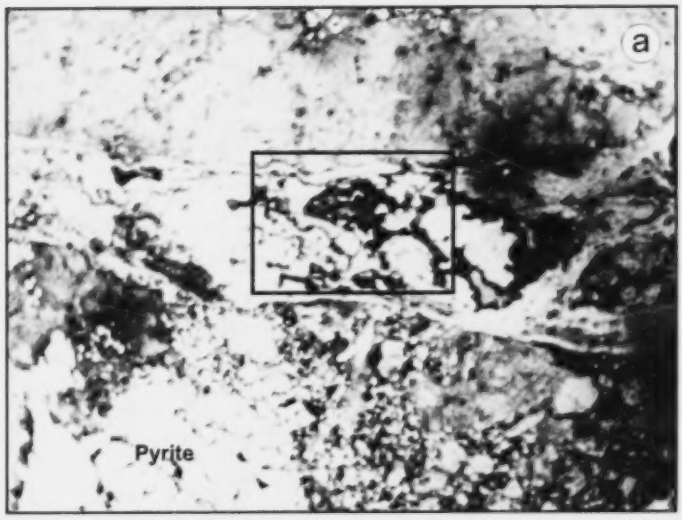

Figure 10a. Photomicrograph showing later sulphide–iron-oxide–sericite vein trending left to right. Vein cuts albitized sedimentary rocks of the Greys Gulch Formation, and earlier sulphide-only vein (pyrite). Section is from core of drillhole M04-05 (32.5 m) at the Malachite occurrence.

Photographed under combined plane-polarized light and reflected light. Field of view is ~5.4 mm.

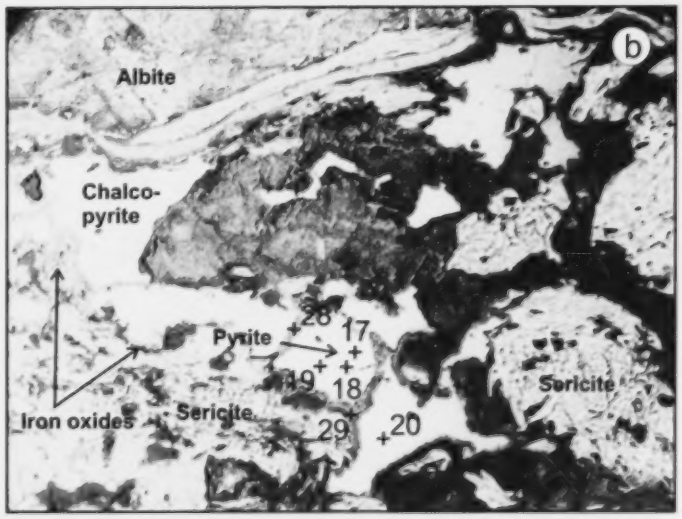

Figure 10b. Close-up of rectangular area in Figure 10a. This later vein, which cross-cuts albite in host sedimentary rocks, contains 1) sericite, and 2) equant pyrite within chalcopyrite rimmed by iron oxides. Sample is from core of drillhole M04-05 (32.5 m) at the Malachite occurrence.

Photographed under combined plane-polarized light and reflected light. Field of view ~2.[illegible]n.

Numbered crosses mark microprobe sample points (see Appendix 1).

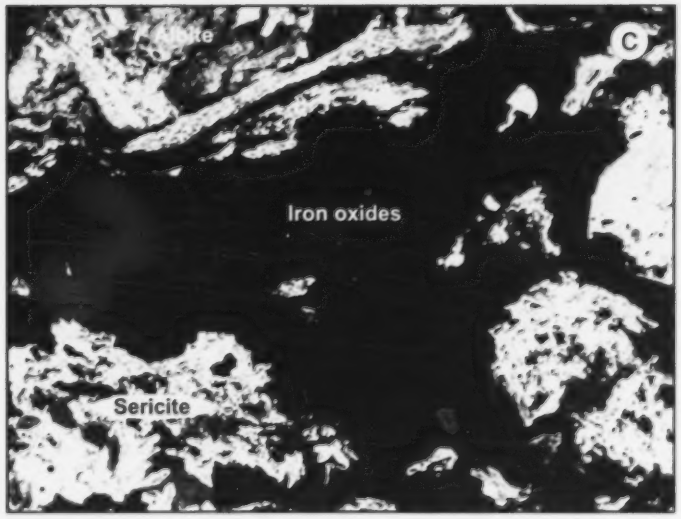

Figure 10c. Same as in Figure 10b but photographed under crossed polarizers.

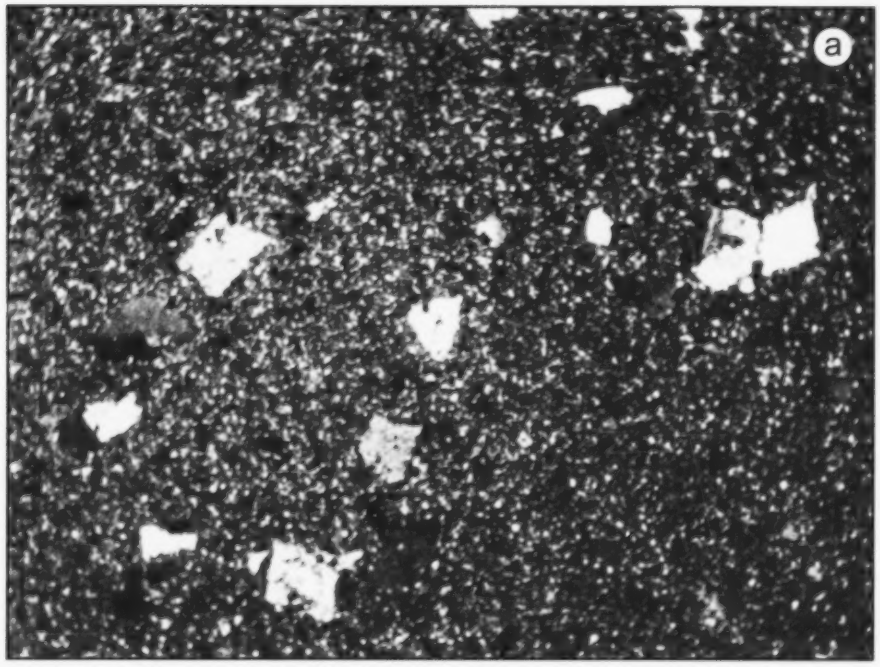

Figure 11a. Photomicrograph of carbonate porphyroblasts in carbonate-altered siltstone of the Greys Gulch Formation. Sample is from core of drillhole M04-05 (176.6 m) at the Malachite occurrence. Photographed under crossed polarizers. Field of view is ~ 2.6 mm.

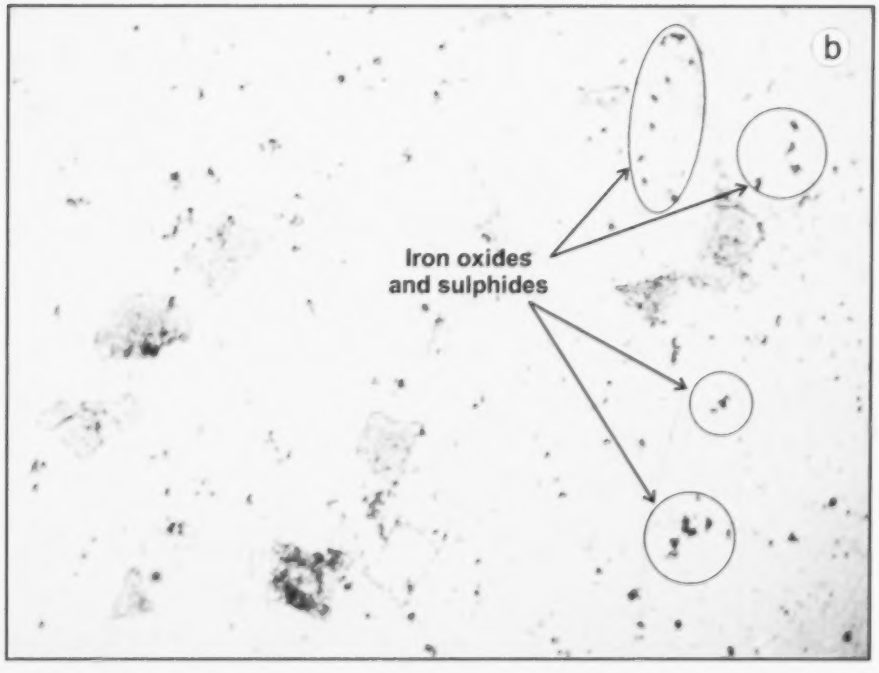

Figure 11b. Same sample as in Figure 11a, photographed under plane-polarized light. Note abundant disseminated iron oxides and subordinate sulphides.

sulphide phases have iron-oxide rims. Second, no evidence exists of a decrease in iron oxide with increasing depth, as would be expected if the iron-oxide rims were a weathering phenomenon.

Metal Associations

Assay data from Montoro Resources (Clark 2004, 2005) show correlations between several elements. A very strong correlation exists between Co and As, with a Pearson correlation coefficient of 0.91 (Table 2). Elevated Co and As values are directly related to the presence of cobaltite. The As content generally does not exceed 2000 ppm, except in drillholes M04-04 to M04-06, where reported values are higher than 2000 ppm. The As content tends to increase in later sulphide–iron-oxide–sericite vein sulphides (Type 1) and in the zone of disseminated sulphides (Type 2). The Bi content ranges from below the detection limit of 0.1 ppm up to 25 ppm (Clark 2004, 2005); however, several higher assays of between 10 ppm and 25 ppm are concentrated in drillholes M04-04 to M04-07.

Elevated Cu is attributed to abundant chalcopyrite, and no evidence was found for other copper phases, in contrast to what had been suggested by previous workers. Cu grades reported from the Malachite occurrence are consistent and generally less than 5000 ppm; however, several assays higher than 5000 ppm are reported from drillholes M04-04 to M04-06. Chalcopyrite occurs as fracture fillings in earlier pyrite but more commonly as irregular masses with later spongy pyrite (Fig. 9a) or as disseminations in sedimentary rocks, where it is associated with iron oxides and cobaltite (Fig. 9c).

Table 2. Pearson correlation coefficients among selected metals for assay data from the Ramsay–Pitre and Malachite occurrences. All data are from Clark (2004, 2005).

Sedimentary Rocks (number of samples (n) = 425)							
	Co	**As**	**Ni**	**Fe**	**Cu**	**Zn**	**Au**
Co							
As	0.91						
Ni	0.48	0.51					
Fe	0.16	0.19	0.35				
Cu	0.19	0.28	0.13	0.33			
Zn	0.01	0.03	0.22	0.43	0.10		
Au	0.44	0.42	0.36	0.34	0.26	-0.05	
Gabbroic Dykes (n = 83)							
	Co	**As**	**Ni**	**Fe**	**Cu**	**Zn**	**Au**
Co							
As	0.89						
Ni	0.08	0.08					
Fe	-0.01	-0.14	0.18				
Cu	0.59	0.73	0.07	0.00			
Zn	0.24	0.26	0.32	0.08	0.33		
Au	0.50	0.50	0.16	-0.15	0.29	0.10	

Assay data (Clark 2004, 2005) indicate that sedimentary rocks within the alteration zone are typically elevated in Cu, Co and locally Au, with the highest values occurring in zones with higher concentrations of sulphides and/or iron oxides. The highest Cu grade reported is 3.03% over 0.5 m; the best Co grade is 8860 ppm over 1 m. The Cu content in mineralized zones is roughly inversely proportional to the CaO content. Gold content is commonly above the detection limit (5 ppb) and locally is up to 440 ppb. Sedimentary rocks with elevated Au contents also tend to have higher CaO contents (3.0–8.0%). The absence of free gold in petrographic samples suggests that Au is refractory and likely occurs in pyrite, given the very low abundance of arsenopyrite in the system. However, incorporation of Au into other sulphide phases such as chalcopyrite and cobaltite cannot be ruled out. Microprobe analyses specifically for Au were conducted at a 15 kV accelerating voltage and a 200 nA beam current with count times of 1000 seconds and a detection limit lowered to 100 ppm. Yet even under these operating conditions, Au was not detected in the pyrite grains analyzed.

The analyzed samples in Table 1 have very low Ag contents, but assay data reported in assessment files show Ag values ranging from 0.1 to 10 ppm. Although a few higher Ag assays are derived from altered zones in the gabbro, most of the higher Ag assays come from carbonate-altered sedimentary rocks adjacent to mafic dykes. The Au content is generally low with an average of 18 ppb for 508 samples; however, samples from drillholes M04-05, -06 and -09 show several assays that exceed 100 ppb Au (Clark 2004, 2005). This is interesting, as it suggests that gold mineralization increases toward the northeast, approaching the Ramsay Brook Fault (Fig. 1).

ALTERATION

In general, the alteration-induced mass change of various elements is similar for both sedimentary rocks and gabbroic dykes (see below), implying that both rock types were affected by the same fluids. However, alteration is better developed and more widespread in the sedimentary rocks.

Sedimentary Rocks

Sedimentary rocks near the Ramsay–Pitre and Malachite occurrences are affected by hydrothermal alteration. Most are significantly depleted in Ba, which ranges from 9 ppm to 24 ppm (Table 1). These values are considerably lower than the average Ba contents of sandstone and shale (170 ppm and 550 ppm, respectively; Rose et al. 1979). The atypically low Ba in the sedimentary rocks might be a function of a sediment source that was anomalously low in Ba. Alternatively, Ba may have been removed by hydrothermal processes. Specifically, the destruction of K-feldspar, which apart from barite is the mineral phase that most commonly accounts for most of the Ba budget in sedimentary rocks, could account for the low Ba in these samples.

In addition to the pervasive Ca (± Mn–Fe) carbonate that overlaps the mineralization zone described above, most of the sedimentary rocks have high Na_2O and very low K_2O.

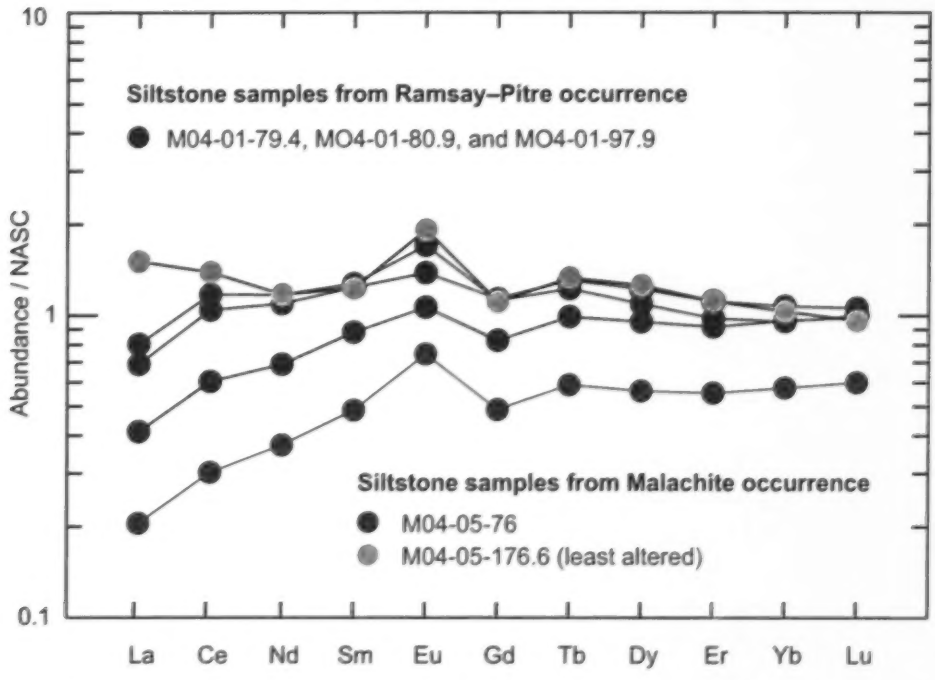

Figure 12. Rare-earth-element abundances in siltstone samples (Greys Gulch Formation) from the Ramsay–Pitre and Malachite occurrences, normalized to the North American Shale Composite (NASC). Normalization values are from Gromet et al. (1984).

Sedimentary rocks (shale to fine-grained sandstone) typically contain more K than Na and have K_2O:Na_2O ratios in the range of 2 to 3 (Pettijohn 1975). In contrast, K_2O/Na_2O for the dataset from the report area ranges between 0.02 and 0.05. Petrographic analysis of sedimentary rocks adjacent to sulphide veins (e.g., sample M04-05-32.5) shows evidence of pervasive albitization (Fig. 10a–10c), which accounts for the elevated Na_2O in these rocks. Most have fairly flat light-rare-earth-element (LREE)-depleted profiles, with a few samples having a slightly positive Eu anomaly (Fig. 12). The positive Eu anomalies may be the result of Eu having been incorporated into hydrothermal albite.

Gabbroic Dykes

The one sample of bleached, altered gabbro (M04-05-20.6) shows depletions in K, Rb, Cs, Tl, Ba, Sr, Ti, Sc, and Cr relative to the two samples of unaltered gabbro (M04-05-20.5 and -28) in the extended-element plot (Fig. 7d). (The Tl content of the altered sample is below detection limits and is omitted from the plot.) Ca and Mg contents in the altered sample are 43% and 20%, respectively, of Ca and Mg contents in the unaltered samples. The depletion of large-ion lithophile elements (e.g., K, Rb, Sr, and Ba) is attributed to their loss to the hydrothermal fluid during feldspar-destructive alteration of the gabbro. The loss of Cr (and Mg) is attributed to the breakdown of olivine by, and the loss of Cr to, the hydrothermal fluid. The altered sample also has elevated Pb, Th, U, Zn, Cu, and Ni contents relative to those of the unaltered samples.

The slightly higher Zr content of the altered sample relative to that of the unaltered samples is attributed to an overall mass loss for M04-05-20.6 (presuming Zr immobility). Similarly, the higher Th content of the altered sample is attributed to the immobility of Th and an overall mass loss for the sample due to alteration. The elevated Cu, Pb, and Zn contents in the altered sample probably reflect composition of the hydrothermal fluid. However, Ni likely was liberated during olivine destruction (see comment on Cr, above) and then precipitated with pyrite in the sulphide veins, a conclusion that is supported by the gersdorffite (NiAsS) rims on some earlier pyrite grains (Fig. 9b). This scenario implies that the mineralizing fluid became enriched in Ni sometime after sulphide deposition began (see ***Paragenetic Relationships***, below).

The altered gabbro sample has gained Na relative to the unaltered rocks, which is consistent with the sodic metasomatism recognized in the altered sedimentary rocks. Although the U content of the altered sample is low (2.4 ppm), it is seven times that of the unaltered gabbros and is similar to the lowest U contents of altered sedimentary rocks (Table 1). These numbers suggest that the mineralizing fluid was able to transport U in addition to the Ni, Cu, Co and other elements cited above.

SULPHUR ISOTOPES

The sulphur content of the eight samples analyzed specifically for this study is highly varied (Table 1). The two samples of unaltered gabbro (M04-05-20.5 and -28) contain 0.05% and 0.08% S, respectively, whereas the sample of altered gabbro contains 17.6% S. The five sedimentary samples contain between 0.009% and 1.15% S.

As part of this investigation, a total of six core samples of sulphide-vein material were collected for bulk sulphur isotopic analysis: two samples from drillhole M04-01 at the Ramsay–Pitre occurrence, and four samples from drillhole M04-05 at the Malachite occurrence (Table 3).

Table 3. Bulk sulphur isotope data from the Ramsay–Pitre and Malachite occurrences.

Sample No.	Occurrence	Host Rock	Drillhole and Depth (m)	Delta of Peak
1	Ramsay–Pitre	gabbro	M04-01-61.8	6.69
2	Ramsay–Pitre	siltstone	M04-01-97.9	7.01
3	Malachite	gabbro	M04-05-20.6	6.66
4	Malachite	siltstone	M04-05-38.7	6.59
5	Malachite	siltstone	M04-05-76.0	6.35
6	Malachite	siltstone	M04-05-152.7	3.46

Note: Analyses conducted at Memorial University, St. John's, Newfoundland.

The sulphur isotope contents of these pyrite-dominant samples (Table 3) yielded $\delta^{34}S$ values of between 3.46‰ and 7.01‰ (avg. = 6.13‰). These values are marginally heavier than magmatic sulphur, which has a narrow $\delta^{34}S$ range of approximately -5 to +5‰. Although the six samples form a small dataset, the similarity in results for five of the samples (results ranged from 6.35‰ to 7.01‰) implies a common source for the associated hydrothermal

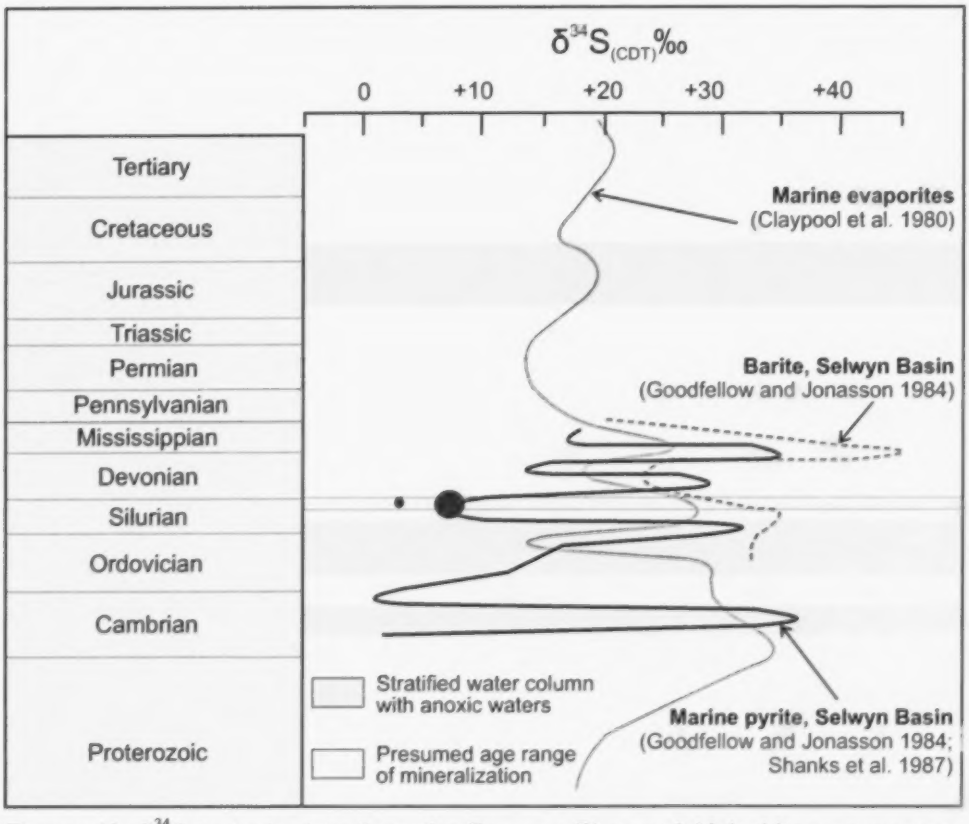

Figure 13. $\delta^{34}S$ isotopic data from the Ramsay–Pitre and Malachite occurrences, northern New Brunswick. Most S data (large green circle) from the six analyzed samples fall on the marine pyrite curve (red line) of Goodfellow and Jonasson (1984) and Shanks et al. (1987). Only one sample (small green circle) shows a slightly lighter $\delta^{34}S$ value.

fluids. If an Early Devonian age of mineralization is presumed, these five samples (Fig. 13) fall along the line of marine pyrite (Goodfellow and Jonasson 1984; Shanks et al. 1987), suggesting that sulphur may have been derived from sedimentary rocks of the Greys Gulch Formation.

One sample (M04-05-152.7) returned a lighter, more magmatic $\delta^{34}S$ value of 3.46‰ (Table 3; Fig. 13). This prompts the speculation that sulphur in the mineralization at the Ramsay–Pitre and Malachite occurrences is the product of magmatic sulphur (~0‰) having mixed with circulating groundwater that scavenged heavier (>10‰) sulphur from the underlying stratigraphic succession. Sedimentary rocks of the Early Devonian Greys Gulch Formation and Silurian Chaleurs Group constitute the footwall stratigraphy. All of these rocks were deposited under fairly oxidizing conditions and are not known to contain an abundance of either pyrite or sulphate minerals. Consequently, their potential as a sulphur source is limited. The sulphur thus was likely derived from more deeply circulating fluids interacting with Ordovician basement sedimentary and volcanic rocks of the Miramichi Zone (Fig. 1, inset), including those of the Bathurst Mining Camp. These basement rocks are known to contain abundant pyrite of relatively heavy (+15‰ to +20‰) sulphur (McCutcheon et al. 1993).

PARAGENETIC RELATIONSHIPS

Information is not available to determine the precise timing of mineralization at the Ramsay–Pitre and Malachite occurrences. However, the mineralization must be younger than sedimentary rocks of the Early Devonian Greys Gulch Formation (Wilson 2005) and either younger than or coeval with the associated gabbroic dykes. If the dykes were emplaced with the Ramsay Brook Gabbro (dated by $^{40}Ar/^{39}Ar$ as 374 ± 6 Ma), mineralization and alteration could be as young as Late Devonian. Regardless of ambiguity in the absolute age of the Ramsay–Pitre and Malachite mineralization, the relative timing of mineralogical changes that mirror evolution of the hydrothermal system can be divided into early, middle, and late stages (Fig. 14). These mineralogical paragenetic relationships are described below.

Early Stage

The fairly limited alteration of the gabbroic dykes suggests that dyke emplacement occurred after lithification of the host sedimentary rocks and was synchronous with, or slightly younger than, the envelope of sodic–calcic metasomatism (formation of calcite and albite). However, it is possible that the more limited alteration of the dykes is due to the lower permeability and porosity of the gabbroic rocks rather than to the timing of dyke emplacement relative to alteration.

Middle Stage

Sulphide Veins

Sulphide-only veins were emplaced within, but more commonly immediately adjacent to, the gabbroic dykes. The veins contain two generations of pyrite formed during the middle mineralizing stage.

The earlier pyrite occurs as equant grains (Fig. 9a, 9b) that generally exceed 1000 μ and contain minor inclusions of pyrrhotite and chalcopyrite, suggesting that the latter minerals were in equilibrium at least locally during this stage of mineralization. The earlier pyrite is overgrown by the later spongy anhedral pyrite, which contains numerous silicate inclusions (sericite) along with subordinate arsenopyrite, chalcopyrite, and grey sphalerite (Fig. 9a). The earlier pyrite is also cut by numerous curvilinear fractures filled by white sphalerite (Fig. 9a, 14) containing less than 3% Fe (Fig. 9a–points 16, 26, and 27; Appendix 1).

Microprobe analyses were conducted of the earlier pyrite (Fig. 9a–points 10–13; Fig. 9b–points 21–23) and later spongy pyrite (Fig. 9a–points 14, 15) in the sulphide-only veins. Analyses were also conducted of a small equant pyrite grain in the cross-cutting sulphide–iron-oxide–sericite vein (Fig. 10b–points 17, 18). Results indicate that all of the pyrite contains minor amounts of Co (≤0.25%). Analyses also reveal a slight tendency for Co to increase from earlier to later stages: in the earlier pyrite, higher Co values are obtained from the rims whereas in the later pyrite, higher values predominate throughout. This suggests that cobaltite was deposited later than equant pyrite.

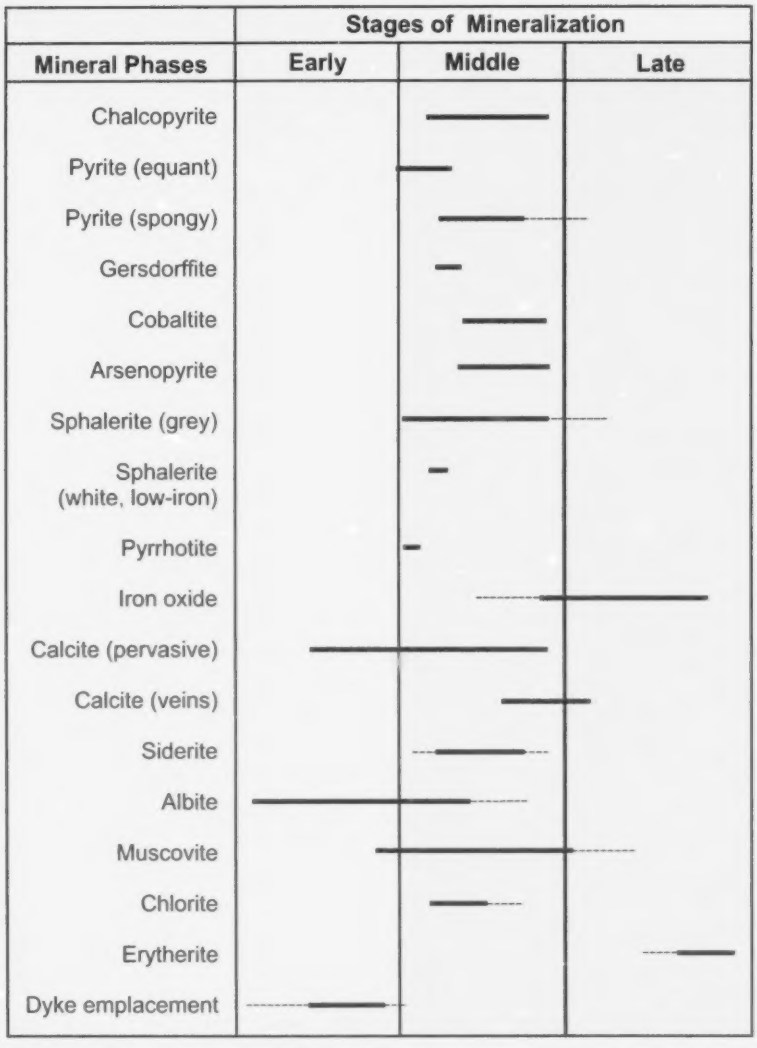

Figure 14. Schematic diagram of proposed timing of various carbonate, sulphide, silicate, and oxide mineral phases, relative to gabbroic dyke emplacement at the Ramsay–Pitre and Malachite occurrences. Dashed lines represent uncertainty with respect to timing.

Chalcopyrite commonly occurs as irregular masses within the spongy pyrite and within fracture fillings in the earlier equant pyrite (Fig. 9a); and as disseminated blebs in sedimentary rocks, where it is associated with iron oxides and cobaltite (Fig. 9c). Microprobe analyses indicate that the earlier pyrite locally has an As content (≤0.08%) that is slightly above detection limits (Fig. 9b–points 21, 22; Appendix 1). Higher As content in the pyrite rims suggests that arsenopyrite deposition likely coincided with cobaltite–chalcopyrite deposition and took place after earlier equant pyrite deposition.

Thin (<90 μ) rims of gersdorffite (NiAsS) on the earlier equant pyrite indicate that the mineralizing fluid became enriched in Ni and As toward the end of earlier pyrite deposition (Fig. 9b). Microprobe analysis of the gersdorffite shows that it contains more than 1% Co and up to 1.4% Sb (Fig. 9b–points 24, 25; Appendix 1), which implies that Co and Sb enrichment accompanied Ni and As.

Disseminated Sulphides

Disseminated sulphides (chalcopyrite, cobaltite, and subordinate arsenopyrite and pyrite) were emplaced within carbonate-altered sedimentary rocks distal to the gabbroic dykes. The paragenetic relationship between vein mineralization (proximal) and disseminated mineralization (distal) is uncertain. The two types may have been synchronous, reflecting varied physicochemical conditions in proximal and distal parts of the system. However, Co enrichment toward rims of the earlier equant pyrite in sulphide-only veins, coupled with the higher Co (and Cu) in enveloping later spongy pyrite in the veins, suggests that the Co–Cu-rich disseminated sulphides are more likely equivalent to the later (middle stage) spongy pyrite than to the earlier (middle stage) equant pyrite (Fig. 14).

Alternatively, the zone of disseminated sulphides may reflect early widespread mineralization coincident with sodic–calcic metasomatism, whereas some sulphide veins may represent a later prograde (increasing temperature), spatially restricted event. Supporting evidence for the latter interpretation comes from the observations that 1) sulphide veins have not been encountered outside the envelope of carbonate-altered rock that hosts the disseminated mineralization, and 2) the sulphide veins cut apparently stratabound alteration (Fig. 4), suggesting that veins postdate at least some of this alteration.

Late Stage

In the zone of disseminated sulphide mineralization, chalcopyrite (locally overgrowing cobaltite) is almost always mantled by a thin rim of iron oxides (Fig. 9c). Likewise, in the late sulphide–iron-oxide–sericite vein (Fig. 10a) that cuts the earlier sulphide-only vein, the small equant pyrite crystal noted above is overgrown by chalcopyrite that in turn is overgrown by iron oxides (Fig. 10b), indicating that oxide growth overlaps with the timing of late potassic alteration.

Discussion

Cobalt mineralization in New Brunswick is limited, occurring most commonly as intra-magmatic deposits associated with nickeliferous mafic intrusions, such as in the St. Stephen and Goodwin Lake deposits (Rose and Johnson 1990; NBDNR 2009). However, the Cu–Co–Au association such as occurs in the Ramsay–Pitre and Malachite occurrences has been reported from only a few other New Brunswick localities, in which the deposits are variously classified as being hosted by sedimentary rocks or related to contact metamorphism (skarn) or mafic intrusions. None of these classifications adequately explains all of the attributes recognized at the Ramsay–Pitre and Malachite occurrences. In particular, they do not account for the fairly widespread (distal) sodic–calcic metasomatism with disseminated copper–cobalt–gold–iron-oxide mineralization, and the much less extensive (proximal or prograde) potassic alteration and sulphide vein system.

A similar Cu–Au–Fe-oxide association occurs approximately 6.5 km west of the Malachite occurrence at Big Pit (Fig. 1; URN 1434), where an auriferous hematite–chalcopyrite vein cuts

mafic flows of the Greys Gulch Formation. The east–west-striking, northerly dipping vein is spatially associated with a splay of the McIntyre Brook Fault and has returned assays showing Au contents of up to 10 g/t (Smith 1999b). Although the Big Pit occurrence is fairly small, its mineralization style is best classified as an iron-oxide–copper–gold (IOCG) system, the first of its kind to be recognized in northern New Brunswick (Rose and Johnson 1990; NBDNR 2009). IOCG mineralization has also been documented about 150 km north-northeast of Ramsay Brook at Mont-de-l'Aigle in the Gaspésie region of Québec (Simard et al. 2006).

Although many IOCG subtypes exist, each with a unique set of characteristics, the following characteristics are shared by many of these deposits (Pollard 2002; Porter 2002; Corriveau 2007).

- *Mineralization style*: sulphide-deficient but not necessarily sulphide absent; low-Ti magnetite- and/or hematite-bearing hydrothermal veins, breccias, massive lenses and disseminated mineralization; ore metals include Cu, Au, Ag, U, rare-earth elements, Bi, Co, Nb, and F.

- *Association with intrusions/volcanic rocks*: large-scale continental I- or A-type magmas or alkaline carbonatites.

- *Alteration*: proximal-scale potassic–iron oxide, and regional-scale sodic–calcic or potassic.

- *Mineralization depth*: shallow- to mid-crustal depths.

- *Tectonic setting*: associated with rift settings marked by bimodal volcanism and typically associated with crustal-scale faults; orogenic collapse settings commonly invoked as an IOCG setting.

Several of these characteristics are recognized at the Ramsay–Pitre and Malachite occurrences, namely the Cu–Co–Au–Fe-oxide association, the widespread sodic–calcic metasomatism, the proximal potassic alteration, the continental rift setting, and the proximity to major faults.

Similarly, many features of the Mont-de-l'Aigle IOCG deposits (Simard et al. 2006) can be recognized at the Ramsay–Pitre and Malachite occurrences. These features include 1) proximity to major regional faults, 2) Silurian–Early Devonian host rocks, and 3) the presence of mafic intrusions (and felsic intrusions in the case of Mont-de-l'Aigle). The alteration style and paragenetic relationships at the Ramsay–Pitre and Malachite occurrences also resemble those at Mont-de-l'Aigle (Simard et al. 2006). Specifically, alteration of the dykes at both the New Brunswick and Québec locales is characterized by gains in Na_2O, CaO, MnO, and Zn, and decreases in K_2O, Ba, Sr, and Rb. Likewise, second-stage alteration at both sites is characterized by K_2O enrichment. On the other hand, carbonate host rocks at Mont-de-l'Aigle have undergone very different mass changes relative to the dykes (i.e., decalcification and

silicification); siliciclastic sedimentary host rocks at the Ramsay–Pitre and Malachite occurrences, conversely, have undergone mass changes similar to those of the dykes.

An obvious spatial relationship exists between the gabbroic dykes and alteration–mineralization phenomena at the Ramsay–Pitre and Malachite occurrences. The elevated Co, Ni, and Bi contents suggest that mafic melts may have contributed metals to the mineralizing fluids. Mafic magma-derived fluids have been proposed as the metal source for some IOCG systems, but felsic to intermediate magmatic fluids are more commonly invoked as such a source.

The slight increase in Co, Cu, Au, and Bi from southwest to northeast in the mineralized area, coupled with the one sulphur isotope sample that returned a light, more magmatic $\delta^{34}S$ (3.46‰) from the Malachite occurrence, implies that the magmatic source of the mineralizing fluid is to the northeast. Several gold occurrences are known from the area north and northeast of the Malachite occurrence, most of which are spatially associated with mafic intrusions, faults, and zones of iron-carbonate alteration (Fig. 1; Ruitenberg et al. 1989). It is possible they are all part of the same system as Ramsay–Pitre and Malachite; however, more work needs to be done before this can be confirmed.

Some ambiguities remain with respect to timing of alteration and mineralization. Nonetheless, the evolution of the hydrothermal system at the Ramsay–Pitre and Malachite occurrences could be explained by the following sequential model.

1. The transtensional tectonic setting proposed for the Tobique–Chaleurs Zone and abundance of mafic volcanic rocks and intrusions in the Ramsay Brook area (Fig. 1) make it feasible to postulate the emplacement of gabbroic magma at depth. Crystallization and cooling of this body could have generated a magmatic fluid rich in Na–Ca–CO_2 and also containing As, Co, Cu, Au, Bi, and Fe.

2. Given the fairly consistent $\delta^{34}S$ of sulphide mineralization (6.35–7.0‰), it is likely that circulating groundwater was entrained in the hydrothermal cell. This groundwater probably contributed sulphur to the system by dissolving sulphate or sulphide minerals from sedimentary rocks of the Greys Gulch Formation or older sedimentary and volcanic units deeper in the footwall. Some of the Cu (± Au) also may have been sourced from these rocks.

3. Mixing of the circulating groundwater and entrained magmatic fluid would have generated the large halo of albite–carbonate alteration (sodic–calcic metasomatism) in sedimentary rocks of the Greys Gulch Formation. This same fluid also may have been responsible for the formation of disseminated Cu–Co–Au–Fe-oxide (Type 2) mineralization.

4. Gabbroic dykes from the main intrusion were emplaced into the early-formed carbonate-alteration zone. Cooling of the dykes and continued cooling of the larger intrusion likely

generated additional volumes of circulating fluids, which further altered the country rocks as well as margins of the dykes and small zones within the dykes.

5. The close spatial relationship between sulphide veins and dykes, and the fact that dykes are locally cut by sulphide veins and alteration, implies that the sulphide veins formed shortly after the dykes were emplaced. Therefore, the sulphide-vein (Type 1) mineralization reflects a proximal or prograde part of the system. This interpretation is supported by the fact that potassic alteration is associated with late Type 1 sulphide–iron-oxide–sericite-bearing veins in the Ramsay–Pitre and Malachite occurrences—an alteration type recognized elsewhere as a proximal part of an IOCG system.

CONCLUSIONS

The mineralization, alteration style, and host rocks of the Ramsay–Pitre and Malachite occurrences are similar in many respects, making it likely that the two showings are part of the same mineralization system. Geophysical anomalies from magnetometer and VLF surveys reported by Montoro Resources (Clark 2004, 2005) suggest that the dyke swarm encountered in drilling and trenching continues to the north-northeast. The increased number of mafic dykes, coupled with higher Au and Co assays for the Malachite occurrence relative to the Ramsay–Pitre occurrence, suggests that mineralization continues and possibly increases from southwest to northeast. Likewise, the one sulphur isotope sample returning a lighter (more magmatic) $\delta^{34}S$ value and the marginally higher Bi values at the Malachite occurrence both suggest that the core of the hydrothermal system lies to the northeast of that occurrence.

Many aspects of the Ramsay–Pitre and Malachite mineralization system are consistent with features associated with iron-oxide–copper–gold (IOCG) systems. Fairly widespread and varyingly intense sodic–calcic metasomatism affects most of the sedimentary host rocks and intrusions in the Ramsay–Pitre–Malachite system. Mineralization in this metasomatized zone is manifested as disseminated iron oxides with subordinate arsenopyrite and chalcopyrite. In drillcore samples analyzed for this study, the disseminated blebs of chalcopyrite almost always have thin rims of iron oxides. A less well-developed phase of potassic metasomatism is evident in a sulphide–iron-oxide–sericite vein that is spatially associated with, but later than, sulphide-only veins. The veins cut the earlier sodic–calcic alteration; they are dominated by pyrite and subordinate chalcopyrite, cobaltite, gersdorffite, sphalerite, and arsenopyrite. The vein mineralization and potassic alteration together likely represent a more proximal and possibly prograde part of the system.

Mineralized grades and widths reported to date from the Ramsay–Pitre and Malachite occurrences are subeconomic. However, recognition of an IOCG-style of mineralization in an area that has received limited exploration greatly enhances the potential for further discovery. It should be noted that a cluster of gold occurrences featuring iron-carbonate alteration lies about 8 km north-northeast of the Malachite occurrence. Given that IOCG systems are characterized by large halos of alteration and mineralization, these gold occurrences could be related to the Ramsay–Pitre–Malachite system.

In addition, crustal-scale faults, which are commonly invoked as fluid conduits in IOCG systems, have been mapped in the area. For example, two major splays of the Rocky Brook–Millstream Fault (Fig. 1, inset)—the Ramsay Brook and Greys Gulch faults—lie less than 3 km north of the Malachite occurrence (Fig. 1). These faults, or some as yet unrecognized subsidiary structures, may have controlled dyke emplacement or hydrothermal fluid flow at the Ramsay–Pitre and Malachite occurrences.

Future exploration efforts in the district should be concentrated in areas on or adjacent to major structural breaks such as the Rocky Brook–Millstream Fault or one of its splays. In terms of geochemical vectoring, areas that display coincident sodic–calcic enrichment and potassium depletion may offer the strongest exploration prospects.

ACKNOWLEDGEMENTS

Thank you to Rufus Smith for allowing access to the Malachite property and to Dan Legacy for providing assistance at the core shed. Sulphur isotope analyses were conducted by Alison Pye of Memorial University, St. John's, Newfoundland. Douglas Hall of the Microscopy and Microanalysis Facility, University of New Brunswick, Fredericton, conducted the microprobe analyses. Thank you also to Steve McCutcheon, Reg Wilson, and Sean McClenaghan (all with the Geological Surveys Branch (GSB), New Brunswick Department of Natural Resources) for thoughtful discussions. The report also benefitted from critical reviews by Steve McCutcheon and Les Fyffe (GSB).

REFERENCES

Clark, D. 2002. Report of work on the Malachite property for Log House Construction Ltd. New Brunswick Department of Natural Resources; Minerals, Policy and Planning Division, Assessment File 475585.

Clark, D. 2004. Report of work on the Malachite property for Montoro Resources Inc. New Brunswick Department of Natural Resources; Minerals, Policy and Planning Division, Assessment File 475768.

Clark, D. 2005. Report of work on the Malachite property for Montoro Resources Inc. New Brunswick Department of Natural Resources; Minerals, Policy and Planning Division, Assessment File 476113.

Claypool, G.E., Holser, W.T., Kaplan, I.R., Sakai, H., and Zak, I. 1980. The age curves of sulfur and oxygen isotopes in marine sulfate and their mutual interpretation. Chemical Geology, **28**, p. 199–260.

Corriveau, L. 2007. Iron oxide–copper–gold deposits: a Canadian perspective. *In* Mineral Deposits of Canada: A Synthesis of Major Deposit-Types, District Metallogeny, and Evolution of Geological Provinces and Exploration Methods. *Edited by* W.D. Goodfellow. Geological Association of Canada, Mineral Deposits Division, Special Publication No. 5, p. 307–328.

Debon, F., and Le Fort, P. 1983. A chemical–mineralogical classification of common plutonic rocks and associations. Transactions of the Royal Society of Edinburgh, Earth Sciences, **73**, p. 135–149.

Dostal, J., Wilson, R.A., and Keppie, D. 1989. Geochemistry of Siluro–Devonian Tobique belt in northern and central New Brunswick (Canada). Canadian Journal of Earth Science, **26,** p. 1282–1296.

Fyffe, L. 1971. Junction of Ramsay and Murray Brooks. New Brunswick Department of Natural Resources; Mineral Resources Branch, Map Plate 71-48.

Fyffe, L. 1974. Geology of head of McCormack, Ferguson and Ramsay Brooks. New Brunswick Department of Natural Resources; Minerals Resources Branch, Map Plate 74-159.

Goodfellow, W.D., and Jonasson, I.R. 1984. Ocean stagnation and ventilation defined by $\delta^{34}S$ secular

trends for barite and pyrite, Selwyn Basin, Yukon. Geology, **12**, p. 583–586.

Gromet, L.P., Dymek, R.F., Haskin, L.A., and Korotev, R.L. 1984. The "North American Shale Composite": its compilation, major and trace element characteristics. Geochimica et Cosmochimica Acta, **48**, p. 2469–2482.

Le Maitre, R.W., Bateman, P., Dudek, A., Keller, J., Lameyre Le Bas, M.J., Sabine, P.A., Schmid, R., Sorensen, H., Streckeisen, A., Wolley, A.R., and Zanettin, B. 1989. A Classification of Igneous Rocks and Glossary of Terms. Blackwell, Oxford, 193 p.

McCutcheon, S.R., Langton, J.P., van Staal, C.R., and Lentz, D.R. 1993. Stratigraphy, tectonic setting and massive sulphide deposits of the Bathurst Mining Camp, northern New Brunswick. *In* Guidebook to the Metallogeny of the Bathurst Camp. *Edited by* S.R. McCutcheon and D.R. Lentz. Trip No. 4, Bathurst '93, 3rd Annual Field Conference, Geological Society, Canadian Institute of Mining and Metallurgy, p. 1–39.

Mersereau, T. 1998. Report of work on the Malachite property for Log House Construction Ltd. New Brunswick Department of Natural Resources; Minerals and Energy Division, Assessment File 475160.

Murphy, R.B. 1989. Geochemistry of the Siluro–Devonian mafic volcanic rocks and associated gabbroic intrusions, Upsalquitch Forks area, New Brunswick. Unpublished M.Sc. thesis, Acadia University, Wolfville, Nova Scotia, Canada, 290 p.

New Brunswick Department of Natural Resources. 2009. New Brunswick mineral occurrence database. Minerals, Policy and Planning Division. http://dnre-mrne.gnb.ca/mineraloccurrence/. Accessed December 2009.

Pettijohn, F.J. 1975. Sedimentary Rocks, 3rd edition. Harper & Row Publishers, New York, 628 p.

Pitre, N., 1991. Report of work on the Ramsay Brook group. New Brunswick Department of Natural Resources; Mineral Resources, Assessment File 474071.

Pitre, N., 1992. Report of work on the Ramsay Brook Group. New Brunswick Department of Natural Resources; Mineral Resources, Assessment File 474223.

Pitre, N., 1993. Report of work on the Ramsay Brook Group. New Brunswick Department of Natural Resources; Mineral Resources, Assessment File 474361.

Pitre, N., 1995. Report of work on the Ramsay Brook Group. New Brunswick Department of Natural Resources; Minerals and Energy Division, Assessment File 474585.

Pollard, P.J. 2002. Magmatic fluid and metal source for Fe-oxide–Cu–Au mineralization. *In* Hydrothermal Iron-Oxide–Copper–Gold and Related Deposits: A Global Perspective. *Edited by* T.M. Porter. PGC Publishing, Adelaide, Australia, **1**, 2nd edition, 349 p., p. 27–42.

Porter, T.M. 2002. Hydrothermal iron-oxide–copper-gold and related deposits. *In* Hydrothermal Iron-Oxide–Copper–Gold and Related Deposits: A Global Perspective. *Edited by* T.M. Porter. PGC Publishing, Adelaide, Australia, **1**, 2nd edition, 349 p., p. 3–5.

Rose, A.W., Hawkes, H.E., and Webb, J.S. 1979. Geochemistry in Mineral Exploration, 2nd edition. Academic Press Inc. (London) Ltd., 657 p.

Rose, D.G., and Johnson, S.C. 1990. New Brunswick computerized mineral occurrence database. New Brunswick Department of Natural Resources and Energy; Mineral Resources, Mineral Resource Report 3.

Ruitenberg, A.A., McCutcheon, S.R., Watters, S.E., McLeod, D.M., Burton, D.M., and Hoy, D. 1989. Field guide to gold occurrences in New Brunswick. New Brunswick Department of Natural Resources; Minerals and Energy Division, Field Guide No. 1, 63 p.

Shanks, W.C. III, Woodruff, L.G., Jilson, G.A., Jennings, D.S., Modene, J.S., and Ryan, B.D. 1987. Sulfur and lead isotope studies of stratiform Zn–Pb–Ag deposits, Anvil range, Yukon: basinal brine exhalation and anoxic bottom-water mixing. Economic Geology, **82**, p. 600–634.

Simard, M., Beaudoin, G., Bernard, J., and Hupé, A. 2006. Metallogeny of the Mont-de-l'Aigle IOCG deposit, Gaspé Peninsula, Québec, Canada. Mineralium Deposita, **41**, p. 607–636.

Smith R. 1999a. Report of work on the Malachite property for Log House Construction Ltd. New Brunswick Department of Natural Resources; Minerals and Energy Division, Assessment File 475275.

Smith R. 1999b. Report of work on the Big Pit property for Log House Construction Ltd. New Brunswick Department of Natural Resources; Minerals and Energy Division, Assessment File 475175.

Smith R. 2001. Report of work on the Malachite property for Log House Construction Ltd. New Brunswick Department of Natural Resources; Minerals, Policy and Planning Division, Assessment File 475384.

Smith R. 2002. Report of work on the Malachite property for Log House Construction Ltd. New Brunswick Department of Natural Resources; Minerals, Policy and Planning Division, Assessment File 475494.

Taylor, S.R., and McLennan, S.M. 1985. The Continental Crust: Its Composition and Evolution: An Examination of the Geochemical Record Preserved in Sedimentary Rocks. Blackwell Scientific Publications, Oxford, 312 p.

van Staal, C.R., and De Roo, J.A. 1995. Mid-Paleozoic tectonic evolution of the Canadian Appalachian Central Mobile Belt in northern New Brunswick, Canada: collision, extensional collapse and dextral transpression. *In* Current Perspectives in the Appalachian–Caledonian Orogen. *Edited by* J.P. Hibbard, C.R. van Staal, and P.A. Cawood. Geological Association of Canada, Special Paper 41, p. 367–389.

Walker, J.A., and McCutcheon, S.R. 1990. Geology of Upsalquitch Forks area (21 O/10), New Brunswick. New Brunswick Department of Natural Resources and Energy; Mineral Resources, Map Plate 90-24.

Walker, J.A., and McCutcheon, S.R. 1995. Siluro–Devonian stratigraphy of the Chaleurs Bay Synclinorium, northern New Brunswick. *In* Current Research 1994. *Edited by* S.A.A. Merlini. New Brunswick Department of Natural Resources; Minerals and Energy Division, Miscellaneous Report 18, p. 225–244.

Wilson, R.A. 2003. Geology of the Ramsay Brook area (NTS 21 O/10a), Restigouche County, New Brunswick. New Brunswick Department of Natural Resources; Minerals, Policy and Planning Division, Map Plate 2003-20.

Wilson, R.A. 2005. Geology of the McCormack Lake area (NTS 21 O/10b), Restigouche and Northumberland Counties, New Brunswick. New Brunswick Department of Natural Resources; Minerals, Policy and Planning Division, Map Plate 2005-60.

Wilson, R.A., and Kamo, S. 2008. New U–Pb ages from the Chaleurs and Dalhousie Groups: implications for regional correlations and tectonic evolution of northern New Brunswick. *In* Geological Investigations in New Brunswick for 2007. *Edited by* G.L. Martin. New Brunswick Department of Natural Resources; Minerals, Policy and Planning Division, Mineral Resource Report 2008-1, p. 55–57.

Winchester, J.A., and Floyd, P.A. 1977. Geochemical magma type discrimination: application to altered and metamorphosed basic igneous rocks. Earth and Planetary Science Letters, **28**, p. 459–469.

Appendix 1. Microprobe analyses of element wt % in sulphides from the Ramsay Brook–Pitre and Malachite occurrences, northern New Brunswick.

Notes: 1. Pt # refers to sample points shown on Figures 9a–9c, and Figure 10b. 2. See p. 46 and 51 for data on microprobe operating conditions.

Pt #	Fig. #	S	Fe	Co	Cu	Ni	Zn	As	Sb	Au	Total	X (mm)	Y (mm)	Label	Phase
1	Fig. 9c	19.93	10.92	23.95	0.1889	N/A	N/A	44.51	0.2082	0.0358	99.75	56.257	36.9202	URN1339aspyAcore	Cobaltite
2	Fig. 9c	19.35	9.12	26.1	0.1082	N/A	N/A	44.96	0.137	0.0083	99.79	56.263	36.9172	URN1339aspyArim	Cobaltite
3	Fig. 9c	34.58	30.89	0.1237	34.95	N/A	N/A	0	0.0669	0	100.61	56.2142	36.9782	URN1339CpyCore	Chalcopyrite
4	Fig. 9c	34.65	30.34	0.29	35.07	N/A	N/A	0	0	0	100.35	56.2255	36.9902	URN1339CpyRim	Chalcopyrite
5	Fig. 9c	19.62	10.11	26.59	1.0716	N/A	N/A	44.89	0.0495	0.0482	102.38	56.2428	36.8219	URN1339 Aspy in Cpy2	Cobaltite
5	Fig. 9c	19.67	9.68	26.82	0.9618	N/A	N/A	44.76	0.1274	0	102.02	56.245	36.8219	URN1339 Aspy in Cpy2	Cobaltite
6	Fig. 9c	34.58	30.36	0.7064	34.74	N/A	N/A	0.0444	0.0101	0	100.45	56.2482	36.8142	URN1339 Cpy2	Chalcopyrite
7	Fig. 9c	34.61	29.72	0.3994	35.3	N/A	N/A	0.0012	0	0	100.02	56.2605	36.7969	URN1339 Cpy2	Chalcopyrite
8	Fig. 9c	34.58	30.07	0.1222	34.56	N/A	N/A	0.0128	0	0	99.35	56.1982	36.7994	URN1339 Cpy2	Chalcopyrite
9	Fig. 9c	34.44	29.9	0.2891	34.46	N/A	N/A	0	0.0378	0.0399	99.16	56.2682	36.8147	URN1339 Cpy2	Chalcopyrite
10	Fig. 9a	54.45	47.58	0.101	0	N/A	N/A	0	0.0253	0.0589	102.21	22.7245	10.0644	M0401 Py	Pyrite
11	Fig. 9a	54.21	46.95	0.0675	0.0487	N/A	N/A	0	0	0.0005	101.28	22.8298	10.0374	M0401 Py	Pyrite
12	Fig. 9a	54.41	47.17	0.1301	0	N/A	N/A	0	0.0494	0	101.76	22.94	10.0082	M0401 Py	Pyrite
13	Fig. 9a	54.39	46.94	0.0882	0.0025	N/A	N/A	0	0.0004	0.0355	101.46	22.971	9.9672	M0401 Py	Pyrite
14	Fig. 9a	54.24	46.84	0.2474	0.0401	N/A	N/A	0	0.0264	0.0086	101.4	23.049	9.9454	M0401 Py	Pyrite
15	Fig. 9a	54.86	46.94	0.0586	0.0503	N/A	N/A	0	0.0359	0	101.95	23.0602	9.8807	M0401 Py	Pyrite
17	Fig. 10b	53.41	46.59	0.0836	0.5075	N/A	N/A	0	0.0234	0	100.61	23.5703	41.4039	M0405A py core	Pyrite
18	Fig. 10b	53.56	45.82	0.0669	0.7509	N/A	N/A	0	0	0.0231	100.22	23.5703	41.3869	M0405A py rim	Pyrite
19	Fig. 10b	34.76	29.89	0.0821	34.9	N/A	N/A	0	0.0053	0	99.64	23.5452	41.3722	M0405A cpy	Chalcopyrite
20	Fig. 10b	34.57	30.13	0.0371	35.07	N/A	N/A	0.0275	0.0445	0	99.88	23.6592	41.3509	M0405A cpy	Chalcopyrite

	S	Fe	Co	Cu	As	Sb	Au
Detection Limit (wt %)	0.02	0.05	0.04	0.06	0.03	0.04	0.08
Peak Counting Time (sec)	30	40	80	80	80	80	100
Standard	Marcasite	Marcasite	Metal	Metal	InAs	Metal	Metal

Appendix 1 *(cont'd).*

Pt #	Fig. #	S	Fe	Co	Cu	Ni	Zn	As	Sb	Au	Total	X (mm)	Y (mm)	Label	Phase
16	Fig. 9a	33.43	2.9993	0	0.0462	0.0123	65.06	0	0.1577	0	101.71	22.8365	10.1249	M0401 grey phase	Sphalerite
21	Fig. 9b	53.54	46.63	0.1283	0	0.073	0.0103	0.0807	0	0.0291	100.49	16.3698	42.2229	M0405B py	Pyrite
22	Fig. 9b	53.72	47.23	0.1304	0	0.0492	0.0508	0.0134	0	0.0407	101.24	16.0325	42.1967	M0405B py	Pyrite
23	Fig. 9b	53.56	46.97	0.0915	0.033	0.0241	0	0	0.0554	0	100.74	15.8602	42.2409	M0405B py	Pyrite
24	Fig. 9b	18.98	0.417	1.0439	0	34.52	0	45.03	1.4262	0.0394	101.45	15.7805	41.3674	M0405B aspy	Gersdorffite
25	Fig. 9b	18.98	0.4237	1.2306	0	34.46	0	45.44	1.1867	0.0097	101.73	15.7612	42.3542	M0405B aspy	Gersdorffite
26	Fig. 9a	33.19	2.8727	0	0.0619	0	64.96	0	0.0409	0	101.13	22.6898	10.1952	M0401 grey phase	Sphalerite
27	Fig. 9a	32.99	2.4129	0.0072	0.1949	0	65.86	0	0	0.0162	101.48	22.6392	10.2359	M0401 adj sphalerite	Sphalerite

	S	Fe	Co	Cu	Ni	Zn	As	Sb	Au
Detection Limit (wt %)	0.02	0.05	0.04	0.06	0.05	0.07	0.03	0.04	0.08
Peak Counting Time (sec)	30	40	80	80	80	80	80	80	100
Standard	Marcasite	Marcasite	Metal	Metal	Metal	Zns	Inas	Metal	Metal

Pt #	Fig. #	SO_2	FeO	CoO	CuO	NiO	ZnO	As_2O_3	Sb_2O_3	AuO_2	Total	X (mm)	Y (mm)	Label
28	Fig. 10b	40.7	24.46	0.9827	50.42	0.5653	0	9.28	0	0.0047	126.41	23.5138	41.3557	M0405A Feoxide
28 *	Fig. 10b	18.84	24.56	0.9206	29.57	0.7859	0	13.33	0	0	88.01	23.5188	41.3597	M0405A Feoxide
29	Fig. 10b	4.33	43.61	1.0896	6.73	0.9637	0	11.64	0	0.0357	68.41	23.613	41.3144	M0405A Feoxide
30	Fig. 9c	60.97	8.01	34.32	25.95	2.1661	0	4.37	0.0687	0	135.86	56.2715	36.8474	URN1339 Feoxide

28 * = duplicate analysis

	S	Fe	Co	Cu	Ni	Zn	As	Sb	Au
Detection Limit (wt %)	0.05	0.07	0.05	0.07	0.06	0.08	0.04	0.05	0.09
Peak Counting Time (sec)	30	40	80	80	80	80	80	80	100
Standard	Marcasite	Marcasite	Metal	Metal	Metal	ZnS	InAs	Metal	Metal

THE APPALACHIAN GLACIER COMPLEX, AND THE MIDDLE–LATE PLEISTOCENE HISTORY OF WEST-CENTRAL NEW BRUNSWICK, CANADA

ALLEN A. SEAMAN

Geological Surveys Branch, New Brunswick Department of Natural Resources,
P.O. Box 6000, Fredericton, New Brunswick, CANADA E3B 5H1 *(Allen.Seaman@gnb.ca)*

Seaman, A.A. 2009. The Appalachian Glacier Complex, and the Middle–Late Pleistocene history of west-central New Brunswick, Canada. *In* Geological Investigations in New Brunswick for 2008. *Edited by* G.L. Martin. New Brunswick Department of Natural Resources; Minerals, Policy and Planning Division, Mineral Resource Report 2009-2, p. 66–140.

Glaciation of the Canadian Maritime provinces has previously been ascribed to the actions of the Appalachian Glacier Complex during the Wisconsinan Stage of the Late Pleistocene. In contrast, the glaciation of adjacent Maine has been attributed to the continental Laurentide Ice Sheet. An analysis of glacial phenomena and chronology in west-central New Brunswick indicates that much of the region's glacial activity is attributable to the Appalachian Glacier Complex, although the Laurentide Ice Sheet probably played a role during the Early Wisconsinan.

A new non-finite date (>51.7 ka) for the newly defined Half Moon Sediments, previously interpreted to be of mid-Wisconsinan age, indicates that they are instead of Sangamonian Interglacial age (c. 130–75 ka). The 'Lower till' underlying these and similar fluvial sediments in a previously defined Pleistocene stratigraphy for central and northern New Brunswick is interpreted to be of probable Illinoian age (c. 200–130 ka). This till, as well as other evidence for early eastward ice flow that formerly had been assigned to the early part of the Early Wisconsinan, is attributed to the newly defined Northumberland Phase of the Illinoian Appalachian Glacier Complex. The till is now referred to informally as the 'Northumberland till.'

Other glacial phenomena in west-central New Brunswick are attributable to the previously defined phases of the Wisconsinan Appalachian Glacier Complex. The southeast- to south-southeast-trending Caledonia Phase of the Early–Middle Wisconsinan was responsible for producing glacially streamlined landforms, significant glacial dispersal, and till deposition (the 'Caledonia till'). It is interpreted to reflect the combined actions of both the Laurentide Ice Sheet and the Notre Dame Ice Divide. The Late Wisconsinan maximum is represented by the Escuminac Phase, with south to southwest (and perhaps west) ice flow from the Escuminac Ice Centre in the Gulf of St. Lawrence. During the subsequent Scotian Phase, glacial retreat and thinning led to breakup of the Escuminac glacier and the initiation of eastward to northeastward ice flow from the Central Maine Ice Centre.

Further glacial waning led to the Chignecto Phase, during which ice flow was northward from the Fundy Highlands Ice Divide. At the end of the Chignecto Phase, rising waters of the Late Glacial De Geer Sea partitioned the Fundy Highlands Ice Divide, leading to the development of Inland Sea Acadia in the Saint John River valley. The area southwest of the river was deglaciated by regional stagnation. To the northeast, the remnant Gaspereau Ice Centre was reactivated during the Collins Pond Phase, correlative with the brief

Younger Dryas Stadial. Only locally did these Late Wisconsinan phases develop their own till. In large part, their action was confined to the generation of small-scale glacial erosion marks and local reworking of the Caledonia till into a hybrid till with Caledonia physical and chemical properties but a realigned fabric.

La glaciation des provinces maritimes du Canada a déjà été décrite comme s'inscrivant dans le cycle de glaciation des Appalaches, survenu durant l'étage glaciaire du Wisconsinien, au Pléistocène tardif. Par ailleurs, la glaciation de l'État adjacent du Maine aurait été causée par la plaque glaciaire des Laurentides. Une analyse du phénomène de glaciation et des périodes glaciaires de l'ouest et du centre du Nouveau-Brunswick indique qu'une bonne partie de l'activité de glaciation de la région s'inscrirait dans le cadre du cycle de glaciation des Appalaches, même s'il faut tout de même prendre en compte que la plaque glaciaire des Laurentides a probablement eu une incidence au début du Wisconsinien.

Une nouvelle datation indéterminée (de plus de 51,7 millions d'années) des nouveaux sédiments en demi-lune découverts a été établie. Auparavant, l'interprétation chronologique de ces sédiments avait ciblé une datation du milieu du Wisconsinien. Or, il s'agirait plutôt de sédiments du stade interglaciaire sangamonien (dont la formation remonterait à une période comprise entre 130 et 75 millions d'années). La strate de till inférieure sous-jacente et les autres roches sédimentaires fluviatiles apparentées dans une stratigraphie dont il a déjà été établi qu'elle datait du Pléistocène dans le centre et le nord du Nouveau-Brunswick seraient probablement de l'Illinoien (soit entre 200 et 130 millions d'années). La présence de ce till, tout comme d'autres observations d'un écoulement glaciaire vers l'est qui avaient au départ été attribuées au tout début du Wisconsinien, seraient maintenant attribuées à la phase de Northumberland récemment définie connue comme l'Illinoien, du cycle de glaciation des Appalaches. Ce till est maintenant communément désigné comme le « till de Northumberland ».

D'autres phénomènes glaciaires dans l'ouest et le centre du Nouveau-Brunswick sont attribuables aux phases déjà définies du cycle de glaciation des Appalaches appartenant au Wisconsinien. Ainsi, l'écoulement glaciaire Caledonia du sud-est vers le sud-sud-est du Wisconsinien précoce à moyen a été à l'origine de formes terrestres induites par le mouvement des glaciers, d'une importante dispersion glaciaire, et de l'accumulation de till (soit le « till Caledonia »). Les scientifiques interprètent maintenant ces formations comme ayant subi les actions combinées de la plaque glaciaire des Laurentides et de la ligne de partage glaciaire Notre-Dame. L'étendue glaciaire maximale de la fin du Wisconsinien correspond à la phase Escuminac, caractérisée par un écoulement glaciaire du sud vers le sud-ouest (et vraisemblablement vers l'ouest), à partir du pôle glaciaire d'Escuminac dans le golfe du Saint-Laurent. Au cours de la phase néo-écossaise qui a suivi, le retrait des glaciers et l'amincissement de la plaque glaciaire a provoqué la désintégration du glacier Escuminac, puis engendré un mouvement d'écoulement glaciaire de l'est vers le nord-est, à partir du pôle glaciaire dans la région centrale du Maine.

L'amincissement continu des glaces a donné lieu à la phase de Chignecto, au cours de laquelle un écoulement glaciaire est survenu vers le nord, à partir de la ligne de partage glaciaire de haute-terres Fundy. À la fin de la phase de Chignecto, la crue des eaux provoquée par la formation de la mer tardiglaciaire De Geer a entraîné la scission de la ligne de partage glaciaire de haute-terres Fundy, ce qui a donné lieu à la formation de la mer intérieure acadienne, dans la vallée du fleuve Saint-Jean. Dans la région située au

sud-ouest du fleuve, les glaces ont disparu en raison de la stagnation régionale. Dans le nord-est, le pôle glaciaire résiduel de Gaspereau a connu un regain d'existence au cours de la phase de Collins Pond, en parallèle avec le bref stade glaciaire du Dryas précoce. Ce n'est qu'en certains endroits isolés que ces phases de la fin du Wisconsin ont donné lieu à la formation de till régional. Pour une large part, cette action s'est limitée à de petites traces d'érosion laissées par les glaciers et un refaçonnement du till Caledonia, ce qui a produit un till hybride possédant les propriétés physico-chimiques du till Caledonia, mais d'une nouvelle composition.

INTRODUCTION

At first glance, the surficial geology of the report area in west-central New Brunswick (Fig. 1) exhibits an appearance of simplicity. In comparison with nearby Nova Scotia, where thick Late Pleistocene sequences are common (Stea et al. 1998; Stea 2004), tills in New Brunswick are generally less than 3 m in thickness (Rampton et al. 1984). They typically overlie bedrock, apparently as a single stratigraphic unit. As such, they theoretically comprise the tripartite basal sequence of deformation till, lodgement till, and basal melt-out till, locally overlain by supraglacial ablation till and associated glaciofluvial, glaciolacustrine, or glaciomarine deposits (Seaman 2004). Rarely are more than two of these till types exposed at any one site; multiple tills of differing ages are exposed at only a few known sites (Rampton et al. 1984; Rappol 1989; Lamothe 1992; Seaman 2004; Seaman and McCoy 2008).

In contrast, the glacial erosion record of New Brunswick is extremely complex. On the basis of the striae record, Rampton et al. (1984, their Fig. 27) identified eight different Wisconsinan-age (Fig. 2) ice-flow patterns in west-central New Brunswick, as well as two areas with local flow attributed to decaying ice caps. Seaman et al. (1993) identified 16 separate ice-flow directions of regional extent in southwestern New Brunswick, in addition to several other directions of apparently local extent. Up to a dozen different striae sets, each marking a different ice-flow direction, have been observed on a single outcrop surface (Seaman 2000a).

The complex glacial history of west-central New Brunswick was first recognized by Chalmers (1884, 1885, 1890a, 1895, 1902), who ascribed glaciation to a regional 'Appalachian system of glaciers' (Chalmers 1890b, 1898a). Conversely, Goldthwait (1924), based on his work in Nova Scotia, advocated an alternative scenario wherein the Maritime provinces were glaciated by the far more extensive Laurentide Ice Sheet. Goldthwait's interpretation gained favour in Maritime Canada and also in adjacent New England, where Wisconsinan glaciation by the Laurentide Ice Sheet was (and remains, e.g., Borns et al. 2004) the standard model. In the absence of evidence for glacial or non-glacial events of Early or Middle Pleistocene age, all glacial events in New Brunswick were interpreted as Late Pleistocene—that is, of Wisconsinan age (Fig. 2; Gadd 1973).

Prest and Grant (1969) subsequently revived Chalmers' concept of glaciation in Maritime Canada by large local ice caps. They argued that the Laurentian Channel (traversing the modern Gulf of St. Lawrence and adjacent lower part of the St. Lawrence River valley) would have diverted a significant volume of the Laurentide Ice Sheet toward the east.

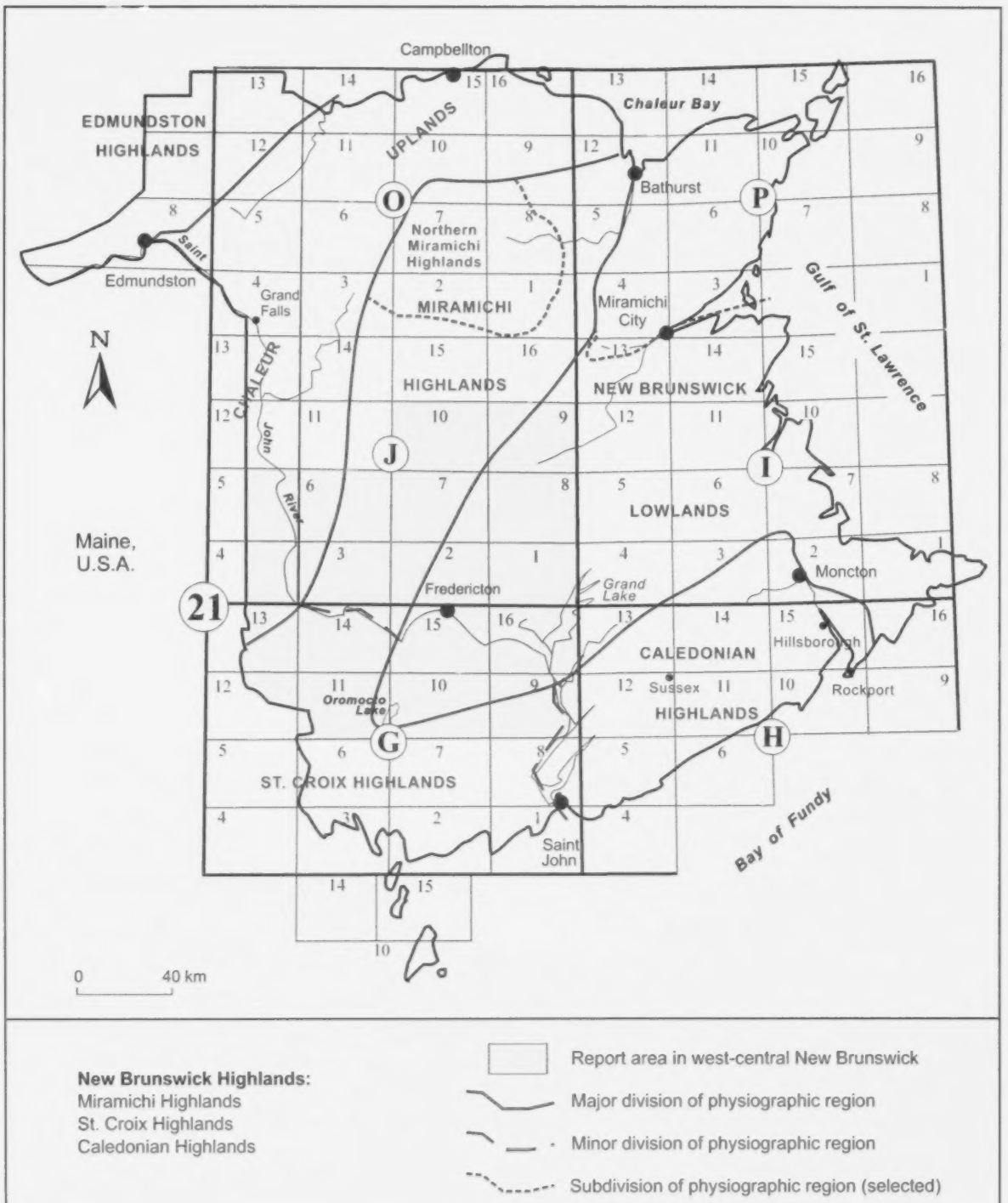

Figure 1. Location map of report area in west-central New Brunswick. Figure shows National Topographic System (NTS) map areas and some of New Brunswick's physiographic regions (after Rampton et al. 1984). See Figure 4 for expanded view of the report area and adjacent map areas in southern New Brunswick.

Epoch	Stage		^{14}C Age (ka)	Glacial Phase	Glacier Source	Features in West-Central New Brunswick
HOLOCENE			10			• alluvial deposits in stream valleys • colluvial deposits on steep slopes • bog deposits in topographic depressions • draining of Lake Acadia
PLEISTOCENE	Wisconsinan	Late	10	Collins Pond	Gaspereau Ice Centre	• Younger Dryas till at ice margins • Glacial Lake Acadia (Saint John River valley)
			11			• disintegration moraine formation • glaciofluvial deposits • Inland Sea Acadia (Saint John River valley)
			13	Chignecto	Fundy Highlands Ice Divide	• scattered N-trending striae • reorientation of Fredericton drumlins
			15	Scotian	Central Maine Ice Centre	• 'Scotian till' (in NE) • ENE glacial dispersal (in NE) • E- to NE-trending striae
			18	Escuminac	Escuminac Ice Centre	• local hybridization of 'Caledonia till' • common S- to SW-trending striae • possibly rare W-trending striae
			22		Inactive ice cover	• possibly local striation of bedrock
		Middle	30			
			40			
		Early	55	Caledonia	Laurentide Ice Sheet	• SE-trending fluted bedrock • 'Caledonia till' • SE to SSE glacial dispersal trains • common SE- to SSE-trending striae • ? early flow from highland ice caps ?
			75			
	Sangamonian				Deglaciated	• Half Moon Sediments • 'intertill sediments' (Lamothe 1992)
			130			
	Illinoian			Northumberland	White Mountains–Megantic Hills Ice Divide	• ESE-trending fluted bedrock • 'Northumberland till' • Carlisle ESE-trending dispersal train • old E- to ESE-trending striae
			200			

Figure 2. Stratigraphic column for the Quaternary geology of west-central New Brunswick.

They suggested instead that glaciation in the Maritimes was due to glaciers of limited size that extended only a short distance beyond modern shorelines. These divergent interpretations—one invoking the Laurentian Ice Sheet and the other advocating what came to be named the 'Appalachian Glacier Complex' (Stea 2004)—were termed the 'maximum' and 'minimum' models, respectively.

Grant (1977) presented additional arguments for the minimum model, based on investigations in Nova Scotia. Rampton et al. (1984), in their summary of New Brunswick's glacial history, identified four local glacial source areas: 1) the North Maine Ice Divide in northern Maine and adjacent New Brunswick, 2) the Notre Dame Ice Divide in Gaspésie, 3) the Gaspereau Ice Centre in central New Brunswick, and 4) the Escuminac Ice Centre in the western Gulf of St. Lawrence. Influenced by the minimum model, they also identified two nunatak zones in the province: one of Wisconsinan age in the Northern Miramichi Highlands in northern New Brunswick, and one of Late Wisconsinan age in the Caledonian Highlands in the southeast (Fig. 1).

Subsequent investigations in the onshore and offshore areas of the Maritimes revealed that elements of both the maximum and minimum models were correct. For example, it is now generally accepted that Late Wisconsinan glaciers extended to the continental shelf edge off Nova Scotia (Stea et al. 1998), as postulated in the maximum model, and that the proposed nunatak zones in New Brunswick were glaciated during the Late Wisconsinan (Seaman 2004). However, this extensive Late Wisconsinan glaciation is currently ascribed to the Appalachian Glacier Complex rather than to the Laurentide Ice Sheet.

Stea et al. (1998) and Stea (2004) published a revised Wisconsinan glacial framework for Maritime Canada, based on improved dating methods and on correlation with data from the Atlantic continental shelf. The framework identified five phases of glaciation, as shown below (Table 1).

Table 1. Wisconsinan glaciation phases in Maritime Canada, after Stea et al. (1998) and Stea (2004).

Stage	Phase	Age (ka)	Comments / Events
Late Wisconsinan	Collins Pond	c. 11–10	Phase corresponds with the Younger Dryas Stadial, during which remnant 'seed' glaciers were reactivated.
Late Wisconsinan	Chignecto	c. 13–12.5 (minor readvance)	Scotian Ice Divide broke into small separate ice caps, perhaps due to drawdown into the Bay of Fundy, prior to deglaciation of much of the Maritimes.
Late Wisconsinan	Scotian	c. 18–15	Thinning ice cover led to development of the Scotian Ice Divide over Nova Scotia, followed by glacial retreat c. 15–13 ka due to rising sea levels.
Late Wisconsinan	Escuminac	c. 22–18	Corresponds to Late Wisconsinan maximum, during which the Appalachian Glacier Complex extended eastward to continental shelf edge.
Early–Middle Wisconsinan	Caledonia	c. 75–40	–

Note: All dates in this report are cited in terms of uncalibrated radiocarbon years.

These glacial phases are conceptually similar to those of Rampton et al. (1984) in that they relate to glacial episodes and flow patterns. They differ from the earlier ones of Gadd (1973), which identified inferred ice-marginal positions at specific times during deglaciation. Stea et al. (1998) and Stea (2004) plotted their glacial phases on a regional map that encompasses eastern New Brunswick. The New Brunswick data were derived in part from the work of Pronk et al. (1989) in northeastern New Brunswick and of Foisy and Prichonnet (1991) in the eastern Caledonian Highlands (Fig. 1).

The current report summarizes the Pleistocene stratigraphy of west-central New Brunswick and shows how the area's complex glacial record correlates with the glacial model of Stea et al. (1998) and Stea (2004). Only limited revision of that model is required to explain observations in west-central New Brunswick, chief of which relate to the identification of a new phase, the Northumberland Phase, which precedes the Caledonia Phase and is interpreted to be of Illinoian age (compare Table 1 with Fig. 2). Due to the absence of strong dating control and stratigraphic continuity, many age assignments and correlations made herein are tenuous. However, the sequence of glacial events suggested by the Appalachian Glacier Complex model for the Wisconsinan is largely compatible with the glacial chronology of Seaman et al. (1993) for southwestern New Brunswick.

The remainder of this report is divided into three main sections: 1) the glacial phenomena of west-central New Brunswick, 2) the glacial stratigraphy of west-central New Brunswick, and 3) the glacial and interglacial history of the province, with particular emphasis on how that history affected and pertains to west-central New Brunswick.

Glacial Phenomena of West-Central New Brunswick

Introduction

The glacial phenomena of west-central New Brunswick are discussed below under:

- glacial erosion features and bedrock weathering, and
- glacial sediments (including basal till, ablation till, till fabric and glacial dispersal trends, and Canadian Shield erratics).

Glacial Erosion Features and Bedrock Weathering

Large-Scale Features

Large-scale bedrock flutings represent periods of extensive glacial erosion. The digital elevation model of west-central New Brunswick (Fig. 3) highlights an extensive area of large-scale bedrock fluting with an east-southeast trend, extending from the international border with Maine into central New Brunswick. Scattered, streamlined bedrock hills with this trend had been noted in the area, but the magnitude of these flutings was not apparent until such high-resolution, high-elevation imagery became available.

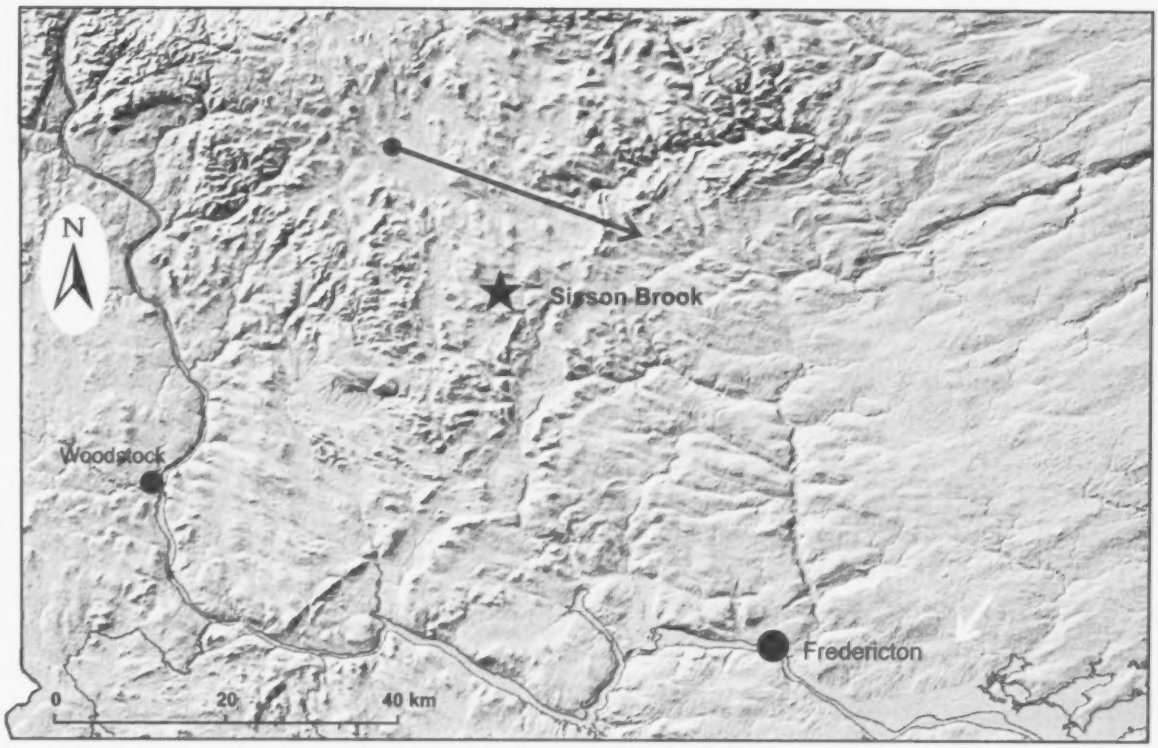

Figure 3. High-resolution image of west-central New Brunswick, showing large-scale east-southeast-trending bedrock fluting (red arrow). Also shown are southwest-trending fluting (yellow arrow: lower right corner) and east-northeast-trending fluting (yellow arrow: upper right corner). The high-resolution imagery data are from the Shuttle Radar Topographic Mission digital elevation model.

In contrast, conventional aerial photographs and topographic maps clearly reveal smaller, southeast-trending, glacially streamlined bedrock landforms in the McAdam area (Fig. 4) to the southwest (Stumpf et al. 1997). The fact that these southeast-trending landforms are more visible suggests that they overprint the larger scale landforms and thus relate to a later phase of glacial erosion and deposition.

Bedrock Weathering

Despite the apparent magnitude of glacial erosion in the province, weathered rock, particularly granite, is common in west-central New Brunswick. The preserved weathered granite is typically characterized by granular disintegration and the development of corestones. It resembles the lowermost part of Zone II or underlying Zones III or IV (Thomas 1974) of the characteristic granite weathering profile. The weathered rock is commonly overlain by relatively unweathered till (Fig. 5; Table 2; Chalmers 1898b) and locally is subject to glaciogenic deformation (Fig. 6; Broster and Seaman 1991). Weathered granite has even been observed at the up-ice end of a southeast-trending glacially streamlined bedrock hill at Parker Lake Ridge, 2 km west of Bolton Lake (Forest City map area, Fig. 4). Weathered bedrock is therefore an indicator of the fairly limited erosive ability of glaciers that inundated New Brunswick.

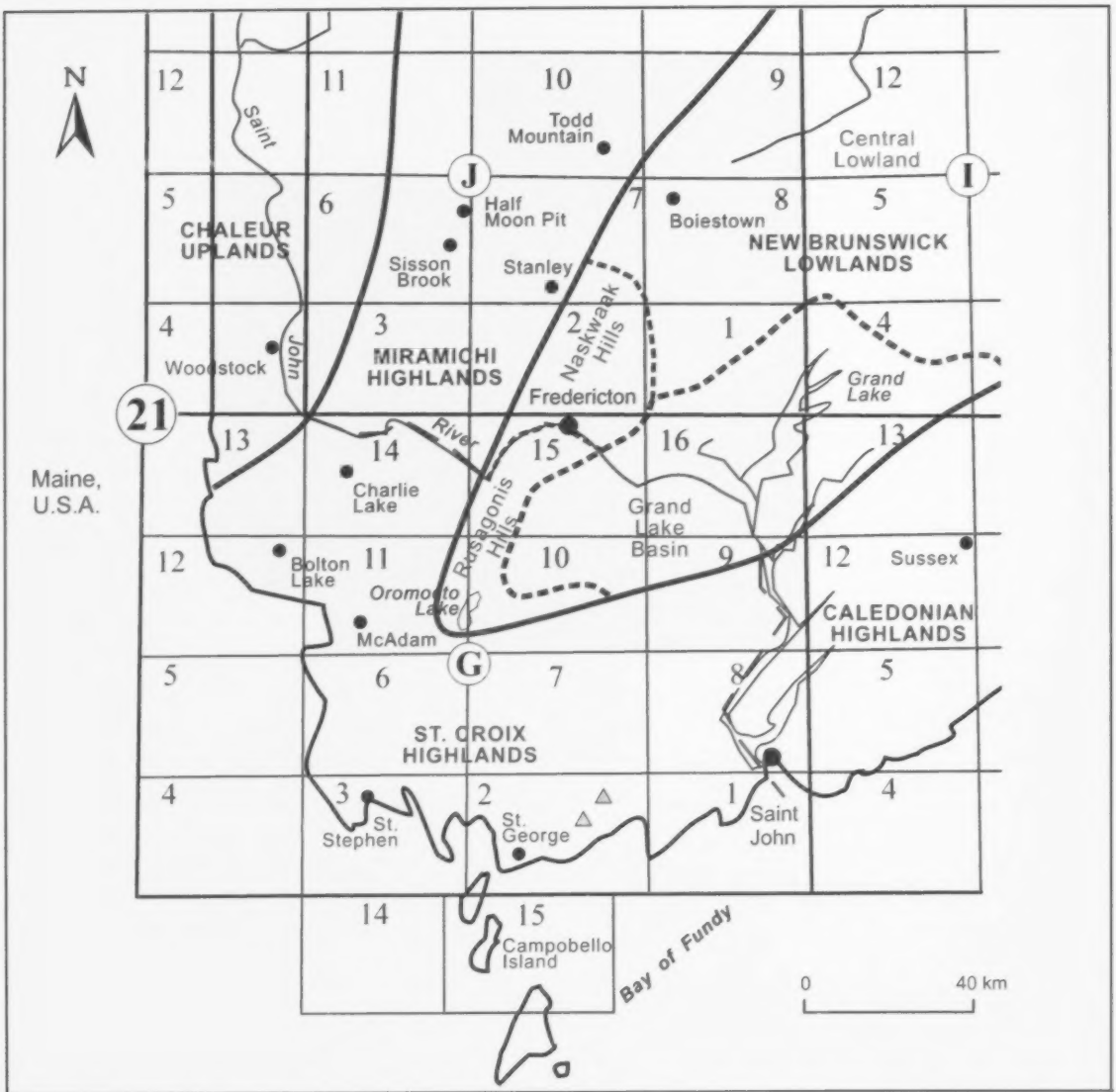

NTS Map Sheet	Map Area
21 G/02	St. George
21 G/06	Rollingdam
21 G/10	Fredericton Junction
21 G/12	Forest City
21 G/13	Fosterville
21 G/14	Canterbury
21 G/15	Fredericton
21 I/12	Blackville
21 J/03	Millville
21 J/06	Coldstream
21 J/07	Napadogan
21 J/09	Doaktown
21 J/10	Hayesville

△ Pennfield–Utopia delta complex

△ Pocologan delta complex

Report area in west-central New Brunswick

Major division of physiographic region

Minor division of physiographic region

Subdivision of physiographic region (selected)

Figure 4. Larger scale view of the report area, showing the place names, NTS map sheets, and NTS map areas referred to in the text. See Figure 1 for the location of this area in New Brunswick.

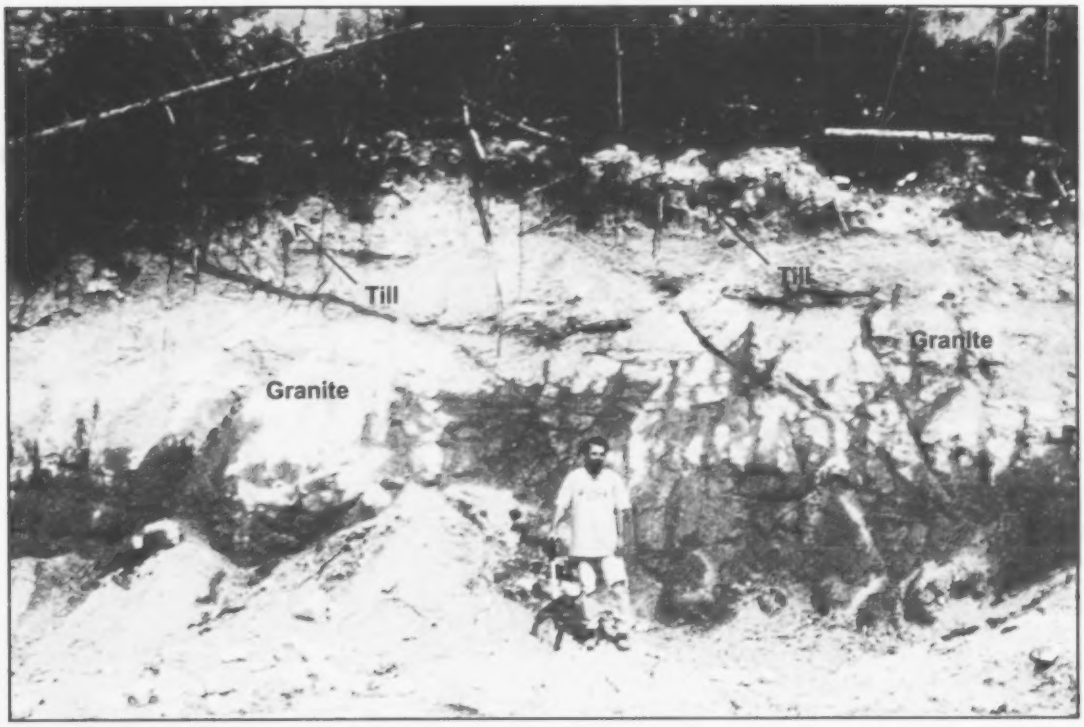

Figure 5. Thin basal till (with swallow-nest holes) overlying weathered granite bedrock at site AS030047, Hayesville map area (Fig. 4; Table 2).

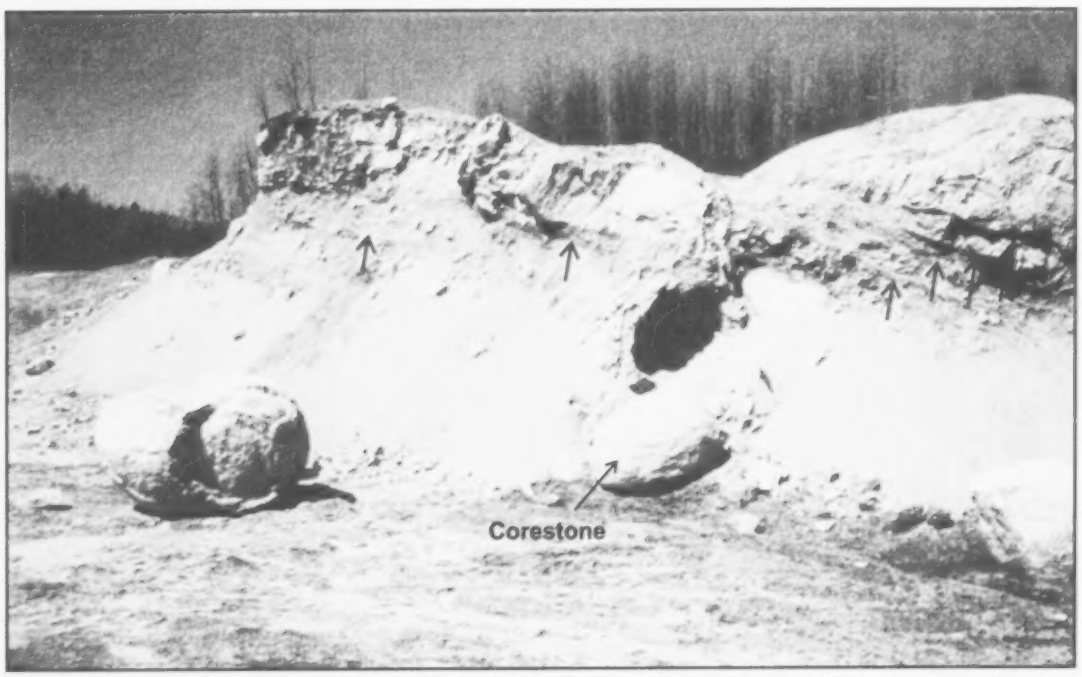

Figure 6. Glaciotectonic thrusting of weathered granite containing corestones near Charlie Lake, Canterbury map area (Fig. 4; Table 2). Red arrows indicate northward-dipping fault planes.

Table 2. Location details for sample sites shown as photographic figures in this report. Appendices 1 and/or 2 give additional data for some (**) sites.

	Site Number	NTS Map Area	Map Sheet	Latitude	Longitude
Fig. 5	AS030047	Hayesville	21 J/10	46°37.6'N	66°50.6'W
Fig. 6	near Charlie Lake	Canterbury	21 G/14	45°53.4'N	67°23.2'W
Fig. 8	97AS0009	Millville	21 J/03	46°06.5'N	67°22.3'W
Fig. 9	HV-P11.5 **	Hayesville	21 J/10	46°33.5'N	66°40.7'W
Fig. 11	HV-H19	Forest City	21 G/12	45°39.6'N	67°37.1'W
Fig. 12	FJ 88-40 **	Fredericton Junction	21 G/10	45°34.7'N	66°40.5'W
Fig. 13	CS-SB-01 **	Coldstream	21 J/06	46°22.2'N	67°02.8'W
Fig. 16	CS-W10b **	Coldstream	21 J/06	46°20.3'N	67°01.8'W
Fig. 17	MV-Q14 **	Millville	21 J/03	46°00.8'N	67°09.9'W
Fig. 18	AS030012a **	Coldstream	21 J/06	46°27.6'N	67°00.1'W
Fig. 19	AS030014a **	Coldstream	21 J/06	46°27.8'N	67°00.4'W
Fig. 20, 25	Sisson Brook exploration trench	Coldstream	21 J/06	46°22.2'N	67°02.8'W
Fig. 22	site FV-3	Fosterville	21 G/13	45°56.7'N	67°30.3'W
Fig. 24	site G2-119 (of Finamore and Seaman 1988)	St. George	21 G/02	45°07.4'N	66°49.4'W

Lee (1962) suggested that bedrock weathering in west-central New Brunswick was post-Carboniferous but pre-Wisconsinan. However, Anderson (1968) postulated that granite weathering began when the rocks were unroofed in the Late Devonian. Wang et al. (1981), working with residual granitic soils in northern New Brunswick, interpreted the weathering as pre-Wisconsinan and probably pre-Pleistocene. Rampton et al. (1984) identified the Caledonian Highlands and Northern Miramichi Highlands (Fig. 1) as nunatak zones, the former in the Late Wisconsinan and the latter throughout the Wisconsinan (Fig. 2), in part to account for deeply weathered granite in those areas. Rampton et al. (1984) argued that the weathered rock indicated a long interval of non-glaciation, implying it was both pre-Wisconsinan and Wisconsinan. However, subsequent investigations revealed that the weathered granite was overlain by till with only a Holocene weathering profile, and that similar weathered granite was locally present on most of the many granite batholiths elsewhere in New Brunswick. In addition, weathered basalt, gabbro, siltstone, sandstone, and conglomerate have been observed beneath Wisconsinan till.

The paleomagnetic signature of gossans (weathered orebodies) in northern New Brunswick indicates that gossan formation began no later than 1.05 Ma and no earlier than 2.3 ± 0.3 Ma (Symons et al. 1996). Gossanization and presumably other bedrock weathering in New Brunswick was therefore the result of Pleistocene weathering processes. Various lines of evidence support this interpretation.

- Tropical weathering depths are typically 20 m to 50 m, rarely exceeding 150 m, because erosion continually removes material from the profile top while weathering proceeds at the

bottom (Thomas 1974). Erosion of the Laurentide Ice Sheet by the Keewatin Ice Divide of the Laurentide Ice Sheet during the Wisconsinan removed 6 m to 20 m from the Canadian Shield (Kaszycki and Shilts 1980). Therefore, a few glacial cycles should be sufficient to remove any pre-Pleistocene regolith.

However, in northern New Brunswick, weathered granite appears in depths of up to 26 m (Veillette and Nixon 1982)—a remarkable thickness to have survived millions of years of subaerial erosional processes, plus several million years of glacial and periglacial erosional processes. Such a thickness strongly implies minimal glacial erosion throughout the Pleistocene. Yet this is contradicted by the presence of large-scale glacially streamlined bedrock landforms, and by the absence of evidence for a Pleistocene-long stratigraphy. Therefore, renewed weathering during interglacial or interstadial periods must have occurred.

- Many granites become disaggregated to considerable depth without significant chemical change; the very low clay content and preserved feldspars in such material (as is commonly observed in west-central New Brunswick) indicate comparatively recent alteration (Thomas 1974). Casual observations by the author confirm that granites in west-central New Brunswick can weather rapidly. In 1981, for example, in the Skiff Lake Granite (Forest City map area; Fig. 4; Lutes 1987), granite outcrops visible on 1976-vintage aerial photographs were devoid of glacial striae. However, the outcrops exposed after 1976 by road-building activities commonly exhibited striae. When water was splashed on these fresher bedrock surfaces to enhance striae visibility, air was audibly expelled from pore spaces as the water permeated the rock surface. This suggests that granite porosity allowed the glaciated surface to weather so quickly under current climatic conditions that exposed striae were eradicated in fewer than five years.

- The rapid weathering of granite may also be due in part to groundwater movement (Hunt 1972; Thomas 1974) and not just to surficial weathering processes. Weathering caused by groundwater activity may take place today beneath relatively unweathered till, as well as having occurred during previous interstadials or interglacials.

Given the foregoing points of evidence, most of the bedrock weathered in New Brunswick before the Pleistocene was likely eroded by Early Pleistocene glaciers. Newer weathered rock would have been generated during the interglacial and interstadial intervals before being at least partially removed during subsequent glacial intervals. Therefore, much of the weathered bedrock in west-central New Brunswick today probably was formed in the Late Pleistocene, in particular during the Sangamonian Interglacial Stage (Fig. 2). Moreover, weathering will have continued under current interstadial or interglacial conditions.

Small-Scale Features

Despite the widespread occurrence of weathered bedrock in west-central New Brunswick, glacially polished and striated bedrock surfaces are common, particularly on the harder and less permeable lithotypes such as fine-grained igneous rocks, wackes, and metasedimentary

rocks. The small-scale glacial erosion features range in size from striae to roches moutonnées. The smoothed stoss sides and angular lee sides of the latter, plus smaller features such as rat-tails, wedge and nailhead striae, and crescentic scars provide definitive evidence of ice-flow direction (Prest 1983; Seaman 1991, his Fig. 7).

Lists of glacial striae in the province, including parts of west-central New Brunswick, have been published by several authors (Robb 1851; Hind 1865; Mathew *[Matthew] 1*879; Chalmers 1884, 1885, 1890a, 1895, 1902). The author used data from these lists, as well as from geological maps and reports, and field investigations conducted in 1988, to generate an ice-flow direction map for New Brunswick (Seaman 1989a, 1989b; summarized as ranges in Seaman 1991). This work enabled the identification of definite striae trends in west-central New Brunswick, ranging from north-northeastward (018°) clockwise to southwestward (231°). Subsequent investigations have added rare westward-, northwestward-, and northward-trending ice-flow indicators to the known ice-flow trends. Figures 7a and 7b show plots of observed striae trends in west-central New Brunswick, determined on the basis of all currently available data, and grouped into their respective NTS map areas (Fig. 4).

Striae Chronology

In the absence of a depositional stratigraphy, Rampton et al. (1984) attempted to develop an erosional stratigraphy for New Brunswick, using cross-cutting relationships between striae sets. On the basis of limited available data, the authors suggested multiple interacting ice centres. They also implied parallel ice-flow events of different age. For example, they proposed an early Caledonia flow pattern that paralleled the later Tay and St. Stephen flow patterns. They also noted that some striae assigned to the eastward-trending Kent flow pattern might actually belong to an earlier east-trending ice-flow event.

Subsequent striae mapping studies by Seaman (1991) showed that the limits placed on supposed individual ice centres in west-central New Brunswick were simply an artefact of incomplete data. This led Seaman et al. (1993) to propose glaciation by a single regional ice centre that migrated over time, generating the observed variety of ice-flow directions. The striae chronology of Seaman et al. (1993, their Fig. 7, 8) suggested initial southward flow, followed by a shift to southeastward flow, then back to southward and southwestward, and then a shift back to southward followed by southeastward, eastward, and east-northeastward. Such a chronology can encompass up to three separate ice-flow events with the same specific trend in the southeast-to-south compass sector.

More recently, several new sites have been investigated with definitive cross-cutting relationships (cross-cutting striae on rat-tails, bevelled grooves, or bevelled outcrop surfaces), all of which are compatible with the chronology of Seaman et al. (1993). These cross-cutting relationships (Table 3) in southern New Brunswick confirm that every ice-flow direction between 130° and 185° may have occurred at least twice. For example, at site 97AS0009 in the Millville map area (Fig. 4), fine to medium striae with a north–south orientation occur on an older roche moutonnée with parallel, medium to coarse striae trending toward 150° (Fig. 8a,

8b). A similar cross-cut chronology appears elsewhere in the region. However, at site 98AS0281, also in the Millville map area, an early south-trending rat-tail that formed behind an epidote 'knot' is strongly cross-cut by later striae with a 150° trend. This latter chronology occurs at several other sites in southwestern New Brunswick and also was observed by Chalmers (1890a, his site No. 89) in the southeast.

In general, there is no way to reliably age-correlate striae sets with similar trends between one outcrop and another. Therefore, it is impossible to state with certainty the relative ages of the two foregoing flow trends. Did the trends shift from 180° to 150° to 180°, or from 150° to 180° to 150°? Or was the situation even more complex than these two scenarios? The same restriction applies to other pairs of striae trends that show conflicting cross-cutting relationships. Note that such conflicting relationships are not restricted to west-central New Brunswick, as similar observations have been made in northeastern New Brunswick (Parkhill and Doiron 2003).

Glacial Sediments

Basal Till

Basal till represents the dominant surficial material of glacial origin in west-central New Brunswick, outside of valleys that may contain significant accumulations of ablation till, or of glaciofluvial, glaciolacustrine, or glaciomarine sediments. As noted above, the basal till may consist of deformation, lodgement, and basal melt-out till (Fig. 9). Since 1990, multiple basal till types have been sampled at several individual sites in the report area as part of the ongoing till geochemistry investigations by the New Brunswick Department of Natural Resources (NBDNR). Analytical results indicate that the deformation tills, commonly of the subtype referred to as local till (Dreimanis 1976), are geochemically and physically more representative of local bedrock than are the other two basal till types. Lodgement and basal melt-out tills are geochemically and lithologically indistinguishable, but the latter tills tend to be less compact and somewhat coarser than the former.

Rampton (1984) mapped most of west-central New Brunswick as either 'morainal veneer' (till that is generally <0.5 m thick over bedrock) or 'morainal blanket' (till that is 0.5–3 m thick). Subsequent till geochemistry work (e.g., Seaman 2007) suggested that basal till is rarely less than 0.5 m thick, except locally on steep bedrock slopes, and that 'morainal blanket' is the norm. Moreover, till can be locally extremely thick, particularly in valleys. One study describes 47.5 m of till overlying sand and gravel in a borehole at the mouth of the Oromocto River east of Fredericton (Lee 1957, his locality 18BH; Appendix 2). Another study reports a borehole (Lamothe 1990a, No. 3033) in the Keswick River valley northwest of Fredericton that penetrated "an impressive 60 m of continuous till which is visually consistent in terms of texture and colour" (Lamothe 1992, p. 16); Lamothe (1992) noted no significant geochemical variation in the 66 samples collected from the borehole core. In contrast, Seaman and McCoy (2008) used geochemistry, fabric, and textural characteristics to identify three different basal tills in an approximately 7 m deep exploration trench at Sisson Brook (Fig. 4), 38 km north-northwest of Fredericton.

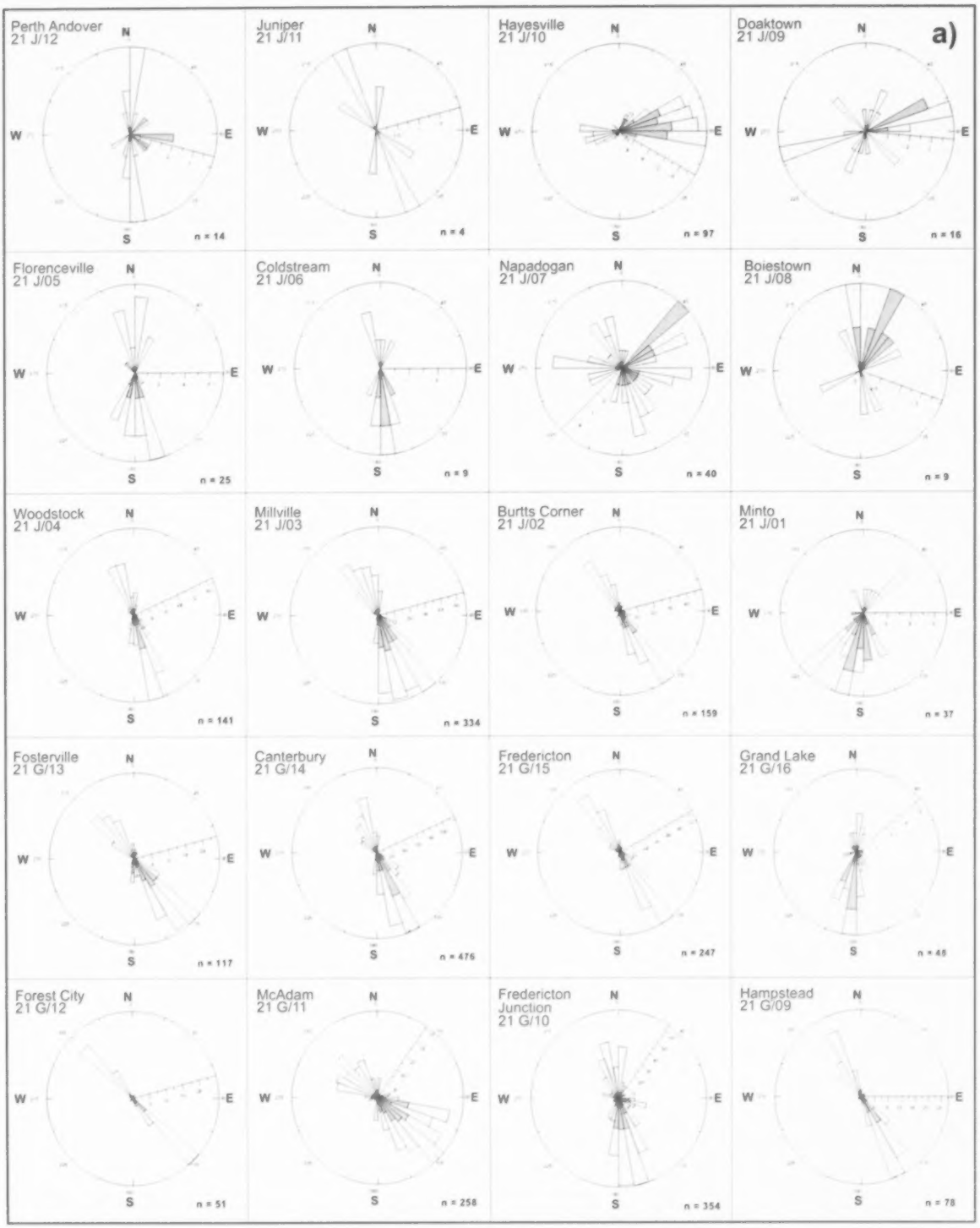

Figure 7. Summary diagrams of glacial striae trends in west-central New Brunswick. Green shows definite azimuths of ice flow, as indicated by rat-tails and other small-scale glacial features. Yellow shows striae of indefinite orientation with both possible azimuths of ice flow plotted. This figure (Fig. 7a) presents rose diagrams, which magnify the most common striae trends.

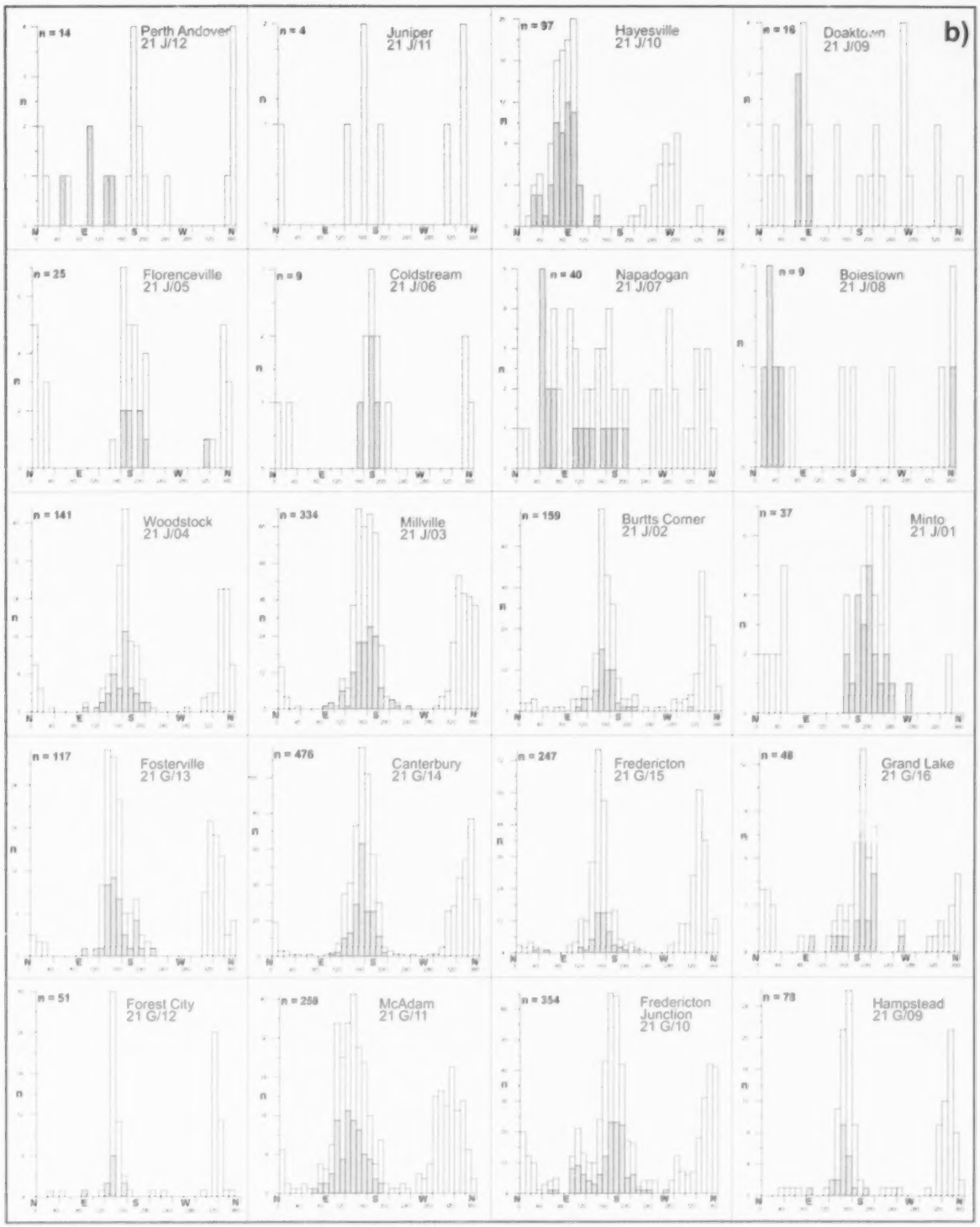

Figure 7b. Diagrams showing the same azimuths of ice flow as in Figure 7a, but plotted as histograms. The histograms reveal that, while the dominant ice-flow trend varies from one NTS map area to the next, the same trends tend to occur throughout the report area. n = number of measurements.

Table 3. Cross-cutting relationships among striae in southern and central New Brunswick.

Unique			Contradictory			
A	B	A→B	A	B	A→B	B→A
025°	090°	G	055°	095°		R&P
040°	025°	G, R	060°	100°	R&P	
040°	175°	R&P	065°	100°		G
050°	070°	R	065°	105°	R&P	
055°	045°	G	070 °	110°		R&P
055°	070°	G	090°	145°	R&P	
090°	065°	R&P	090°	150°		G
100°	115°	G	115°	125°	R	
105°	045°	G	115°	130°		G
115°	150°	G	120°	130°	G	
120 °	140°	G	125°	160°		R
120°	200°	R&P	130°	160°		R
120°	255°	R&P	130°	165°	R&P	R&P
130 °	095°	R&P	130°	175°		G
135°	075°	ML	135°	170°	R&P	
135°	090°	G	135°	150°		G, R
140°	075°	R	140°	150°	G, R	G, R
140°	100°	R	145°	155°	G, R	
140°	105°	G	140°	160°	G, R	G, R
140°	130°	G	140°	165°	G	G, R
140°	210°	R	145°	165°	G	R
145°	105°	R	140°	170°	G, R	
150°	190°	G	140°	175°		G
150°	200°	G	145°	170°		R&P
155°	060°	G	150°	160°	G, R	
155°	070°	G	150°	165°	G	R
155°	190°	R	150°	170°	G, R	
155°	200°	R&P	155°	160°	G	G
155°	225°	R&P	155°	165°		R
155°	255°	R&P	155°	170°	G, R	
160°	100°	R	160°	165°	G	
160°	115°	G	160°	170°	G	G
165°	095°	R&P	145°	180°	G	
165°	105°	G, R	150°	175°	G, R	
165°	270°	R	155°	175°		Ch
175°	115°	R	150°	180°	G, R	R
175°	180°	R	150°	185°	R	
180°	120°	R	155°	180°	R&P	
180°	195°	G	160°	175°		R
185°	125°	R	165°	180°	G, R	
185°	260°	R	170°	175°		R
195°	135°	G, R	165°	185°	Ch	R
210°	190°	R	165°	200°	R&P	Ch
220°	100°	G	170°	190°		G
220°	120°	G	175°	190°	R	
220°	130°	G	180°	200°	R	
220°	200°	R&P	180°	205°		G
225°	290°	R&P	175°	210°	R	
240°	130°	G				
255°	200°	R&P				

Codes Used

G	Cross-cut groove or coarse striae
R	Cross-cut rat-tail or glacial fluting
Ch	From Chalmers (1884)
ML	From Lamothe (1990b)
R&P	From Rampton and Paradis (1981a–c)
	NTS 21 J
	NTS 21 G
	NTS 21 G and 21 J
	NTS 21 G, 21 H, and 21 J
	NTS 21 H
	NTS 21 I

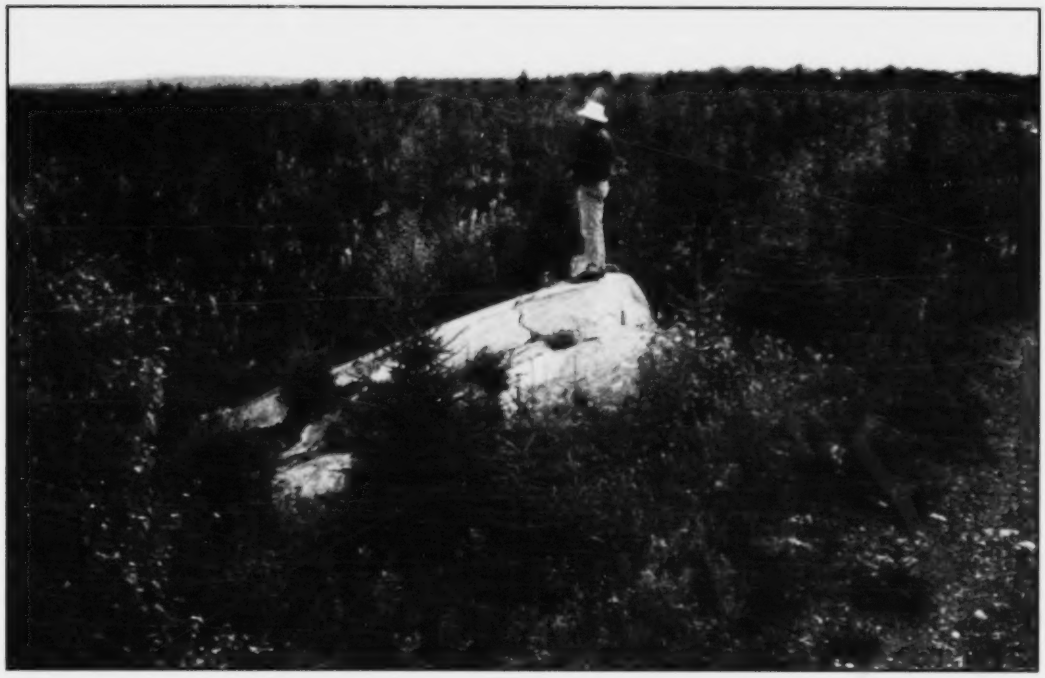

Figure 8a. Roche moutonnée oriented south-southeast at site 97AS0009, Millville map area (Fig. 4; Table 2).

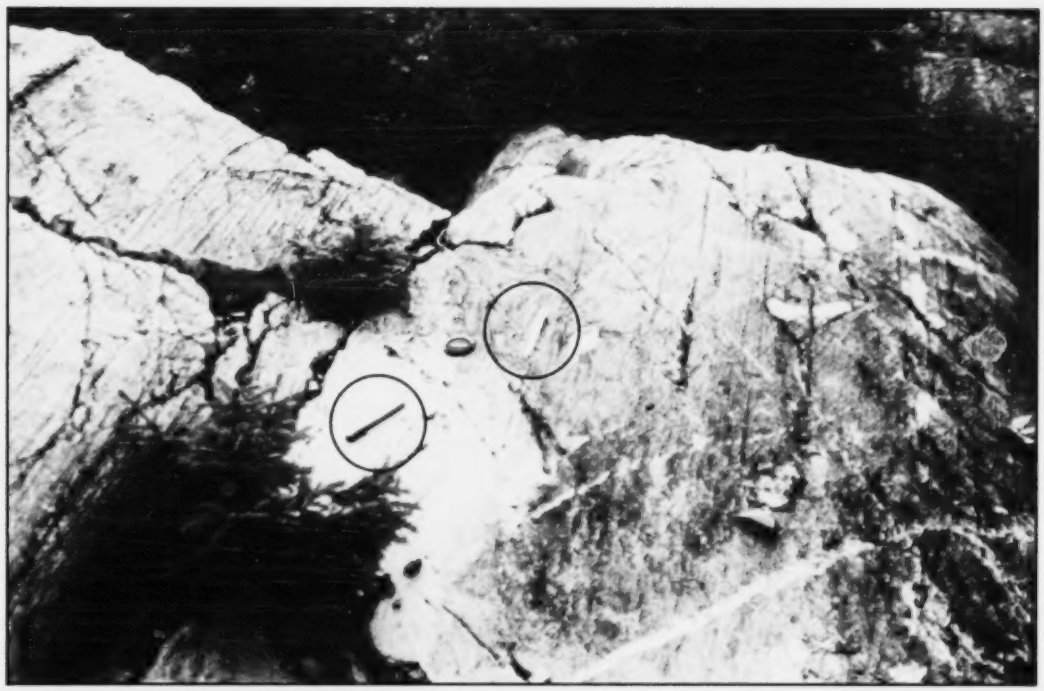

Figure 8b. Upper surface of the roche moutonnée in Figure 8a, showing parallel 150° ± 2° medium to coarse striae (circled white pen) cross-cut by later 181° ± 2° fine to medium striae (circled blue pen).

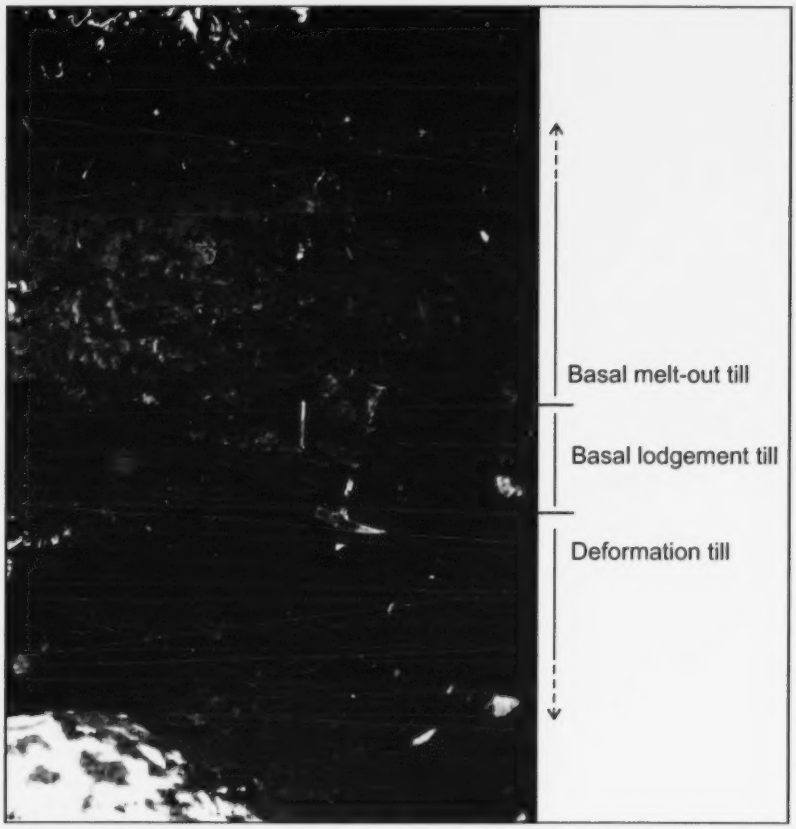

Figure 9. Basal melt-out till, basal lodgement till, and deformation till at site HV-P11.5 near Todd Mountain, Hayesville map area (Fig. 4; Table 2). Hammer handle is 30 cm long.

Thick basal till may also be present in drumlins. These features are most common in the southwestern part of the report area, where their southeast trends are comparable with those of large-scale bedrock flutings in the same area. Without excavating or seismic profiling, it cannot be determined whether some apparent drumlins are composed of till, till with a rock core, or rock with a till blanket or veneer. About 9+ m of sandy till was observed in a cut through one of several drumlins in a small drumlin field immediately southeast of Fredericton (Lee 1957). Several boreholes were subsequently drilled in the field, and one core was stored at the NBDNR core building in Fredericton. The upper 5.8 m of material was not recovered, but the lower 17.7 m, overlying bedrock, was logged (J.J. Thibault, pers. comm., 1986) as a uniform, reddish, sandy silt to silty sand till. Stoss faces on some of the Fredericton drumlins appear to be to the south-southeast (Fig. 10), suggesting shaping by ice flow toward the north-northwest.

Ablation Till

Ablation till is also known as superglacial or supraglacial melt-out till (Dreimanis 1976). It appears throughout west-central New Brunswick but is most common in the southwestern part of the report area. Mappable ablation moraines tend to lie in topographic depressions (Seaman et al. 1993). The ablation till typically thins upslope into a patchy veneer or blanket over basal till, transitioning into surface boulder accumulations of varied concentration (Seaman 1992). This suggests that the deglaciation of west-central New Brunswick occurred by regional stagnation and downwasting (Seaman et al. 1993), rather than by ice-marginal retreat, as suggested by Gadd (1973) and Rampton et al. (1984).

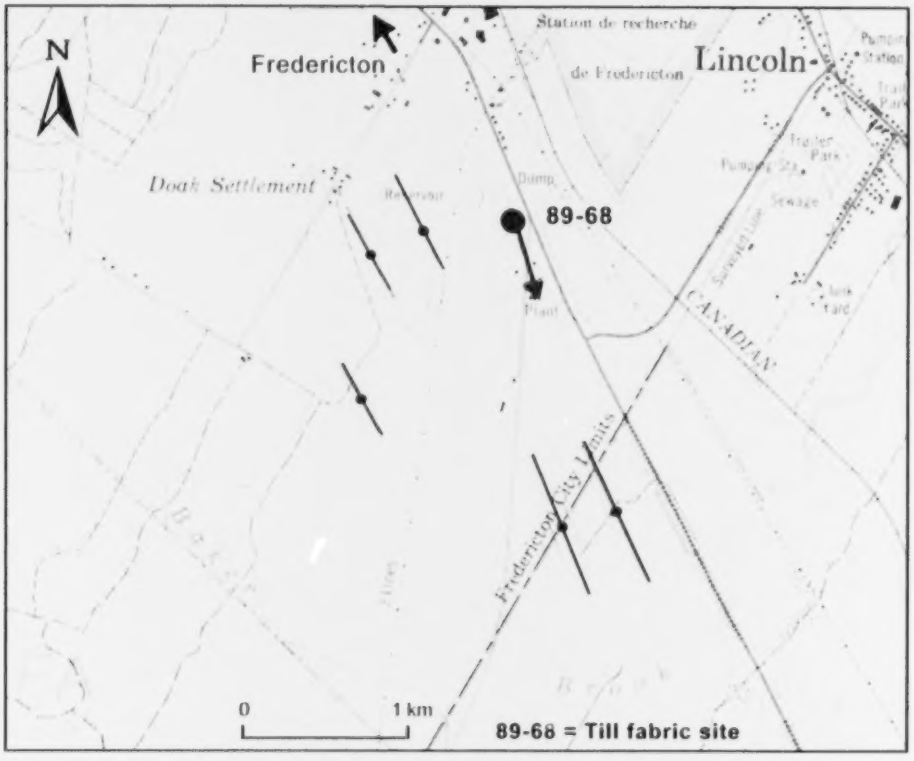

Figure 10. Fredericton drumlin field (short red lines) in the Fredericton map area (Fig. 4). The apparent south-southeast stoss faces (blunter ends of the topographic contours) imply formation or reworking by north-northwest ice flow.

Ablation till is the last strictly glacial deposit of a melting glacier and thus is expected to contain more distally derived material than would the underlying basal till (Dreimanis 1976). However, this is commonly not the case in southwestern New Brunswick (Seaman 1992; Stumpf 1995). For example, ablation till over the Skiff Lake Granite tends to be more granitic than the underlying lodgement till (Seaman 1992). At site FC-22 (site FC-E19b in Seaman 1999a), a pebble sample from the surface ablation till unit contained 86% granitic clasts, whereas a similar sample from the immediately underlying basal till contained only 9% granitic clasts (Seaman 1992, 1999a). Granitic hills in this area are glacially streamlined and mantled by basal till dominated by pebbles of distal derivation. In addition, many of the granitic boulders are somewhat rounded, suggesting they were entrained as corestones from previously weathered bedrock. Therefore, granitic material in the ablation till (Fig. 11) could not be derived from late-glacial nunataks in this area.

Hicock (1987) described a similar relationship in northern Ontario, where a relatively proximal non-calcareous ablation till overlies a distal calcareous basal till sequence down-ice of an upland area. To explain the relationship, he proposed a standing wave analogy, whereby proximal material eroded from the stoss side of the upland was upsheared into the englacial and supraglacial zones by compressive flow; down-ice, in the lee of the upland, extending flow led to downshearing of distal material from the englacial zone into the basal zone and subsequent deposition as a distal basal till. Later downwasting of the Laurentide Ice Sheet deposited the more proximal material from the upper part of the glacier as ablation till.

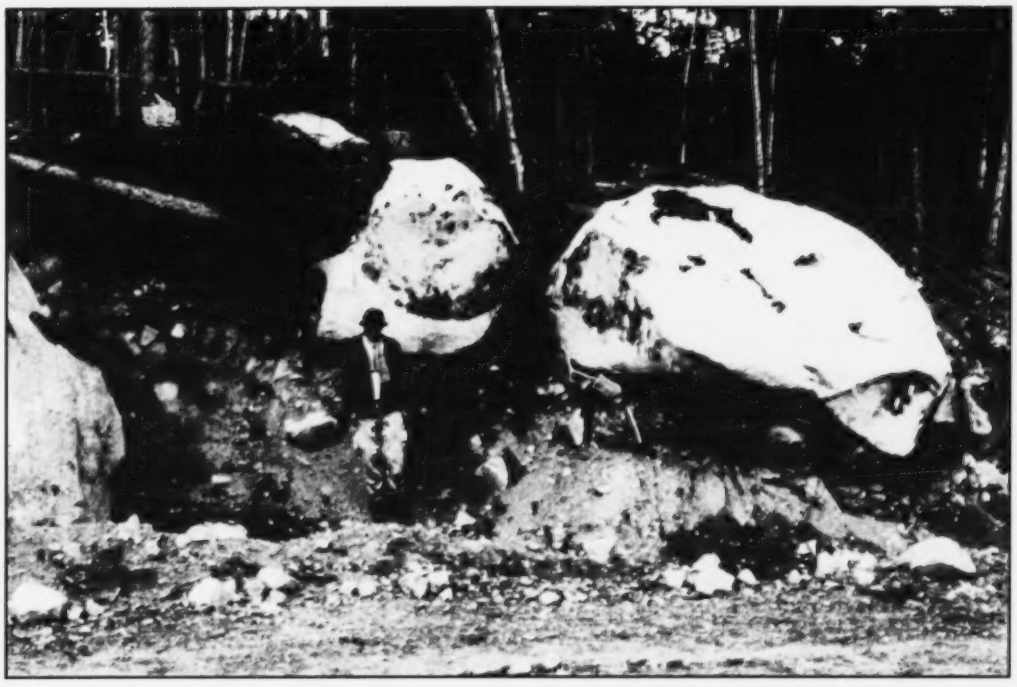

Figure 11. Ablation till, 150 m west of site HV-H19, Forest City map area (Fig. 4; Table 2).

Hicock's analogy involves an essentially unidirectional ice-flow vector, a simpler context than in west-central New Brunswick, where multiple ice-flow vectors were present in the same ice mass. However, the analogy applies to the hilly granitic terrain of west-central New Brunswick. Upshearing by compressive flow in the stoss zone early in the glacial episode carried granitic material into the upper part of the glacier, while downshearing deposited distal till in the lee zones. With subsequent shifts in the ice-flow vector, the distal basal till was spread over much of the granitic terrain. Meanwhile, the proximal material, eventually deposited as ablation till, was transported over a circuitous route (Seaman 2004). Consequently, upon glacial stagnation and melt-out, the granitic supraglacial material, which was derived either from the local bedrock or more likely from similar granitic units along the structural trend to the northeast, was coincidentally deposited onto the underlying distal till.

Till Fabric Trends

The orientations of basal till fabrics from west-central New Brunswick show a diversity comparable with that of the striae (Appendix 1). Trends can vary significantly over only a few kilometres (Seaman 1991, 2006). Till fabric trends from southwestern New Brunswick were originally interpreted to be of questionable value, due to the limitations imposed by clast shape (Seaman 1991). In hilly areas, many till fabrics are aligned parallel to the trend of bedrock slope (Sacré 1989; Seaman et al. 2005). Such till fabric trends could indicate fabric reorientation by postdepositional downslope movement (Sacré 1989; Lamothe 1992). However, Seaman et al. (2005) showed that the till fabric at one site (HV-NP07 in Appendix 1) was parallel to the last of three striae sets on an adjacent bedrock outcrop, indicating that the fabric was generated by late downslope movement of a glacier.

Several problems are associated with till fabric measurements.

- Clasts in the subglacial environment can be aligned either longitudinal or transverse to the direction of glacial flow (Flint 1971). It is commonly assumed that a unidirectional fabric (Fig. 12) with a significant degree of imbrication is formed by longitudinal clast orientation, with the ice-flow direction indicated by the average updip azimuth. A bidirectional fabric with updip trends in opposing directions may indicate either a transverse fabric or a longitudinal fabric with no significant imbrication. A trimodal fabric (Fig. 13) could indicate a transverse fabric with a superimposed longitudinal fabric that identifies the azimuth of ice flow.

- Fabric orientation can be affected by clast content of the till. In till with sparse clasts, pebbles can align with the subglacial stress field without interclast interference. However, in a gravelly till (common in west-central New Brunswick), interactions between clasts can force individual pebbles to lodge in an alignment oblique to the stress field. The result is a more diffuse fabric with a greater uncertainty range around the statistically inferred ice-flow trend.

- Till fabrics are measured with respect to the horizontal. Theoretically, longitudinally aligned clasts are generally deposited with an imbrication that lies up-ice with respect to the depositional surface (Flint 1971). However, this depositional surface typically differs from the horizontal, and may or may not lie parallel to the bedrock surface. In addition, end-over-end overturning of clasts can result in clasts with reverse imbrication with respect to ice flow.

Consequently, till fabrics alone cannot be used to infer ice-flow direction.

The variety of till fabrics in west-central New Brunswick is now interpreted to be largely the result of local reworking of previously deposited till by glaciers of limited erosive power. Piotrowski et al. (2004) provided a conceptual model for this phenomenon, recognizing that the subglacial bed could comprise a mosaic of deforming and stable zones. Therefore, an earlier deposited till at one location may be reworked during a subsequent ice-flow phase, while the same till at nearby sites may be reworked by a different ice-flow phase, or not reworked at all. Tills formed by one ice-flow event, and then reworked and reoriented by a later ice-flow event, are referred to as hybrid tills (Allard 2003; Allard and Pronk 2003).

Glacial Dispersal Trains

In 1990, the NBDNR began regional till geochemistry investigations in the highland areas of west-central New Brunswick, using a 2 km sample grid spacing. Recently, the Department commenced reconnaissance-scale till geochemistry sampling over the New Brunswick Lowlands (Fig. 1) and marginal parts of the adjacent highland areas, using a 10 km sample grid spacing (Seaman 2007). Despite the complexity exhibited by the glacial striae and till fabric data, these till geochemistry investigations have identified several major glacial dispersal trains (Fig. 14).

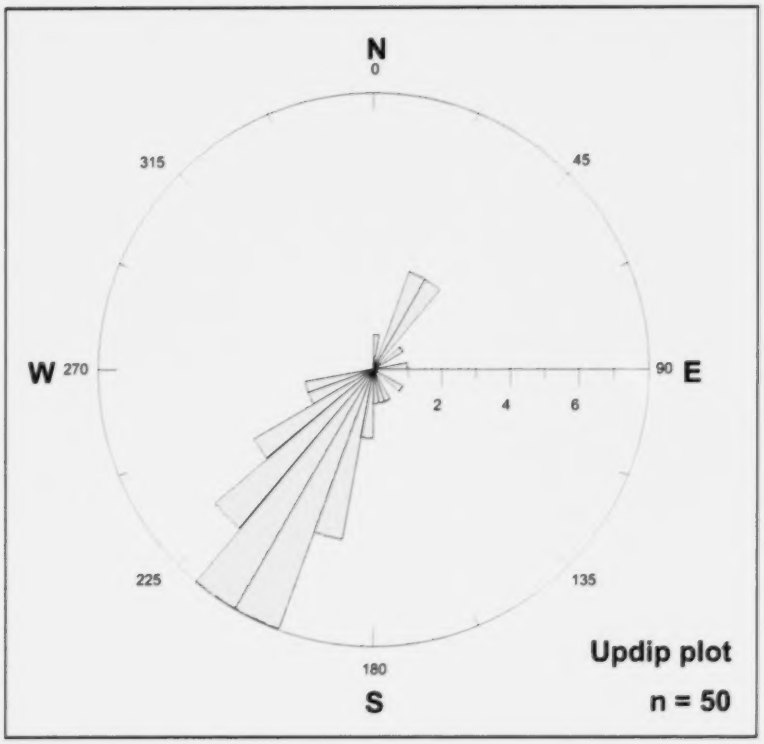

Figure 12. Unidirectional till fabric at site FJ 88-40, Fredericton Junction map area (Fig. 4; Table 2). n = number of measurements.

Fabric is interpreted to indicate a south-southwest to southwest ice flow.

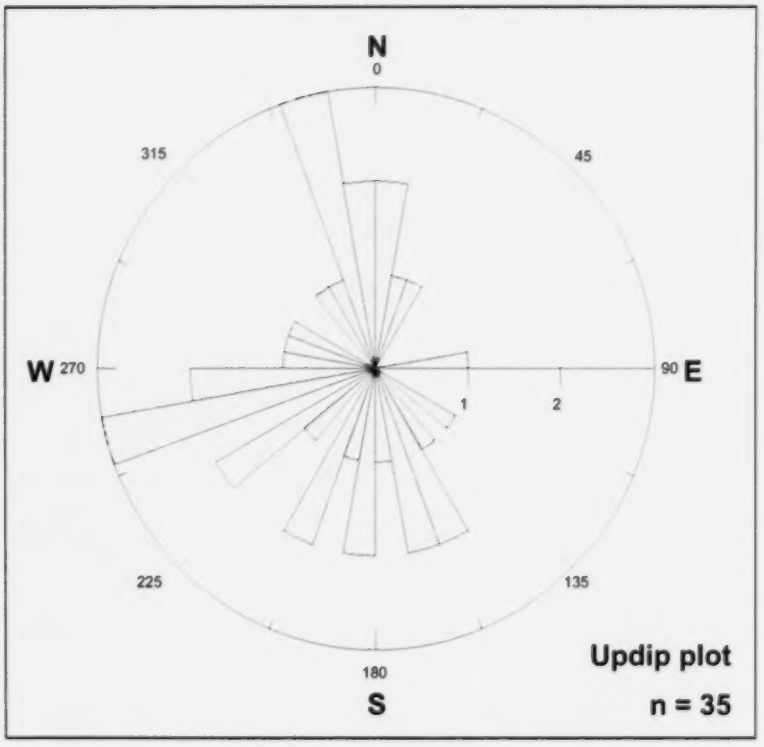

Figure 13. Trimodal till fabric at site CS-SB-01, Sisson Brook, Coldstream map area (Fig. 4; Table 2).

Fabric is interpreted to indicate a west-southwest ice flow, with transverse clasts aligned to the north-northwest and south-southeast.

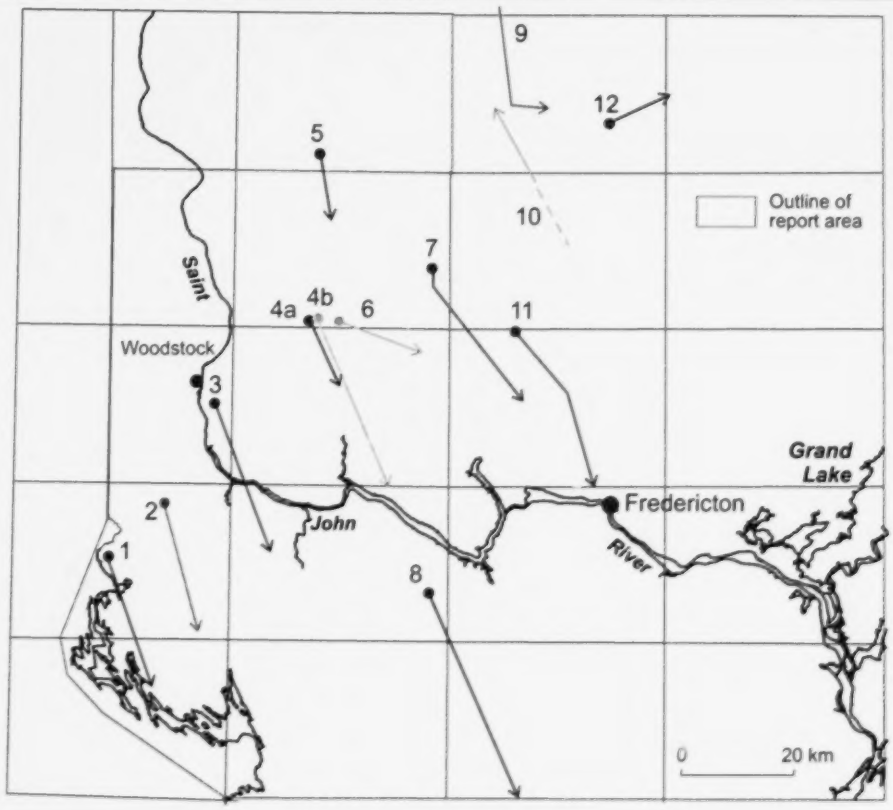

	Dispersal Train	Dispersal Indicator
1	Poplar Mountain	gold
2	Oak Mountain	mafic volcanic clasts
3	Connell Mountain	copper
4a	Cloverdale	arsenic and antimony
4b	Cloverdale	reddish till
5	Foreston	lead and zinc
6	Carlisle	reddish till
7	Sisson Brook	bismuth and tungsten
8	Lake George	antimony
9	Clearwater Brook	gabbric clasts
10	McLean Brook	clayey material
11	Fredericksburg	barium
12	Trout Lake	beryllium and granitic clasts

Figure 14. Major glacial dispersal trains in the report area. Figure 1 shows the location of this area in west-central New Brunswick.

Indications of early east-southeastward dispersal appear in the western part of the report area, where Seaman (2000a) identified a fragmentary east-southeast trending dispersal train of reddish till derived from an outlier of red Carboniferous clastic sedimentary rocks of the Carlisle Formation. Clasts of this reddish till occur in the regional yellowish brown till of the area (Seaman 2004), confirming that the east-southeastward dispersal was an earlier event.

In central New Brunswick, dispersal from the Sisson Brook tungsten–molybdenum–copper deposit is aligned southward for the first few kilometres, probably due to deflection of basal ice flow by the north-northeast trending Nashwaak Ridge (Seaman 2002). The dispersal direction then is aligned southeastward from where basal ice crested the ridge. The dispersal train for bismuth from this source extends for at least 26 km (Fig. 15). Southeastward glacial dispersal is also reported for southwestern New Brunswick (Allard 2003; Allard and Pronk 2003).

A short distance to the east of Sisson Brook, a dogleg dispersal train in barium associated with the Fredericksburg antimony anomaly (Fig. 14; Seaman 2008) appears to trend first southeast, and then south-southeast (Seaman 2007). This suggests that the southeastward dispersal preceded that toward the south-southeast. In the western part of west-central New Brunswick, the dominant trend is south-southeastward (Seaman 2000a). Evidence for south-southeastward dispersal also occurs in the northern part of the Hayesville map area (Fig. 4; Seaman et al. 2005).

In the northern part of the report area, dispersal trains trend toward the east to northeast (Sacré 1989; Lamothe 1992; Seaman et al. 2005), and tend to be shorter than those elsewhere in the region. They truncate south-southeast-trending dispersal trains, suggesting they are related to a younger glacial event (Seaman 2006). Evidence for late north-northwestward dispersal also occurs in this area (Seaman et al. 2005; Seaman 2006).

Many of these dispersal trains are characterized by either irregular margins or 'gaps' in the contours defining the train, as exhibited by the Sisson Brook dispersal train (Fig. 15). Both of these characteristics could result from dispersal trains being formed during one ice-flow event and then being reworked or partially buried by one or more subsequent events. However, these characteristics could also result from variations in till thickness and sampling depth (A.G. Pronk, pers. comm., 2009).

Two examples show that dispersal trains in west-central New Brunswick have undergone local reworking or burial.

1. At site CS-W10b (Table 2; Appendix 1), in highly anomalous till within the proximal part of the Sisson Brook dispersal train, the till fabric orientation (Fig. 16) exhibits an updip imbrication to the northeast with an average dip of 14° with respect to the horizontal. The bedrock surface slopes northeastward, so the actual angle of imbrication with respect to the probable depositional surface is greater.

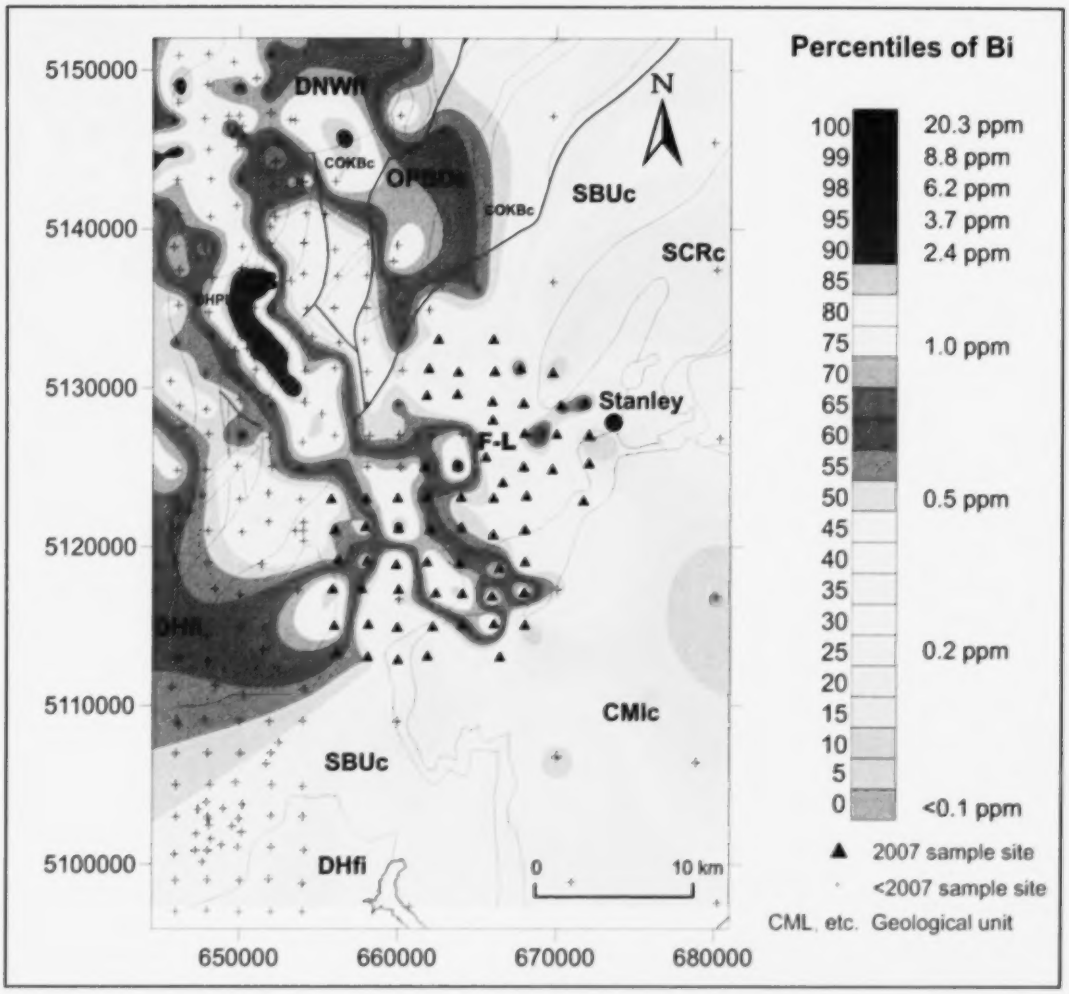

Figure 15. Sisson Brook bismuth (Bi) dispersal train in basal till. Figure 4 shows the location of the Village of Stanley (marked here) in west-central New Brunswick.

Fine striae with this trend occur about 15 km to the east-northeast on bedrock surfaces at sites AS030004 and AS030009. At site AS030004, ice-flow direction is indicated by bevelling of an older groove and lee-side plucking. Site AS030009 exhibits ten striae sets, ranging in orientation from northeastward clockwise through to southward. The northeast-trending striae set (flow direction confirmed by wedge striae, lee-side plucking, and a knob-and-tail in the lee of a cherty horizon) was one of the younger sets; it bevelled an east-southeast-trending groove and was finer and more abundant than the southeast- to south-oriented sets. The till fabric at nearby site AS030005 (on a north-facing slope) also had a northeast orientation.

Therefore, the fabric at site CS-W10b most likely is longitudinal, and thus it is interpreted as a hybrid till. The till was formed during the southeast-trending ice-flow event, and then was reworked and reoriented by a later northeast-trending ice-flow event—one powerful enough to remobilize till at this site but not to transport it a significant distance.

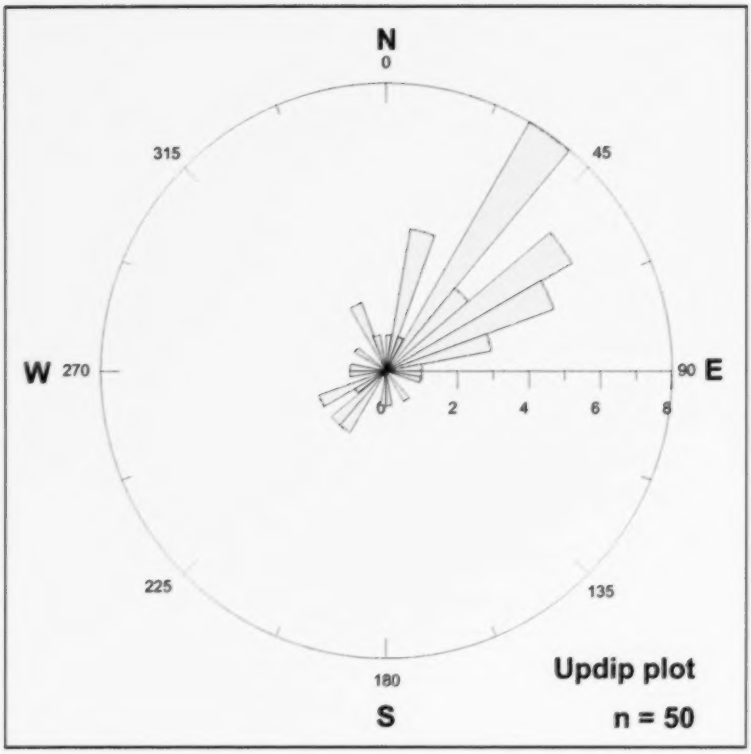

Figure 16. Till fabric plot for site CS-W10b, in the head of the Sisson Brook dispersal train, Coldstream map area (Fig. 4; Table 2). n = number of measurements.

Fabric is interpreted to indicate a northeastward ice flow.

2. The reddish till in the Cloverdale dispersal train (Seaman 2000a) extends discontinuously for approximately 27 km. Till material in the dispersal train is red to reddish brown (Munsell® colour hues 2.5 YR to 5 YR) grading to brown (7.5 YR hue) and lies in an area of dominantly yellowish brown (10 YR hue) to olive brown (2.5 Y hue) till. At site MV-Q14 (Appendix 1) near the southernmost extent of the dispersal train, the till fabric lies parallel to the south-southeast trend of the train, with an updip imbrication suggesting ice flow in that direction.

   This reddish till contrasts markedly with till at site 98AS0061 (Appendix 1), situated 6 km north-northwest of MV-Q14 and close to a south-southeast-trending striae site of Rampton and Paradis (1981a). The 98AS0061 till is yellowish brown with a fabric indicating deposition by a south-southwest-flowing glacier. However, reddish brown till lies 650 m northwest, 2.5 km southeast, and 2.5 km southeast of site 98AS0061; as well, brown till lies 1 km to the north. This suggests that, near site 98AS0061, the reddish brown till of the dispersal train was removed or buried by the later south-southwestward ice-flow event. Such an interpretation is supported by the presence of mottled red and grey till (possibly reflecting incomplete mixing of reddish into greyish till) overlying the sand and gravel at nearby site J3-40 (Appendix 2; Finamore 1981).

Precambrian Shield Erratics

The presence of erratic pebbles, cobbles, or boulders derived from Precambrian Shield rocks of Québec—the so-called 'Laurentide erratics'—are significant in identifying whether New Brunswick glacial deposits were formed by the Laurentide Ice Sheet or the Appalachian Glacier Complex. Rampton et al. (1984, p. 41) report that "Laurentide erratics in New

Brunswick are confined mainly to the Saint John River valley and adjacent areas" in northwestern New Brunswick. Pronk et al. (1989) also observed Precambrian Shield erratics only in the area adjacent to the upper Saint John River valley, west of the Miramichi Highlands, and north of the Grand Falls area (Fig. 1).

To resolve whether Laurentide or Appalachian glaciation was involved in the Late Wisconsinan glaciation of New Brunswick, the late Dr. V.K. Prest collected boulder samples from several New Brunswick localities during the late 1980s and early 1990s. Potassium–argon dates were reported for 19 of these boulders (Hunt and Roddick 1987, 1991, 1992a, 1992b), including four from the Woodstock area in west-central New Brunswick. The dates were accompanied by Prest's commentary on individual boulders and their inferred glacial geological significance. Three of the eight boulders that returned Precambrian ages were from southeastern New Brunswick; they were interpreted to represent dispersal from Precambrian bedrock sources in the Caledonian Highlands. Four of the other Precambrian boulders were from the upper Saint John River valley and were interpreted as Laurentide erratics.

The one remaining Precambrian boulder (Hunt and Roddick 1992b, GSC 92-84) was found by Dr. Prest and the author in a farm fencerow approximately 10 km west-northwest of Woodstock. Prest (*in* Hunt and Roddick 1992b) noted that the Precambrian age of this boulder was surprising, given its occurrence with a Devonian boulder (GSC 92-85), and suggested that their association indicated incursion of a glacier from Maine. This would imply east-northeastward ice flow from the nearest Precambrian source in western Maine. However, the date for the anomalous boulder falls within the range of the four boulders attributed to a Laurentide source. Also, a cobble of the distinctive Deboullie syenite from northern Maine was subsequently found in a fencerow at site WS-H04, 4 km north-northwest of Woodstock (Seaman 2000b). Therefore, a Laurentide origin for this Precambrian-age boulder is now considered more likely than an Appalachian origin.

Laurentide erratics possibly may have been dispersed even farther south. Mathew *[Matthew]* (1879, p. 2) reported a boulder of labradorite in the St. Stephen area, "which Dr. T.S. Hunt recognized as the kind of rock which occurs in the Laurentian of the Province of Québec." However, as mafic to ultramafic rocks occur in the St. Stephen Pluton (McLeod et al. 1994), this boulder more likely was of local derivation.

In the absence of radiometric dates, the age identification of Precambrian Laurentide erratics is problematic. A comment by Prest (*in* Hunt and Roddick 1991, p. 137) on a boulder of Silurian age is particularly pertinent: "Were it not for the K–Ar date, the granitoid rocks in the esker would, from their appearance, have been assigned to a Precambrian source by those favouring Laurentide ice over New Brunswick." Prest and Grant (1969) made a similar observation concerning dates for apparent Laurentide erratics from Prince Edward Island. Therefore, while Prest's boulder-dating project conclusively identified Laurentide erratics in northwestern New Brunswick, it also raised the possibility that some previously identified 'Laurentide' erratics actually derive from local highland sources of Phanerozoic age.

GLACIAL STRATIGRAPHY OF WEST-CENTRAL NEW BRUNSWICK

Introduction

The following discussion of glacial stratigraphy in west-central New Brunswick focuses on several multiple till sections and buried fluvial deposits, as well as significant sections in the Miramichi Lake Valley, Todd Mountain, and Sisson Brook areas (Fig. 4).

Multiple Till Sections and Buried Fluvial Deposits

As noted earlier, multiple till sections are comparatively rare in New Brunswick. Rampton et al. (1984) identified a number of sites where two or more apparently different tills were in stratigraphic superposition. At some sites, the superimposed tills were of differing colour, while at others, the tills were separated by intertill sediments, usually of inferred glaciofluvial origin.

The author has observed several sections of apparent multiple lodgement till in west-central New Brunswick. Geochemical and lithological analyses indicated that, for most of these sections, the 'two' tills are simply different facies of the same till. The best studied example is at site MV-Q14 noted above under ***Glacial Dispersal Trains***. There, a fresh roadcut section (Fig. 17) exposed 1.1 m of dark reddish brown till over 0.6+ m of yellowish brown till. The variation in geochemical and lithological values between the two till units was comparable to that between field duplicate samples from a single unit at other sites. As well, till fabric trends of MV-Q14-1 and -2 (Appendix 1) were essentially the same, parallel to the trend of the dispersal train (Seaman 1999b).

Site MV-Q14 therefore reflects only one period of glacial dispersal and one till: the lower unit simply reflects the first 25 km of glacial transport, and the upper unit the arrival of material from the Carlisle Formation, about 25 km distant. Rappol and Stoltenberg (1985) reported similar observations from The Netherlands, where 'petrographic stratification' developed in a single till, reflecting the distribution of bedrock lithotypes in the up-ice direction. Similar explanations may account for some other sites where two apparent tills of visibly different character are superposed. However, the sites may also indicate variations in the mode of glacier flow, in the source area (i.e., ice-flow trend), or in oxidation arising from differing texture (Rampton et al. 1984).

Some sections in the Saint John River valley, primarily in northwestern New Brunswick, expose two tills separated by thick sequences of intertill sediments; the tills have been interpreted as representing two glacial phases separated by an interstadial or interglacial period (Rampton et al. 1984; Rappol 1989; Lamothe 1992). Several fluvial deposits buried by till are known from west-central New Brunswick, as are several buried glaciolacustrine deposits and ablation till deposits (Appendix 2). The lower number of buried deposit sites south of the Saint John River suggests that the glacial history north and east of the river may be different or more complex.

Figure 17. Dark reddish brown (5 YR 3/4) till over yellowish brown (10 YR 5/4) till at site MV-Q14, Millville map area (Fig. 4; Table 2).

Head of rock hammer is sitting on the contact. Hammer handle is 30 cm long.

Most of the foregoing sites appear to contain no datable organic material, making it impossible to place accurate age constraints on the overlying till. However, three sites in west-central New Brunswick—Half Moon Pit in the Miramichi Lake Valley, Todd Mountain, and Sisson Brook—have returned radiocarbon dates that impose some constraints. These sites are discussed below.

Miramichi Lake Valley

Half Moon Pit Site

The Half Moon Pit site (Fig. 4) is a roadside borrow pit where till overlies "oxidized organic-bearing and colluviated sand" (Lamothe 1992, p. 19). It lies in the broad valley occupied by Miramichi Lake, south of the modern Southwest Miramichi River. The valley extends southeastward from the river at Half Moon Cove, just east of Deersdale, to Miramichi Lake and then northeastward back to the river near its confluence with Otter Brook, west of Otter Slide Mountain.

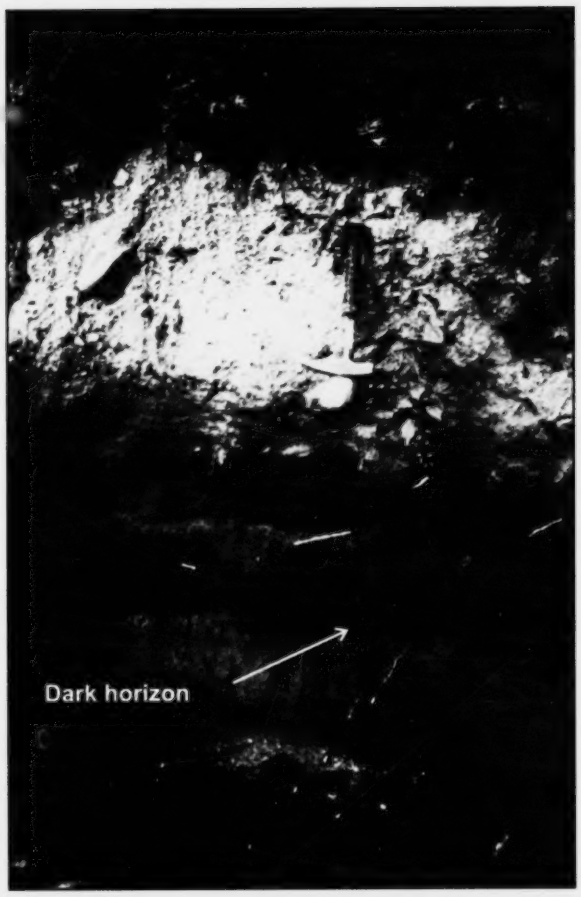

Figure 18. Compact, fissile till (behind the hammer) overlying stratified sand at the Half Moon Pit section, site AS030012a, Coldstream map area (Fig. 4; Table 2).

Dark horizon within the stratified sand contains charcoal that was sampled for radiocarbon dating. Hammer handle is 30 cm long.

The organic-bearing section at the Half Moon Pit site (site AS030012a in Appendix 2; Lamothe 1992, his Fig. 16) exhibits 0.7 m of compact and fissile basal till, with soil development in the upper 0.3 m The basal till overlies 1.6 m of stratified silty sand, which in turn overlies 0.2+ m of gravelly sand; at a depth of about 1.2 m, the silty sand unit contains a roughly 0.1 m thick horizon of organic silt containing charcoal fragments (Fig. 18). The charcoal-bearing material contains angular quartz and feldspar grains, some of the latter being weathered. The presence of both weathered and unweathered feldspar grains suggests that exposed granite was being actively weathered at the time of sediment deposition.

A bulk sample consisting of fragments of conifer charcoal, possibly pine, from the organic silt unit was dated at >36 ka (GSC-4199; McNeely and McCuaig 1991; Lamothe 1992). R.J. Mott (*in* McNeely and McCuaig 1991, p. 31) reported that the associated pollen indicated open conditions, but that "no specific age relationship is apparent." However, Lamothe (1992) interpreted these organic-bearing sediments as representing a Wisconsinan interstadial rather than the Sangamonian Interglacial, basing his conclusion on an interpretation of regional stratigraphy and on his inference that the organic sediments represent a climate that was cooler than at present.

The Half Moon Pit site is particularly critical to interpreting the glacial history of New Brunswick. It is one of only four known sites with non-finite radiocarbon dates in the province,

and the only one outside of southeastern New Brunswick. The three other locations are 1) the mastodon site at Hillsborough (Fig. 1), 2) a site just north of Sussex (Fig. 4), hereafter called the McGregor Brook site, and 3) a site near Springdale just east of Sussex, discovered by Marc Foisy in 1989 (Seaman 2004).

After evaluating the paleoenvironmental conditions and age-dating limitations, Harington et al. (1993) interpreted the age of the Hillsborough mastodon as late Sangamonian Interglacial (Fig. 2), probably Marine Isotope Stage 5a. Rampton et al. (1984, p. 41) interpreted organics and underlying sediments at the McGregor Brook site (BGS-806 in their Table 2) to be of "interglacial age." Seaman (2004) suggested that the organics at both the McGregor Brook and Springdale sites could be mid-Wisconsinan, on the basis of identifying a till with an east–west fabric separating the organic-bearing diamicton at McGregor Brook from weathered gravel at the section base. The McGregor Brook and Springdale sites require further work to determine whether the organics are interstadial or interglacial (Seaman 2004).

Because evidence for mid-Wisconsinan deglaciation is lacking in adjacent Nova Scotia (Stea et al. 1992), evidence for its occurrence in New Brunswick, at a higher latitude, must be considered suspect. Consequently, a new charcoal sample from the Half Moon Pit site was radiocarbon-dated by the Radiochronology Laboratory at l'Université Laval, using Accelerator Mass Spectrometry. The resulting date was >51.7 ka (ULA-1337). The laboratory report notes that the $^{14}C/C$ ratio was 'very close to zero after background subtraction, and the corresponding ^{14}C age is quoted as a lower limit at 2 sigma.' Therefore, the true age of the sample is probably considerably greater than 52 ka.

The Middle Wisconsinan encompasses the time period between approximately 55 ka and 30 ka (Kirby and Andrews 1999). Stea et al. (1998) and Stea (2004) indicate that the first Wisconsinan glaciation in Maritime Canada persisted until approximately 40 ka. The new date for the Half Moon Pit section therefore indicates that host sediments at the Half Moon Pit site are unlikely to be Middle Wisconsinan.

At a number of sites in Nova Scotia for which similar non-finite radiocarbon dates were obtained, subsequent dating by other methods has confirmed a Sangamonian age for the host deposits (Stea et al. 1998). Therefore, the buried sand and gravel at the Half Moon Pit site are interpreted as Sangamonian. Deposition during the Sangamonian could account for the weathered feldspar grains observed in association with the charcoal. Since bulk radiocarbon dates similar to those for GSC-4199 were obtained for the two sites near Sussex, and since those sites lie between Half Moon Pit and Hillsborough, the organic-bearing sediments near Sussex are also inferred to be of probable Sangamonian age.

The following additional sections (Table 4; Appendix 2) were examined by the author near the organic-bearing section at Half Moon Pit site (AS030012a).

Table 4. Descriptions of sections located near the Half Moon Pit site (AS030012a).

Site	Location Relative to Site AS030012a	Observations
AS030012b	~30 m to the north	0.8 m of till (with soil) with southeast-trending fabric overlies 1.6+ m of poorly sorted, slightly cobbly, sandy gravel
AS030012c	~15 m to the north	0.8 m of basal till (with soil) overlies 1.3+ m of gravelly sand, similar to that at base of site AS030012a
AS030012d	~8 m to the south	1.15 m of till (with soil) overlies 0.8+ m of silty sand, similar to that at AS030012a but without an obvious organic-bearing horizon
AS030012e	~30 m to the south	1.2 m of till (with soil) overlies 0.3 m of gritty sand that in turn overlies 0.4+ m of sandy gravel

On the basis of these four sites and the new age date, it appears that the organic-bearing material lies in a channel-fill sequence in Sangamonian fluvial deposits of the ancestral Southwest Miramichi River.

Shallow drilling near the base of the Half Moon Pit section encountered either bedrock or a large boulder, but lower till in this area is assumed (Lamothe 1992). Lamothe correlated the lower till with other lower till in boreholes and sections in both northwestern and northeastern New Brunswick (Lamothe 1992, his Fig. 23). Lamothe (1992) interpreted the surface till at the Half Moon Pit site as the regional surface till of Late Wisconsinan age.

Half Moon Sediments

Although Rampton and Paradis (1981a) and Rampton (1984) mapped the Miramichi Lake valley as part of a large lacustrine basin, subsequent till sampling in the area has revealed no evidence for extensive lacustrine deposits. At three sample sites in the northeast corner of the Coldstream map area (Fig. 4), soil development was in the underlying till (Seaman 2002). Till is also the soil parent material at site ND-BC03.5 (Appendices 1, 2; Seaman 2007) and eight other sites in the northwest corner of the Napadogan map area (Fig. 4; A.G. Pronk and G.R. Boldon, pers. comm., 2009). However, at a nearby pit section (site AS970015 in Appendix 2) situated at a slightly lower elevation than site ND-BC03.5, a sand layer, 0.5 m thick, was observed overlying the till when the site was first visited in 1997. As site AS970015 lies only 200 m from Miramichi Lake, this surficial sand simply indicates a former lake level a few metres above the current level.

In addition to the Half Moon Pit sections, buried sand and gravel has been observed at three other locations in the Miramichi Lake valley.

- The borrow pit noted above (sites 97AS0015, AS030010, and ND-BC03.5 in Appendices 1 and 2) exposed 0.7 m of basal till with north-trending fabric overlying 2.1+ m of silty to gravelly sand. Silty sand was encountered in a probe hole extending 0.6 m below the pit base.

Figure 19. About 13 m of fluvial sand and gravel overlain by thin (~0.7 m thick) till at site AS030014a, Coldstream map area (Fig. 4; Table 2).

- About 600 m northwest of the Half Moon Pit site, another pit (AS030014a in Appendix 2) exposes 0.7 m of till (with soil) overlying about 13 m of mostly sand and gravelly sand, with some beds of sandy gravel to sandy cobble gravel (Fig. 19).

- In a pit complex near Half Moon Cove (AS030013 in Appendix 2), several sections expose till both overlying and underlying sandy gravel. A till fabric measured in section AS030013b (Appendix 1) was parallel to that at the Half Moon Pit site but of apparent opposite trend.

Cursory paleocurrent measurements at sites 97AS0015 and AS030014 suggest that the flow of the ancestral Southwest Miramichi River was opposite to its current trend, implying that the river possibly served as a tributary of the Saint John River at that time.

The buried sand or gravel in the above sections is interpreted to represent remnants of a large alluvial plain that occupied the Miramichi Lake valley during the Sangamonian. A ditch cut at site AS030011 (Appendix 1) between sites AS030012 and AS030014 exposed 1.1 m of till (with soil), with a south-southeast-trending fabric, similar to that at site AS030012b. A soil probe was used to examine the material to a depth of 1.8 m. Stoniness prevented probing to a greater depth. The lower 0.1 m of till was sandier than the upper part and somewhat less compact, implying gradation into a sandy material. This suggests that the low hill between the above two sites is also underlain by sand and gravel. A similar stratigraphy may be present elsewhere in the Miramichi Lake valley. Therefore, the valley may host a significant reserve of granular material, much greater than earlier estimates (Hunter and Lavergne 1982, their site J7-04). It is suggested that the name 'Half Moon Sediments' be used for these buried Sangamonian fluvial sediments and that the Half Moon Pit site of Lamothe (1992) be selected as the type section.

Todd Mountain

The Todd Mountain site (Fig. 4) was discovered during a Geological Survey of Canada trenching program carried out in 1986 (Sacré 1989; Lamothe 1992) and is significant as the first New Brunswick site to show conclusive evidence for Younger Dryas glaciation (Fig. 2). The section exposed 2 m to 4+ m of sandy brown till overlying organic-bearing clayey diamicton that in turn overlay a sandy brownish grey till (Lamothe 1992, his Fig. 21). A sample of the organic material was dated at 11.5 ka (McNeely and McCuaig 1991: GSC-4277), proving that the overlying till was younger and hence compatible with a Younger Dryas age (11–10 ka). The age of the underlying till was disputed. Lamothe (1992) interpreted it as the regional Late Wisconsinan till, equivalent to the surface till in the Half Moon Pit. However, Sacré (1989) suggested that all till in the trench belonged to a single (Younger Dryas) unit, with the organic-bearing diamicton being transported from elsewhere and deposited in the till.

Observations made at the Sisson Brook site (see below) indicate that the Younger Dryas till may not differ visibly from the underlying older till but may be geochemically distinct. Geochemical data in Lamothe (1990b) suggest that the upper and lower till may be geochemically similar, except for their arsenic values, which are approximately 30% higher in the lower till than in the upper till. Therefore, either of the two interpretations above may be correct, as the upper and lower till units could be facies of the same till, or different tills of similar composition.

Lamothe (1992) interpreted the Younger Dryas till at this site as having been deposited by a glacier flowing from the west. However, Seaman (2006) presented evidence of its formation by the Gaspereau Ice Centre of central New Brunswick, flowing toward the northwest.

Sisson Brook

The Sisson Brook site (Fig. 4; Table 2) occurs in an exploration trench (Fig. 20) excavated by Geodex Minerals Ltd. over Zone III of the Sisson Brook tungsten–molybdenum–copper deposit. This site is of particular importance, not only for being the second confirmed Younger Dryas till site in New Brunswick, but also for exposing an identifiable multiple till sequence (Seaman and McCoy 2008).

The lower till is exposed only at the western extremity of the trench, where it appears to occupy a topographic depression over a fault zone. Its maximum thickness is greater than 3 m. It has a geochemical signature that reflects both the underlying bedrock mineralization and a granitic source. The latter feature, combined with the relatively high clay content and east-southeast-trending till fabric (sites CS-SB-02 and CS-SB-05 in Appendix 1), indicates a source area to the west. Seaman and McCoy (2008) correlated this till with the 'early Caledonia Phase' of Seaman (2004), inferred at the time to be Early Wisconsinan.

The middle till is up to 2.5 m thick and directly overlies the bedrock in the trench, except at its western extremity, where it overlies the lower till. It is anomalous in many elements, its

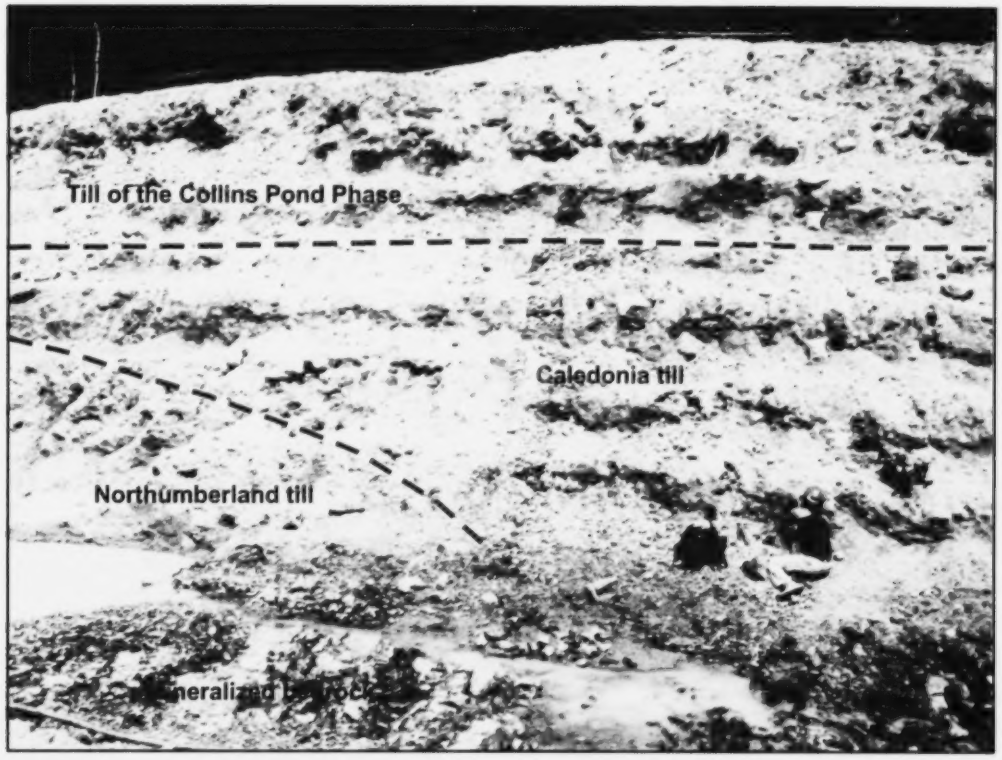

Figure 20. Till section in the Geodex Minerals Ltd. exploration trench at Sisson Brook, Coldstream map area (Fig. 4; Table 2). Boundaries between till units are approximate and are defined primarily by geochemistry (see Seaman and McCoy 2008).

geochemical signature reflecting mineralization in the underlying bedrock (Seaman and McCoy 2008). The single fabric measured in this till had a south-southwest orientation (CS-SB-03 in Appendix 1). Seaman and McCoy (2008) suggested that this till was a hybrid, deposited during an earlier glacial phase and then reoriented during a later south-southwest Late Wisconsinan ice-flow event. However, such an orientation parallels Nashwaak Ridge, the crest line of which lies 900 m to the east-southeast. As noted under ***Glacial Dispersal Trains***, the dispersal train from Sisson Brook extends southward for a several kilometres before assuming a southeast trend at the ridge crest. Therefore, the above till fabric trend may also reflect the local flow direction of the basal ice when the dispersal train formed, rather than the result of reworking during a later, south-southwest-trending ice-flow phase.

The upper till is about 1 m to 3 m thick, consists in part of reworked glaciofluvial deposits, and contains organic materials dated at about 11 ka (Seaman and McCoy 2008). It is incised by a small channel from which basal peat was sampled and dated at approximately 10.6 ka (Seaman and McCoy 2008: TO-13585). This till was therefore deposited early in the Younger Dryas Stadial. Till fabrics (CS-SB-01, CS-SB-04, and CS-SB-06 in Appendix 1) and deformation structures indicate it was deposited by a west- to northwest-flowing glacier. This implies that the Gaspereau Ice Centre (as defined by Seaman 2006) was thick enough to overtop the approximately 100 m elevation of Nashwaak Ridge immediately to the east. The till largely masks the geochemical signature of the underlying tills and bedrock at Sisson Brook.

The Sisson Brook site is notable, not just for its multiple tills, but also for its regional stratigraphic significance. Ablation moraines in this valley were interpreted as marking the eastern limits of flow from the North Maine Ice Divide at their Millville/Dungarvon phase maximum extent (Rampton and Paradis 1981a; Rampton et al. 1984). Rampton et al. (1984) assigned an age of 12.7 ka for this ice marginal position. However, the presence of Younger Dryas basal till in the valley means that associated ablation till, which overlies the surface basal till and thus is stratigraphically part of the upper till, was deposited by the melting Younger Dryas glacier. The site thus marks the approximate western margin of the Gaspereau Ice Centre of central New Brunswick, c. 10.7 ka.

GLACIAL AND INTERGLACIAL HISTORY

Introduction

The glacial and interglacial history of New Brunswick as discussed below reflects the stratigraphic divisions and glaciation phases shown in Figure 2. From oldest to youngest, these are the Illinoian (Northumberland Phase), Sangamonian Interglacial, Early–Middle Wisconsinan (Caledonia Phase), Middle Wisconsinan, and Late Wisconsinan (Escuminac, Scotian, Chignecto, and Collins Pond phases). Figure 21 (a–f) depicts the phase names and interpreted ice-flow patterns associated with these Middle–Late Pleistocene glaciers that affected New Brunswick.

Illinoian: Northumberland Phase (new phase)

Definition

As detailed earlier under ***Half Moon Pit Site***, Lamothe (1992) correlated till underlying the Half Moon Sediments with the lowermost till in boreholes and sections in northwestern New Brunswick along the middle and upper Saint John River valley. Lower till at these latter sites had an east–west fabric (Rampton et al. 1984; Rappol 1989; Lamothe 1992). The presence of clasts of Deboullie syenite from a source area in northern Maine (Rappol 1988) indicates that this till was deposited by an eastward-flowing glacier (Rappol 1989).

At one site, located near Grand Falls (Fig. 1), Rampton et al. (1984) noted oxidation to a depth of 1 m in the surface of the lower till. They suggested this indicated a pre-Wisconsinan age but made no specific age assignment. With the Half Moon Sediments now assigned to the Sangamonian Interglacial, this lower till is interpreted to most likely represent the penultimate glaciation—that is, the Illinoian Glacial Stage (c. 200–130 ka; Fig. 2).

The early eastward ice-flow event in the Maritime provinces had been assigned to the early part of the Caledonia Phase (Rampton et al. 1984; Stea et al. 1998; Stea 2004). However, the Caledonia Phase of glaciation was originally defined as Early–Middle Wisconsinan (Rampton and Paradis 1981b, 1981c). Thus, it is inconsistent to refer to this earlier eastward flow event as 'early Caledonia Phase', as suggested by Seaman (2004), if it is in fact Illinoian. Rampton et al. (1984, p. 41) also questioned their assignment of this early eastward flow to the

Caledonia Phase, noting that "analysis of the probable source of the glacier ice producing the eastward trending striae and the Caledonia flow pattern places this assignment in doubt."

Stea et al. (1998) and Stea (2004) attributed the early eastward glacial flow event to the Northumberland Glacier, originally defined by Chalmers (1895). Consequently, the name 'Northumberland Phase' is proposed for this probable Illinoian glaciation of the Maritime provinces (Fig. 21a). The associated till, referred to as the 'Lower till' by Lamothe (1992), is referred to informally herein as the 'Northumberland till.'

West-Central New Brunswick

Rampton and Paradis (1981a) reported early, east-trending striae from one site just south of Woodstock in west-central New Brunswick. Several striae with an east to east-southeast trend have since been noted in west-central New Brunswick that 'appear to be old.' For example, at site 98AS0074 in the east-central part of the Millville map area (Fig. 4), east-southeast-trending grooves and fine to coarse striae appear to be older than fine to medium striae of southeast orientation. However, as younger striae with this trend are also known from the area, assigning eastward-trending striae on a particular outcrop to the Northumberland Phase is problematic. On the other hand, the early, east-southeast-trending, large-scale bedrock fluting (Fig. 3) can be reasonably assigned to the Northumberland Phase. Its muted appearance suggests that it represents the earliest surviving phase of glaciation in the area.

The early, discontinuous, east-southeast-trending reddish till dispersal train from the Carlisle Formation (see ***Glacial Dispersal Trains***) is also assigned to the Northumberland Phase. This dispersal train lies in the area of large-scale bedrock fluting. Also, the clasts of reddish till in the regional yellowish brown till at site MV-X02d (Millville map area) confirms this was an early dispersal event (Seaman 2000a). Clasts of older till appear at numerous sites in west-central New Brunswick. At some sites, the reworked material may be Northumberland till. However, given the complexity of glacial events and the presence of hybrid tills, younger tills may also have been reworked during even younger glacial phases. For example, a 'boulder' of compact brown till in reddish brown till at site BC-K01 may be the result of reworking by the Gaspereau Ice Centre during the Younger Dryas Stadial (Seaman 2008).

As noted earlier under ***Sisson Brook***, the physical and geochemical characteristics of the lower till in the Sisson Brook exploration trench indicate deposition by an east-southeast-flowing glacier. This site also lies in the area of large-scale east-southeast bedrock fluting, about 15 km north of the eastern end of the reddish dispersal train mentioned above. Therefore, the lower till at the Sisson Brook site is now interpreted as the Northumberland till. Pending discovery of a datable section to confirm the Northumberland till as Illinoian, it is suggested that this site, as described by Seaman and McCoy (2008), serve as a temporary type section.

Source Area

Rampton et al. (1984) postulated an Appalachian source for this early eastward flow, from a glacier over the eastern flank of the Megantic Hills in Québec, the White Mountains of New

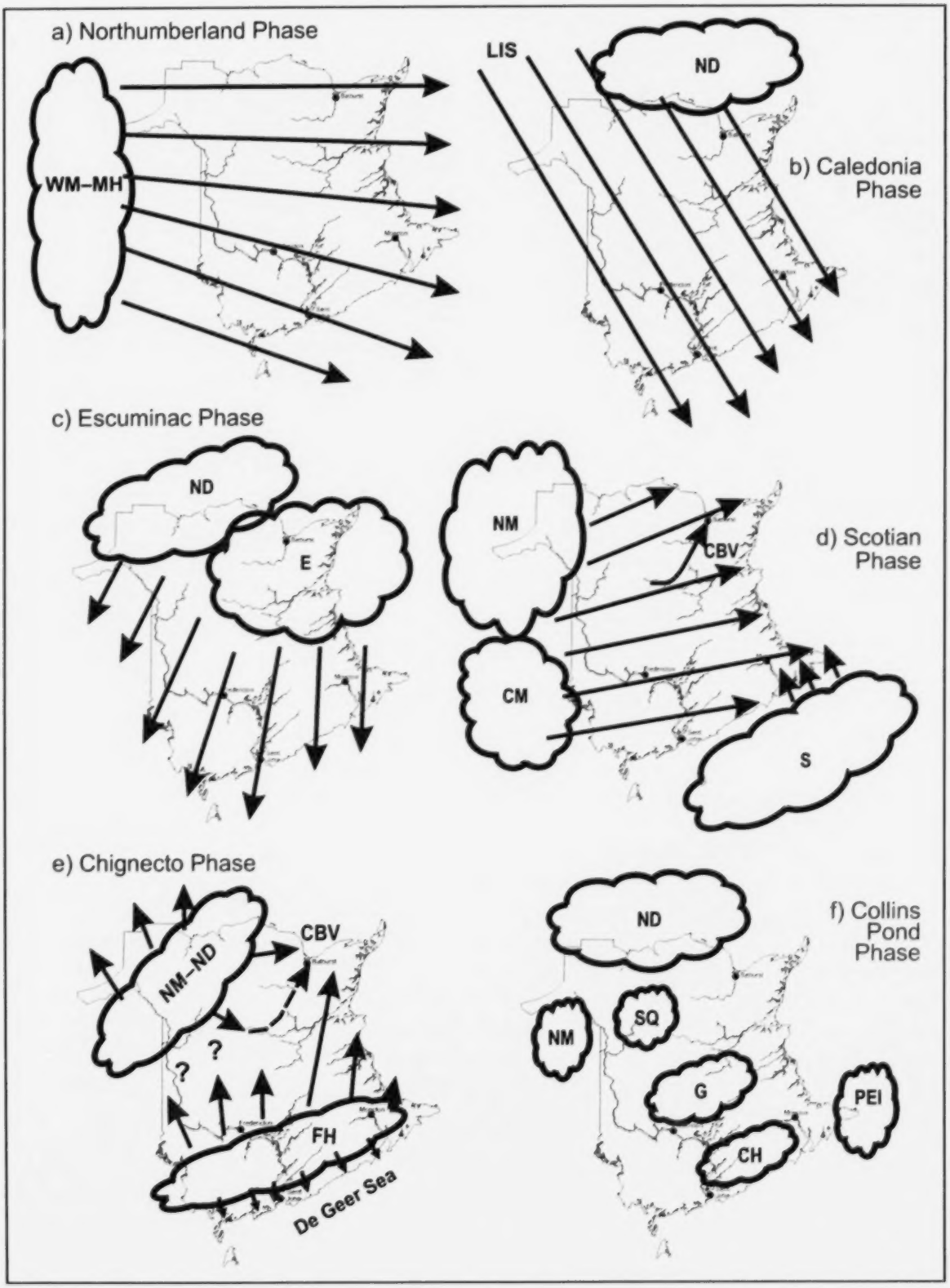

Figure 21. Appalachian Glacier Complex: phases and regional ice-flow patterns (legend on facing page).

Legend for Figure 21 *(on facing page)*			
Figure	**Glaciation Phase**	**Stage**	**Age (ka)**
21a	Northumberland	Illinoian	c. 200–130
21b	Caledonia	Early–Middle Wisconsinan	c. 75–40
21c	Escuminac (Late Wisconsinan maximum)	Late Wisconsinan	c. 22–18
21d	Scotian	Late Wisconsinan	c. 18–15
21e	Chignecto	Late Wisconsinan	c. 15–12.5
21f	Collins Pond	Late Wisconsinan	c. 11–10

CBV	Curventon–Bathurst valley ice stream	**ND**	Notre Dame Ice Divide
CH	Caledonian Highlands Ice Centre	**NM**	North Maine Ice Divide
CM	Central Maine Ice Centre	**PEI**	Prince Edward Island Ice Centre
E	Escuminac Ice Centre	**S**	Scotian Ice Divide
FH	Fundy Highlands Ice Divide	**SQ**	Saint Quentin Ice Centre
G	Gaspereau Ice Centre	**WM–MH**	White Mountains–Megantic Hills Ice Divide
LIS	Laurentide Ice Sheet		

England, or central Maine. If the east-southeastward trend of the large-scale bedrock fluting in west-central New Brunswick is projected to the west-northwest, a possible source area can be suggested between Woodstock and Québec City. The Deboullie syenite clasts in this till (Rappol 1988, 1989) suggest that the most likely source for the glacial flow was west of northern Maine, around an axis of accumulation suggested by Elson (1987) for a glaciation of inferred mid-Wisconsinan age.

Ice flow from this divide may have generated the lower till in the upper Saint John River valley (Rappol 1989), but if so, the ice divide is older than originally proposed by Elson (1987). The name 'White Mountains–Megantic Hills Ice Divide' is suggested for this area of Illinoian glacial outflow. Figure 21a depicts the presumed regional ice-flow pattern of the White Mountains–Megantic Hills Ice Divide during the Northumberland Phase.

Recently, three shallow trenches (site AS090002) were examined at the Flume Ridge tungsten property of Geodex Minerals Ltd., in the northeast corner of the Rollingdam map area (Fig. 4). Much of the exposed bedrock was roughened by weathering. However, it is possible to discern east-southeast-trending striae cross-cutting an eastward-trending rat-tail at one location, and grooves created by the eastward transport of plucked blocks at another location. These striae are attributed to the Northumberland Phase, as later striae trending south-southeast were observed at one location, and others trending east-northeast were observed at three locations. The relationship between the east- and east-southeast-trending striae suggests that the Northumberland Phase began with eastward flow and then transitioned to east-southeastward flow.

The magnitude of the large-scale, east-southeast-trending bedrock fluting in west-central New Brunswick suggests that the White Mountains–Megantic Hills Ice Divide of the Appalachian Glacier Complex maintained a relatively uniform flow vector for a considerable period of time. The timespan of the Illinoian Stage would be ample for such erosion.

Regional Correlation

Tills attributed to the Illinoian (Marine Isotope Stage 6) have long been known from southern Ontario and Québec. These include the York Till (Karrow et al. 2001), and the Baie-Saint-Paul Glacial Complex, Bécancour Till, Johnville Till, Portneuf Till, and Rigaud Till (Clet-Pellerin and Occhietti 2000). Several of the Québec tills, such as the Bécancour Till (Lamothe 1989) and Johnville Till (McDonald and Shilts 1971), were initially interpreted as Wisconsinan. Tills of Illinoian age have also been identified in Nova Scotia; these include the Red Head and Little Brook tills of the southern mainland, and the Miller Creek Till of the central mainland (Stea et al. 1998; Stea 2004).

The Northumberland till is interpreted as chronologically correlative with the above Illinoian tills and also with the St. Francis Till in northern Maine, which exhibits a similar fabric and stratigraphic context (Genes et al. 1981). Similarly, the lower till at the McGregor Brook site near Sussex, with its east–west fabric and position beneath organic materials of non-finite age (Seaman 2004), is now interpreted as part of the Northumberland till. The underlying weathered gravels at the McGregor Brook site (Rampton et al. 1984; Seaman 2004) are now interpreted as pre-Illinoian rather than Sangamonian. They may be correlative with the Bridgewater or Mabou conglomerates of Nova Scotia, which occur in a similar stratigraphic context (Stea et al. 1998; Stea 2004).

Sangamonian Interglacial

The Half Moon Sediments are now assigned to the Sangamonian (c. 130–75 ka). As mentioned earlier, the Half Moon Pit site's organic-bearing channel-fill sequence may indicate a climate cooler than today (Lamothe 1992). If so, the sequence may correlate with the latter part of the Sangamonian (Marine Isotope Stage 5a), making these sediments correlative with the 'blue clay' hosting the Hillsborough mastodon.

None of the buried gravels in west-central New Brunswick exhibit the kind of weathering seen in buried gravels at the McGregor Brook site. Therefore, it is inferred that none are pre-Illinoian. Some of these buried gravel deposits, particularly those south of, west of, and within the Saint John River valley (Appendix 2), may be correlative with the Half Moon Sediments. Alternatively, they may relate to earlier substages of the Sangamonian. Except for the Half Moon Sediments, the buried gravel deposits north and east of the river could be of similar age, or much younger, as a glacial readvance occurred in central New Brunswick during the Younger Dryas Stadial at the end of the Late Wisconsinan (Seaman 2006; see below).

Clet-Pellerin and Occhietti (2000, p. 44) note that the Illinoian glaciation in southern Ontario and Québec "eroded most of the older Quaternary deposits, and left a very discontinuous till cover which in most cases directly overlies the bedrock." Their description is compatible with observations of the Northumberland till in New Brunswick. It also suggests that much of the regolith generated by preglacial weathering was stripped away during the Illinoian, supporting the interpretation above that much of the weathered bedrock seen today was probably weathered during the Sangamonian.

Early–Middle Wisconsinan: Caledonia Phase

Definition

The Caledonia Phase was initially defined by Rampton and Paradis (1981b, 1981c) as the earliest Wisconsinan glaciation, associated with eastward to southeastward ice movements over the Caledonian Highlands and adjacent areas of southeastern New Brunswick. However, Rampton et al. (1984) questioned the assignment of the early eastward flow to the Caledonia Phase; that flow is assigned herein to the earlier Northumberland Phase, as noted above.

Southeast- to south-southeast-trending striae of the Caledonia Phase occur on the surface of a marine wave-cut bedrock bench near Rockport (Fig. 1), southeastern New Brunswick (Rampton and Paradis 1981c). The formation of a similar bedrock bench in adjacent Nova Scotia was attributed to a higher sea level during the Sangamonian Interglacial (Grant 1977). Rampton and Paradis (1981b, 1981c) therefore assigned the Caledonia Phase to either the Early or Middle Wisconsinan. Stea et al. (1998) and Stea (2004) subsequently assigned the Caledonia Phase to the Early Wisconsinan and approximately the first half of the Middle Wisconsinan (c. 75 to 40 ka). Probable confirmation of this timing comes from the offshore stratigraphy. Stea et al. (1998) assigned the Hartlen Till of Nova Scotia to the Caledonia Phase and mapped its extent to the continental shelf edge. They noted that the younger Lawrencetown Till (which they assigned to the Escuminac Phase of the Late Wisconsinan) also extends to the shelf edge and that, at average glacial flow rates, there would be insufficient time for both till sheets to be deposited during the span of just the Late Wisconsinan.

West-Central New Brunswick and Adjacent Areas

Evidence for southeast to south-southeast ice flow is widespread across New Brunswick (Seaman 1989a, 1989b). This early ice-flow event is documented, not just in southeastern New Brunswick (as indicated above), but also in southwestern (Seaman et al. 1993; Allard 2003; Allard and Pronk 2003; Seaman 2004), northwestern (Rappol 1989), and northeastern (Pronk et al. 1989; Parkhill and Doiron 2003) New Brunswick. Applying the principle of Occam's razor, these early southeast to south-southeast flows most likely relate to the same glacial event, namely the Caledonia Phase. Others (Allard 2003; Allard and Pronk 2003) have suggested that till with a southeast-trending fabric in southwestern New Brunswick was deposited during the Caledonia Phase, or have attributed the southeast-trending bedrock flutings in the area to that phase (Seaman 2004). Pending the definition of formal type sections, it is suggested that this till be informally named the 'Caledonia till.' Because the till is equivalent to Lamothe's (1992) 'Upper till,' the Half Moon Pit site is suggested herein as the temporary type section.

In the eastern Caledonian Highlands (Fig. 1), an early north-northwest ice flow from the highlands preceded the influx of the southeast-flowing Caledonia Phase glacier (Foisy and Prichonnet 1991). This may indicate that a local Appalachian glacier developed in the area of the Caledonian Highlands before the major Caledonia Phase glaciation. However, Illinoian

glaciation also could have ended with remnant glaciers over the highlands, analogous to what transpired at the end of the Late Wisconsinan (see below). Future work will be required to differentiate between these two possibilities. The complex striae record of west-central New Brunswick may in part reflect minor Illinoian or Early Wisconsinan ice-flow trends that were paralleled by later Wisconsinan ice flows—flows that, at least locally, were not powerful enough to erase previously formed striae.

Evidence for the Caledonia Phase is widespread in west-central New Brunswick. It includes the 1) southeast-trending streamlined bedrock landforms in the southwestern part of this area, 2) southeast-trending Sisson Brook and Fredericksburg dispersal trains, and 3) dispersal trains with a south-southeast trend (Fig. 14). Till comprising these dispersal trains is interpreted as Caledonia till. Many southeast- to south-southeast-trending striae (Fig. 7a, 7b) were probably generated during this phase, particularly those associated with grooves, coarse striae, and large rat-tails.

The striae chronology of Seaman et al. (1993) indicates that the Caledonia Phase began with south-southeastward flow and then transitioned to southeastward flow before returning to south-southeastward flow. The dogleg barium dispersal train from Fredericksburg (Fig. 14) also indicates a transition from southeastward to south-southeastward flow. The southeast to south-southeast trends of the dispersal trains parallel the till fabric at several sites, particularly the fabric of till overlying the Half Moon Sediments at their type section and the fabric of lower till near Charlie Lake (Broster and Seaman 1991). The glaciotectonic faulting of weathered granite near Charlie Lake is compatible with south-southeastward displacement and thus is also assigned to the Caledonia Phase.

Observations in the Charlie Lake area clearly show the relative chronological age of the Caledonia Phase. The surface till overlying the glaciotectonized weathered bedrock has a south-southwest- to southwest-trending fabric (Broster and Seaman 1991) (AS 89-42 and AS 89-55 in Appendix 1), paralleling the flow of the later Escuminac Phase (see below). This relationship is confirmed by striae cross-cutting relationships (Table 3; Fig. 22a, 22b).

Source Area

The source of the Caledonia Phase glacier has been a contentious issue. Rampton et al. (1984) suggested it was their Gaspereau Ice Centre in central New Brunswick; Stea et al. (1998) and Stea (2004) also attributed the Caledonia Phase glaciation of Nova Scotia to the Gaspereau Ice Centre (Fig. 21f). Pronk et al. (1989) suggested that the early southeastward ice flow in northern New Brunswick was affected by local Appalachian ice. In contrast, other investigators attributed the early southeast ice flow to the Laurentide Ice Sheet (Rappol 1989; Lamothe 1992; Parkhill and Doiron 2003).

The issue of Laurentide inundation in adjacent Gaspésie has also been highly debated. Rappol (1993) documented Laurentide erratics in western Gaspésie and northwestern New Brunswick. David and Lebuis (1985) presented evidence supporting inundation of western

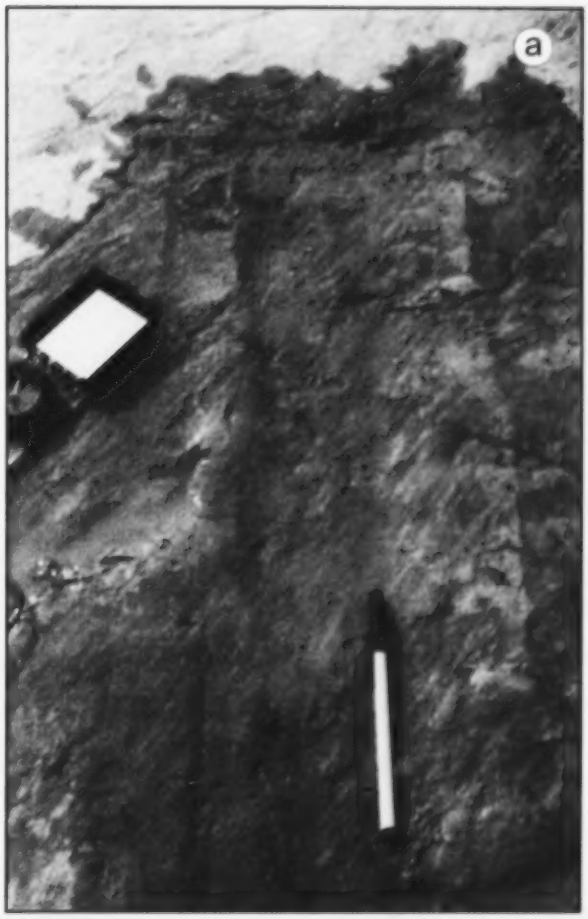

Figure 22. Grooves, rat-tails, and striae at site FV-3, Fosterville map area (Fig. 4; Table 2).

The large south-southeast-trending grooves (Fig. 22a) and rat-tails (Fig. 22b) are features of the Caledonia Phase (indicated by pen). Both features are cross-cut by later, south-southwest-trending striae of the Escuminac Phase (indicated by compass).

Gaspésie by the Laurentide Ice Sheet. Charbonneau and David (1993) interpreted the event as being Early Wisconsinan. However, Olejczyk and Gray (2007) disputed this interpretation, insisting there is no evidence that the Laurentide Ice Sheet crossed northern Gaspésie, even before the late-glacial maximum.

The Gaspereau Ice Centre cannot be the source of glaciation features attributed to the southeast-trending Caledonia Phase in southwestern, west-central, or northern New Brunswick. Rather, those features require a source farther to the northwest. Contenders might be the North Maine–Notre Dame Ice Divide, as originally defined by Rampton et al. (1984) or the Laurentide Ice Sheet as suggested by Parkhill and Doiron (2003). In the New Brunswick context, it is difficult to choose between these two sources since, as noted by Flint (1951, p. 25), "this direction of flow would have been assumed by glacier ice regardless of whether it originated in New Brunswick or were part of the great Laurentide Ice Sheet."

The foregoing contrasting points of view suggest that the Caledonia Phase glacier was sourced from either 1) the Laurentide Ice Sheet, 2) the North Maine–Notre Dame Ice Divide of the Appalachian Glacier Complex, or 3) a combination of the two ice masses.

The first possibility is easily dismissed. The Laurentide Ice Sheet would have needed to traverse all of Gaspésie to account for the Caledonia flow pattern in northeastern New Brunswick, Prince Edward Island, and much of Nova Scotia. Since it did not cross northern Gaspésie (Olejczyk and Gray 2007), the Laurentide Ice Sheet alone could not have generated the Caledonia Phase flow pattern.

However, if the Appalachian Glacier Complex was solely responsible for the Caledonia Phase, the Laurentide erratics in northwestern New Brunswick and western Gaspésie must be explained. The erratics are most abundant in intertill gravels in the Saint John River valley area (Rampton et al. 1984). According to Rappol and Russell (1989, p. 134), the erratics "...tend to be more abundant in the upper bouldery zones of till and associated ice contact deposits formed during final deglaciation, than in silty and compact subglacial till," indicating they had arrived by the latest ice cover, representing far-travelled englacial material.

Taking into account the probable Sangamonian age of the intertill sediments, the relative sparseness of Laurentide erratics, and their preferential emplacement in melt-out deposits, the presence of these erratics could be explained via the following sequence of events.

- The erractics were derived from the erosion of an older Laurentide till and introduced into northwestern New Brunswick as part of the englacial debris transported from the White Mountains–Megantic Hills Ice Divide during the Northumberland Phase;
- they were deposited as part of surficial ablation lags, ablation till, or glaciofluvial deposits during deglaciation following the Northumberland Phase;
- many of the surficial erratics were eroded into the Saint John River valley during subaerial transport processes active during the Sangamonian Interglacial;

- erratics from the Northumberland Phase ablation and glaciofluvial deposits were re-entrained during the Caledonia Phase; others were reworked from the Sangamonian fluvial deposits;
- the erratics migrated upward into englacial or supraglacial positions; and
- the erratics were finally deposited from melt-out of glaciers at the end of the Wisconsinan.

This scenario accounts for the Laurentide erratics in northwestern New Brunswick but involves a complex sequence of events that would be difficult to confirm and is considered unlikely.

A simpler explanation for the erratics involves direct action of the Laurentide Ice Sheet. Such an explanation also supports the third possibility (above), namely that the Laurentide Ice Sheet *and* the Notre Dame Ice Divide of the Appalachian Glacier Complex provided the most probable source of the Caledonia Phase of glaciation. Under this combined scenario, the Caledonia Phase would begin with the Laurentide Ice Sheet inundating northwestern New Brunswick while northeastern New Brunswick was overridden by ice from the Notre Dame Ice Divide. These glaciers may have encountered others growing northward from the Caledonian Highlands area (Foisy and Prichonnet 1991) and assimilated them to form a continuous ice cover over New Brunswick. The Caledonia Phase glacier would therefore be composed largely of local Appalachian ice, but would flow southeastward under the driving force of the Laurentide Ice Sheet (Lamothe 1992).

The flow from the Notre Dame Ice Divide may have become more dominant over time, as suggested by 1) the shift from southeastward flow to south-southeastward flow during the Caledonia Phase, as indicated by striae chronology, 2) the divergence between fluted bedrock trend and dominant till dispersal trend in west-central New Brunswick, and 3) the dogleg barium dispersal train from the Fredericksburg area. The increase in dominance could have resulted from enhanced accumulation over the Notre Dame Ice Divide, growth of the St. Lawrence valley ice stream diverting much of the Laurentide Ice Sheet to the east, or a combination of these or other factors.

In the context of west-central New Brunswick, the above scenario means that the glacier crossing the area during the Caledonia Phase was technically the Laurentide Ice Sheet. This interpretation is supported by the single Precambrian erratic in the Woodstock area (Hunt and Roddick 1992b). Several reasons could explain why more such erratics have not been observed in the area.

- The Laurentide basal debris may have been diverted eastward down the Laurentian Channel, resulting in relatively clean ice entering New Brunswick (Pronk et al. 1989). The Laurentide erratics were likely derived from the englacial load of the Laurentide Ice Sheet (Rappol and Russell 1989), which probably entered northwestern New Brunswick via transverse valleys through the Notre Dame Mountains (A.G. Pronk, pers. comm., 2009). Therefore, most of the material transported and deposited by the Laurentide Ice Sheet in New Brunswick would be of local Appalachian origin.

- Laurentide erratics may be indistinguishable from younger local rocks of similar appearance (Lamothe 1992). Radiometric dating of individual pebbles, cobbles, and boulders would be needed to determine whether they were derived from Laurentian or Appalachian sources.

- No deglaciation interval existed between the Caledonia Phase and subsequent Late Wisconsinan glacial phases described below. Two of these later phases had a component of westward flow in west-central or northwestern New Brunswick (Fig. 21a–21f). Therefore, many of the Laurentide erratics brought into western New Brunswick may subsequently have been transported westward into Maine and deposited there upon deglaciation.

Regional Correlation

The Caledonia till is stratigraphically equivalent to the 'Upper till' of Lamothe (1992). He interpreted it as the regional surface till in the Saint John River valley–Miramichi Highlands area and assigned it to the Late Wisconsinan. However, his interpretation was predicated on the Half Moon Sediments being mid-Wisconsinan, which means that the till's reassignment herein to the Early Wisconsinan does not change the relative relationships in Lamothe's regional stratigraphic framework. The till over the Caledonian Highlands (Fig. 1), with its south-southeast-trending dispersal trains (Munn 1995; Munn et al. 1996), is also interpreted as Caledonia till, as is the organic-bearing diamicton at the McGregor Brook site near Sussex.

Several named tills of Early Wisconsinan age have been identified in Nova Scotia (Stea et al. 1998; Stea 2004). In the central mainland area these are the McCarron Brook Till, East Milford Till, and Hartlen Till. On Cape Breton Island, the Early Wisconsinan is represented by the Richmond Till. All of these tills are inferred to be correlative with the Caledonia till.

Middle Wisconsinan

As noted above, Lamothe (1992) interpreted the Half Moon Sediments as mid-Wisconsinan. On the basis of a similar non-finite age, Seaman (2004) suggested that the organic sediments at the McGregor Brook site could also be mid-Wisconsinan, if the underlying till was Early Wisconsinan. However, the new chronological model resulting from the new date for the Half Moon Sediments removes the need for a mid-Wisconsinan deglaciation at McGregor Brook, and brings New Brunswick stratigraphy into accordance with that of Nova Scotia.

Stea et al. (1998) and Stea (2004) interpret the Caledonia Phase glaciation as persisting throughout the first part of the Middle Wisconsinan. They also note the absence of evidence for widespread glacial retreat from Maritime Canada during the latter part of the Wisconsinan (c. 40–22 ka). According to Stea et al. (1998), a calving bay developed in the Laurentian Channel in the Gulf of St. Lawrence, with ice covering Prince Edward Island, the Magdalen Shelf, and adjacent New Brunswick; another, small calving bay existed in the outer Bay of Fundy, with the ice margin lying close to the modern St. Croix Highlands shoreline (Fig. 1). The similarity in 'freshness' of Caledonia Phase striae and Late Wisconsinan striae on the same bedrock surfaces (Fig. 22a, 22b) implies that both generations of striae were first

weathered at the same time. This supports the interpretation of continued glaciation of west-central New Brunswick throughout the mid-Wisconsinan.

West-central New Brunswick has no known glacial features relating to the latter part of the Middle Wisconsinan. The ice was likely thin and therefore frozen to the underlying substrate. However, locally it may have been at the pressure melting point and thus capable of flow. Such local flow could account in part for the complex striae record in the area.

Late Wisconsinan: Escuminac Phase

Definition

The following definition is derived from Stea et al. (1998). The Escuminac Phase represents the classical Late Wisconsinan Maximum, c. 22 ka to 18 ka. The Late Wisconsinan till sheet extends to the continental shelf margin and correlates with the Lawrencetown Till of Nova Scotia. Southward to southwestward flow trajectories in most of Nova Scotia and Prince Edward Island indicate that the glacial source area was an ice centre on the Magdalen Shelf in the Gulf of St. Lawrence, previously defined (Rampton et al. 1984) as the Escuminac Ice Centre. The reddish coloration of the Lawrencetown Till is attributed to hematitic sediments in the source area.

West-Central New Brunswick and Adjacent Areas

For the Escuminac Ice Centre to have affected west-central New Brunswick, the ice flow would have been southwestward. Striae (Fig. 7a, 7b) and till fabrics with south to southwest trends are common in this area (Appendix 1), while those with southwest to west trends are less common. However, the apparent absence of significant dispersal trains of similar trend suggests that flow from the Escuminac Ice Centre was comparatively weak in this area. Its effects seem to have been limited to the generating of striae (Fig. 22a, 22b) and local reworking of the Caledonia till (Allard 2003; Allard and Pronk 2003). The reworking involved only limited transport without significant erosion of the underlying bedrock; this produced a hybrid till with Caledonia physical and chemical characteristics but an Escuminac fabric.

In contrast with the above observations, the area west of Grand Lake is characterized by southwest-trending fluting and southwest-trending striae (Rampton and Paradis 1981a: their Minto phase). Fluting here is much finer than that associated with the Northumberland Phase (Fig. 3). No parallel dispersal has been observed in this area (Seaman 2007). Therefore, the fluting may have developed in the Caledonia till rather than from deposition of 'Escuminac till.' Further investigation is required to confirm this interpretation.

This southwest-trending fluting extends across the Saint John River valley (Fig. 3). Thus, it cannot be attributed to actions of the later Gaspereau Ice Centre during the Collins Pond Phase, as that ice centre was confined to northeast of the Saint John River (see below).

Late Wisconsinan: Scotian Phase

Definition

Around 18 ka, calving induced by sea level rise caused the Escuminac Ice Centre to begin retreating from its maximum position at the continental shelf margin (Stea et al. 1998). Drawdown into marine channels such as the Bay of Fundy caused the Escuminac glacier to break into local ice divides or ice centres, initiating the Scotian Phase (c. 18–15 ka). During this phase, the Scotian Ice Divide was active over Nova Scotia and is correlated with an ice-marginal position on the Scotian Shelf east of Nova Scotia (Stea et al. 1998).

West-Central New Brunswick and Adjacent Areas

A similar ice divide or ice centre affected west-central New Brunswick. Seaman et al. (1993) identified a transition from southwestward ice flow, now attributed to the Escuminac Phase, to southeast to east to east-northeast flow. The latter flow directions are represented by the Passamaquoddy Diversion, Kent, and Tuadook–Renous flow patterns of Rampton et al. (1984), which they assigned to their Bantalor phase. These flow patterns probably reflect drawdown toward the Laurentian Channel ice stream in the Gulf of St. Lawrence.

Striae presumed to relate to the above flow patterns are comparatively rare but occur across much of west-central New Brunswick (Fig. 7a, 7b). This implies that, at the time of their formation, the source ice centre lay to the west, probably in central Maine. The name 'Central Maine Ice Centre' is therefore proposed for the Scotian Phase ice centre that flowed through west-central New Brunswick. Trends and relative ages similar to those seen in west-central New Brunswick also occur in northern New Brunswick (Pronk et al. 1989; Rappol 1989; Lamothe 1992; Parkhill and Doiron 2003). This suggests that the Central Maine Ice Centre may have been contiguous with the North Maine Ice Divide during the Scotian Phase (Fig. 21d).

The strength of the Tuadook–Renous flow pattern in the northern part of the report area is indicated by several features. These include the associated east-northeast-trending large-scale fluting (Fig. 3), the Trout Lake dispersal train (Fig. 14), and several lesser dispersal trains in the Hayesville map area (Fig. 4) that are of parallel trend. The northeastward curvature of the Tuadook–Renous flowlines into the Curventon–Bathurst valley (Rampton et al. 1984) indicates that an ice stream developed in this area, fed by the Central Maine Ice Centre to the west and flowing into Bathurst Bay to the northeast. The enhanced velocity of the ice stream likely was responsible for the fluting and glacial dispersal associated with this flow pattern.

The distinct dispersal trains in the northern part of west-central New Brunswick indicate that, unlike the Escuminac ice flow, the Scotian ice flow was powerful or fast enough here to generate its own till. Some of the new till may have been generated by reworking of the pre-existing Caledonia till. However, the distinct dispersal trains extend back to known source areas, indicating that some new material was entrained from local bedrock. Therefore, this till is interpreted as a separate till, informally referred to as the 'Scotian till.'

Indicators of eastward to northeastward glacial dispersal are common in northeastern New Brunswick (Pronk et al. 1989; Parkhill and Doiron 2003). Some of the eastward dispersal may be attributed to the earlier Northumberland Phase. However, some probably took place during the Scotian Phase, as this area was also subject to drawdown into the Curventon–Bathurst valley and an ice stream in Chaleur Bay. Therefore, the surface till in northeastern New Brunswick is tentatively correlated with the Scotian till. It should be noted that, if this correlation is correct, the 'Upper till' of Lamothe (1992) in the northeast will not be correlative with similar till in west-central New Brunswick, attributed above to the Caledonia Phase.

Late Wisconsinan: Chignecto Phase

Definition

The Scotian Phase glaciers began to retreat from their maximum extent around 15 ka, due to climatic warming and associated sea-level rise (Stea et al. 1998). Stea et al. (1998) and Stea (2004) related the Chignecto Phase specifically to a minor glacial readvance that occurred around 13 ka to 12.5 ka. That definition is expanded herein to encompass the time interval from 15 ka to 13 ka, during which new ice divides were active following the breakup or migration of the Scotian Phase ice centres and divides. Therefore, the minor readvance is now interpreted to represent merely the 'last gasp' of the Chignecto Phase.

It should be noted that this Chignecto Phase has no direct correlation with the 'Chignecto phase' of Rampton et al. (1984), which they identified as the first Late Wisconsinan phase, approximately equivalent to what is now called the Escuminac Phase.

West-Central New Brunswick and Adjacent Areas

The rising late-glacial sea level led to formation of the De Geer Sea in the Gulf of Maine–Bay of Fundy area (Lougee 1954). Development of the De Geer Sea signalled the end of the Central Maine Ice Centre. The New Brunswick Highlands (Fig. 1) extend into eastern Maine, where they are flanked to the northwest and west by the Coastal Lowlands of western and central Maine (Denny 1982). Therefore, calving into rising marine waters caused much greater ice retreat in Maine than in adjacent New Brunswick, where the highlands extend to the Bay of Fundy shore. Consequently, the centre of ice flow migrated from central Maine into southern New Brunswick. Evidence for late northward ice flow in west-central and southwestern New Brunswick indicates that the outflow centre lay over the St. Croix Highlands (Fig. 1). Another late ice centre also may have overlain the Caledonian Highlands (Fig. 1; Foisy and Prichonnet 1991). Consequently, the glacial effects of the Chignecto Phase in southern New Brunswick are interpreted to be due to the newly defined 'Fundy Highlands Ice Divide,' overlying the St. Croix and Caledonian highlands (Fig. 21e).

In southwestern New Brunswick, calving into the De Geer Sea caused the Fundy Highlands Ice Divide margin to retreat to the Bay of Fundy shoreline (Seaman 1989c). The Campobello moraine on Campobello Island, St. George moraine, Pennfield–Utopia and Pocologan delta complexes, and Sheldon Point moraine in Saint John—all in southwestern New Brunswick

(Fig. 4)—are interpreted to mark late Chignecto Phase ice margins formed in contact with the De Geer Sea (Seaman et al. 1993). Farther east, the ice margin was probably defined by steep cliffs along the northern shore of the Bay of Fundy. The ice margin there was probably an ice cliff similar to that seen locally at the margin of the modern Columbia Icefield in Alberta (Fig. 23).

The transition from the Central Maine Ice Centre of the Scotian Phase to the Fundy Highlands Ice Divide of the Chignecto Phase was probably gradual. The northeast-trending Harcourt and Doaktown flow patterns (Rampton et al. 1984) may relate to this period of transition. Northwest-trending striae (Prest *in* Hunt and Roddick 1992b) northwest of Woodstock, north-northeast-trending rat-tails in the Magaguadavic River valley southwest of Oromocto Lake (S. Allard, pers. comm., 2003), and the apparent north-northwest trend of the Fredericton drumlins (Fig. 10) are all interpreted to relate to northward ice flow from the Fundy Highlands Ice Divide during the Chignecto Phase. The north-northwest-trending McLean Brook dispersal train (Fig. 14) and the north-trending striae near Boiestown (Lamothe 1990b) could relate to this phase. However, they may also have been formed during the later Collins Pond Phase.

In southwestern New Brunswick, the minor readvance at the end of the Chignecto Phase is recorded in the St. George moraine. Readvance of the Fundy Highlands Ice Divide deposited basal till over the northern face of the moraine and generated deformation structures in the underlying glaciomarine sediments (Fig. 24). The age of this glacial readvance has not been directly dated. However, its age is bracketed by dates on shells from the Pennfield delta complex to the east and from glaciomarine deposits in the St. Croix River estuary to the west (Gadd 1973). The sample from the former location gave an uncorrected date of 13.0 ka (GSC-882); two others from the latter area gave uncorrected dates of 12.3 ka (GSC-795, GSC-886). Because the St. George moraine lies only a few kilometres west of the delta complex, the readvance probably occurred shortly after 13 ka. It is therefore contemporaneous with the Chignecto Phase readvance in Nova Scotia and eastern New Brunswick reported by Stea et al. (1998) and Stea (2004).

Late Wisconsinan: Deglaciation

The Chignecto Phase in southwestern and west-central New Brunswick was probably terminated by the incursion of an arm of the De Geer Sea into the Saint John River valley, creating Inland Sea Acadia (Rampton et al. 1984). This would have partitioned the Fundy Highlands Ice Divide from south to north. The partitioning probably occurred shortly after the Chignecto Phase readvance, as Rampton et al. (1984: BGS-684) reported a date of 12.7 ka for an organic deposit overlying glacial deposits in the Saint John River valley in the Woodstock area, indicating that the valley was open by that time.

Corroborating evidence for the 12.7 ka date comes from the Saint John River valley near Grand Lake east of Fredericton, where organic material at a core depth of 28.68 m gave an age of 11.3 ka (Dickinson 2008: TO-13071). An additional 30 m of silty clay and clay lay below this level, overlying about 4 m of sand, followed by 5 m of till overlying bedrock. Lamination in the silt–clay sequence showed a nominal 28.5 laminae per 610 mm of core for an average

Figure 23. An ice cliff at the eastern edge of the Columbia Icefield, Alberta, viewed from the Icefield Parkway. The southern margin of the Fundy Highlands Ice Divide east of Saint John probably was similar, but with waters of the De Geer Sea below the cliff instead of vegetation.

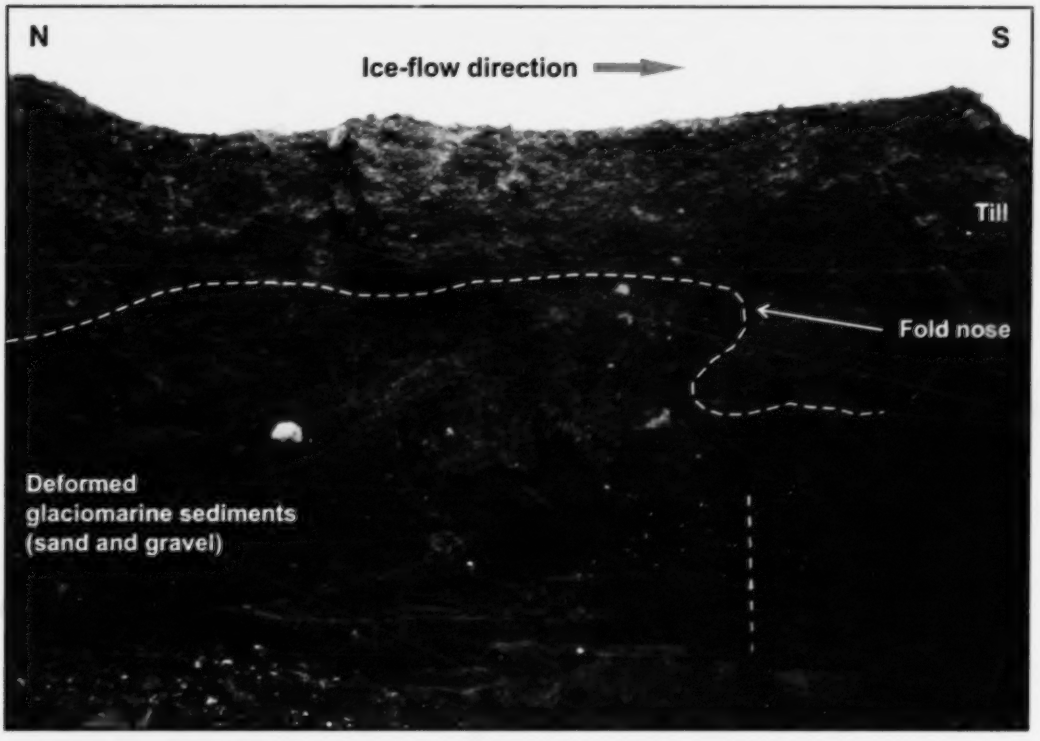

Figure 24. Basal till of the Chignecto Phase overlying glaciotectonically deformed (see fold) glaciomarine sediments of the St. George moraine, site G2-119 of Finamore and Seaman (1988), St. George map area (Fig. 4; Table 2). Scale units = 10 cm.

thickness of about 20 mm (Dickinson 2008). This is similar to thicknesses recorded in silt–clay couplets in rhythmites in the upper part of the glaciolacustrine sequence in the Fredericton area (Seaman 1982, his Plate XVI). If most of these rhythmites are varves, indicating annual deposition of each couplet, then initial inundation of the Saint John River valley by Inland Sea Acadia can be estimated to have occurred around 12.8 ka. Geochemical analyses confirm that the initial waterbody in the Saint John River valley was estuarine (Dickinson 2008), as proposed by Seaman (1982), and not lacustrine, as proposed by Lee (1957) and subsequently by Seaman (2004).

Deglaciation of southwestern New Brunswick appears to have been due to downwasting of a stagnant glacier. Evidence for this occurs in the extensive accumulations of ablation till in topographic lows and in the massive, preserved dendritic subglacial drainage system that terminated in the Pennfield–Utopia and Pocologan delta complexes (Fig. 4; Seaman et al. 1993). Rampton et al. (1984) interpreted the trend of the esker system to indicate the last ice-flow direction before deglaciation. However, the esker system under a stagnant glacier follows the subglacial hydrographic gradient, and its parallelism with observed striae trends of earlier glacial phases is merely coincidental.

Unlike the underlying basal till, the ablation till southwest of the Saint John River valley in west-central New Brunswick is commonly of local character. This likely is due to the complex glacial dynamics of the Caledonia, Escuminac, Scotian, and Chignecto phases, which may have produced the following scenario. The ablation material first was entrained by upshearing out of the basal zone (see analogy of Hicock 1987 under ***Ablation Till***) during the Caledonia Phase and then transported southeastward to south-southeastward. It remained fairly stationary during the mid-Wisconsinan before being transported southward, southwestward, and possibly westward during the Escuminac Phase. With the subsequent breakdown of the Escuminac Ice Centre and development of the Central Maine Ice Centre during the Scotian Phase, the ablation material was transported toward the east to northeast. Finally, during the Chignecto Phase, it was transported northward to northwestward. As a consequence, when the glacier began downwasting after the Chignecto Phase readvance, the ablation material was coincidentally close to its point of origin, having in effect taken an englacial or supraglacial 'tour' of southwestern New Brunswick and adjacent Maine.

A basal organic date from Splan Pond (formerly Basswood Road Lake; Seaman et al. 1993) north of St. Stephen (Fig. 4) indicates that the extreme southwest of New Brunswick was deglaciated by 12.6 ka (Mott 1975: GSC-1067). On the basis of pollen profiles, Mott discounted older dates on Little Lake in the Pennfield–Utopia delta complex as anomalously old. Twig fragments from near the base of a profile at Mayflower Lake, Saint John (also in southern New Brunswick), gave a date of 12.0 ka (Levesque et al. 1993: TO-1947).

The following additional dates are of significance to the interpretation of deglaciation in west-central New Brunswick.

- A date of 11.5 ka was obtained for twig fragments situated 12 cm above the base of cores from Pine Ridge Pond in the Magaguadavic River outwash plain west of Oromocto Lake (Levesque et al. 1994: Beta-55257). This date indicates that outwash deposition in the valley ended about 12 ka or shortly thereafter.

- Similar fragments from about 15 cm above the base of a profile from Killarney Lake in Fredericton returned a date of 11.2 ka (Levesque et al. 1993: TO-3001).

Together, these dates suggest that the area southwest of the Saint John River valley was completely deglaciated before 11.0 ka.

Central New Brunswick likely was not completely deglaciated after the end of the Chignecto Phase, as much of the area became reglaciated during the Younger Dryas Stadial (Collins Pond Phase). Nova Scotian evidence (see below) suggests that Younger Dryas glaciers readvanced for only a few tens of kilometres. Therefore, much of the New Brunswick Lowlands north of the Saint John River were probably still covered by a remnant Late Wisconsinan glacier that became the Gaspereau Ice Centre, described below.

Late Wisconsinan: Collins Pond Phase

Definition

The Collins Pond Phase (c. 11–10 ka) is correlative with the Younger Dryas Stadial, a millennial-scale cold interval at the end of the Wisconsinan Stage that followed a period of general climatic amelioration. Calculations by Levesque et al. (1994), for example, indicate that the summer surface water temperature of Pine Ridge Pond in the Magaguadavic River outwash plain dropped almost 12°C from a late-glacial high of 21.6°C during this interval. The phase was named for the first site in Nova Scotia that yielded unequivocal evidence for a Younger Dryas till overlying slightly older organic deposits (Stea and Mott 1989; Stea et al. 1998).

West-Central New Brunswick and Adjacent Areas

The western part of the Central Lowland and adjacent parts of the New Brunswick Highlands were demonstrably occupied by a glacier during the Younger Dryas (Seaman 2006). The area corresponds to that of the 'Gaspereau Ice Centre' as originally defined by Rampton et al. (1984). However, the Gaspereau Ice Centre was not an outflow centre during the Early Wisconsinan or earlier parts of the Late Wisconsinan (as had been assumed by Rampton et al. 1984). Hence, Seaman (2006) redefined the Gaspereau Ice Centre as specifically a Younger Dryas ice cap.

Seaman (2006) initially placed the western margin of the Gaspereau Ice Centre at the approximate position of the roughly 100 m high topographic feature known informally as Nashwaak Ridge. However, the Sisson Brook exploration trench of Geodex Minerals Ltd., immediately west of the ridge, exposed an organic-bearing surface till (Fig. 25) dated as Younger Dryas (Seaman and McCoy 2008). Thus, the Gaspereau Ice Centre not only had

Figure 25. Deformed organic silt in till of the Collins Pond Phase (Younger Dryas) at Sisson Brook, Coldstream map area (Fig. 4; Table 2). Overturned fold (dashed line) indicates deformation by westward-flowing ice of the Gaspereau Ice Centre. Hammer handle is 30 cm long.

reached farther west than originally proposed by Seaman (2006), but also was sufficiently thick to easily overtop Nashwaak Ridge. Dates on organic material in the Younger Dryas till and from the base of an overlying channel fill indicate that the ice centre readvanced rapidly, reaching its maximum extent shortly after 11.0 ka (Seaman and McCoy 2008). It persisted at its maximum extent in this area for at most 400 years before retreating to the east of Nashwaak Ridge.

The rapid advance of the Gaspereau Ice Centre to its maximum western position is compatible with its development from a remnant Late Wisconsinan glacier that persisted in the western New Brunswick Lowlands following the Chignecto Phase. In Nova Scotia, the readvance of glaciers of the Collins Pond Phase was in the order of 10 km to 20 km (R.R. Stea, pers. comm., 2009). Formation of the Gaspereau Ice Centre by 'instantaneous glacierization' (Ives et al. 1975) is considered less likely. Such 'glacierization' would involve "widespread and rapid expansion and coalescence of permanent snowbanks" (Ives et al. 1975, p. 121) in elevated areas of relatively flat topography, due to lowering of the regional snowline—a process more likely to occur in highlands than in lowlands.

The full extent of the Gaspereau Ice Centre in central New Brunswick remains to be determined. Seaman (2006) suggested it may have occupied the Grand Lake Basin (Fig. 4). However, Dickinson (2008) showed conclusively that the southern part of the Grand Lake Basin was not glaciated during the Younger Dryas. The ice margin therefore lay north of the

Saint John River valley. A calving front may have existed in the shallow, northern part of the Grand Lake Basin. The persistence of Younger Dryas ice in this part of the basin would explain the discordantly low 'marine' limits observed in the area by Rampton and Paradis (1981a).

According to Dickinson (2008), the body of water in the Saint John River valley may have transitioned from brackish (estuarine) to fresh at about the beginning of the Younger Dryas. Seaman (2004) suggested that the valley may have been dammed by readvance of a remnant glacier over the Caledonian Highlands, creating Glacial Lake Acadia. However, Dickinson (2008) presented an alternate hypothesis that the dam was created by the inland migration of the peripheral bulge, which raised the sill to the south above the prevailing sea level. Irrespective of the mechanism, the consequence would be the same: Inland Sea Acadia gradually transitioned into freshwater Glacial Lake Acadia, as saline water of the former was diluted by the continued inflow of fresh meltwater from the Gaspereau Ice Centre and other Younger Dryas ice centres in the Saint John River basin (Fig. 21f).

The maximum southwestern extent of the Gaspereau Ice Centre would be limited by Glacial Lake Acadia. It now seems probable that the Nashwaak, Jones Forks, and Keswick glaciofluvial deltas (Seaman 1982) were formed, at least in part, during the Collins Pond Phase. These deltas, in tributary streams north of the Saint John River valley, lie immediately south of the area overrun by the Gaspereau Ice Centre. The extensive ablation moraines in the eastern part of the Millville map area (Fig. 4) to the west may mark the western limits of the Gaspereau Ice Centre, as the south-southeast-trending Cloverdale dispersal train (Seaman 2001) appears to have undergone little modification after the Escuminac Phase.

The northern and eastern extents of the Gaspereau Ice Centre have yet to be determined. The lack of evidence for glacial over-riding in Joe Lake (Levesque et al. 1993) just north of the Hayesville map area (Fig. 4) indicates that it did not extend this far northward (Seaman 2006). However, evidence from other sites suggests that the northern margin of the ice centre may have lain north of the Southwest Miramichi River. These sites (see Appendix 2) include 1) the 1.8 m of till overlying glaciofluvial sediments at site HV-DE02, 2) buried or reworked glaciolacustrine deposits in the Southwest Miramichi River valley at sites HV-B08a, HV-F12a, and HV-T11a, and 3) the buried ablation till in the Doaktown map area (Fig. 4) at site DT-E07. It is tentatively suggested that the Despres Lake esker and related deposits in the Blackville map area (Fig. 4; Seaman 1983) were formed near the eastern limit of the Gaspereau Ice Centre. Farther southeast, the Gaspereau Ice Centre may have been contiguous with the Caledonian Highlands Ice Centre (Foisy and Prichonnet 1991), or the one over Prince Edward Island and adjacent Nova Scotia (Stea et al. 1998; Stea 2004).

The date of c. 10.6 ka for basal peat from the surface channel at Sisson Brook (Seaman and McCoy 2008) indicates that the Gaspereau Ice Centre began to wane shortly after it reached its maximum extent in west-central New Brunswick. It is presumed to have largely dissipated by the beginning of the Holocene, c. 10 ka. However, it may have persisted longer, as the only constraint to date is a near-basal organic date of c. 8.2 ka (Rampton et al. 1984; Seaman 2006: BGS 77) from a bog between Fredericton and Grand Lake.

DISCUSSION

Five of the conundrums regarding the glacial history of New Brunswick have been that:

- New Brunswick apparently lacked glacial deposits older than the Wisconsinan, despite the widespread preservation of weathered bedrock interpreted to be preglacial;
- the glacial striae record in New Brunswick featured multiple ice-flow trends, some recurring;
- a common lack of parallelism appeared to exist between the direction of glacial dispersal and the last direction of ice flow as recorded by glacial striae;
- except for in major valleys, New Brunswick lacks the thick depositional till sequences so typical of Nova Scotia, and
- in areas devoid of nunataks, supraglacial ablation till of proximal derivation occurs locally overlying basal till of distal derivation.

The first of these conundrums can be resolved by identifying the Northumberland till (the 'Lower till' of Lamothe 1992) as of probable Illinoian age, and interpreting much of the preserved weathered rock as Sangamonian. The absence of even older tills is consistent with observations in Ontario and Québec. Clet-Pellerin and Occhietti (2000, p. 44) report that during the Illinoian glaciation "ice sheets eroded most of the older Quaternary deposits, and left a very discontinuous till cover which in most cases directly overlies the bedrock." With the identification of the Northumberland till, the glacial stratigraphy of New Brunswick is now comparable to that of Ontario, Québec, and Nova Scotia.

The second conundrum is readily explained by the Appalachian Glacier Complex model of Stea et al. (1998) and Stea (2004). With ice flowing at different times from different ice centres or ice divides in widely separated geographic areas, a complex glacial erosion record is to be expected. In addition, the sequence of ice-flow phases in the Appalachian Glacier Complex model explains much of the previously developed erosional chronology of Seaman et al. (1993). The lack of evidence for a period of subaerial exposure between the Wisconsinan striae sets is due to continuous ice cover; the varying flow directions merely represent changes in outflow centre within a single ice mass (Seaman et al. 1993).

The third conundrum is explained by interpreting the flow of the Appalachian Glacier Complex to have grown less powerful over time, due to decreased ice thickness or flow velocity. Under such conditions, the later flows were generally too weak to generate a new till. Instead, they locally reworked the older till, often just enough to reorient its fabric and locally add a few striae to suitable underlying bedrock surfaces. Therefore, a striae record was created for the new phase but not an accompanying depositional record. The till was not transported far enough to remove it from the general area of pre-existing dispersal trains.

The fourth conundrum is also explained by the relative weakness of Late Wisconsinan glacial flows across New Brunswick. In essence, while thick tills were being deposited in Nova Scotia, the pre-existing Caledonia till in much of New Brunswick was either being eroded or merely being reworked with the addition of little if any new material.

The fifth conundrum is explained by the entrainment and deposition model of Hicock (1987), described under ***Ablation Till***, combined with the multiple flow directions resulting from diverse actions of the Appalachian Glacier Complex.

Clet-Pellerin and Occhietti (2000) noted the rare occurrence of older deposits beneath the Illinoian till in Ontario and Québec. A similar situation probably accounts for the weathered gravel at the McGregor Brook site (Rampton et al. 1984). Organics at this site, with a non-finite data of >35 ka (BGS-806), are presumed to be comparable in age to the Half Moon Sediments. The underlying till with its east–west fabric (Seaman 2004) is therefore interpreted to be the Northumberland till. The underlying weathered gravel thus represents a pre-Illinoian fluvial deposit, which could be earlier Pleistocene or even pre-Pleistocene.

CONCLUSIONS

Much of the evidence relating to the glaciation of west-central New Brunswick can be attributed to actions of the Appalachian Glacier Complex, beginning in the Middle Pleistocene (Illinoian Glaciation), and resuming in the Late Pleistocene (Wisconsinan Glaciation). The history of the Middle–Late Pleistocene in this area is now interpreted to comprise ten climatic or glacial periods.

1. Evidence of the Early–Middle Pleistocene glacial events in New Brunswick was largely eroded and/or transported offshore by eastward to east-southeastward flow from the White Mountains–Megantic Hills Ice Divide during the Northumberland Phase (Illinoian Glacial Stage) at the end of the Middle Pleistocene (c. 200–130 ka). In west-central New Brunswick, large- and small-scale glacial erosion features and scattered, generally buried, remnants of the Northumberland till remain as evidence for this phase.

2. The Late Pleistocene began with the complete deglaciation of New Brunswick (Sangamonian Interglacial Stage, c. 130–75 ka). Fluvial sediments interpreted to be of this age are now known from the Miramichi Lake valley (the Half Moon Sediments). Sediments of possibly similar age occur in the Saint John River valley area and northeastern New Brunswick (as evidenced in Lamothe 1992). Much of the weathered bedrock in west-central New Brunswick was probably formed during this interglacial interval.

3. The Wisconsinan glaciation in New Brunswick began with the Caledonia Phase (Early–Middle Wisconsinan, c. 75–40 ka), a southeast- to south-southeast-trending flow that traversed the Maritime provinces. The source of glaciation—either the Laurentide Ice Sheet or the North Maine–Notre Dame Ice Divide—has been much debated. However, it now seems most likely that western New Brunswick was inundated by the Laurentide Ice Sheet, while parallel flow from the Notre Dame Ice Divide inundated eastern New Brunswick. The Caledonia Phase glaciation was the most important in west-central New Brunswick. It involved significant glacial erosion, the generation of most dispersal trains in west-central New Brunswick, and the deposition of Caledonia till, which is the surface till throughout much of the area.

4. The Middle Wisconsinan deglaciation (c. 40–22 ka) was such in name only for New Brunswick, as the entire province remained ice-bound. However, the ice was thinner than during the Caledonia Phase and probably was frozen to the underlying substrate. Its effects on the underlying landscape, if any, were minimal.

5. The Late Wisconsinan glaciation began with the Escuminac Phase, which corresponds to the late-glacial maximum (c. 22–18 ka). Ice flow was southward to southwestward, and possibly westward, from the Escuminac Ice Centre over the Gulf of St. Lawrence. In west-central New Brunswick, the effects of this phase were largely limited to small-scale erosion and reworking of the Caledonia till. However, an Escuminac till may have been formed west of Grand Lake, where southwest-oriented glacial fluting occurs.

6. Thinning of the Escuminac glacier led to its retreat from its maximum position and its breakdown into an ice divide over Nova Scotia and an ice centre in central Maine during the Scotian Phase (c. 18–15 ka). Flow from the Central Maine Ice Centre was eastward to northeastward across west-central New Brunswick. As with the Escuminac Phase, the effects of this phase were generally limited. However, a Scotian till was deposited in parts of the Doaktown and Hayesville areas, accompanied by comparatively short glacial dispersal trains.

7. The rising level of the De Geer Sea following the Scotian Phase caused rapid glacial calving in the Bay of Fundy and adjacent lowland areas. During the Chignecto Phase (c. 15–13 ka), the flow centre migrated from the Central Maine Ice Centre to the Fundy Highlands Ice Divide, established over the New Brunswick Highlands area adjacent to the Bay of Fundy. Northward ice flow from this ice divide generated only limited evidence for its passage in west-central New Brunswick, namely a few scattered striae and reorientation of the Fredericton drumlins.

8. With partitioning of the Fundy Highlands Ice Divide by invasion of the De Geer Sea into the Saint John River valley, the Chignecto Phase was terminated. The ice mass southwest of the river became stagnant and in time disappeared by downwasting. Deglaciation was complete in that area prior to 11 ka.

9. Climatic deterioration at the beginning of the Younger Dryas Stadial (c. 11 ka) led to modest readvance of the Gaspereau Ice Centre from a remnant glacier northeast of the Saint John River valley.

10. Final deglaciation of the area occupied by the Gaspereau Ice Centre probably occurred around the end of the Younger Dryas Stadial (c. 10 ka) or early in the Holocene.

ACKNOWLEDGEMENTS

This paper was critically reviewed by Serge Allard and Toon Pronk of the New Brunswick Department of Natural Resources. An earlier draft was reviewed by Dr. Pam Dickinson. Its content was improved by their comments and by discussions with Dr. Ralph Stea, formerly of the Nova Scotia Department of Natural Resources. Figures were prepared by Terry Leonard.

REFERENCES

Allard, S. 2003. Geochemistry, lithology, and depositional history of the Rollingdam (NTS 21 G/06) map area till, southwestern New Brunswick. New Brunswick Department of Natural Resources and Energy; Minerals, Policy and Planning Division, Open File 2003-2, 218 p.

Allard, S., and Pronk, T. 2003. Glacial history of southwestern New Brunswick: challenges to drift prospecting. *In* Current Research 2002. *Edited by* B.M.W. Carroll. New Brunswick Department of Natural Resources; Minerals, Policy and Planning Division, Mineral Resource Report 2003-4, p. 1–11.

Anderson, F.D. 1968. Woodstock, Millville, and Coldstream map areas, York and Carleton counties, New Brunswick. Geological Survey of Canada, Memoir 353, 69 p.

Borns, H.W., Jr., Doner, L.A., Dorion, C.C., Jacobsen, G.L. Jr., Kaplan, M.R., Kreutz, K.J., Lowell, T.V., Thompson, W.B., and Weddle, T.K. 2004. The deglaciation of Maine, U.S.A. *In* Quaternary Glaciations–Extent and Chronology, Part II: North America. *Edited by* J. Ehlers and P.L. Gibbard. Developments in Quaternary Science, **2b**. Elsevier, Amsterdam, p. 89–109.

Broster, B.E., and Seaman, A.A. 1991. Glacigenic rafting of weathered granite: Charlie Lake, New Brunswick. Canadian Journal of Earth Sciences, **28**, p. 649–654.

Chalmers, R. 1884. Report on the surface geology of western New Brunswick with special reference to the area included in York and Carleton counties. Geological and Natural History Survey of Canada, Report of Progress, 1882–1884, Part GG, 47 p.

Chalmers, R. 1885. Preliminary report on the surface geology of New Brunswick. Geological and Natural History Survey of Canada, Annual Report, **I**, Part GG, 58 p.

Chalmers, R. 1890a. Report on the surface geology of southern New Brunswick to accompany ¼ sheet maps 1S.W., 1S.E., and 1N.E. Geological and Natural History Survey of Canada, Annual Report, **IV** (1888–1889), Part N, 92 p.

Chalmers, R. 1890b. The glaciation of the Cordillera and the Laurentide: correspondence. The American Geologist, **VI**, p. 324–325.

Chalmers, R. 1895. Report on the surface geology of eastern New Brunswick, north-eastern Nova Scotia and a portion of Prince Edward Island, to accompany ¼ sheet maps, No. 2 S.E, No. 5 S.W. and No. 4 N.W. Geological Survey of Canada, Annual Report, **VII** (1894), Part M, 149 p.

Chalmers, R. 1898a. Report on the surface geology and auriferous deposits of south-eastern Québec. Geological Survey of Canada, Annual Report, **X** (1897), Part J, 69 p.

Chalmers, R. 1898b. The pre-glacial decay of rocks in eastern Canada. American Journal of Science, **155**, p. 273–282.

Chalmers, R. 1902. Report on the surface geology shown on the Fredericton and Andover quarter-sheet maps, New Brunswick. Geological Survey of Canada, Annual Report, **XII** (1899), Part M, 41 p.

Charbonneau, R., and David, P.P. 1993. Glacial dispersal of rock debris in central Gaspésie, Québec, Canada. Canadian Journal of Earth Sciences, **30**, p. 1697–1707.

Clet-Pellerin, M., and Occhietti, S. 2000. Pleistocene palynostratigraphy in the St. Lawrence valley and middle estuary. Quaternary International, **68–71**, p. 39–57.

David, P.P., and Lebuis, J. 1985. Glacial maximum and deglaciation of western Gaspé, Québec, Canada. *In* Late Pleistocene History of Northeastern New England and Adjacent Québec. *Edited by* H.W. Borns,

Jr., P. LaSalle, and W.B. Thompson. Geological Society of America, Special Paper 197, p. 85–109.

Denny, C.S. 1982. Geomorphology of New England. United States Geological Survey, Professional Paper 1208, 18 p.

Dickinson, P.J. 2008. Geomorphological processes and the development of the lower Saint John River human landscape. Unpublished Ph.D. thesis, University of New Brunswick, Fredericton, 203 p.

Dreimanis, A. 1976. Tills: their origin and properties. *In* Glacial Till. *Edited by* R.F. Legget. The Royal Society of Canada Special Publications, No. 12, p. 11–49.

Elson, J.A. 1987. West-southwest dispersal of pillow-lava boulders, Philipsburg–Sutton region, Eastern Townships, Québec. Canadian Journal of Earth Sciences, **24**, p. 985–991.

Finamore, P.F. 1981. Granular aggregate resources of the Woodstock and Millville map-areas, New Brunswick (N.T.S. 21 J/4 and 21 J/3). New Brunswick Department of Natural Resources; Mineral Development Branch, Open File Report No. 81-4, 145 p.

Finamore, P.F., and Seaman, A.A. 1988. Granular aggregate resources, St. George (NTS 21 G/2) map area, New Brunswick. New Brunswick Department of Natural Resources and Energy; Minerals and Energy Division, Open File Report No. 88-2, 105 p.

Flint, R.F. 1951. Highland centers of former glacial outflow in northeastern North America. Bulletin of the Geological Society of America, **62**, p. 21–38.

Flint, R.F. 1971. Glacial and Quaternary Geology. John Wiley and Sons, Inc., New York, 892 p.

Foisy, M., and Prichonnet, G. 1991. A reconstruction of glacial events in south-eastern New Brunswick. Canadian Journal of Earth Sciences, **28**, p. 1594–1612.

Gadd, N.R. 1973. Quaternary geology of southwest New Brunswick with particular reference to Fredericton area. Geological Survey of Canada, Paper 71-34, 31 p.

Genes, A.N., Newman, W.A., and Brewer, T.B. 1981. Late Wisconsinan glaciation models of northern Maine and adjacent Canada. Quaternary Research, **16**, p. 48-65.

Goldthwait, J.W. 1924. Physiography of Nova Scotia. Canada Department of Mines, Geological Survey, Memoir 140, 179 p.

Grant, D.R. 1977. Glacial style and ice limits, the Quaternary stratigraphic record, and changes of land and ocean level in the Atlantic Provinces, Canada. Géographie physique et Quaternaire, **XXXI**, p. 247–260.

Harington, C.R., Grant, D.R., and Mott, R.J. 1993. The Hillsborough, New Brunswick, mastodon and comments on other Pleistocene mastodon fossils from Nova Scotia. Canadian Journal of Earth Sciences, **30**, p. 1242–1253.

Hicock, S.R. 1987. Genesis of carbonate till in the lee sides of Precambrian Shield uplands, Hemlo area, Ontario. Canadian Journal of Earth Sciences, **24**, 2004–2015.

Hind, H.Y. 1865. A preliminary report on the geology of New Brunswick, together with a special report on the distribution of the "Québec Group" in the Province. Journal of the Assembly of New Brunswick, Appendix 8, 293 p.

Hunt, C.B. 1972. Geology of Soils: Their Evolution, Classification, and Uses. W.H. Freeman and Company, San Francisco, 344 p.

Hunt, P.A., and Roddick, J.C. 1987. A compilation of K–Ar ages, Report 17. *In* Radiogenic Age and Isotope Studies: Report 1. Geological Survey of Canada, Paper 87-2, p. 143–210.

Hunt, P.A., and Roddick, J.C. 1991. A compilation of K–Ar ages, Report 20. *In* Radiogenic Age and Isotope Studies: Report 4. Geological Survey of Canada, Paper 90-2, p. 113–143.

Hunt, P.A., and Roddick, J.C. 1992a. A compilation of K–Ar ages, Report 21. *In* Radiogenic Age and Isotope Studies: Report 5. Geological Survey of Canada, Paper 91-2, p. 207–261.

Hunt, P.A., and Roddick, J.C. 1992b. A compilation of K–Ar and ^{40}Ar–^{39}Ar ages: Report 22. *In* Radiogenic Age and Isotope Studies: Report 6. Geological Survey of Canada, Paper 92-2, p. 179–226.

Hunter, M., and Lavergne, C. (GeoCon Inc.). 1982. Granular aggregate resources of Coldstream (21 J/6), Napadogan (21 J/7), Hayesville (21 J/10), and Juniper (21 J/11), New Brunswick. New Brunswick

Department of Natural Resources; Mineral Resources Division, Open File Report No. 82-2, 209 p.

Ives, J.D., Andrews, J.T., and Barry, R.G. 1975. Growth and decay of the Laurentide Ice Sheet and comparisons with Fenno-Scandinavia. Naturwissenschaften, **62**, p. 118–125.

Karrow, P.F., McAndrews, J.H., Miller, B.B., Morgan, A.V., Seymour, K.L., and White, O.L. 2001. Illinoian to Late Wisconsinan stratigraphy at Woodbridge, Ontario. Canadian Journal of Earth Sciences, **38**, p. 921–942.

Kaszycki, C.A., and Shilts, W.W. 1980. Glacial erosion of the Canadian Shield–calculation of average depths. Atomic Energy of Canada, Technical Record TR-106, 37 p.

Kirby, M.E., and Andrews, J.T. 1999. Mid-Wisconsinan Laurentide Ice Sheet growth and decay: implications for Heinrich events 3 and 4. Paleoceanography, **14**, p. 211–223.

Lamothe, M. 1989. A new framework for the Pleistocene stratigraphy of the central St. Lawrence Lowland, southern Québec. Géographie physique et Quaternaire, **43**, p. 119–129.

Lamothe, M. 1990a. Overburden drilling program in the Saint John River valley and the Baie des Chaleurs coastal area of northern New Brunswick: till geochemistry and borehole logs. Geological Survey of Canada, Open File 2149, 84 p.

Lamothe, M. 1990b. Till geochemistry in the vicinity of the Late Devonian granites of the Hayesville area, central New Brunswick. Geological Survey of Canada, Open File 2217, 66 p.

Lamothe, M. 1992. Pleistocene stratigraphy and till geochemistry of the Miramichi Zone, New Brunswick. Geological Survey of Canada, Bulletin 433, 58 p.

Lee, H.A. 1957. Surficial geology of Fredericton, York and Sunbury counties, New Brunswick. Geological Survey of Canada, Paper 56-2, 11 p.

Lee, H.A. 1962. Surficial geology of Canterbury, Woodstock, Florenceville and Andover map-areas; York, Carleton and Victoria counties, New Brunswick. Geological Survey of Canada, Paper 62-12, 8 p.

Levesque, A.J., Mayle, F.E., Walker, I.R., and Cwynar, L.C. 1993. A previously recognized late-glacial cold event in eastern North America. Nature, **361**, p. 623–626.

Levesque, A.J., Cwynar, L.C., and Walker, I.R. 1994. A multiproxy investigation of late-glacial climate and vegetation change at Pine Ridge Pond, southwest New Brunswick, Canada. Quaternary Research, **42**, p. 316–327.

Lougee, R.J. 1954. The role of up-warping in the post-glacial history of Canada: Part II, the Maritime region and the St. John valley. Revue Canadienne de Géographie, **VIII**, p. 3–52.

Lutes, G.G. 1987. Geology and geochemistry of the Pokiok Batholith, New Brunswick. New Brunswick Department of Natural Resources and Energy; Minerals and Energy Division, Report of Investigation 22, 55 p.

Mathew [*Matthew*], G.F. 1879. Report on the superficial geology of southern New Brunswick. Geological Survey of Canada, Report of Progress for 1877–78, Part EE, 36 p.

McDonald, B.C., and Shilts, W.W. 1971. Quaternary stratigraphy and events in southeastern Québec. Geological Society of America Bulletin, **82**, p. 683–698.

McLeod, M.J., Johnson, S.C., and Ruitenberg, A.A. 1994. Geological map of southwestern New Brunswick. New Brunswick Department of Natural Resources and Energy; Mineral Resources, Map NR-5.

McNeely, R., and McCuaig, S. 1991. Geological Survey of Canada radiocarbon dates XXIX. Geological Survey of Canada, Paper 89-7, 134 p.

Mott, R.J. 1975. Palynological studies of lake sediment profiles from southwestern New Brunswick. Canadian Journal of Earth Sciences, **12**, p. 273–288.

Munn, M.D. 1995. Till lithology and geochemistry in the Waterford area, New Brunswick. New Brunswick Department of Natural Resources and Energy; Minerals and Energy Division, Open File Report 95-4, 170 p.

Munn, M.D., Broster, B.E., and Pronk, A.G. 1996. Geochemical dispersal in till: Waterford area, New Brunswick. Atlantic Geology, **32**, p. 269–279.

Olejczyk, P., and Gray, J.T. 2007. The relative influence of Laurentide and local ice sheets during the last glacial maximum in the eastern Chic-Chocs Range, northern Gaspé Peninsula, Québec. Canadian Journal of Earth Sciences, **44**, p. 1603–1625.

Parkhill, M.A., and Doiron, A. 2003. Quaternary geology of the Bathurst Mining Camp and implications for base metal exploration using drift prospecting. Economic Geology, Monograph 11, p. 631–660.

Piotrowski, J.A., Larsen, N.K., and Junge, F.W. 2004. Reflections on soft subglacial beds as a mosaic of deforming and stable spots. Quaternary Science Reviews, **23**, p. 993–1000.

Prest, V.K. 1983. Canada's heritage of glacial features / L'heritage glaciaire du Canada. Geological Survey of Canada, Miscellaneous Report 28 / Commission géologique du Canada, Rapport divers 28, 119 p.

Prest, V.K., and Grant, D.R. 1969. Retreat of the last ice sheet from the Maritime Provinces–Gulf of St. Lawrence region. Geological Survey of Canada, Paper 69-33, 15 p.

Pronk, A.G., Bobrowsky, P.T., and Parkhill, M.A. 1989. An interpretation of late Quaternary glacial flow indicators in the Baie des Chaleurs region, northern New Brunswick. Géographie physique et Quaternaire, **43**, p. 179–190.

Rampton, V.N. 1984. Surficial geology, New Brunswick. Geological Survey of Canada, Map 1594A.

Rampton, V.N., and Paradis, S. 1981a. Quaternary geology of Woodstock map area (21 J), New Brunswick. New Brunswick Department of Natural Resources; Mineral Development Branch, Map Report 81-1, 37 p.

Rampton, V.N., and Paradis, S. 1981b. Quaternary geology of Moncton map area (21 I), New Brunswick. New Brunswick Department of Natural Resources; Mineral Development Branch, Map Report 81-2, 31 p.

Rampton, V.N., and Paradis, S. 1981c. Quaternary geology of Amherst map area (21 H), New Brunswick. New Brunswick Department of Natural Resources; Mineral Development Branch, Map Report 81-3, 36 p.

Rampton, V.N., Gauthier, R.C., Thibault, J., and Seaman, A.A. 1984. Quaternary geology of New Brunswick. Geological Survey of Canada, Memoir 416, 77 p.

Rappol, M. 1988. Glacial dispersal of Deboullie syenite, northern Maine, into western New Brunswick. *In* Current Research, Part B, Geological Survey of Canada, Paper 88-1B, p. 49–53.

Rappol, M. 1989. Glacial history and stratigraphy of northwestern New Brunswick. Géographie physique et Quaternaire, **43**, p. 191-206.

Rappol, M. 1993. Ice flow and glacial transport in lower St. Lawrence, Québec. Geological Survey of Canada, Paper 90-19, 28 p.

Rappol, M., and Russell, H. 1989. Glacial dispersal of Precambrian Shield and local Appalachian rocks in the lower St. Lawrence region in western Gaspésie, Québec, and in adjacent New Brunswick. *In* Current Research, Part B, Geological Survey of Canada, Paper 89-1B, p. 127–136.

Rappol, M., and Stoltenberg, H.M.K. 1985. Compositional variability of Saalian till in The Netherlands and its origin. Boreas, **14**, 33–50.

Robb, J. 1851. Notice of observations on drift striae in New Brunswick. Proceedings of the American Association for the Advancement of Science, **4**, p. 349–351.

Sacré, J.P. 1989. Stratigraphy, lithology, and geochemistry of till in the Hayesville map-area, central New Brunswick. Unpublished M.Sc. thesis, University of Waterloo, Ontario, Canada, 155 p.

Seaman, A.A. 1982. The late Quaternary history of the Burtts Corner area, New Brunswick. New Brunswick Department of Natural Resources; Mineral Resources Division, Open File Report 83-2, 105 p.

Seaman, A.A. 1983. Granular aggregate resources, Blackville (N.T.S. 21 I/12), New Brunswick. New Brunswick Department of Natural Resources; Mineral Resources Division, Open File Report 83-12, 73 p.

Seaman, A.A. 1988. Granular aggregate resources, Hampstead (NTS 21 G/9) map area, New Brunswick. New Brunswick Department of Natural Resources and Energy; Minerals and Energy Division, Open File Report 88-4, 53 p.

Seaman, A.A. 1989a. Glacial striae trends in New Brunswick: a compilation. New Brunswick Department of Natural Resources and Energy; Minerals and Energy Division, Open File Report 89-34, 136 p.

Seaman, A.A. 1989b. Glacial ice-flow directions in New Brunswick. New Brunswick Department of Natural Resources and Energy; Minerals and Energy Division, Plate 89-11.

Seaman, A.A. 1989c. Late Wisconsinan glaciation and deglaciation of the St. Croix Highlands area, southwestern New Brunswick [abstract]. *In* Late Glacial and Post-Glacial Processes and Environments in Montane and Adjacent Areas. Canadian Quaternary Association, CANQUA 1989, Edmonton, Alberta, Program and Abstracts, p. 46.

Seaman, A.A. 1991. Complex glacial ice-flow events in New Brunswick with particular reference to the Oromocto Lake area, and implications for drift prospecting. New Brunswick Department of Natural Resources and Energy; Mineral Resources, Geoscience Report 89-2, 48 p.

Seaman, A.A. 1992. Till geochemistry of part of the Forest City (NTS 21 G/12) map area, York County, New Brunswick. New Brunswick Department of Natural Resources and Energy; Mineral Resources, Open File Report 92-6, 88 p.

Seaman, A.A. 1999a. Till geochemistry of the New Brunswick part of the Forest City (NTS 21 G/12) and Fosterville (NTS 21 G/13) map areas, York and Carleton counties: site and geochemical data. New Brunswick Department of Natural Resources and Energy; Minerals and Energy Division, Open File 99-7, 67 p.

Seaman, A.A. 1999b. Follow-up till geochemistry in the Millville (NTS 21 J/3) map area, York County, New Brunswick. *In* Current Research 1998. *Edited by* B.M.W. Carroll. New Brunswick Department of Natural Resources and Energy; Minerals and Energy Division, Mineral Resource Report 99-4, p. 45–55.

Seaman, A.A. 2000a. Glacial dispersal in west-central New Brunswick [abstract]. Atlantic Geology, **36**, p. 71–72.

Seaman, A.A. 2000b. Till geochemistry and glacial dispersal in the eastern part of the Woodstock (NTS 21 J/04) map area, Carleton County, New Brunswick. *In* Current Research 1999. *Edited by* B.M.W. Carroll. New Brunswick Department of Natural Resources and Energy; Minerals and Energy Division, Mineral Resource Report 2000-4, p. 51–71.

Seaman, A.A. 2001. The Cloverdale As–Sb dispersal train, and other till geochemical anomalies in the west half of the Coldstream (NTS 21 J/06) map area, Carleton and York counties, New Brunswick. *In* Current Research 2000. *Edited by* B.M.W. Carroll. New Brunswick Department of Natural Resources and Energy; Minerals and Energy Division, Mineral Resource Report 2001-4, p. 97–110.

Seaman, A.A. 2002. Surficial geology and till geochemistry of the eastern two-thirds of the Coldstream (NTS 21 J/06) map area, York and Carleton counties, New Brunswick. *In* Current Research 2001. *Edited by* B.M.W. Carroll. New Brunswick Department of Natural Resources and Energy; Minerals, Policy and Planning Division, Mineral Resource Report 2002-4, p. 81–103.

Seaman, A.A. 2003. Follow-up till geochemistry, Coldstream (NTS 21 J/06) map area and part of the adjacent Napadogan (NTS 21 J/07) map area, York and Carleton counties, New Brunswick. New Brunswick Department of Natural Resources; Minerals, Policy and Planning Division, Open File 2003-11, 103 p.

Seaman, A.A. 2004. Late Pleistocene history of New Brunswick, Canada. *In* Quaternary Glaciations–Extent and Chronology, Part II: North America. *Edited by* J. Ehlers and P.L. Gibbard. Developments in Quaternary Science, **2b**. Elsevier, Amsterdam, p. 151–167.

Seaman, A.A. 2006. A new interpretation of the late glacial history of central New Brunswick: the Gaspereau Ice Centre as a Younger Dryas ice cap. *In* Geological Investigations in New Brunswick for 2005. *Edited by* G.L. Martin. New Brunswick Department of Natural Resources; Minerals, Policy and Planning Division, Mineral Resource Report 2006-3, p. 1–36.

Seaman, A.A. 2007. Reconnaissance till geochemistry of NTS 21 J/01, J/02, J/07, and J/08 map areas (parts of York, Sunbury, Northumberland, and Queens counties), central New Brunswick: site and geochemical data. New Brunswick Department of Natural Resources; Minerals, Policy and Planning Division, Open File (CD-ROM) 2007-8, 95 p.

Seaman, A.A. 2008. Till geochemistry of the Fredericksburg–South Tay River area, parts of the Burtts Corner and Napadogan map areas (NTS 21 J/02 and 21 J/07), York County, west-central New Brunswick. New Brunswick Department of Natural Resources; Minerals, Policy and Planning Division, Open File (CD-ROM) 2008-6, 55 p.

Seaman, A.A., and McCoy, S.M. 2008. Multiple Wisconsinan tills in the Sisson Brook exploration trench of Geodex Minerals Ltd., York County, west-central New Brunswick. *In* Geological Investigations in New Brunswick for 2007. *Edited by* G.L. Martin. New Brunswick Department of Natural Resources; Minerals, Policy and Planning Division, Mineral Resource Report 2008-1, p. 1–34.

Seaman, A.A., and Thibault, J.J. 1986. Granular aggregate resources of the Central Lowland area, east-central New Brunswick. New Brunswick Department of Forests, Mines and Energy; Mineral Resources Division, Open File Report 86-1, 213 p.

Seaman, A.A., Broster, B.E., Cwynar, L.C., Lamothe, M., Miller, R.F., and Thibault, J.J. 1993. Field guide to the Quaternary geology of southwestern New Brunswick. New Brunswick Department of Natural Resources and Energy; Mineral Resources, Open File Report 93-1, 102 p.

Seaman, A.A., Allard, S., Pronk, A.G., and Boldon, G.R. 2005. 'Ultratrace' ICP–MS values for till samples from the Hayesville (NTS 21 J/10) map area; York, Carleton, and Northumberland counties, central New Brunswick. New Brunswick Department of Natural Resources; Minerals, Policy and Planning Division, Open File (Digital) 2005-10, 84 p.

Stea, R.R. 2004. The Appalachian Glacier Complex in Maritime Canada. *In* Quaternary Glaciation–Extent and Chronology, Part II: North America. *Edited by* J. Ehlers and P.L. Gibbard. Developments in Quaternary Science, **2b**. Elsevier, Amsterdam, p. 213–232.

Stea, R.R., and Mott, R.J. 1989. Deglaciation environments and evidence for glaciers of Younger Dryas age in Nova Scotia, Canada. Boreas, **18**, p. 169–187.

Stea, R.R., Mott, R.J., Belknap, D.F., and Radtke, U. 1992. The pre-late Wisconsinan chronology of Nova Scotia, Canada. *In* The Last Interglacial / Glacial Transition in North America. *Edited by* P.U. Clark and P.D. Lea. Geological Society of America, Special Paper 270, p. 185–206.

Stea, R.R., Piper, D.J.W., Fader, G.B.J., and Boyd, R. 1998. Wisconsinan glacial and sea-level history of Maritime Canada and the adjacent continental shelf: a correlation of land and sea events. Geological Society of America Bulletin, **110**, p. 821–845.

Stumpf, A.J. 1995. Quaternary geology and dispersal patterns of the McAdam (NTS 21 G/11) map area, York County, New Brunswick. New Brunswick Department of Natural Resources and Energy; Minerals and Energy Division, Open File Report 95-5, 218 p.

Stumpf, A.J., Broster, B.E., and Seaman, A.A. 1997. Lithological and geochemical dispersal in till: McAdam area, New Brunswick. Atlantic Geology, **33**, p. 31–42.

Symons, D.T.A., Lewchuk, M.T., and Boyle, D.R. 1996. Pliocene–Pleistocene genesis for the Murray Brook and Heath Steele Au–Ag gossan ore deposits, New Brunswick, from paleomagnetism. Canadian Journal of Earth Sciences, **33**, p. 1–11.

Thomas, M.F. 1974. Tropical Geomorphology: A Study of Weathering and Landform Development in Warm Climates. The MacMillan Press Ltd., London, 332 p.

Veillette, J.J., and Nixon, F.M. 1982. Saprolite in the Big Bald Mountain area, New Brunswick. *In* Current Research, Part B, Geological Survey of Canada, Paper 82-1B, p. 63–70.

Wang, C., Ross, G.J., and Rees, H.W. 1981. Characteristics of residual and colluvial soils developed on granite and of the associated pre-Wisconsin landforms in north-central New Brunswick. Canadian Journal of Earth Sciences, **18**, p. 487–494.

Appendix 1. Till fabrics in west-central New Brunswick.

Site No.	Alternate Site No.	NTS Map Area	Easting NAD27	Northing NAD27	n°	Mean Up-dip a-axis Trend	Std. Dev.	Mean Angle of Imbric.†	Topog. Expos-ure ‡	Sugg't'd Ice-flow Trend	Min. a:b Axis Ratio	Colour	Sugg. Ice-flow Phase **	Comments
AS 88-16a	FJ 88-16a	21 G/10	672825	5054200	30 (3)	064°	36°	29°	NNE	ENE	1.4:1	5 YR 4/3	S	very compact till, across road from site AS 88-16b; nearby sandstone outcrop exhibits 3 striae sets, with average trends of 183° (oldest), 201°, and 164°
AS 88-16b	FJ 88-16b	21 G/10	672850	5054225	30 (3)	098° / 278°	34°	0°	NNE	E / W	1.5:1	5 YR 4/3	S	very compact till; underlying sandstone bedrock exhibits 10 different striae sets, with average trends of 093°, 101°, 110°, 122°, 153°, 161°, 170°, 180°, 191°, and 201° (see Seaman 1991)
AS 88-39	FJ 88-39	21 G/10	675925	5058000	50 (19)	130°	25°	15°	NNW	SE	1.4:1	5 YR 4/3	Ca	thin, very compact till, with numerous weathered sandstone clasts; overlies dark reddish brown siltstone
AS 88-40	FJ 88-40	21 G/10	681450	5049800	50 (1)	213°	22°	12°	S	SSW	1.4:1	5 YR 5/3	E	compact till
AS 88-41	FJ 88-41	21 G/10	678275	5044650	50 (2)	298°	37°	16°	SW	WNW	1.5:1	5 YR 4/3	Ch?	cobbly, moderately compact till
AS 88-43	FJ 88-43	21 G/10	659950	5046025	50 (5)	139°	30°	28°	SE	SE	1.4:1	10 YR 4/3	Ca	compact till
AS 88-45	FJ 88-45	21 G/10	666775	5049000	50 (0)	266°	40°	10°	WNW	W	1.4:1	5 YR 4/3	E?	compact till
CB MP-2	FJ MP-2	21 G/10	675025	5043300	25 (2)	140°	19°	13°	ESE	SE	1.6:1	5 YR 4/4	Ca	stony, compact till (C. Bianchi)
CB MP-4	FJ MP-4	21 G/10	675475	5041900	25 (8)	207°	19°	26°	W	SSW	1.3:1	5 YR 3/4	E	compact till (C. Bianchi)
CB MP-19	FJ MP-19	21 G/10	676950	5042000	25 (1)	152°	29°	14°	SSW	SSE	1.5:1	5 YR 3/4	Ca	compact till (C. Bianchi)
CB MP-21	FJ MP-21	21 G/10	676450	5046550	25 (8)	296°	32°	1°	NNE	WNW / ESE	1.7:1	5 YR 4/4	Ch?	stony, compact till; overlies one flank of an ablation till ridge (C. Bianchi)
CB MP-29	FJ MP-29	21 G/10	676750	5048700	25 (4)	001°	30°	7°	S	S?	1.6:1	5 YR 4/4	E?	stony, very compact till (C. Bianchi)
AS 88-44	MA 88-44	21 G/11	644350	5048550	50 (1)	129°	26°	18°	SSE	SE	1.5:1	10 YR 5/4	Ca	compact till
AS 88-48	MA 88-48	21 G/11	638025	5052175	50 (10)	286°	28°	6°	SW	WNW	1.5:1	2.5 Y 6/4	Ch?	moderately compact till; an ablation lag of large boulders is on surface in the area, grading into an ablation till blanket to the north
AS 89-57	MA 89-57	21 G/11	655525	5063400	25 (0)	114°	22°	18°	E	ESE	1.5:1	10 YR 4/3	N	very compact, fissile till

Site No.	Alternate Site No.	NTS Map Area	Easting NAD27	Northing NAD27	n*	Mean Up-dip a-axis Trend	Std. Dev.	Mean Angle of Imbric.†	Topog. Expos-ure ‡	Sugg't'd Ice-flow Trend	Min. a:b Axis Ratio	Colour	Sugg. Ice-flow Phase **	Comments
AS FC-22	FC-E19b-3	21 G/12	602125	5056725	25 (3)	089°	36°	12°	ENE	E	1.6:1	2.5 Y4/4	S	stony, compact till; overlain by ~1.75 m of ablation till: geochemical sample 22Bm (Seaman 1992), FC-E19b-3 (Seaman 1999a)
AS 89-42	CB 89-42	21 G/14	625250	5081500	25 (0)	036°	32°	9°	SE	NE	1.5:1	2.5 Y 6/6	Ch	moderately compact till with sandy lenses, overlying glaciotectonized granite (Broster and Seaman 1991, site 1); assumed to indicate SW ice flow
AS 89-51	CB 89-51	21 G/14	651125	5081900	25 (4)	010°	23°	10°	E	N	1.6:1	10 YR 4/4	Ch	compact to very compact till overlying weathered reddish brown (5 YR 4/3) siltstone
AS 89-55	CB 89-55	21 G/14	625200	5082950	25 (0)	192°	34°	9°	SE	SSW	1.5:1	2.5 Y 5/4	E	fissile till overlying granitic deformation till (Broster and Seaman 1991, site 2)
AS 89-56	CB 89-56	21 G/14	636575	5073525	25 (1)	231°	31°	20°	NW/SE col	SW	1.5:1	2.5 Y 5/4	E	very compact, fissile till
AS 89-66	CB 89-66	21 G/14	644425	5074925	25 (1)	004°	26°	24°	NNE	N	1.5:1	2.5 Y 5/4	Ch	very compact till
AS 89-1	FT 89-1	21 G/15	679000	5085600	50 (1)	191°	35°	3°	NE	S	1.4:1	5 YR 5/3	E	compact till
AS 89-68-1	FT 89-68-1	21 G/15	685300	5085500	9 (1)	004° / 184°	31°	0°	E	N / S	1.5:1	n/a	E?,Ch?	2.5 to 2.7 m above base of section
AS 89-68-2	FT 89-68-2	21 G/15	685300	5085500	25 (2)	156°	33°	9°	E	SSE	1.5:1	n/a	Ca	1.8 to 2.0 m above base of section
AS 89-68-3	FT 89-68-3	21 G/15	685300	5085500	25 (4)	166°	20	1°	E	SSE / NNW	1.5:1	n/a	Ca	1.1 to 1.3 m above base of section
MT-S03.5		21 J/01	724110	5119665	50 (15)	322°	35°	9°	NW	NW	1.5:1	10 YR 5/4	CP	compact basal till; appear to be 2 slightly different colours, with one slightly siltier and less compact than the other; indicator of subglacial reworking ?
BC-D01		21 J/02	661785	5123080	40 (17)	138°	20°	39°	ENE	SE	1.5:1	10 YR 4/4	Ca	compact to very compact basal till
98AS0061		21 J/03	640175	5102575	40 (2)	206°	28°	8°	WNW	SSW	1.5:1	10 YR 5/4	E	compact basal till; fabric is parallel to valley trend; Finamore (1981) observed till over sand and gravel at a site 125 m to the west
MV-Q14-1		21 J/03	642050	5096925	50 (0)	166°	21°	14°	S	SSE	1.4:1	5 YR 3/4	Ca	compact basal till, in valley bottom; geochemically and is

Site No.	Alternate Site No.	NTS Map Area	Easting NAD27	Northing NAD27	n°	Mean Up-dip a-axis Trend	Std. Dev.	Mean Angle of Imbric.†	Topog. Expos-ure ‡	Sugg'ted Ice-flow Trend	Min. a:b Axis Ratio	Colour	Sugg. Ice-flow Phase **	Comments
														lithologically similar to the lower till
MV-Q14-2		21 J/03	642050	5096925	50 (1)	159° / 339°	30°	0°	S	SSE / NNW	1.6:1	10 YR 5/4	Ca	compact basal till, in valley bottom; geochemically and lithologically similar to upper till
AS030011	CS-WX03a	21 J/06	653150	5146890	50 (7)	149°	32°	31°	NNE	SSE	1.5:1	10 YR 5/3	Ca	compact basal till, becoming sandier and less compact at a depth of 1.6 m; overlain by 0.6 m of basal meltout till
AS030012b	CS-WX03b-1	21 J/06	653460	5146830	50 (2)	140°	46°	16°	NNE	SE	1.5:1	10 YR 4/3	Ca	compact, fissile, basal till; Half Moon Pit section; till overlies organic-bearing sand; organic material dated at >36 ka, GSC-4199 (Lamothe 1992)
AS030013b	CS-VW02	21 J/06	651020	5149480	50 (4)	322°	29°	5°	NNE	NW / SE	1.5:1	10 YR 4/4	Ca	compact, fissile, basal till; overlain by 0.6 m of gravelly sand; overlies 0.3 m sandy gravel and 0.7+ m of sand and gravelly sand
AS030025		21 J/06	648050	5144230	30 (3)	262°	23°	33°	SW	W	1.6:1	10 YR 4/3	CP	very compact basal till
CS-SB-01		21 J/06	650210	5136735	35 (22)	264°	22°	14°	SE	W	1.6:1	n/a	CP	Younger Dryas till; south face of exploration trench; twigs from organic 'boulders' in this till were dated at 10.99 ka, TO-13588, and 11.03 ka, TO-13589 (Seaman and McCoy 2008)
CS-SB-02		21 J/06	650180	5136750	40 (6)	115°	36°	9°	SE	ESE	1.5:1	5 Y 5/2	N	oldest till; west face of trench (see Seaman and McCoy 2008)
CS-SB-03		21 J/06	650195	5136740	30 (3)	212°	38°	11°	SE	SSW	1.5:1	10 YR 5/3	Ca?,E?	intermediate till; south face of trench, ~15 m west of CS-SB-02 (see Seaman and McCoy 2008); parallel to trend of Nashwaak Ridge to the east
CS-SB-04		21 J/06	650195	5136740	35 (15)	129°	26°	7°	SE	NW / SE	1.5:1	10 YR 4/3	CP	Younger Dryas till, 1.2 to 1.4 m above SB-03; peak in fabric suggests ice flow toward the WNW (see Seaman and McCoy 2008)
CS-SB-05		21 J/06	650185	5136755	40 (8)	103°	36°	1°	SE	ESE / WNW	1.5:1	10 YR 5/2	N	oldest till; north face of trench across from SB-03 and SB-04; 1.2 to 1.4 m above the bedrock surface (see Seaman and McCoy 2008)
CS-SB-06-2		21 J/06	650225	5136735	40 (8)	290°	25°	15°	SE	WNW	1.5:1	10 YR 5/1	CP	organic-rich Younger Dryas till; south face of trench, ~ 15 m east of CS-SB-01 (see Seaman and

Site No.	Alternate Site No.	NTS Map Area	Easting NAD27	Northing NAD27	n*	Mean Up-dip a-axis Trend	Std. Dev.	Mean Angle of Imbric.†	Topog. Exposure ‡	Sugg't'd Ice-flow Trend	Min. a:b Axis Ratio	Colour	Sugg. Ice-flow Phase **	Comments
														McCoy 2008)
CS-T09-2		21 J/06	648020	5134750	50 (9)	142°	28°	4°	crest	SE	1.5:1	2.5 Y 5/4	Ca	compact to very compact basal till, in a Rogen moraine; overlain by 0.85 m of meltout till
CS-TV03		21 J/06	649270	5147090	30 (5)	333°	32°	15°	NW	NNW	1.5:1	10 YR 5/6	Ch	very compact basal till
CS-V08-2		21 J/06	650050	5137190	30 (7)	035°	19°	19°	NE	NE	1.5:1	2.5 Y 5/4	S	compact to very compact basal till; overlain by 0.85 m of probable Younger Dryas meltout till (see Seaman and McCoy 2008)
CS-V10.5a-1		21 J/06	649640	5132320	50 (2)	265°	47°	14°	SW	W	1.6:1	10 YR 5/6	CP	thin, very compact basal till; overlies 0.25 m of laminated sand
CS-V10.5a-3		21 J/06	649640	5132320	50 (4)	261°	33°	2°	SW	W	1.6:1	10 YR 5/3	CP	compact basal till; overlain by 0.25 m of laminated sand
CS-W07		21 J/06	651850	5139050	50 (6)	192°	21°	23°	WNW	SSW	1.5:1	2.5 Y 5/4	E	compact basal till
CS-W08.5		21 J/06	651350	5136020	50 (0)	095°	33°	28°	E	E	1.5:1	10 YR 5/4	S	compact basal till
CS-W09		21 J/06	651950	5134960	60 (6)	267°	38°	33°	crest	W	1.5:1	10 YR 5/4	CP	compact to very compact basal till
CS-W10b		21 J/06	651560	5133220	50 (1)	043°	31°	14°	NE	NE	1.5:1	2.5 Y 4/4	S	compact basal till
CS-WX08		21 J/06	653210	5136730	50 (13)	150°	31°	27°	E	SSE	1.5:1	2.5 Y 5/4	Ca	moderately compact till
CS-WX11.5b		21 J/06	653270	5130050	30 (6)	117°	32°	19°	SE	ESE	1.5:1	10 YR 5/3	N	compact to very compact basal till
CS-X14		21 J/06	653720	5124940	30 (6)	013°	31°	22°	NE	NNE	1.5:1	10 YR 5/4	Ch	compact basal till
AS030005	ND-FG06	21 J/07	665370	5141210	60 (1)	042°	29°	18°	N	NE	1.4:1	10 YR 4/6	S	thin, compact basal till; overlies gravelly deformation till
AS030010	ND-BC03.5	21 J/07	656780	5140790	50 (2)	353°	36°	16°	N	N	1.5:1	10 YR 4/6	Ch?,CP?	thin, very compact basal till; overlies 2.8+ m of predominantly sand or gravelly sand, but locally as coarse as cobbly sandy gravel (Half Moon Sediments)
AS030048-1	ND-FG08.5-1	21 J/07	664930	5136180	50 (6)	296°	25°	31°	WNW	WNW	1.5:1	10 YR 5/6	Ch?,CP?	thin, compact basal lodgement till
AS030048-2	ND-FG08.5-2	21 J/07	664930	5136180	30 (0)	282°	39°	5°	WNW	WNW	1.5:1	10 YR 3/4	Ch?,CP?	~0.5 m thick lens (?) of moderately loose sandy gravel, basal meltout till (?)
AS030048-3	ND-FG08.5-3	21 J/07	664930	5136180	30 (0)	299°	21°	33°	WNW	WNW	1.5:1	10 YR 5/6	Ch?,CP?	very compact basal lodgement till
AS030054	ND-	21 J/07	658910	5133470	50	219°	33°	27°	SSW	SW	1.5:1	10 YR	E	compact to very compact basal

Site No.	Alternate Site No.	NTS Map Area	Easting NAD27	Northing NAD27	n*	Mean Up-d/p a-axis Trend	Std. Dev.	Mean Angle of Imbric.†	Topog. Expos-ure ‡	Sugg't'd Ice-flow Trend	Min. a:b Axis Ratio	Colour	Sugg. Ice-flow Phase **	Comments
	CD10				(21)							5/3		lodgement till
AS030055	ND-D07.5	21 J/07	659640	5137970	30 (5)	139°	26°	11°	NE	SE	1.5:1	10 YR 5/4	Ca	compact basal lodgement till
AS030060	ND-EF03.5	21 J/07	662800	5146080	50 (9)	043°	41°	18°	SSE	NW	1.5:1	10 YR 5/3	S	very compact basal lodgement till
ND-A5b		21 J/07	653900	5142930	50 (2)	199°	39°	6°	E	SSW	1.5:1	10 YR 5/3	E	very compact basal till
ND-G12-1		21 J/07	665925	5129090	40 (2)	329°	17°	3°	NW	NNW	1.5:1	10 YR 5/3	CP?	compact basal till; overlies 0.8 m of sandy gravel that, in turn, overlies a geochemically different basal till (see Seaman 2008)
BT-G13.5		21 J/08	704260	5128030	50 (10)	148°	36°	14°	ESE	SSE	1.5:1	10 YR 4/3	Ca	moderately compact to compact, sandy till
AS030015	HV-P11.75	21 J/10	677980	5157560	60 (12)	166°	29°	16°	S	SSE	1.5:1	10 YR 3/4	Ca	very compact basal till
AS030039-1	HV-CD03.5-1	21 J/10	659240	5174020	30 (1)	266°	18°	17°	WNW	W	1.5:1	10 YR 4/4	E?	moderately compact to compact basal till
AS030039-2	HV-CD03.5-2	21 J/10	659240	5174020	30 (1)	268°	22°	19°	WNW	W	1.5:1	10 YR 5/4	E?	compact to very compact basal till
AS030049	HV-DE02	21 J/10	660920	5176790	60 (3)	359°	31°	10°	crest	N	1.5:1	10 YR 4/4	Ch?,CP?	very compact basal lodgement till; overlies 13.5+ m of interbedded sand, sandy gravel, and gravel
AS030050	HV-FG07.5	21 J/10	665180	5166300	50 (10)	100°	32°	8°	SW	E	1.5:1	10 YR 5/4	N?,S?	thin, compact basal till; overlies moderately loose, granitic deformation till
AS030051	HV-C12b	21 J/10	657820	5157420	30 (3)	041°	16°	17°	NE	NE	1.5:1	10 YR 4/3	S	moderately compact basal till
AS030052	HV-C08	21 J/10	658440	5164930	50 (9)	118°	33°	13°	SE	ESE	1.5:1	10 YR 5/4	N	moderately compact basal till
AS030053-1	HV-P11.5-1	21 J/10	678010	5158530	30 (1)	148°	15°	12°	NE	SSE	1.5:1	10 YR 5/4	CP	moderately compact to compact basal till; no significant imbrication with respect to the bedrock slope, probably due to post-depositional downslope movement
AS030053-2	HV-P11.5-2	21 J/10	678010	5158530	30 (4)	334°	17°	5°	NE	NNW	1.5:1	10 YR 4/3	CP	compact to very compact basal till; mixing zone between basal till and underlying rubble-like deformation till
AS030057	HV-DE14.5	21 J/10	660740	5152050	50 (8)	097°	30°	15°	E	E	1.5:1	10 YR 5/3	N?,S?	compact to very compact basal lodgement till
AS030059	HV-L13.5	21 J/10	672260	5154180	50 (2)	233°	25°	21°	WNW	SW	1.5:1	10 YR 5/4	E	very compact basal lodgement till

Site No.	Alternate Site No.	NTS Map Area	Easting NAD27	Northing NAD27	n*	Mean Up-dip a-axis Trend	Std. Dev.	Mean Angle of Imbric.†	Topog. Expos-ure ‡	Sugg't'd Ice-flow Trend	Min. a:b Axis Ratio	Colour	Sugg. Ice-flow Phase **	Comments
HV-F12b		21 J/10	664310	5156950	30 (1)	119°	22°	20°	ESE	ESE	1.5:1	7.5 YR 5/3	Ca?	compact basal lodgement till; the roadcut section exposes scattered clayey silt clasts up to boulder size (reworked lacustrine material from the Half Moon Sediments?)
HV-G04		21 J/10	665970	5173060	40 (6)	217°	27°	16°	S	SW	1.5:1	10 YR 6/4	E	very compact basal till
HV-G13b		21 J/10	666650	5155730	45 (0)	091°	32°	1°	NW	E / W	1.5:1	7.5 YR 4/3	E,?S?,CP?	compact to very compact basal till
HV-L11b	HV-X11	21 J/10	671920	5158950	40 (6)	034°	30°	20°	WNW	NE	1.6:1	10 YR 4/3	Ch	basal till
HV-M04.5		21 J/10	673710	5172070	40 (0)	338°	19°	20°	N	NNW	1.5:1	10 YR 5/3	Ch?,CP?	moderately compact to compact basal till
HV-NP07		21 J/10	676600	5166460	25 (2)	075°	23°	19°	ENE	ENE	1.5:1	10 YR 4/3	S	compact basal till
HV-Q01.5		21 J/10	680550	5177600	50 (11)	019°	36°	21°	NNE	NNE	1.5:1	2.5 Y 5/4	Ch?,CP?	moderately compact basal till
HV-Q14		21 J/10	680010	5153330	40 (6)	011°	27°	29°	NNE	N	1.5:1	10 YR 5/3	Ch?,CP?	compact to very compact basal till
HV-R10	HV-R10-1	21 J/10	681890	5160980	30 (1)	188°	21°	12°	SSW	S	1.5:1	10 YR 4/6	E	thin, compact to very compact basal till; overlies gravelly deformation till
HV-T12b		21 J/10	686420	5156400	40 (1)	240°	22°	27°	WNW	WSW	1.5:1	10 YR 5/3	E	compact basal till
HV-TV10		21 J/10	686920	5161120	45 (1)	274°	36°	11°	WNW	W	1.5:1	10 YR 5/4	E?	moderately compact basal till
HV-V05.5		21 J/10	687430	5169500	25 (1)	110°	19°	13°	ESE	ESE	1.6:1	10 YR 5/3	N	compact basal till
HV-V10		21 J/10	688320	5161070	40 (4)	130°	22°	32°	ESE	SE	1.5:1	10 YR 5/4	Ca	moderately compact basal till
HV-W03-2		21 J/10	689980	5174660	45 (4)	340°	29°	16°	N	NNW	1.5:1	2.5 Y 5/4	Ch	compact basal till; overlain by 0.7m of sandy ablation till

Notes:

* Number of pebbles measured (figure in brackets is number of clasts interpreted as transverse, and deleted from the statistical calculation).

† With respect to the horizontal.

‡ Regional slope, determined from the NTS topographic map.

** Ca = Caledonia; Ch = Chignecto; CP = Collins Pond; E = Escuminac; N = Northumberland; S = Scotian.

Appendix 2. Buried ablation till, glaciofluvial, or glaciolacustrine deposits in west-central New Brunswick.

Site No.	NTS Map Area	Easting NAD27	Northing NAD27	Till Thickness (m)	Underlying Deposit Thickness (m)	Underlying Material Type	Comments	Reference
G9-2	21 G/09	719800	5065100	1.4	1.3+	sandy silt / gravelly sand	N face in this pit was 27.5 m high, and mostly covered by slumped material; cobbly sandy gravel was observed toward base of slump-covered section; kame terrace	Seaman 1988
FJ MP-21	21 G/10	676450	5046550	1.05	1.5+	silty sandy gravel with silt pockets	cross-section sketch shows 0.4 m soil plus 0.6+ m of lodgement till overlying the flank of an ablation till ridge (ablation till to the surface at the crest); orientation of the section is not indicated	C.Bianchi, field notes (1989)
3029	21 G/14	621900	5093600	2.7	2.4	silt / till / sandy gravel	borehole section in Saint John River valley; upper till is overlain by 21.9 m of alluvium and silt and clay; lower till is 3.7 m thick, and is underlain by 17.4 m of sand and gravel overlying bedrock	Lamothe 1990a
CB-F14a	21 G/14	627950	5068950	0.71	0.79+	"not a till"	upper unit described as "till-like"	Balzer, field notes (1991)
CB-F14b	21 G/14	627650	5068750	0.74	0.35+	sandy gravel	extremely compact basal till	Seaman, field notes (1995)
Locality 13	21 G/15	662200	5072700	1.1	2.4+	sand	till comprises two units: a thin grey-brown till with numerous shale fragments over a thin reddish brown till with fragments of red conglomerate and granite; underlying sand is cross bedded	Lee 1957
3032	21 G/15	667300	5095800	1.8	1.5	gravelly sand / till / silt	borehole section in Keswick River valley; upper till is overlain by 5.2 m of alluvial sand, 21.9 m of silt and clay, and 2.7 m of gravelly silt and sand; lower till is 17.1 m thick, and is underlain by 12.2 m of laminated silt over bedrock	Lamothe 1990a
3036	21 G/15	666900	5091500	1.7	25.5	interbedded sand, gravel, and till	borehole section in Saint John River valley; upper till is overlain by 11.9 m of sand and gravel, and 11.6 m of laminated silt and clay; sequence underlying upper till includes 4 thin till units up to 1.2 m thick, with sandy gravel at the base over bedrock	Lamothe 1990a

Site No.	NTS Map Area	Easting NAD27	Northing NAD27	Till Thickness (m)	Underlying Deposit Thickness (m)	Underlying Material Type	Comments	Reference
Locality 18BH	21 G/16	696000	5080800	47.5	17.1	gravel and sand	till is overlain by 1.2 m of sand, silt, and clay; no evidence of weathered or organic materials noted in the cuttings	Lee 1957
AS080001	21 G/16	717820	5078675	~1.5	n/a	bouldery gravel	gravel occurs to the surface at the crest of a glaciofluvial ridge; reddish brown basal till is exposed on slope at W end of the pit; orientation of several elongate clasts in the till suggests ice flow toward the SE	Seaman, field notes (2008)
AS080004	21 G/16	715295	5079245	1+	n/a	glaciofluvial	up to ~2 m of sandy gravel overlies basal till within a glaciofluvial sequence; lithology of pebbles in the gravel is consistent with a source to the W	Seaman, field notes (2008)
J1-2	21 J/01	724100	5106300	0.5	4.0	sandy gravel / sand	till in this pit overlies 1.0–2.3 m of sandy gravel / 1.7 –3.0 m of sand; ice-contact stratified drift	Seaman & Thibault 1986
J1-2	21 J/01	724700	5106400	~ 1	3 - 4+	sandy gravel / sand	till in this pit overlies material similar to the above, but predominantly coarse	Seaman & Thibault 1986
J1-2	21 J/01	724100	5105900	~ 1	3 - 4+	sandy gravel / sand	till in this pit overlies material similar to the above, but predominantly fine	Seaman & Thibault 1986
3034	21 J/02	685250	5105850	10.1	5.2	sandy gravel / till	borehole section in the Nashwaak River valley; upper till is overlain by 20.7 m of interbedded sand, silt and clay; lower till is 1.5 m thick over bedrock	Lamothe 1990a
AS090001	21J/02	687880	5105280	~1 - 1.5	~12	sandy gravel with interbeds of sand and gravelly sand	roadcut section exposed by construction of Marysville Bypass on Highway 8; gravel clasts comprise a mix from highland and lowland source areas	Seaman, field notes (2009)
J3-33	21 J/03	645200	5109800	1.0	0.5 - 4.0 +	sandy gravel with local contorted stratification	reddish brown till overlies the gravel deposit; to the SW a grey till was observed, suggesting that two tills may be present	Finamore (1981)
J3-40	21 J/03	640200	5102700	1.5	0.5 +	sand with silt and pebble to cobble gravel	moderately compact, mottled red and grey till	Finamore (1981)

Site No.	NTS Map Area	Easting NAD27	Northing NAD27	Till Thickness (m)	Underlying Deposit Thickness (m)	Underlying Material Type	Comments	Reference
2	21 J/05	596600	5138300	1.8	0.3	sand / till	underlying till is 0.9+ m thick	Lee 1962 (Map 25-1962)
AS030012a; CS-WX03b-2	21 J/06	653470	5146810	0.7	1.8+	organic-bearing sand / gravelly sand	till overlies 1.6 m sand / 0.2+ m gravelly sand; charcoal fragments from the sand dated >36 ka (GSC-4199) and subsequently >51.7 ka (ULA-1337); mid-Wisconsinan site of Lamothe (1992), now interpreted as Sangamonian	Seaman, field notes (2003); Lamothe (1992)
AS030012b; CS-WX03b-1	21 J/06	653455	5146825	0.84	1.58+	sandy gravel	SE-trending till fabric for till; it overlies coarse, sandy gravel; sand and silt were observed below the base of the section, beneath 0.7 m of slump-covered section	Seaman, field notes (2003)
AS030012c	21 J/06	653480	5146825	0.8	1.3+	gravelly sand	till overlies gravelly sand; 1.2 m slumped material lies below base of section	Seaman, field notes (2003)
AS030012d	21 J/06	653470	5146800	0.65	0.8+	sand	till overlies sand, as at AS030012a, but without an obvious organic-bearing horizon	Seaman, field notes (2003)
AS030012e	21 J/06	653460	5146790	1.2	0.7+	sand / sandy gravel	till overlies 0.3 m gritty sand / 0.4+ m of sandy gravel	Seaman, field notes (2003)
AS030013b; CS-VW02	21 J/06	651020	5149480	1.6	1.0+	sandy gravel / sand	basal till is overlain by 0.6 m of gravelly sand; till fabric suggests ice flow toward the NW	Seaman, field notes (2003)
AS030013d	21 J/06	651065	5149470	0.3	1.0+	sandy gravel / bouldery gravel	till is overlain by 0.7 m of sandy gravel	Seaman, field notes (2003)
AS030013e	21 J/06	651100	5149480	1.0	0.4+	sandy gravel	till is veneered by sandy gravel	Seaman, field notes (2003)
AS030014a	21 J/06	653015	5147175	0.7	12.8+	sand, gravelly sand, sandy gravel	the average of 6 paleocurrent measurements in the underlying sand and gravel unit indicate that meltwater flow was toward the WSW	Seaman, field notes (2003)
AS030014b	21 J/06	652920	5147305	0.8	0.4+	sandy gravel		Seaman, field notes (2003)
97AS0015; AS030010; ND-BC03.5	21 J/07	656785	5145785	0.74	2.8+	sand	till is locally overlain by up to 0.5 m of sand; N-trending till fabric; some deformation of sediment beneath the till plus a truncation surface dipping southward; S-trending paleocurrent in the sand; locally sandy gravel below the till; locally cobbly sandy gravel is present in section beneath the till	Seaman 2007

Site No.	NTS Map Area	Easting NAD27	Northing NAD27	Till Thickness (m)	Underlying Deposit Thickness (m)	Underlying Material Type	Comments	Reference
ND-D12	21 J/07	659965	5128975	0.92	0.3+	sandy gravel	clasts in gravelly unit are subangular; probably ablation till but could be proximal glaciofluvial sediments	Seaman 2003, 2007
ND-E09	21 J/07	661935	5134920	0.79	0.15	sandy gravel	gravel is underlain by another basal till; gravel unit was saturated, preventing sampling of it and the underlying till	Seaman 2003, 2007
ND-G12	21 J/07	665925	51209090	1.21	0.85	sandy gravel / till	gravel unit is underlain by 0.37+ m of basal till; upper till has a NNW-trending till fabric; few elongate clasts observed in the geochemically anomalous lower till	Seaman 2008
DT-E07	21 J/09	700555	5169130	0.76	0.36+	sandy gravel	sandy gravel is ablation till	Seaman, field notes (2008)
HV-B08a	21 J/10	656595	5165455	0.53	unknown	clay loam	underlying material appears to be lacustrine (glaciolacustrine?)	Seaman et al. 2005
J10-10; AS030049; HV-DE02	21 J/10	660915	5176785	1.8	8.7+	gravel / interbedded sand and sandy gravel	site is in a large pit; much of pit face was slump-covered but appeared to be all sand or gravel; a second lift extends approximately 5 m below the base of the upper lift (i.e. ~14+ m of sediments beneath the till); the till has a N-trending fabric	Hunter and Laverge 1982; Seaman et al. 2005
HV-F12a	21 J/10	664270	5156995	0.66	0.18+	clayey silt	underlying material contains rare slaty pebbles; glaciolacustrine	Seaman et al. 2005
HV-S13g	21 J/10	683945	5154955	0.53	0.51+	sandy gravel	sandy gravel is poorly sorted, with subangular to subrounded clasts; glaciofluvial	Seaman et al. 2005
HV-T11a	21 J/10	686015	5158905	0.67	0.23+	clayey silt	clayey silt contains a small lens of fine sand and rare fine gravel dropstones; glaciolacustrine	Seaman et al. 2005

STRATIGRAPHY, GEOCHEMISTRY, AND GEOCHRONOLOGY OF THE ANNIDALE AND NEW RIVER BELTS, AND THE DEVFLOPMENT OF THE PENOBSCOT ARC IN SOUTHERN NEW BRUNSWICK

SUSAN C. JOHNSON [1], MALCOLM J. MCLEOD [1], LESLIE R. FYFFE [2], AND GREGORY R. DUNNING [3]

[1] Geological Surveys Branch, New Brunswick Department of Natural Resources, P.O. 5040, Sussex, New Brunswick, CANADA E4E 5L2 (*susan.johnson@gnb.ca*)

[2] Geological Surveys Branch, New Brunswick Department of Natural Resources, P.O. 6000, Fredericton, New Brunswick, CANADA E3B 5H1

[3] Department of Earth Sciences, Memorial University, St. John's, Newfoundland, CANADA A1B 3X5

Johnson, S.C., McLeod, M.J., Fyffe, L.R., and Dunning, G.R. 2009. Stratigraphy, geochemistry, and geochronology of the Annidale and New River belts, and the development of the Penobscot arc in southern New Brunswick. *In* Geological Investigations in New Brunswick for 2008. *Edited by* G.L. Martin. New Brunswick Department of Natural Resources; Minerals, Policy and Planning Division, Mineral Resource Report 2009-2, p. 141–218.

Late Cambrian–Early Ordovician rocks of the Annidale Group are preserved within the Annidale belt, a northeast-trending, fold-thrust belt situated along the northwestern margin of the New River belt in southern New Brunswick. The Annidale Group comprises the Carpenter Brook, Lawson Brook and East Scotch Settlement formations, which form an assemblage of mafic–intermediate volcanic rocks, marine sedimentary rocks, and rhyolite dome complexes. U–Pb data indicate that rocks of the Annidale Group (c. 497–490 Ma) and adjacent latest Neoproterozoic–earliest Cambrian rocks of the Belleisle Bay Group (c. 540 Ma) in the New River belt both were affected by a younger period of Early–Middle Ordovician magmatism ranging in age from c. 482 to c. 467 Ma. This younger magmatism provides important constraints on the timing of tectonism in the Annidale belt. In particular, structural interleaving of the Annidale Group and its juxtaposition with New River basement must have occurred prior to intrusion of the c. 479 Ma Stewarton Gabbro that stitches their faulted contact.

The geochemical signature of the volcanic and plutonic rocks within the Annidale belt is indicative of suprasubduction zone magmatism. The mafic–intermediate volcanic rocks are subalkaline, mostly tholeiitic to transitional basaltic andesites that exhibit both arc and non-arc geochemical signatures. Most samples show weak to strong negative Nb and Ta and positive Th anomalies on extended rare-earth diagrams and fall clearly within volcanic-arc fields on trace-element discrimination diagrams. One exception is a group of extreme LREE-depleted basalts that are associated locally with plagiogranite and that display concave-upward REE patterns typical of N-MORB affinity, but with uncharacteristically low (0.48–0.54%) TiO_2 values more typical of arc tholeiites.

These new data bearing on the age and tectonic setting of the Annidale Group are in accord with recent models for the tectonic development of the Exploits Subzone, which represents the Gondwanan part of the Dunnage Zone in Newfoundland. Deformation of the Early Cambrian–Early Ordovician (c. 514–486 Ma) Penobscot arc/back-arc complex and

obduction of Exploits Subzone ophiolites onto the Gander margin in Newfoundland occurred prior to development of the younger Victoria arc system (c. 473–454 Ma) from the Early to Middle Ordovician. A new $^{40}Ar/^{39}Ar$ age of c. 444 Ma for metamorphic muscovite in schistose felsic tuff of the Annidale Group suggests that peak metamorphism in the Annidale belt occurred in latest Ordovician–earliest Silurian time, coeval with deformation and metamorphism related to closure of the Tetagouche–Exploits back-arc basin in northern New Brunswick.

Les roches de la fin du Cambrien et du début de l'Ordovicien du groupe Annidale se trouvent dans la ceinture Annidale, une ceinture à plissement et à chevauchement orientée vers le nord-est et située dans la frange nord-ouest de la ceinture New River, dans le sud du Nouveau-Brunswick. Le groupe Annidale comprend les formations Carpenter Brook, Lawson Brook et East Scotch Settlement, qui composent un assemblage de roches mafiques-volcaniques intermédiaires, de roches marines sédimentaires et de complexes de dôme rhyolitique. De nouvelles données sur l'âge U–Pb indiquent que le groupe Annidale, âgé d'environ 497 à 490 Ma, et le groupe adjacent des roches du début du Cambrien (d'environ 540 Ma) de la baie de Belleisle, dans la ceinture New River, ont tous deux été altérés par un magmatisme plus récent de l'Ordovicien, survenu au cours d'une période comprise entre 482 et 467 Ma. Ce magmatisme plus récent donne une indication importante des réserves qui s'imposent quant à la caractérisation de la tectonique de la ceinture Annidale. Plus particulièrement, la lithologie structurale du groupe Annidale et sa juxtaposition près du socle New River ont dû survenir antérieurement à 479 Ma, soit l'âge du gabbro de Stewarton qui émaille sa zone de contact altérée par des failles.

La signature géochimique des roches volcaniques et plutoniques de la ceinture Annidale indique un magmatisme d'une zone de suprasubduction. Les roches mafiques-volcaniques intermédiaires sont des roches subalcalines, et pour l'essentiel des andésites de tholéite et de basalte intermédiaires qui présentent des signatures géochimiques arquées et non arquées. La plupart des échantillons contiennent des anomalies faibles à fortes de Nb négatif et de Ta positif, sur les diagrammes avancés de métal du groupe des terres rares; il s'ensuit que ces échantillons se situent clairement dans la catégorie des champs d'arc volcanique, sur les diagrammes de discrimination des éléments traces. Il y a une exception et il s'agit d'un groupe de basaltes dont l'élimination extrême de terres rares légères est associée localement au plagiogranite. Ces roches présentent une configuration concave vers le haut d'éléments de terres rares, caractéristique d'une affinité N-basalte de dorsale médio-océanique, à la différence toutefois qu'on observe de faibles teneurs de TiO_2 (se situant entre 0,48 et 0,54 %), qui sont généralement davantage associées aux tholéites d'arc.

Ces nouvelles données sur l'âge et le cycle tectonique du groupe Annidale viennent corroborer la modélisation récente de la tectonique de la sous-zone Exploits, qui correspond à la période du continent de Gondwana de la zone de Dunnage, à Terre-Neuve. La déformation du Cambrien et de l'Ordovicien précoces (période comprise environ entre 514 et 486 Ma) du complexe arqué et contre-arqué Penobscot et l'obduction des ophiolites de la sous-zone Exploits dans la marge de Gander, à Terre-Neuve, sont survenues avant le développement du complexe d'arc plus récent de Victoria (survenu il y a environ 473 à 454 Ma), soit entre le début de l'Ordovicien et l'Ordovicien moyen. Une nouvelle datation $^{40}Ar/^{39}Ar$ de 444 Ma de la muscovite métamorphique transformée en tuf

felsique de schiste du groupe Annidale porte à croire que l'activité métamorphique la plus importante dans la ceinture Annidale est survenue à la fin de l'Ordovicien et au début du Silurien, et aurait été contemporaine de la déformation et du métamorphisme associés à la fermeture du bassin de contre-arc Tetagouche–Exploits, dans le nord du Nouveau-Brunswick.

INTRODUCTION

This report focuses on the stratigraphy and tectonic evolution of the Annidale and New River belts in southern New Brunswick. These adjacent belts lie along the southeastern margin of Ganderia within the northern part of the Appalachian Orogen (Fig. 1; Hibbard et al. 2006). An area of approximately 750 km^2 was mapped in the central region of southern New Brunswick, encompassing parts of three 1:50,000-scale NTS map sheets, including the eastern part of 21 G/09, northwestern part of 21 H/12E, and all of 21 H/13. The mapped area is bounded to the southeast by Belleisle Bay and extends from Hampstead in Queens County northeastward across the Saint John River to the Head of Millstream in Kings County (Fig. 2).

The report area is of significant economic interest, as the underlying rocks are host to numerous gold, antimony ± base metal sulphide occurrences, many of which have close spatial associations with faults and/or felsic intrusions. The purpose of this report is to delineate and geochemically characterize major rock units within a more current tectonostratigraphic framework to aid in the development of a metallogenic model for gold occurrences in the region. Geological mapping at a 1:20,000 scale was carried out between 2000 and 2006 by Johnson and McLeod (2000), Johnson (2001a, 2003, 2005), and McLeod (2000, 2005). Chemical analyses of major, trace, and rare-earth elements were conducted on most major mafic and felsic igneous units in the report area.

Radiometric ages on eight rock samples collected in the mapped area were determined by Greg Dunning at Memorial University using the TIMS (U–Pb) method. This report adopts the age spans of the Early Paleozoic series as recently published by the Geological Society of America (Walker et al. 2009): Early Cambrian (542–510 Ma), Middle Cambrian (510–501 Ma), Late Cambrian (501–488 Ma), Early Ordovician (488–472 Ma), and Middle Ordovician (472–461 Ma).

PREVIOUS WORK

Gesner (1841, p. 50–59) conducted the first geological investigation in the area during his third geological survey of the province about 165 years ago. Bailey (1865) subsequently produced one of the first geological maps of the report area and correlated the entire belt with rocks on the Kingston Peninsula, which are now known to be Early Silurian (Barr et al. 2002a). Bailey and Matthew (1872, p. 69–82) later provided a fairly detailed account of the geology in Wickham, Springfield, and Kars parishes, in which they suggested that the pre-Carboniferous rocks were all "Huronian" or Precambrian in age. Regional mapping surveys were later completed in various parts of the report area by Alcock and MacKenzie (1946), MacKenzie (1951, 1964), and Hamilton (1961).

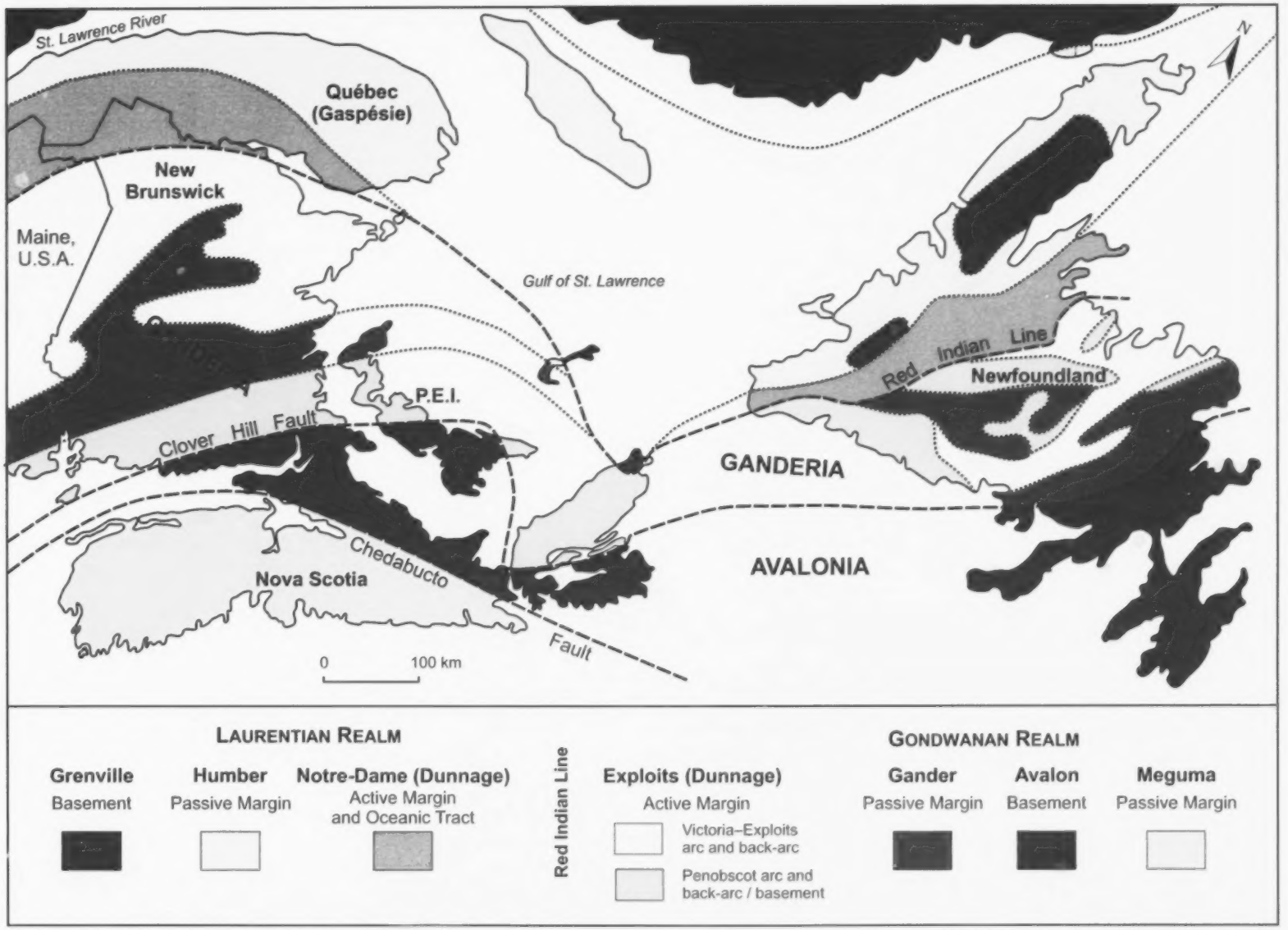

Figure 1. Lithotectonic zonation of the northeastern Appalachian Orogen (modified after Hibbard et al. 2006).

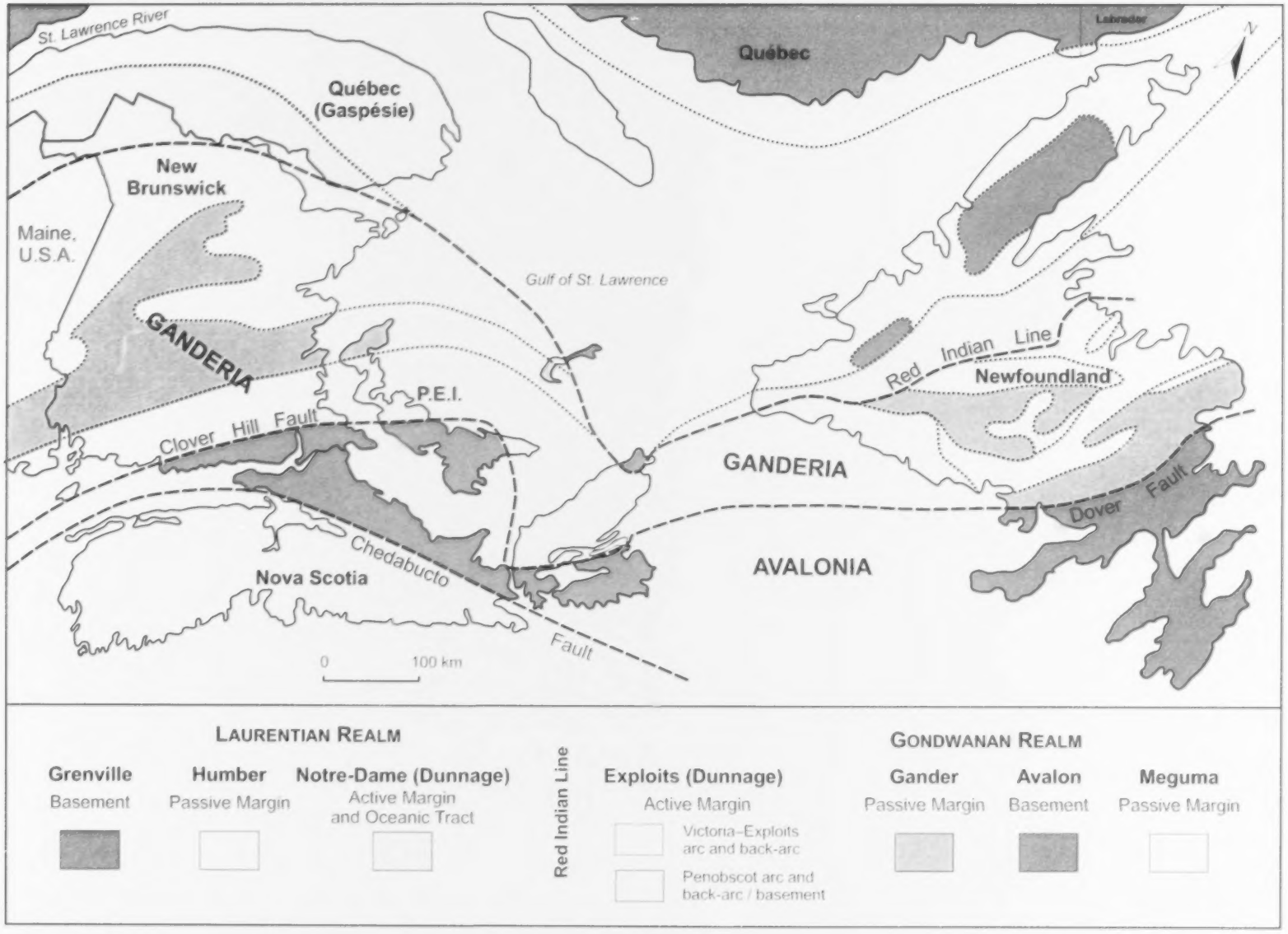

Figure 1. Lithotectonic zonation of the northeastern Appalachian Orogen (modified after Hibbard et al. 2006).

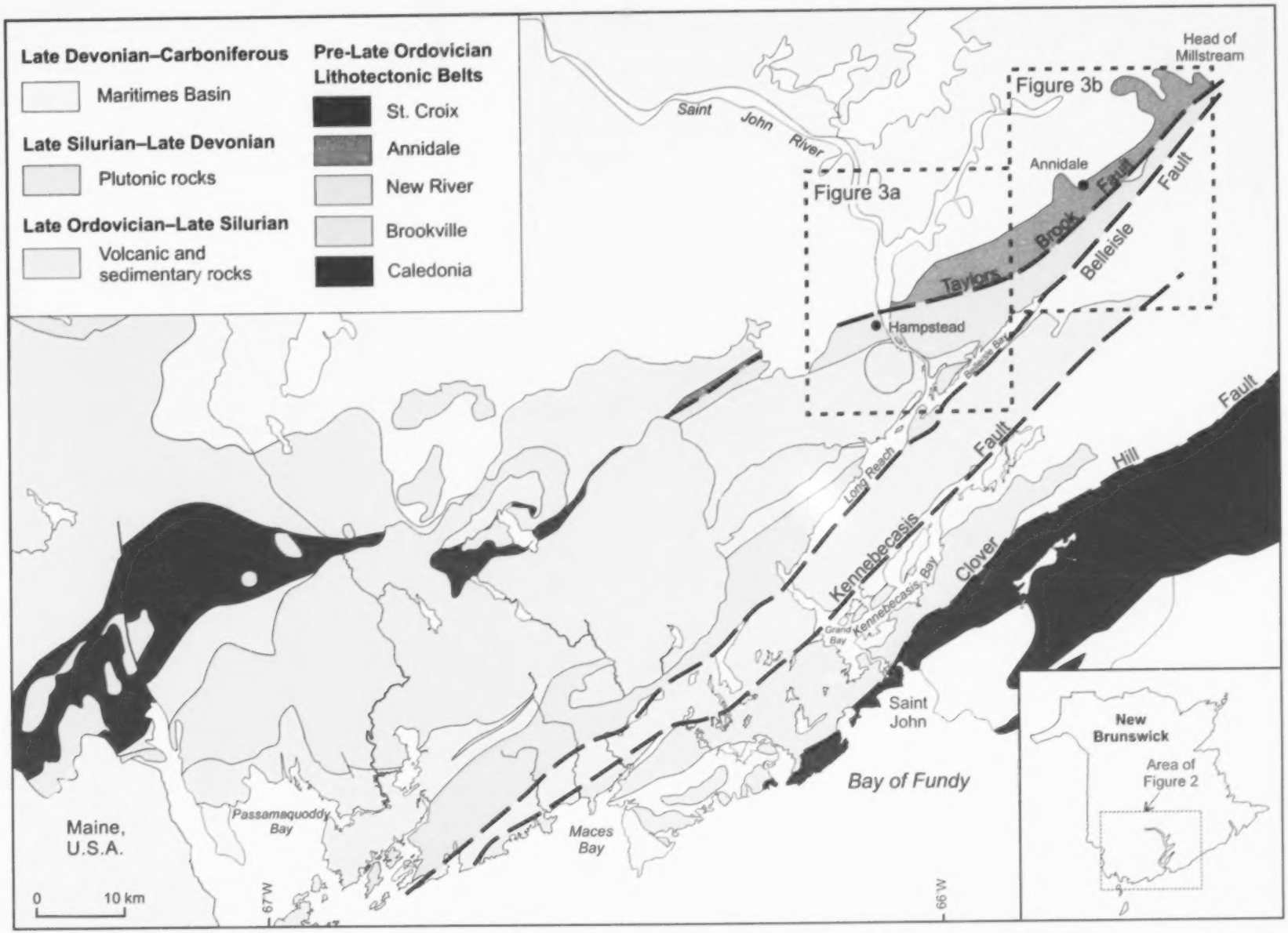

Figure 2. Tectonostratigraphic map of southern New Brunswick, modified after Johnson and Barr (2004).

McCutcheon and Ruitenberg (1987) provided the first comprehensive study on the geology and mineral deposits in the report area. McLeod et al. (1992, 1994) and McLeod (1997) conducted the first U–Pb dating in the Annidale belt. This work revealed that the rhyolite domes in the northern part of the belt (Fig. 3a, 3b) were Late Cambrian, not Carboniferous as previously mapped, highlighting the need for more detailed mapping and U–Pb dating in the area.

More targeted studies included a report on the economic geology of volcanic rocks associated with base metal and gold mineralization in the vicinity of Shannon and Annidale (Lutes 1993) and one on the titanium and phosphate potential of the Stewarton Gabbro (Venugopal 2003). In 2004, the Geological Survey of Canada completed a high-resolution aeromagnetic survey covering the central and northeastern parts of the report area that included a geological interpretation of the results by Thomas and Kiss (2004).

Regional Geological Setting

Southern New Brunswick is divided into five lithotectonic belts on the basis of contrasts in their pre-Late Ordovician stratigraphy and magmatic history (Fig. 2). From northwest to southeast, they include the St. Croix, Annidale, New River, Brookville, and Caledonia belts (Fyffe and Fricker 1987; McLeod et al. 1992, 1994; Johnson and McLeod 1996; White and Barr 1996; Johnson 2001b; Fyffe et al. 2009). All but the Caledonia belt are considered to be correlative with the peri-Gondwanan Gander Zone and Exploits Subzone of the Dunnage Zone in the northern Appalachian Orogen of Newfoundland, collectively referred to as Ganderia (Fig. 1; van Staal et al. 1998; Hibbard et al. 2006). The early Paleozoic rocks comprising the Annidale belt are separated from the predominantly late Neoproterozoic basement rocks of the New River belt by the major, northeast-trending Taylors Brook Fault. The New River belt is juxtaposed to the southeast against volcanic arc-related rocks of the Early Silurian Kingston Group (Barr et al. 2002a) along the Belleisle Fault (Fig. 2).

Reflecting its composite nature, the New River belt contains four distinct, pre-Late Ordovician sequences: 1) Neoproterozoic (c. 625 Ma and c. 555 Ma) arc-related volcanic and plutonic rocks, 2) latest Neoproterozoic–earliest Cambrian (c. 540 Ma) shallow marine to subaerial volcanic and sedimentary rocks of the Belleisle Bay Group (Johnson and McLeod 1996), 3) Early Cambrian quartzose sedimentary rocks of the Matthews Lake Formation; and overlying arc-related volcanic, volcaniclastic, and epiclastic rocks of the c. 514 Ma Mosquito Lake Road Formation (Johnson and McLeod 1996; Johnson 2001b; Johnson and Barr 2004; Bartsch and Barr 2005; Fyffe et al. 2009), and 4) Early–Late Cambrian fossiliferous marine sedimentary and minor rift-related volcanic rocks, some of which are assigned to the Saint John Group (Helmstaedt 1968; Tanoli and Pickerill 1988; Landing et al. 2008). Late Ordovician–Early Silurian rocks of the Mascarene Group form the cover sequence on the older rocks of the New River belt.

Latest Neoproterozoic–earliest Cambrian rocks correlative with the Belleisle Bay Group (sequence 2, above) are abundant in the New River belt of the report area, and older Neoproterozoic rocks (sequence 1) may be present locally (Fig. 3a, 3b). Probable Early

Cambrian quartzose sedimentary rocks similar to those of the Matthews Lake Formation (sequence 3) and Saint John Group (sequence 4) have been recognized overlying the Belleisle Bay Group in the report area. By way of contrast, the adjacent Annidale belt comprises mafic volcanic rocks, felsic tuffs, and dome complexes (dated at c. 497–490 Ma), and sedimentary rocks of the Late Cambrian–Early Ordovician Annidale Group (McLeod et al. 1992, 1994). The belt also contains Early–Middle Ordovician (c. 482–467 Ma) mafic to felsic plutonic rocks and felsic dome complexes that intrude the Annidale Group.

Several major structural panels containing stratigraphic packages that differ in age and lithology as well as deformation style and intensity have been delineated in the report area. The fundamental structure is the Taylors Brook Fault that defines the boundary between the latest Neoproterozoic–earliest Cambrian (c. 540 Ma) rocks of the Belleisle Bay Group and the Late Cambrian–Early Ordovician rocks of the Annidale Group. The Taylors Brook Fault therefore represents a significant regional structure that has telescoped the New River belt against the Annidale belt to the northwest.

Northwest of the Taylors Brook Fault, the Annidale Group is dissected into three major northwesterly transported thrust panels known as the O'Neill Brook, Lawson Brook, and Albright Brook–Taylors Brook thrust panels. These panels are bounded by the northeast-trending Albright Brook Fault and an unnamed, largely cryptic fault to the north that is concealed beneath Carboniferous cover. In the New River belt southeast of the Taylors Brook Fault, significant faults include the northeast-trending Belleisle Fault and Wheaton Brook splay that dissects the Belleisle Bay Group; and the east-northeast-trending Fanning Brook Fault, which defines the boundary between the Belleisle Bay Group and Silurian rocks of the Mascarene Group at the southwestern end of the New River belt (Fig. 3a, 3b).

STRATIGRAPHY OF THE NEW RIVER BELT

In the report area, the New River belt comprises latest Neoproterozoic–earliest Cambrian mafic to felsic volcanic and epiclastic rocks of the Belleisle Bay Group and overlying rocks of the Ketchum Brook and Snider Mountain formations, of probable Early Cambrian age. East of Evandale, an undivided fault-bounded unit containing strongly deformed, phyllitic mafic and felsic volcanic rocks, phyllitic shale, and slate is also tentatively considered to be older than the Belleisle Bay Group (Fig. 3a).

Belleisle Bay Group

The Belleisle Bay Group is regionally extensive, reaching along the western flank of the Belleisle Fault from the Bay of Fundy northeastward to the Head of Millstream, a distance of more than 160 km (Fig. 2). In the former area, the Belleisle Bay Group comprises shallow marine and subaerial mafic breccias, flows, and tuffs, and red felsic pyroclastic and epiclastic rocks of the Simpsons Island Formation (McLeod 1995; Johnson and McLeod 1996). The Simpsons Island Formation has yielded an earliest Cambrian (539 ± 4 Ma) U–Pb age (Barr et al. 2002b). In the report area, the Belleisle Bay Group is divided into the Lobster Brook,

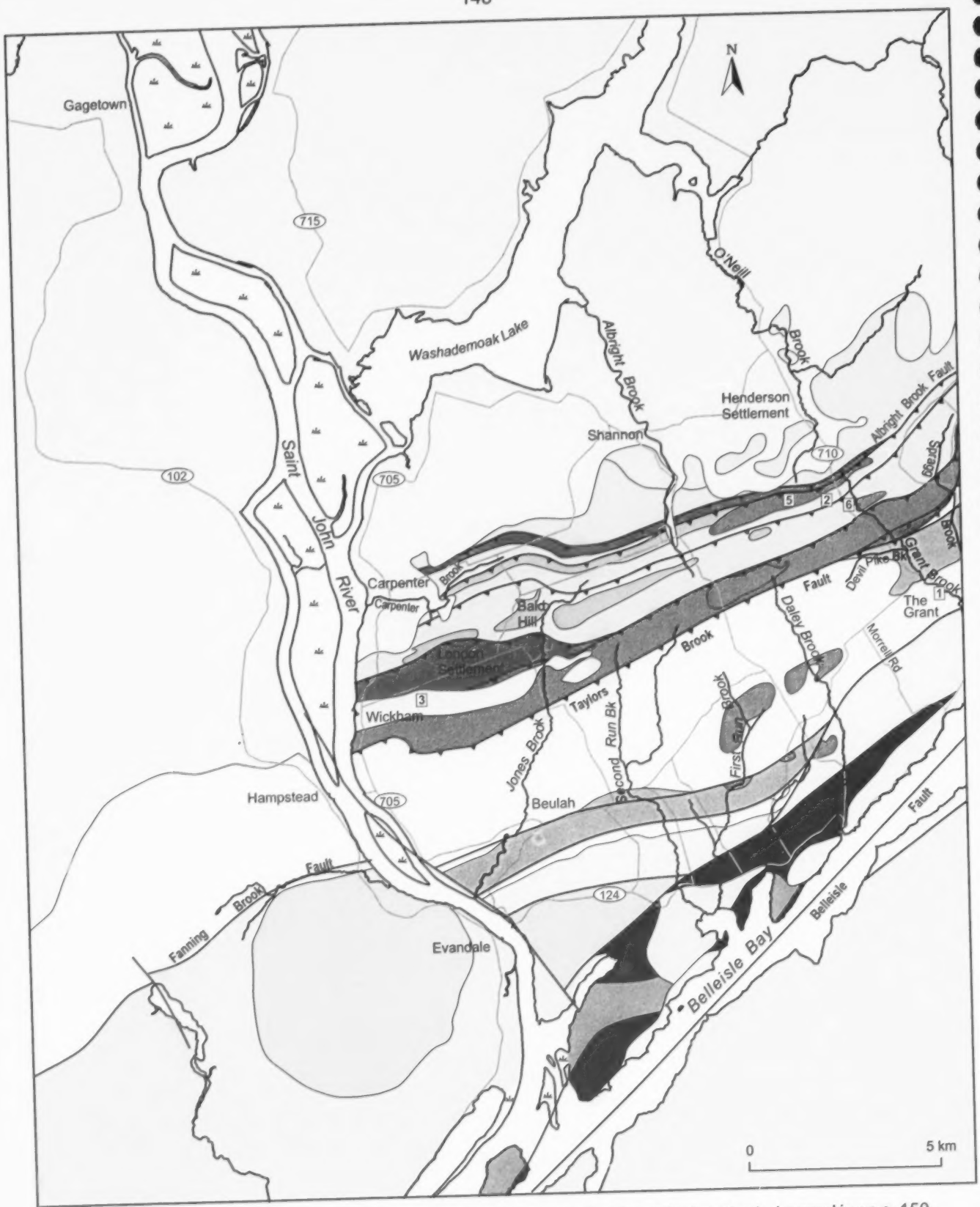

Figure 3a. Geology map of southwestern part of the report area (see Fig. 2 for location). Legend is on p. 150.

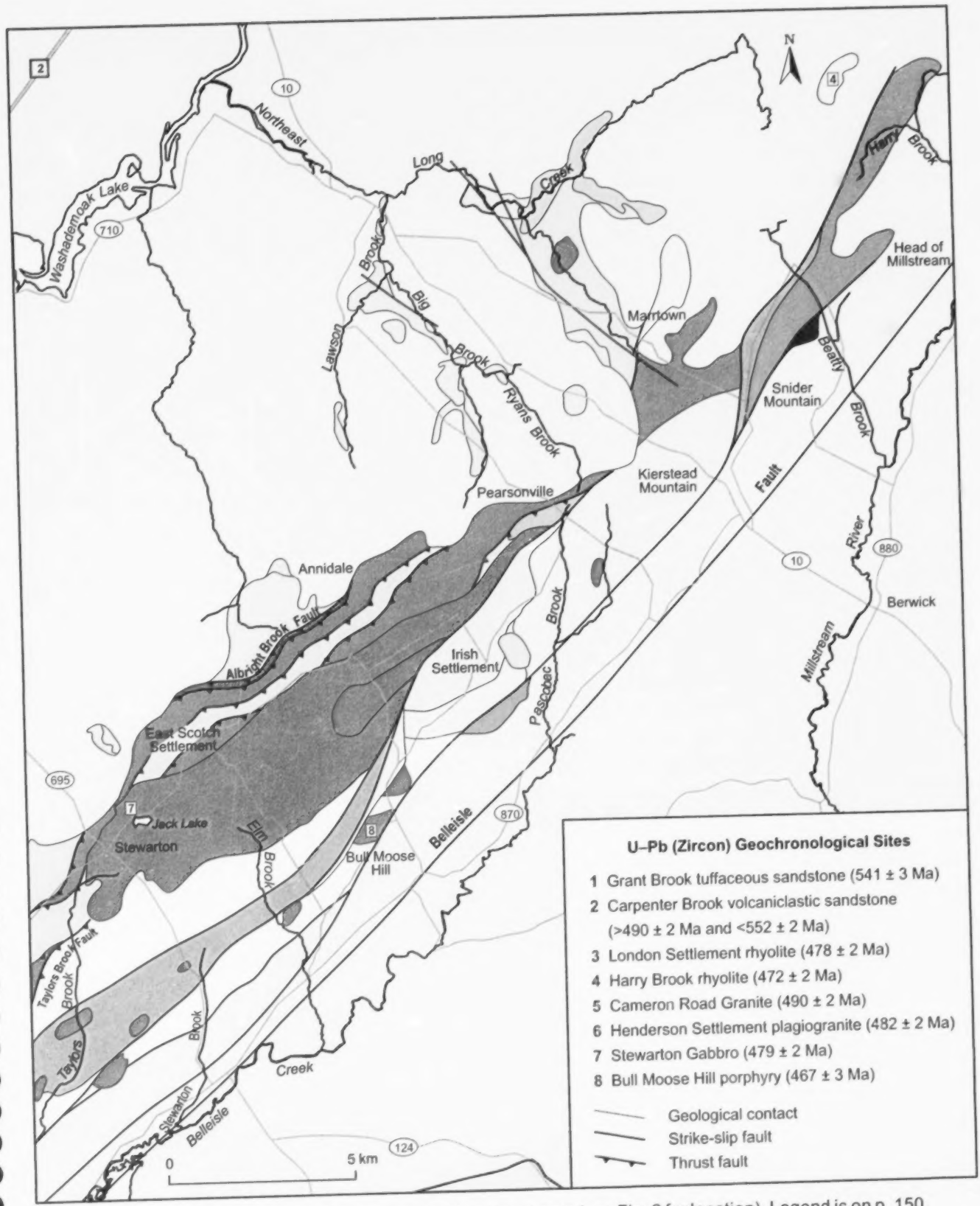

Figure 3b. Geology map of northeastern part of the report area (see Fig. 2 for location). Legend is on p. 150.

Figure 3a. Geology map of southwestern part of the report area (see Fig. 2 for location). Legend is on p. 150.

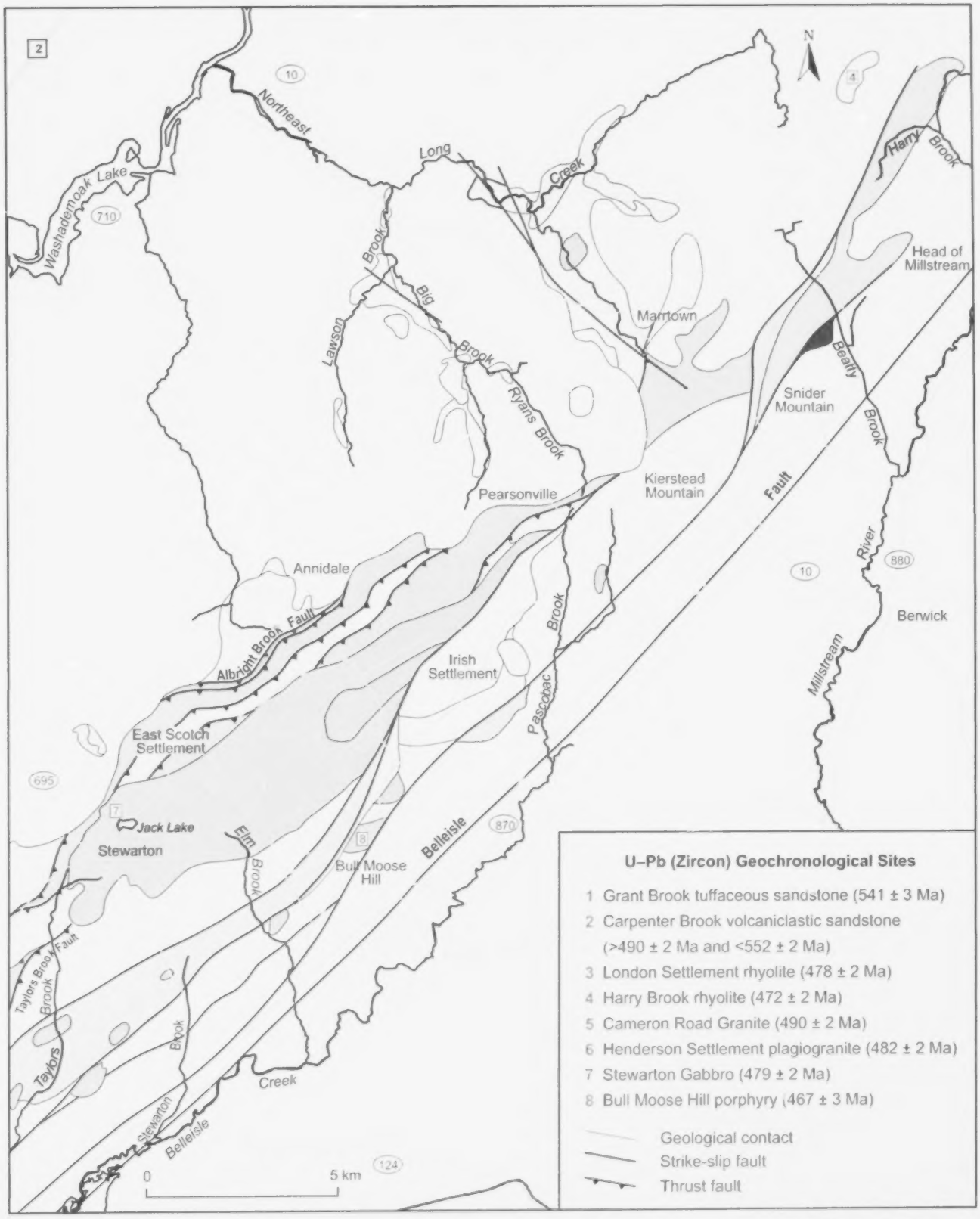

Figure 3b. Geology map of northeastern part of the report area (see Fig. 2 for location). Legend is on p. 150.

LATE DEVONIAN–CARBONIFEROUS

Undivided fluvial sedimentary rocks

LATE SILURIAN–LATE DEVONIAN

Felsic intrusions

Mafic intrusions

EARLY–LATE SILURIAN

KINGSTON, MASCARENE AND KINGSCLEAR GROUPS

Undivided marine sedimentary and volcanic rocks

ANNIDALE BELT

EARLY–MIDDLE ORDOVICIAN

London Settlement/Harry Brook rhyolite dome complexes

LATE CAMBRIAN–MIDDLE ORDOVICIAN

Felsic–intermediate intrusions

Mafic intrusions

LATE CAMBRIAN–EARLY ORDOVICIAN

ANNIDALE GROUP

East Scotch Settlement Formation (sedimentary rocks)

East Scotch Settlement Formation (mafic volcanic rocks)

Lawson Brook Formation

Carpenter Brook Formation

Shannon and Kierstead Mountain rhyolite dome complexes; O'Neill Brook schist

Bald Hill rhyolite dome complex

~ ~ ~ ~ ~ ~ ***Taylors Brook Fault*** ~ ~ ~ ~ ~ ~

NEW RIVER BELT

EARLY CAMBRIAN(?)

Snider Mountain and Ketchum Brook formations

LATE NEOPROTEROZOIC–EARLY CAMBRIAN

BELLEISLE BAY GROUP

Grant Brook Formation (sedimentary/volcaniclastic rocks)

Grant Brook Formation (mafic volcanic rocks)

Lobster Brook Formation

Beulah Camp Formation

Browns Flat Formation

NEOPROTEROZOIC(?)

Mafic and felsic volcanic and sedimentary rocks

Legend for Figures 3a and 3b.

Browns Flat, and Beulah Camp formations southeast of the Wheaton Brook Fault, and the Grant Brook Formation northwest of the fault. Lithological similarities suggest that in general the lower part of the Grant Brook Formation can be correlated with the Browns Flat Formation and its upper part with the Beulah Camp Formation. However, the Grant Brook Formation contains a greater abundance of deeper water sedimentary rocks and is interpreted to represent a more distal basinward facies of the Belleisle Group than is found to the southeast of the Wheaton Brook Fault.

Lobster Brook Formation

The Lobster Brook Formation occurs only in the southwestern part of the report area along the northwestern side of Belleisle Bay (Fig. 3a). It consists predominantly of rhyolite tuffs and rhyolite porphyry, similar to those described in the formation in the Long Reach area by Johnson (2001b). Felsic tuff from the Lobster Brook Formation in that area yielded a latest Neoproterozoic (554 ± 6 Ma) age (McLeod et al. 2003). Contacts with the Browns Flat and Beulah Camp formations are faulted, but the significant discrepancy in age suggests that their contact is probably unconformable or disconformable.

Browns Flat Formation

Well-exposed sections of the Browns Flat Formation occur along the northwestern shore of Belleisle Bay, just south of Highway 124, on the west side of Urquharts Cove and near the mouth of Jenkins Cove (Fig. 3a). The formation consists predominantly of green to grey basalt, basaltic agglomerate, and basaltic lapilli tuff. The volcanic rocks are locally interbedded with reddish brown to maroon pebble to granule conglomerate, sandstone, siltstone, and red to maroon tuffaceous sandstone. Although precise stratigraphic relationships remain uncertain, the upper contact of the Browns Flat Formation is likely gradational with the Beulah Camp Formation, as both formations contain similar red tuffaceous rocks.

Beulah Camp Formation

The most complete exposures of the Beulah Camp Formation occur on Beatty and Harry brooks in the northeastern part of the report area, but the formation also crops out west of Pascobac Brook and on the western shore of Belleisle Bay (Fig. 3a, 3b).

The Beulah Camp Formation consists of reddish maroon to dusky purple and grey pyroclastic, volcaniclastic, and epiclastic rocks. The lower part of the formation comprises massive, thick-bedded, coarse, mafic lithic lapilli tuff containing maroon hematitized basaltic clasts, porphyritic basaltic andesite, and pink felsic lithic–crystal tuffs. The pyroclastic volcanic rocks are overlain, and in part interbedded with, thick-bedded, red and greyish red, coarse-grained volcaniclastic and epiclastic sandstone and conglomerate. On Beatty Brook, they are concordantly succeeded upsection to the northwest by pink to tan feldspathic quartzite and quartzite-pebble conglomerates of the Early Cambrian(?) Snider Mountain Formation. Southwest of the report area, the Beulah Camp Formation is concordantly overlain by late Early Cambrian strata of the Saint John Group along the shore of the Long Reach (Tanoli and Pickerill 1988; Landing and Westrop 1998; Landing et al. 1998; Johnson 2001b).

Grant Brook Formation

The Grant Brook Formation underlies a large part of the report area, extending from the west side of the Saint John River northeastward to Kierstead Mountain (Fig. 3a, 3b). In addition to the type section on Grant Brook, well-preserved sections are found on First Run, Second Run, Taylors Brook, Daley Brook, and in the Morrell Road area in the southwestern part of the New River belt (Fig. 3a); and on Kierstead Mountain and along Pascobac, Stewarton and Elm brooks in the northeastern part (Fig. 3b).

The age and affiliation of the Grant Brook strata has been enigmatic to say the least. McCutcheon and Ruitenberg (1987) considered these rocks to be part of the Queen Brook and Long Reach formations of the Silurian Mascarene Group. This assignment was almost certainly influenced by the fact that the Wheaton Brook Fault defines the boundary between the latest Neoproterozoic–earliest Cambrian Belleisle Bay Group (to the southeast) and the Silurian Mascarene Group (to the northwest) along strike in the Long Reach area (e.g., McCutcheon 1981). Because the Grant Brook strata lie northwest of the Wheaton Brook Fault in the report area, a Silurian age seemed reasonable. McLeod (1997) included Grant Brook strata in a redefined Queen Brook Formation but considered the formation to be part of the Cambro–Ordovician Annidale Group.

Johnson and McLeod (2000) and McLeod (2000) introduced the name 'Grant Brook Formation' for the rocks lying between the Wheaton Brook Fault and the Taylors Brook Fault to the northwest, interpreting them as Silurian. However, new U–Pb data make such an age assignment untenable. Available geochronological and lithological evidence strongly supports a correlation of the Grant Brook Formation with the latest Neoproterozoic–earliest Cambrian rocks of the Belleisle Bay Group exposed southeast of the Wheaton Brook Fault. The relationship between rocks in the type section of the Queen Brook Formation, located west of the Saint John River, and those in the report area more than 30 km to the east, remains uncertain. Due to this uncertainty, we recommend that the Queen Brook Formation be restricted to the area west of the Saint John River until a more definitive correlation can be made.

The Grant Brook Formation is divided into a lower unit predominated by mafic–intermediate volcanic rocks and an overlying unit of clastic sedimentary rocks and minor pyroclastic rocks. The lower unit contains green to grey and locally dusky purple, porphyritic and non-porphyritic basaltic to andesitic flows, vesicular basalt, mafic–intermediate lithic tuff, and phreatic breccia. Accretionary lapilli occur at one locality, suggesting that the rocks were in part deposited subaerially. Plagioclase porphyry and gabbro are common in the mafic sequences.

The upper unit of the Grant Brook Formation comprises a relatively deep-water marine sedimentary facies that is well exposed in the vicinity of Beulah (Fig. 3a). This distal facies grades laterally northeastward into a more proximal, volcano-sedimentary facies exposed in The Grant and Bull Moose Hill areas (Fig. 3a, 3b). The distal facies consists of intercalated light greyish green and dusky purple to maroon siltstone and slate, and thin-bedded, fine-

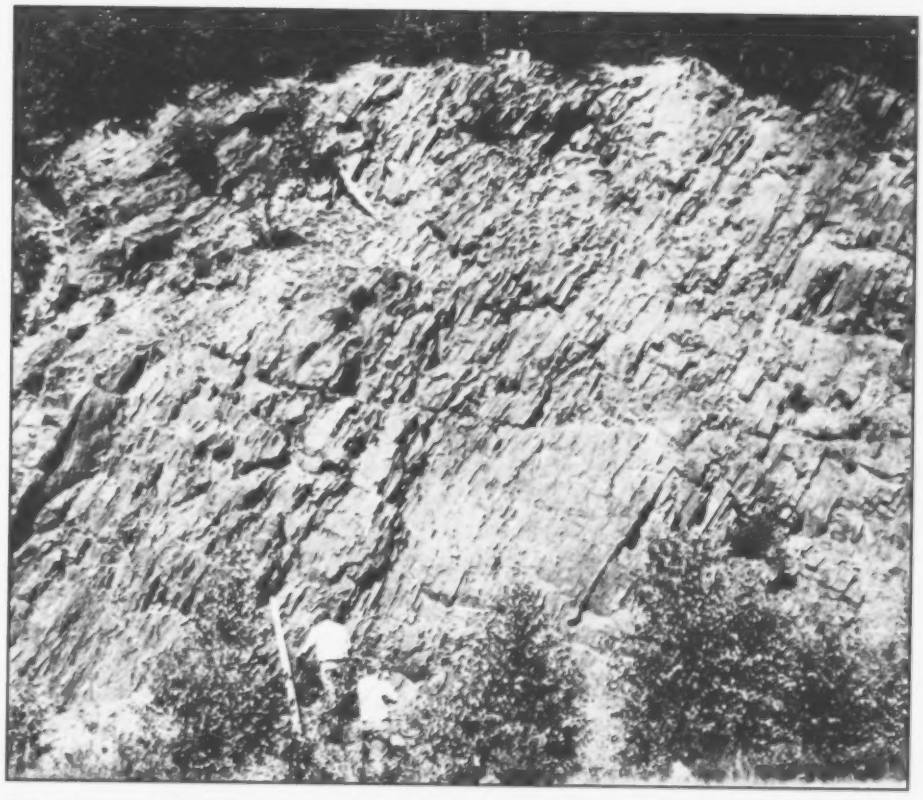

Figure 4. Bedding in the Grant Brook Formation on Highway 710 near The Grant. Each bed consists of maroon siltstone with thin interbeds of greyish green, fine-grained sandstone.

grained siliceous sandstone that is commonly graded. Dark greyish green to maroon, medium-bedded, medium- to coarse-grained, micaceous feldspathic sandstone is present locally. The proximal volcano-sedimentary facies consists of maroon and greyish green, thin- to medium-bedded volcaniclastic sandstone and siltstone (Fig. 4) intercalated with dark maroon to medium grey felsic to intermediate feldspar crystal–lithic and lithic tuffs, and tuffaceous sandstone. Dark greyish green, very thick-bedded, feldspathic micaceous sandstone is exposed in the Bull Moose Hill area. The proximal facies is also distinguished by rhyolite dykes/sills and hackly fractured, siderite-stained, massive red to maroon and green siltstone.

Facing directions in the Devil Pike Brook area (Fig. 3a) suggest that the proximal, volcanic-rich facies in the Grant Brook Formation youngs into micaceous, quartzose sandstone and black shale of the Early Cambrian(?) Ketchum Brook Formation (see below). In contrast, the distal sedimentary facies of the Grant Brook Formation in the western part of the report area dips and youngs southward into thick-bedded orthoquartzite of the Snider Mountain Formation along the lower part of Jones Brook. As previously noted, the Beulah Camp Formation is also overlain by the Snider Mountain Formation, thus occupying a stratigraphic position similar to that of the Grant Brook Formation. Although it is possible that either the Grant Brook or Beulah Camp formations are locally missing due to stratigraphic cut-out, the preferred interpretation is that the pyroclastic rocks in the proximal volcano-sedimentary facies of the Grant Brook Formation are laterally equivalent to volcanic edifices in the Beulah Camp Formation.

The Grant Brook Formation is faulted against the Annidale Group to the northwest along the Taylors Brook Fault. This boundary is stitched by the Stewarton Gabbro, which has produced a broad contact aureole along the southern contact of the intrusion. Intrusive relationships with the c. 479 Ma Stewarton Gabbro and the c. 467 Ma Bull Moose Hill porphyry (see below) clearly demonstrate that the Grant Brook Formation is not part of the Silurian Mascarene Group as was previously thought. Unpublished TIMS (U–Pb) analyses of detrital zircons from felsic tuff on Elms Road north of the Evandale ferry landing provide a maximum age for the Grant Brook Formation. The three single euhedral zircon crystals analyzed gave widely different ages of 607 ± 41 Ma, 556 ± 11 Ma , and 542 ± 9 Ma (Krogh, written comm., 1993), the youngest of which is similar to a new U–Pb zircon age of 541 ± 3 Ma on volcanic zircon from tuffaceous sandstone along Grant Brook (see ***Geochronology***). These data are nearly identical to the earliest Cambrian crystallization age of 539 ± 4 Ma for the Simpsons Island Formation, supporting the interpretation of a close spatial and temporal relationship between the Grant Brook, Beulah Camp, and Simpsons Island formations in the Belleisle Bay Group.

Early Cambrian(?) Units

The Belleisle Bay Group is locally overlain by a sequence of marine sedimentary and basaltic rocks that are tentatively assigned an Early Cambrian age. Although these rocks were included in the Silurian Henderson Brook Formation by McCutcheon and Ruitenberg (1987) and Johnson (2001a), they appear to conformably overlie earliest Cambrian rocks of the Beulah Camp and Grant Brook formations; hence, their Silurian assignment needs to be reassessed. These Early Cambrian(?) rocks occur in three widely separated areas in the report area: on Snider Mountain at the northeastern end of the New River belt; on Taylors Brook, Ketchum Brook, and near The Grant in the central part of the belt; and on tributaries of Jones Brook in the western part of the belt (Fig. 3a). The rocks are divided into two units, namely the Snider Mountain Formation and the conformably overlying Ketchum Brook Formation.

Snider Mountain Formation

Rocks of the Snider Mountain Formation are exposed in several outcrops on the south side of Snider Mountain Road and on Beatty Brook, where they conformably overlie light red, fine- to medium-grained, lithic–feldspathic sandstone of the Beulah Camp Formation.

The Snider Mountain Formation consists of light grey to pink, thick-bedded, vitreous feldspathic quartzite; light grey, granular orthoquartzite; intraformational quartzite-pebble conglomerate; and quartzose sandstone. Similar quartzose sandstones and orthoquartzite overlie the Beulah Camp Formation in the Long Reach area. There, the strata are fossiliferous and have been correlated with the Saint John Group (Landing and Westrop 1998; Landing et al. 1998; Johnson 2001b). This correlation raises the possibility that the Snider Mountain Formation is laterally equivalent to rocks in the Saint John Group. Fyffe et al. (2009) recently proposed a similar facies relationship between the Matthews Lake Formation in the southwestern New River belt, and quartzose rocks of the Saint John Group on Buckmans Creek (Landing et al. 2008). They suggested that the New River belt therefore may contain the only known remnants of the inner and outer platform of Ganderia; however, further

discussion of this topic is beyond the scope of the present paper.

Thick-bedded, white, granular orthoquartzite and minor light grey, slightly feldspathic quartzite is exposed on a small western tributary of Jones Brook about 700 m upstream of where the main branch empties into the Saint John River (Fig. 3a). These rocks are also assigned to the Snider Mountain Formation. At this locality, the quartzite section is only a few metres thick and is concordantly underlain by grey and light green siltstone of the Grant Brook Formation. Dark grey siltstone and fine- to medium-grained quartzose sandstone that overlie the orthoquartzite are assigned to the overlying Ketchum Brook Formation.

Ketchum Brook Formation

The Ketchum Brook Formation is exposed on Taylors and Ketchum brooks and in the area of The Grant along Highway 710, and on Jones Brook and in roadcuts in the Beulah area (Fig. 3a, 3b). It is divided into a lower sedimentary unit and an upper mainly basaltic unit.

The lower unit is dominated by fining upward sequences of light grey, micaceous, thin- to thick-bedded, fine- to medium-grained, slightly feldspathic quartzose sandstone intercalated with dark grey to black laminated siltstone and shale. Thick-bedded (40–50 cm), micaceous, medium-grained quartzose sandstone near the base of the Ketchum Brook Formation is exposed on Ketchum Brook near its junction with Elm Flat Road (Fig. 3a). The quartzose sandstone at this locality is slightly micaceous and interbedded with finer grained, thinner bedded (2 cm), light grey quartzose sandstone and thin-laminated, light green siltstone and shale. On an eastern tributary of Jones Brook, black shale is interbedded with rare limestone and calcareous siltstone with well-developed cone-in-cone structures. Dark grey shale exposed on Highway 705 south of Beulah (Fig. 3a) is conformably overlain by and locally interbedded with greyish green basaltic lithic tuff and light grey, commonly bleached, highly amygdaloidal basalt of the upper unit. The basaltic tuffs are dominated by coarse mafic volcanic lapilli and are locally hematitized to a purplish hue.

OVERVIEW OF THE ANNIDALE BELT

Late Cambrian–Early Ordovician rocks of the Annidale Group are exposed in a northeast-trending fold-thrust belt that is more than 50 km long and up to 10 km wide (Fig. 1). The Annidale Group was first defined in the early 1990s when radiometric dating revealed that a felsic dome complex near Shannon, previously thought to be Carboniferous, was in fact Cambro–Ordovician (McLeod et al. 1992). The stratigraphy and geochemistry of the Annidale Group was described by McLeod et al. (1992, 1994) and Ruitenberg et al. (1993). These authors divided the group into three sequences: the East Scotch Settlement Formation, Lawson Brook Formation, and Canaan Forks sequence. The East Scotch Settlement and Lawson Brook formations were considered to be laterally equivalent to the Early Ordovician Calais Formation in the Cookson Group, located in the St. Croix belt (Fig. 2) along strike to the southwest (McLeod et al. 1992). Turbiditic wacke and shale in the Canaan Forks sequence, exposed in inliers north of the Annidale belt, was considered to be correlative with

the upper part of the Cookson Group and/or overlying basal Kingsclear Group. We concur in general with their correlation but do not consider the Canaan Forks sequence to be part of the Annidale Group as defined in this report.

McLeod et al. (1994) defined the Lawson Brook Formation as comprising rhyolite flows and tuffs with minor mafic volcanic rocks and highly deformed quartz–mica schist, exposed in inliers surrounded by Carboniferous sedimentary rocks along the northwestern flank of the Annidale belt. Most of the mafic volcanic rocks and rhyolite domes exposed just south of the Carboniferous cover in the vicinity of Annidale and Shannon were included in the East Scotch Settlement Formation (Fig. 3a, 3b). The mafic volcanic rocks in the East Scotch Settlement Formation were further divided into northern and southern sequences on the basis of differences in lithology and chemistry (McLeod et al. 1994). The southern sequence, which included the type area of the East Scotch Settlement Formation, was distinguished by a greater volume of sedimentary and tuffaceous rocks. In addition, the basalts in the southern sequence were distinctly low in TiO_2 (0.4–1.2%) relative to those in the northern sequence, which averaged 1.4% to 2.4% TiO_2. Basaltic rocks in the southern sequence also had anomalously high Mg–Cr–Ni contents locally, suggestive of an ultramafic protolith.

The structural complexity, extent of thrusting, and extremely poor exposure has greatly hindered the determination of stratigraphic relationships within the Annidale Group. However, recent U–Pb ages, aided by interpretation of the depositional facies, lithogeochemistry, and structural geometry, necessitated the following revisions to the Annidale Group.

- We suggest that the variations in lithology and chemistry between the northern and southern sequences within the East Scotch Settlement Formation reflect differences in stratigraphic position within the Annidale Group. Consequently, we have revised the East Scotch Settlement Formation to include only the mafic volcanic rocks and black shale that lie south of the Albright Brook Fault (southern sequence of McLeod et al. 1992, 1994).

- The Lawson Brook Formation is expanded to include the mafic volcanic rocks north of the Albright Brook Fault (northern mafic volcanic sequence of McLeod 1992, 1994). These are intercalated with felsic volcanic rocks and associated rhyolite domes at Shannon and Annidale and therefore constitute a bimodal mafic–felsic volcanic assemblage.

- The 'Carpenter Brook Formation' is a new name proposed for a largely sedimentary sequence and associated felsic dome complexes lying south of the Albright Brook Fault. Carpenter Brook strata were previously included in the Queen Brook Formation by McCutcheon and Ruitenberg (1987), McLeod et al. (1992, 1994), and McLeod (1997).

- A thrust panel of mafic volcanic rocks immediately south of the Carpenter Brook Formation and just north of the Taylors Brook Fault is herein included in the East Scotch Settlement Formation. These volcanic rocks were previously considered to be part of the Silurian

Mascarene Group by McCutcheon and Ruitenberg (1987), and in the Ordovician Queen Brook Formation by McLeod (1997).

- The radiometric dating undertaken as part of this study has revealed that the rhyolite dome complexes, despite their lithological similarities, were emplaced during two distinct pulses separated by 15 to 20 million years. On the basis of their differences in age, associated host rocks, and chemistry, the rhyolite dome complexes are divided into five informal suites. Late Cambrian (c. 493 Ma) suites include the Shannon and Kierstead Mountain suites in the Lawson Brook Formation, and the Bald Hill suite in the Carpenter Brook Formation of the Annidale Group. Younger, Early Ordovician (c. 478–472 Ma) dome complexes include the London Settlement and Harry Brook suites that are part of a magmatic event that postdates dome emplacement associated with volcanic activity in the Annidale Group.

Field relationships and new radiometric data described in detail below suggest that the Carpenter Brook sedimentary rocks and laterally interfingering felsic volcanic and volcaniclastic rocks associated with the Bald Hill suite are the oldest components in the Annidale Group. The bimodal volcanic rocks of the Lawson Brook Formation are interpreted to interfinger with and conformably overlie the Carpenter Brook Formation. The Lawson Brook schist (McLeod et al. 1992, 1994) is retained within the Lawson Brook Formation, but is referred to herein as the 'O'Neill Brook schist', named after the only locality where it is exposed (frontispiece, this volume). The basaltic rocks and black shale of the East Scotch Settlement Formation appear to have been deposited disconformably on the Carpenter Brook Formation and therefore represent the youngest part of the Annidale Group.

The majority of rocks in the Annidale Group have been regionally metamorphosed to chlorite- or biotite-grade (McLeod et al. 1992). McLeod et al. (1992) estimated the thickness of the Annidale Group to be about 4 km. However, their estimate did not take into account structural repetition; nor did it include the thickness of the Carpenter Brook Formation, which was not considered part of the group at the time. A more detailed structural study is needed before a confident thickness estimate can be made.

Stratigraphy of the Annidale Belt

Stratigraphy of the Annidale Group is discussed here within the context of three major, northwest-directed thrust panels. The panels were delineated in part by the presence of stratigraphic cut-outs and abrupt changes in metamorphic grade and/or intensity and style of deformation. Units within each structural panel generally young to the south, and only portions of the original stratigraphic order are preserved in each. From north to south, these panels are

- the O'Neill Brook thrust panel, containing the highly deformed Late Cambrian (c. 497 Ma) O'Neill Brook schist;

- the Lawson Brook thrust panel, containing relatively undeformed mafic and felsic volcanic rocks of the Late Cambrian (c. 493 Ma) Lawson Brook Formation; and

- the Albright Brook–Taylors Brook thrust panel, containing an imbricated assemblage of sandstone–shale, volcaniclastic rocks, felsic tuffs, and flows of the Late Cambrian Carpenter Brook Formation; and Late Cambrian–Early Ordovician mafic volcanic rocks and black shale of the East Scotch Settlement Formation.

The last-named structural panel, in the footwall of the Taylors Brook Fault (Fig. 3a, 3b), also contains a number of mafic to felsic intrusions ranging in age from Late Cambrian to Early Ordovician (c. 490 to 472 Ma). The East Scotch Settlement and Carpenter Brook formations are structurally overlain to the south by the Grant Brook Formation of the Belleisle Bay Group, which occupies the hanging wall of the Taylors Brook Fault.

O'Neill Brook Thrust Panel

This northernmost thrust panel contains the O'Neill Brook schist, which is exposed in only two small inliers within Carboniferous conglomerate along O'Neill Brook east of Highway 710 in the Henderson Settlement area (Fig. 3a). The Late Mississippian conglomerate of the Shin Formation is dominated by schist clasts in the area, demonstrating that these Early Carboniferous units are locally derived.

O'Neill Brook Schist

The O'Neill Brook schist is heterogeneous, consisting of pink to tan and light green felsic schist and lesser mafic mica schist. Metamorphic muscovite is abundant in the felsic schist (about 30%) along with a few per cent biotite. The muscovite occurs as individual grains up to 0.5 mm long and in aggregates parallel to the schistose fabric (McLeod et al. 1992), suggesting that protoliths for some of the schistose rocks were likely felsic tuffs and flows. The more mafic layers contain muscovite, finer grained masses of epidote and carbonate, and minor chlorite and biotite. Quartz–plagioclase schist containing coarsely crystalline plagioclase crystals or aggregates in a finely crystalline matrix of quartz and minor muscovite is also present (McLeod et al. 1992). Recent SEM (scanning electron microscope) analyses of the plagioclase in the schist matrix indicate an albitic composition. Mineral assemblages in the O'Neill Brook schist (quartz + albite + muscovite + biotite; quartz + albite + muscovite + chlorite + epidote ± biotite; and quartz + albite ± muscovite) are characteristic of upper greenschist facies metamorphism.

The schistose fabric within the rocks along O'Neill Brook is flat-lying to undulating, dipping shallowly toward the northwest and southeast at approximately 20° to 40° (Fig. 5). Quartz veins commonly parallel the primary schistosity, and both are refolded by a second fabric characterized by mostly southward-verging folds (McLeod et al. 1992). McLeod et al. (1992) reported an igneous crystallization age of 497 ± 10 Ma for coarsely crystalline quartz–muscovite schist within this unit, and described the analyzed zircons as being typical of a rhyolitic protolith. Consequently, they considered the schist to represent a deeper structural level of highly strained tuffaceous rocks within the Lawson Brook Formation, an interpretation with which we concur. The error on the radiometric date obtained from the schist is quite large and within the realm of the age reported for the Lawson Brook Formation (McLeod et al. 1992).

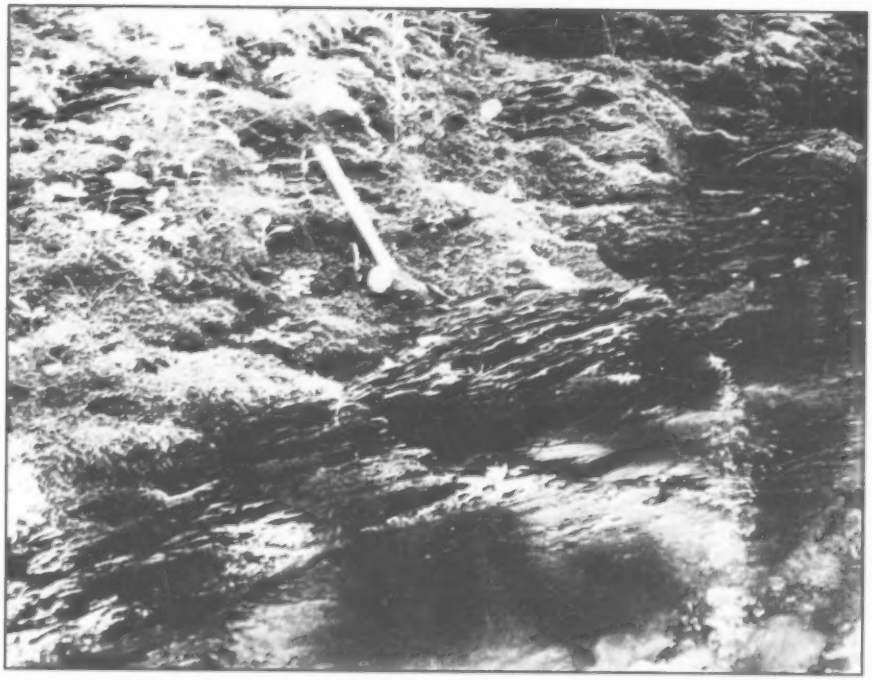

Figure 5. Shallow, north-dipping schistose fabric in the Lawson Brook Formation along O'Neill Brook. Hammer handle is 38 cm long. (Also see frontispiece.)

Lawson Brook Thrust Panel

The structural panel south of the O'Neill Brook schist contains a succession of relatively undeformed volcanic rocks assigned to the Lawson Brook Formation. The fault marking the northern boundary of this panel is not exposed but is indicated by an abrupt contrast in metamorphic grade and deformation intensity between the O'Neill Brook schist and the lower greenschist-grade rocks of the Lawson Brook Formation to the south (Fig. 3a). The location of the fault, beneath a thin cover of flat-lying Carboniferous rocks, is readily apparent on high-resolution aeromagnetic maps of the area (Thomas and Kiss 2004). The presence of a fault in this area is also indicated by tectonic breccia and altered, sheared basalt, black shale, and phyllitic felsic tuff on a tributary of O'Neill Brook less than 500 m south of the proposed location for this fault.

Lawson Brook Formation

The Lawson Brook Formation is exposed in a northeast-trending belt on the southern periphery of the Carboniferous cover, from the Saint John River northeastward to Marrtown (Fig. 3a, 3b). The Lawson Brook Formation terminates to the south against the Albright Brook Fault, where it is structurally overlain by strongly deformed rocks of the Carpenter Brook and East Scotch Settlement formations in the quartz-flooded hanging wall of the fault. The unconformity with Carboniferous sedimentary rocks of the Minto Formation is exposed at several localities, including the Miller quarry near Marrtown (Fig. 6).

The Lawson Brook Formation consists predominantly of basaltic flows, basaltic tuffs, and felsic dome complexes (Fig. 7a, 7b). The mafic volcanic rocks, which are best exposed on logging

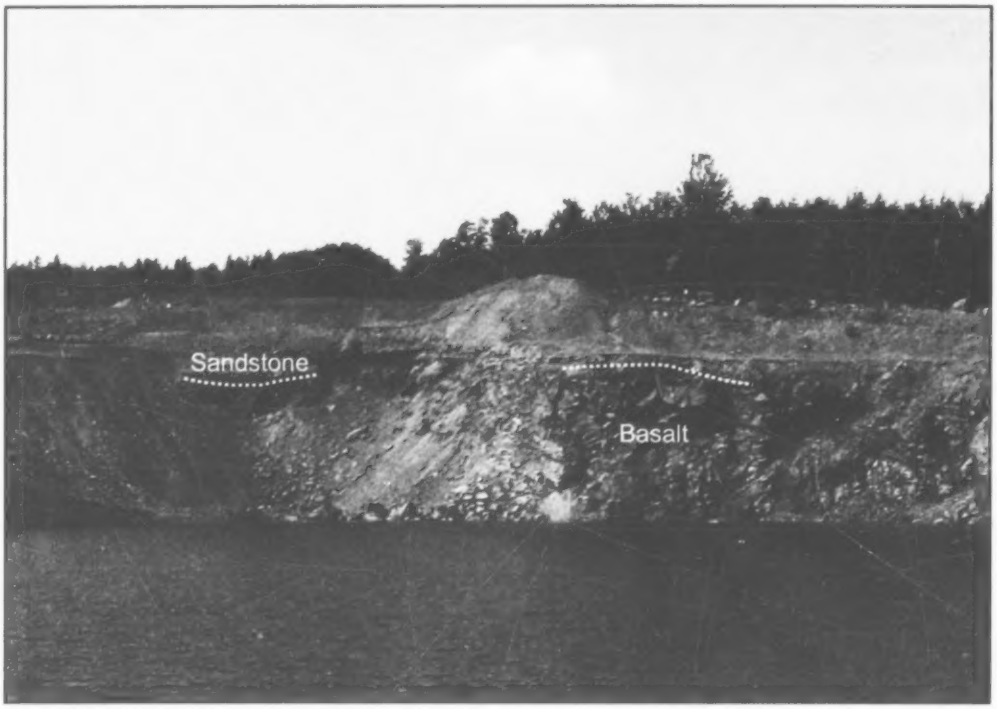

Figure 6. Carboniferous unconformity between sandstone of the Pennsylvanian Minto Formation and basalt of the Cambrian Lawson Brook Formation in the Miller quarry near Marrtown.

roads between Henderson Settlement and Stewarton (Fig. 3a, 3b), comprise a sequence of dark green to greyish green, commonly epidotized pillow lavas, amygdaloidal and vesicular basaltic flows, and hyaloclastite tuffs that contain distinctive bubble wall shards in thin section. The mafic volcanic sequence is at least 500 m thick and is locally interstratified with minor black, locally carbonaceous and pyritiferous shale and rare felsic tuffs. Pillows, almost a metre in length, are locally present within the mafic hyaloclastites (Fig. 7a).

To the northeast, felsic volcanic tuffs and flows are exposed in the valleys of Lawson Brook and Big Brook on the periphery of a subvolcanic rhyolite dome, which forms the adjacent hill between the two brooks (Fig. 3b). The felsic tuffs are medium to thick bedded, reddish pink to light greyish pink, and display eutaxitic banding; locally, they contain a penetrative, shallow-dipping cleavage. Fine-grained, light grey phyllitic sandstone and slate, which are locally interbedded with the tuffs, typically have a distinctive pink weathering and well-developed liesegang banding. These sedimentary rocks resemble those of the Carpenter Brook Formation, which suggests that it and the Lawson Brook Formation are at least partly laterally equivalent.

Shannon and Kierstead Mountain Suites

Felsic dome complexes within the Lawson Brook Formation are divided into the Shannon and Kierstead Mountain suites on the basis of their distinctive chemical traits. The domes are typically ovate to elliptical and form prominent hills covering areas up to 5 km^2. The Shannon suite (Fig. 7b) is exposed in the southwestern and central parts of the report area and includes the felsic domes near Shannon, Henderson Settlement, and Annidale (Fig. 3a, 3b).

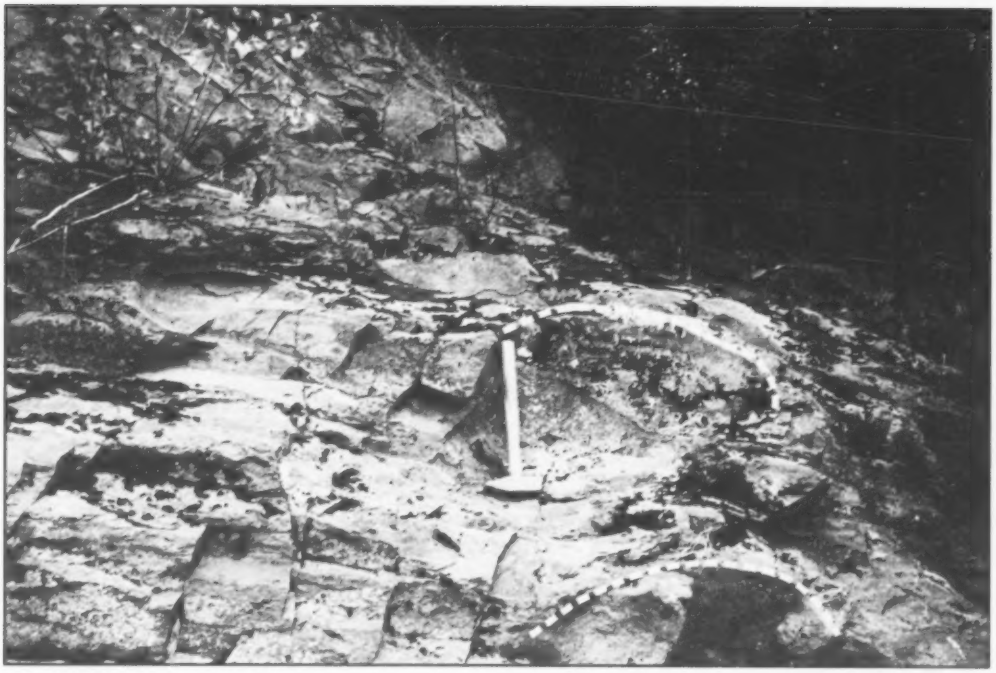

Figure 7a. Pillows (dotted lines) in basalt hyaloclastite sequence of the Lawson Brook Formation along the lower part of Lawson Brook. Hammer handle is 38 cm long.

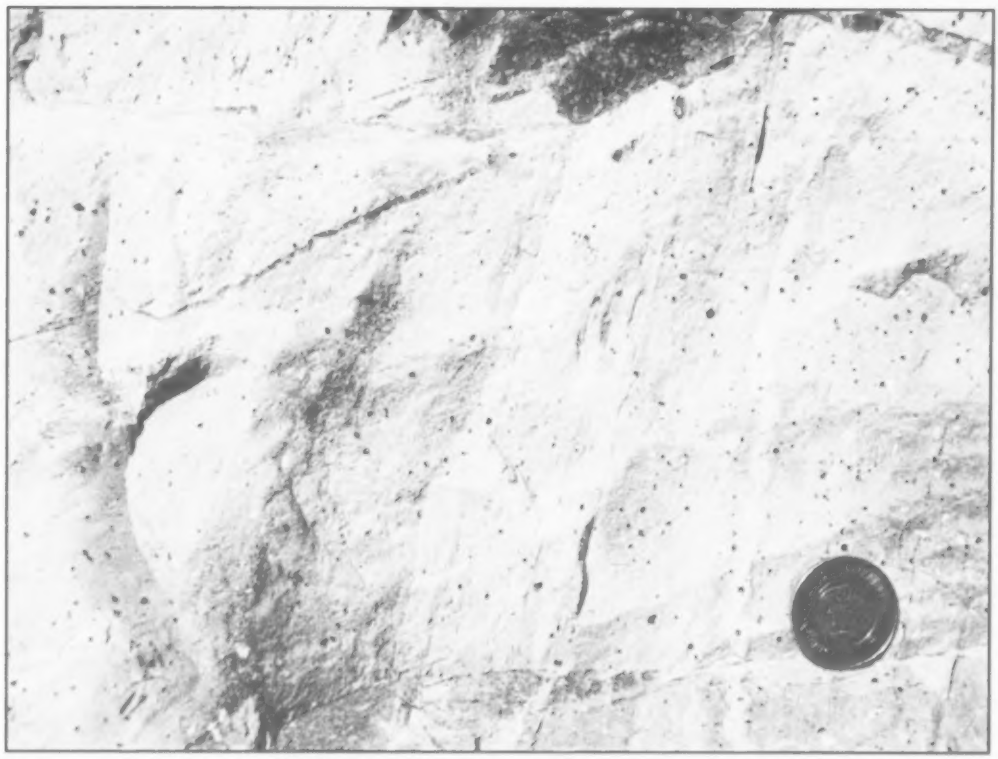

Figure 7b. Porphyritic, flow-banded rhyolite of the Shannon dome complex, east of Henderson Settlement. Coin diameter is 2.8 cm.

The Kierstead Mountain suite, situated in the northeast, includes the domes on Kierstead Mountain and along Lawson Brook and Big Brook in the Marrtown area (Fig. 3b). Both suites consist of slightly porphyritic to non-porphyritic, dark grey, subvolcanic rhyolite with associated felsic tuffs and autobreccia. The domes are locally cored by microgranite (McLeod et al. 1994). Fracturing and silicification is common in the domes, but penetrative fabrics are rarely observed.

The domal rocks are typically massive, glassy, and slightly porphyritic (quartz and/or feldspar), although some display well-developed and/or disaggregated flow-banding (Fig. 7b). The pink coloration of the rhyolite domes is a result of alteration, as fresh interiors are commonly dark grey to black. Autobreccia most commonly contains altered pink rhyolite fragments in a black glassy matrix but can also be composed completely of black rhyolite fragments. The presence of felsic dome material incorporated into the mafic flows of the Lawson Brook Formation, and of mafic tuff blocks within the felsic dome at Shannon, demonstrate that the mafic and felsic phases are comagmatic. The Shannon suite is dated as Late Cambrian (493 ± 2 Ma; McLeod et al. 1992).

Albright Brook–Taylors Brook Thrust Panel

This thrust panel is bounded to the north by the Albright Brook Fault, a significant intra-Annidale Group structure that separates the Lawson Brook Formation in the north from the East Scotch Settlement and Carpenter Brook formations to the south. The hanging wall of this fault is marked by a high-strain zone containing intensely deformed and quartz-flooded rocks. Immediately south of the high-strain zone, the Carpenter Brook and East Scotch Settlement formations are tectonically interleaved through imbricate thrusting and are intruded by numerous felsic to mafic intrusions. The Albright Brook–Taylors Brook thrust panel also contains most of the gold occurrences within the Annidale belt.

Radiometric dating (see ***Geochronology***) indicates that some of the intrusions are essentially coeval with volcanic activity in the Annidale Group, whereas others are distinctly younger. The older intrusions include the penetratively deformed Late Cambrian Cameron Road Granite and the hypabyssal intrusive rocks of the Bald Hill suite. The Early Ordovician Stewarton Gabbro is the largest of the younger intrusions (Fig. 3b). Rhyolite domes in the London Settlement and Harry Brook areas are also part of this younger intrusive episode (Fig. 3a, 3b).

Carpenter Brook Formation

The Carpenter Brook Formation is exposed along Carpenter Brook and the northern parts of Spragg and Taylors brooks (Fig. 3a, 3b). As presently mapped, it does not occur on the west side of the Saint John River; however, distribution of the Annidale Group in that area is poorly known. Rocks assigned to the Carpenter Brook Formation were previously included in the Queen Brook Formation (Silurian of McCutcheon and Ruitenberg 1987; Cambro–Ordovician of McLeod 1997), but we consider the lithological differences and geographical isolation from the Queen Brook type section to warrant separate formation status.

The Carpenter Brook Formation consists mainly of sedimentary rocks, which include a proximal sandstone–siltstone facies and a distal, deeper water siltstone–shale facies. The proximal facies is intercalated with felsic volcanic rocks that are part of a subvolcanic rhyolite dome complex, which is described separately under ***Bald Hill Suite***, below.

The proximal sedimentary facies consists of fining-upward sequences of thin- to medium-bedded, fine- to medium-grained, light to dark greyish green quartzose sandstone (Fig. 8a) interstratified with lesser thick-bedded, dark purple volcaniclastic sandstone, and laminated purple and green siltstone and slate. The volcaniclastic sandstone comprises abundant mafic and felsic volcanic clasts, polydeformed shale clasts, coarse-grained, rounded quartz grains, and feldspar fragments. Sparse detrital muscovite is present in some of the sandstone. The proximal facies grades laterally and upward (southward) into the distal sedimentary facies that comprises light to medium grey silty sandstone, and dark grey shale that locally contains abundant pyrite (Fig. 8b).

The Carpenter Brook Formation also contains rare mafic volcanic rocks, which at one locality near Albright Brook contain intrapillow limestone–marble. A thin but laterally continuous basaltic tuff horizon also extends westward from Cameron Road to the Bald Hill area. Strongly deformed, medium grey, phyllitic felsic tuffaceous rocks (Fig. 9a), light grey, quartz-rich volcaniclastic sandstone (Fig. 9b), greenish grey phyllitic shale, and thin-bedded, fine-grained siliceous sandstone and siltstone occur adjacent to the Albright Brook Fault in the southwestern map area; these rocks are also considered part of the Carpenter Brook Formation.

A maximum age for the Carpenter Brook Formation is latest Neoproterozoic as constrained by the youngest detrital zircons obtained from the quartz-rich volcaniclastic sandstone (c. 552 Ma). A minimum age is indicated by the cross-cutting relationship with the Late Cambrian (c. 490 Ma) Cameron Road Granite. The Late Cambrian age is considered more likely, based on the fact that magmatic activity related to emplacement of the Cameron Road Granite was probably essentially coeval with the volcanic activity associated with the Carpenter Brook Formation.

Bald Hill Suite

The sedimentary rocks in the Carpenter Brook Formation are spatially and temporally associated with peralkaline rhyolite dome complexes named the 'Bald Hill suite.' The suite comprises a series of small rhyolite domes arranged along a preferred axis, parallel to the regional northeast-trending fabric. The suite is best exposed around Bald Hill but also occurs in the Carpenter Brook area and along strike to the northeast (Fig. 3a). Similar felsic volcanic rocks, exposed near Pearsonville several kilometres along strike in the northeastern part of the Annidale belt (Fig. 3b), may also be part of the Bald Hill suite.

Relationships observed in drill core clearly demonstrate that the Bald Hill suite is coeval with sedimentary rocks of the Carpenter Brook Formation. Fine- to coarse-grained, grey and minor

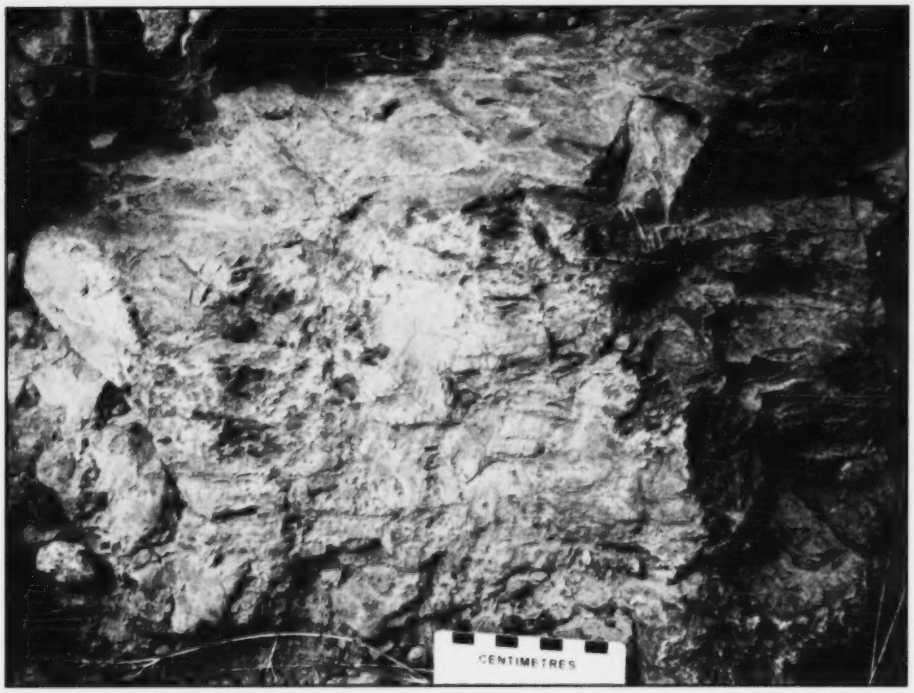

Figure 8a. Light greyish green quartzose sandstone of the Carpenter Brook Formation east of Henderson Settlement. Note vertical bedding laminations and subhorizontal cleavage.

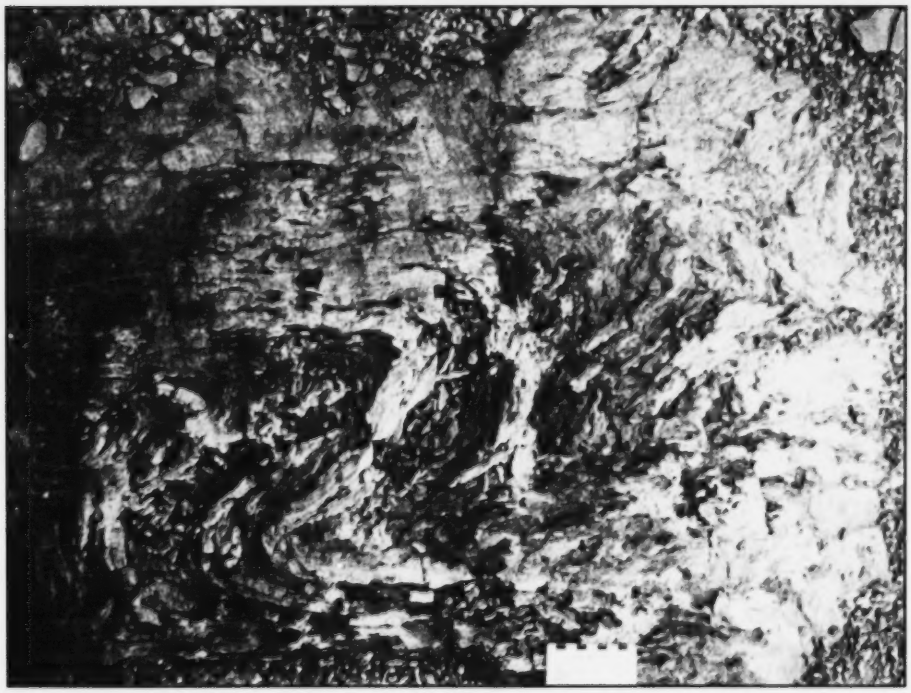

Figure 8b. Tightly folded, interbedded light to medium grey silty sandstone and dark grey shale of the Carpenter Brook Formation, west of Highway 710 and south of Henderson Settlement. Scale divisions indicate 1 cm.

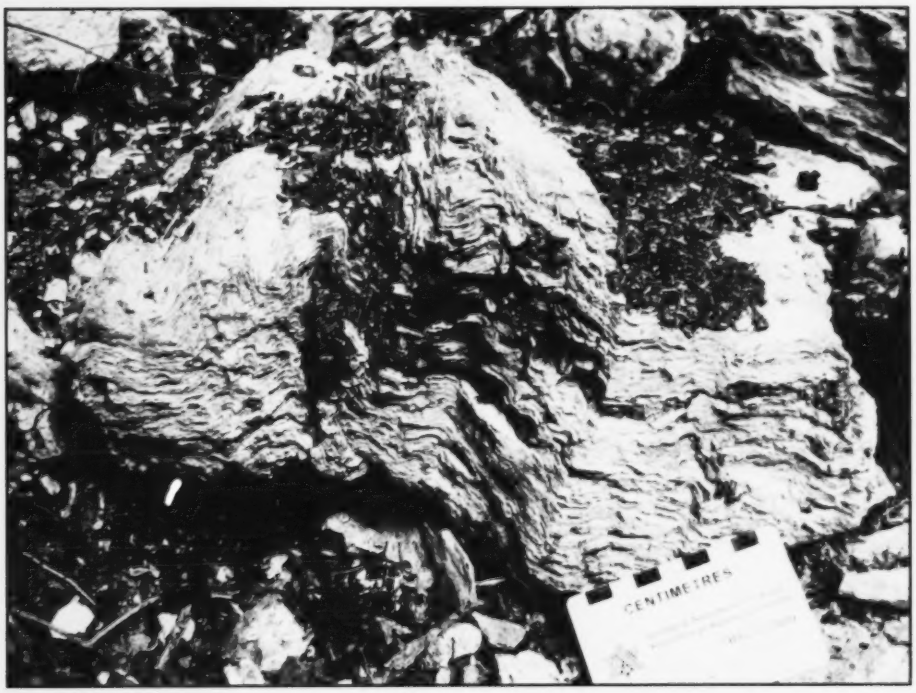

Figure 9a. Polydeformed felsic tuffaceous rocks of the Carpenter Brook Formation, just east of Albright Brook.

Figure 9b. Quartz-rich, light grey volcaniclastic sandstone of the Carpenter Brook Formation just west of Highway 710 (geochronology site 2 on Fig. 3a). Note the abundant quartz veining, which is common adjacent to the Albright Brook Fault.

purple and greyish green volcaniclastic sandstone and siltstone that are characteristic of the Carpenter Brook Formation are intercalated with felsic volcanic rocks associated with the Bald Hill dome. The sandstone is fairly unsorted and contains felsic volcanic debris, most likely from the nearby dome. Extrusive rocks in the suite include grey to tan felsic ash tuff, red to grey felsic pyroclastic breccia, and rhyolite flows. The rhyolite flows are commonly spectacularly spherulitic, containing individual and compound spherulites up to 4 cm in diameter (Fig. 10). The intercalated felsic volcanic and sedimentary rocks are locally intruded by reddish to greyish pink microgranite. Microgranite fragments locally occur within felsic pyroclastic breccia, indicating a close temporal relationship between the intrusive and extrusive phases.

The Bald Hill suite is commonly enriched in sulphides, including pyrite, arsenopyrite, and locally massive stibnite and gold. The rhyolitic volcanic rocks have extremely elevated zirconium levels (870–1242 ppm Zr) that distinguish them from other felsic volcanic rocks associated with other dome complexes in the report area. A sample sent for SEM analysis indicates that the zircon is exceedingly fine grained, typically less than 2 μm in diameter, and most commonly about 1 μm. The rhyolite also contains fine-grained monazite and fluorocarbonates rich in light rare-earth elements (D. Hall, pers. comm., 2008). The latter are commonly associated with alkaline rocks, which is consistent with the chemistry of the Bald Hill suite. Despite the high zirconium content, five samples from this unit yielded no datable zircon when processed for U–Pb dating as part of the present study.

East Scotch Settlement Formation

The East Scotch Settlement Formation is exposed in two narrow, discontinuous fault slivers within the Albright Brook–Taylors Brook thrust panel. The northern sliver extends along the south side of the Albright Brook Fault from Carpenter on the Saint John River northeastward to Annidale. The southern sliver extends along the north side of the Taylors Brook Fault from Wickham on the Saint John River northeastward to Spragg Brook and East Scotch Settlement (Fig. 3a, 3b). On the west side of the Saint John River, west of the report area, similar rocks exposed on Falls Brook and in the Cootehill Ridge area in CFB Gagetown are tentatively assigned to the East Scotch Settlement Formation (McLeod et al. 1992).

In both slivers, the East Scotch Settlement Formation consists predominantly of mafic volcanic rocks and dark grey to black carbonaceous, pyritiferous shale. The volcanic rocks are characterized by strongly deformed, commonly silicified and/or carbonitized and fuchsite-altered, greyish green, basaltic hyaloclastic tuff and agglomerate with lesser vesicular basalt and pillow lavas. The hyaloclastic tuffs are composed almost entirely of well-rounded, large pebble to cobble size basaltic clasts in a basaltic matrix, giving them a 'knobby' appearance (Fig. 11). Intensely deformed, black carbonaceous, pyritiferous shale is locally interbedded with the mafic rocks. Rare outcrops of strongly serpentinized rock, magnesium–chromium–nickel-rich basalt, and extensive fuchsite alteration in the vicinity of Annidale imply the presence of ultramafic rocks in the East Scotch Settlement Formation (McLeod et al. 1992).

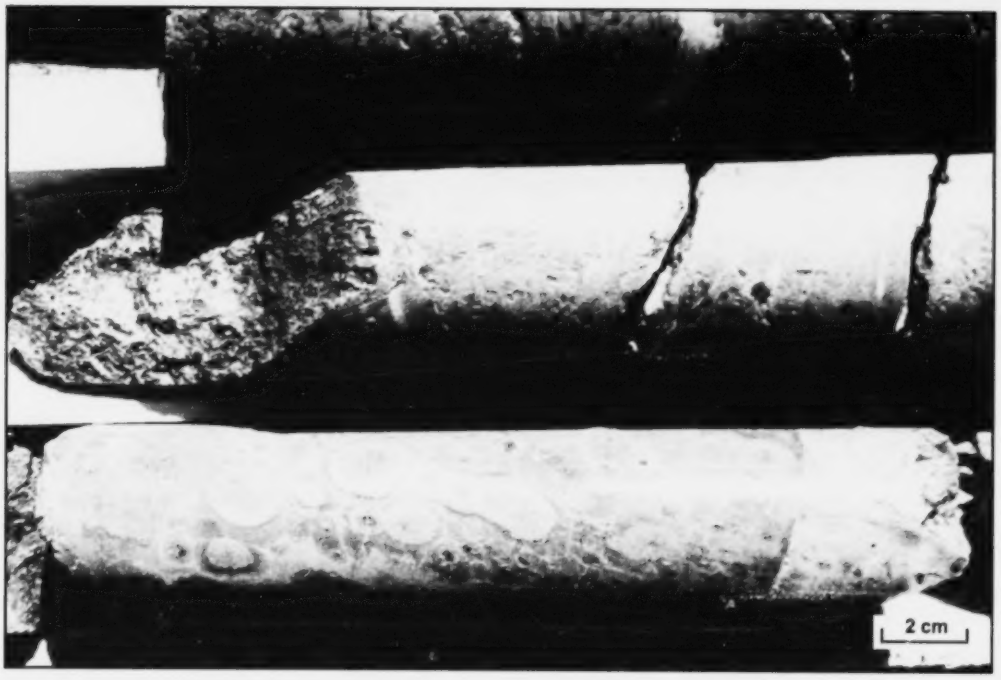

Figure 10. Spherulitic texture in Bald Hill rhyolite from drill core at Bald Hill.

Figure 11. Basaltic hyaloclastic tuff of the East Scotch Settlement Formation, southeast of London Settlement. Note the large basaltic clasts.

A horizon of conglomerate and black shale containing sparse blocks of sandstone occurs in the East Scotch Settlement Formation in the London Settlement area. This horizon occurs in the hanging wall of the thrust fault that separates sedimentary rocks of the East Scotch Settlement Formation from those of the Carpenter Brook Formation to the north. The massive conglomerate beds are exposed along the road between Wickham and London Settlement. They apparently grade east-northeasterly into the black shale beds containing the sandstone blocks, which are exposed just east of Jones Brook. Farther to the east, the horizon apparently thins dramatically or is structurally cut out by a thrust separating mafic volcanic rocks of the East Scotch Settlement Formation from rocks of the Carpenter Brook Formation to the north (Fig. 3a).

The conglomerate contains a variety of angular to rounded, poorly sorted clasts set in a dark grey mudstone matrix. The clasts include light green to grey, fine-grained sandstone and siltstone; and rare light grey, pyritic siliceous sandstone and dark grey porphyritic felsite (Fig. 12a). An interesting feature in the conglomerate is the flattened to spherical and irregular-shaped carbonate concretions. The origin of carbonate concretions in similar beds has been attributed to deep-sea methane venting (Berti et al. 1994), which is consistent with the deep-marine depositional environment proposed for the East Scotch Settlement Formation. The sandstone and siltstone clasts in the conglomerate appear to be derived from the structurally underlying Carpenter Brook Formation and seem to have been lithified before incorporation into the conglomerate. This suggests that the original stratigraphic contact between the East Scotch Settlement and Carpenter Brook formations was a disconformity.

The angular blocks in the black shale (Fig. 12b) to the east of Jones Brook appear to represent boudins of once-continuous sandstone beds. This feature, together with the highly sheared nature of the black shale matrix, suggests that some tectonic activity was taking place at the time of sediment deposition. The conglomerate and laterally equivalent black shale beds are therefore tentatively interpreted to represent the proximal and distal facies of an olistostrome or olistostromal mélange.

The age of the East Scotch Settlement Formation is not well constrained. The formation lies in fault contact with the Grant Brook Formation to the south along the Taylors Brook Fault and is intruded by the Early Ordovician (c. 479 Ma) Stewarton Gabbro. The East Scotch Settlement Formation is interpreted to be unconformably overlain by felsic volcanic rocks that are part of the c. 478 Ma London Settlement suite (described below), although their mutual contact is not exposed. On the basis of evidence given above, the East Scotch Settlement Formation is considered to be younger than the Carpenter Brook Formation and therefore is assigned an age of Late Cambrian to Early Ordovician.

London Settlement Suite

The London Settlement rhyolite dome complex comprises hypabyssal intrusive and extrusive rocks that are exposed within the Albright Brook–Taylors Brook thrust panel from Wickham on the Saint John River eastward to London Settlement (Fig. 3a). The suite consists primarily of

Figure 12a. Conglomerate of the East Scotch Settlement Formation, showing sedimentary and rare felsite clasts in a mudstone matrix, exposed along the road between Wickham and London Settlement.

Figure 12b. Sandstone block in black shale of the East Scotch Settlement Formation, exposed near London Settlement just east of Jones Brook. Hammer handle is 28 cm long.

dark grey to greyish pink, massive to brecciated, porphyritic and aphyric rhyolite and white-weathered, greyish pink felsic lapilli tuff and pyroclastic breccia. The rhyolite autobreccia comprises pinkish rhyolite fragments in a black felsic matrix (Fig. 13), and it is not easily distinguishable from felsic breccia in the Shannon area associated with the much older Lawson Brook Formation. U–Pb dating of a dark grey subvolcanic rhyolite from the suite near Wickham yielded an Early Ordovician age of c. 478 Ma (see ***Geochronology***).

Harry Brook Suite

A younger rhyolite dome complex occurs within the Albright Brook–Taylors Brook thrust panel in the Marrtown–Harry Brook area in the extreme northeastern part of the Annidale belt (Fig. 3b). The enclosing strata for this dome are concealed beneath Carboniferous cover, but mafic volcanic rocks of the East Scotch Settlement Formation crop out nearby, and aeromagnetic trends are consistent with that formation being the host.

The Harry Brook suite consists of pink to reddish rhyolite, spherulitic rhyolite, and rhyolite breccia that show gradations from subvolcanic rhyolite to microgranite over short distances. The rhyolite commonly displays irregular stockwork-like fractures filled with hematite, chlorite. and quartz–chalcedony, as well as large (~5 cm) quartz–chalcedony-filled vugs (Fig. 14). Like the London Settlement suite, the black-matrix rhyolite breccia in the Harry Brook suite is very similar to that in the older domes but is demonstrably younger. U–Pb dating of a vesicular, spherulitic rhyolite in the Harry Brook suite yielded an Early Ordovician age of c. 472 Ma (see ***Geochronology***).

STRATIGRAPHY OF SILURIAN ROCKS

Silurian rocks exposed in the report area belong to three separate sequences. From southeast to northwest, these are the Kingston Group of the Kingston arc (Barr et al. 2002a), the Mascarene Group of the Mascarene Basin (Fyffe et al. 1999), and the Kingsclear Group of the Fredericton Trough (McKerrow and Ziegler 1971; Fyffe 1995). Despite the diverse paleogeographic settings proposed by these authors and others (e.g., van Staal et al. 1998), all three groups are exposed over a distance of less than 25 km perpendicular to the regional strike, attesting to the degree of telescoping in this region.

The Kingston Group lies southeast of the Belleisle Fault and will not herein be considered further. The Mascarene Group, which is exposed between the Belleisle and Taylors Brook faults in the report area, locally forms the cover on the New River belt, consistent with basement–cover relationships in the belt to the southwest (Johnson and McLeod 1996; Fyffe et al. 1999). Strata correlated with the Kingsclear Group occur in the northernmost part of the report area. Although basement is not exposed there, volcanic rocks of the Annidale Group crop out nearby, suggesting that sedimentary rocks of the Kingsclear Group either structurally or stratigraphically overlie the Cambrian–Early Ordovician sequence. Detrital zircon data (Fyffe et al. 2009) also indicate that a similar basement–cover relationship existed between the New River belt and Ordovician Cookson Group of the St. Croix belt by Early Silurian time (Fig. 2).

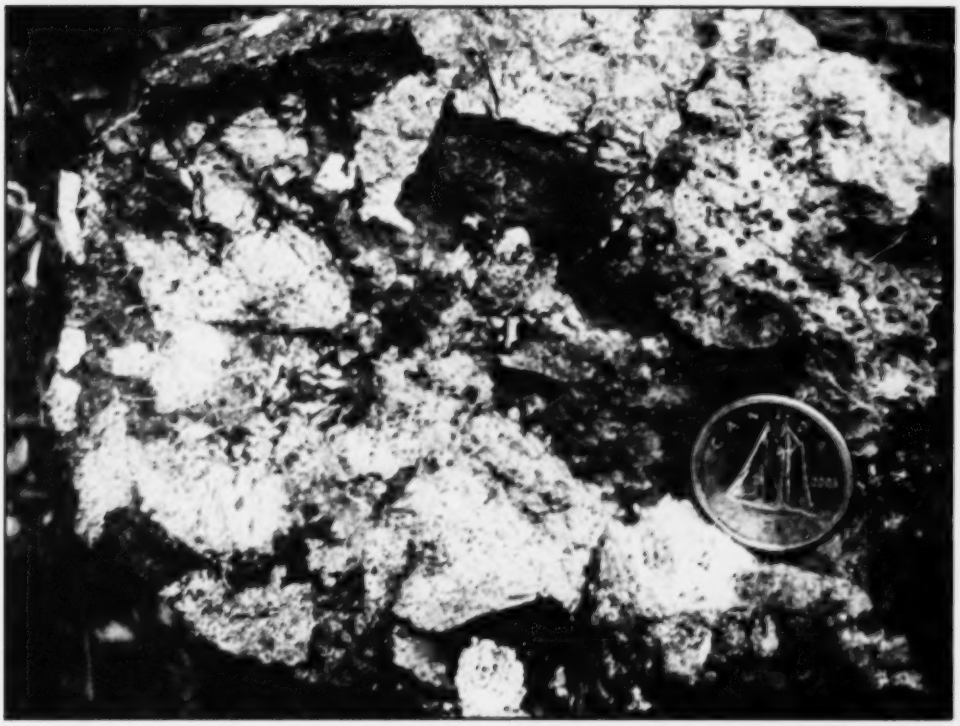

Figure 13. Rhyolite autobreccia of the London Settlement suite, east of Wickham. Coin diameter is 1.7 cm.

Figure 14. Harry Brook rhyolite containing a large, quartz–chalcedony-filled vug, northwest of the headwaters of Harry Brook.

Figure 15. Light grey, medium- to thick-bedded feldspathic sandstone, exposed along the upper part of Northeast Long Creek. Rocks are probably correlative with the Silurian Digdeguash Formation (Kingsclear Group). Hammer handle is 38 cm long.

Kingsclear Group (Long Creek Beds)

Light grey to greenish grey, medium- to thick-bedded, fine- to medium-grained feldspathic sandstone and siltstone (Fig. 15) occur in a small inlier along Northeast Long Creek in the northeastern part of the report area (Fig. 3b). These rocks were formerly considered part of the Canaan Forks sequence (Sheba inlier) of McLeod et al. (1992, 1994).

A number of silicified mafic sills or flows occur within the section. McCutcheon and Ruitenberg (1987) noted thin-banded, sulphide-bearing ironstone in the unit, and the beds are heavily stained with iron due to abundant disseminated pyrite. To the east and south, the unit is intruded by gabbroic to granitic plugs. The strata display a moderately to shallowly north-dipping, well-developed, northeast-trending cleavage that is subparallel to bedding. The contact between the Long Creek beds and Annidale Group is not exposed, but phyllitic siltstone and felsic tuffs of the Lawson Brook Formation are exposed to the west along the creek.

The Long Creek beds are lithologically unlike anything observed in the Annidale Group but are similar to the Middle Ordovician Woodland Formation in the Cookson Group and the Early Silurian Digdeguash Formation in the Kingsclear Group. Following McLeod et al. (1992, 1994), we tentatively assign the Long Creek beds to the latter unit.

Mascarene Group (Henderson Brook Formation)

The Mascarene Group in the report area comprises shallow-marine clastic rocks of the Henderson Brook Formation. The formation is interpreted to lie unconformably on mafic volcanic rocks of the Grant Brook Formation to the southeast and is faulted against the Stewarton Gabbro and mafic volcanic rocks of the East Scotch Settlement Formation to the northwest. Polymictic conglomerate in the Henderson Brook Formation contains clasts of orange and pink rhyolite, dark grey shale and minor mafic volcanic rocks. Such lithologies are common in the Annidale Group, suggesting that it may have been the detritus source.

Shelly fossils in grey feldspathic sandstone on Henderson Brook near Irish Settlement (Fig. 3b) indicate a precise Llandovery C5 (Early Silurian) age (McCutcheon and Boucot 1984) for the formation. McCutcheon and Ruitenberg (1987) also assigned quartzose sedimentary rocks along Ketchum Brook and parts of Taylors Brook to this Silurian unit; however, as discussed above, we consider those rocks to be Early Cambrian.

Plutonic Rocks

The Annidale and Belleisle Bay groups are host to a variety of felsic to mafic intrusions and rare plagiogranite intrusions and lamprophyre dykes. The only intrusive rocks recognized in the report area prior to this study were the Stewarton Gabbro and the larger rhyolite dome complexes near Shannon, Annidale, and Kierstead Mountain. The Stewarton Gabbro was considered to be Devonian (Hamilton 1961; Bennett 1965; McCutcheon and Ruitenberg 1987). The domes were previously thought to be part of either the Late Devonian–Early Carboniferous Piskahegan Group or the Silurian Mascarene Group.

U–Pb dating reported herein indicates that magmatic activity as a whole occurred in two main pulses: one in the Late Cambrian (c. 497–490 Ma) and another in the Early–Middle Ordovician (c. 482–467 Ma). The older intrusions are restricted to the Annidale belt north of the Taylors Brook Fault. They are represented mainly by felsic dome complexes within the Lawson Brook and Carpenter Brook formations but also include the penetratively deformed Cameron Road Granite. The younger intrusions were emplaced in both the Annidale and Belleisle Bay groups and are represented by the Stewarton Gabbro and numerous smaller gabbroic to granitic bodies and hybrid intrusions.

Late Cambrian–Middle Ordovician Intrusions

Cameron Road Granite

The Cameron Road Granite is an elongated, sheet-like intrusion extending along the Albright Brook Fault from Albright Brook northeastward to Grant Brook in the Albright Brook–Taylors Brook thrust panel. The granite is well exposed on Cameron Road and the associated network of logging roads west of Highway 710 to the south of Henderson Settlement (Fig. 3a). A small intrusive body located an additional 3 km to the northeast is also part of this unit. The Cameron Road Granite is the only major intrusion in the report area that exhibits a strong

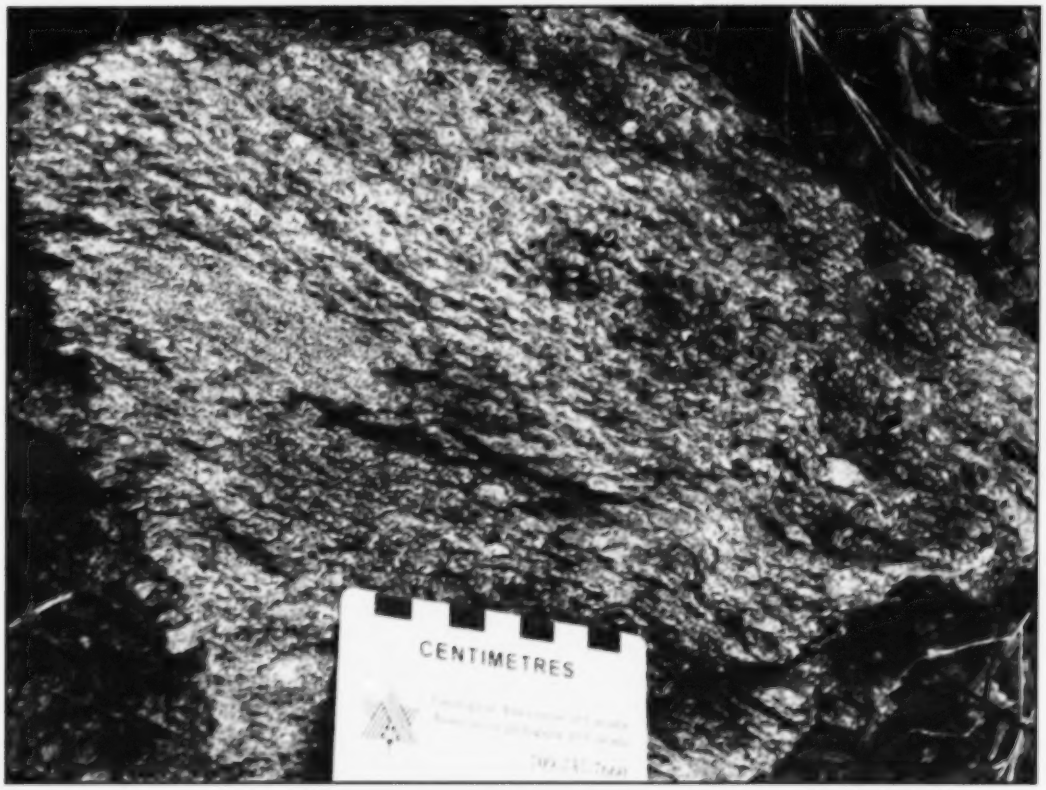

Figure 16. Coarse-grained texture and strong penetrative fabric in the Cameron Road Granite, exposed west of Highway 710, south of Henderson Settlement.

penetrative foliation, although the deformation possibly could be due to its close proximity to the Albright Brook Fault. The intrusion comprises medium grey to greyish pink, seriate, coarse- to fine-grained granite containing abundant, closely packed, large rounded quartz phenocrysts and glomerocrysts averaging 1 cm across (Fig. 16).

At its southwestern end, the Cameron Road Granite displays a finer grained, chilled margin against contorted and quartz-veined grey sandstone and phyllitic siltstone of the Carpenter Brook Formation. The intrusion is chemically similar to granite sheets that occur in the Carpenter Brook Formation, as observed in drill core from south of the intrusion (see ***Geochemistry***). U–Pb dating of this intrusion yielded a Late Cambrian age of 490 ± 2 Ma (see ***Geochronology***).

Plagiogranite

Plagiogranite intrusions occur as two separate bodies within the Albright Brook–Taylors Brook thrust panel. The first is a small (<1 km by 200 m) hypabyssal felsic intrusion that intrudes shale of the Carpenter Brook Formation along Grant Brook near Henderson Settlement (Fig. 3a). U–Pb dating of this intrusion, referred to as the 'Henderson Settlement plagiogranite' (Fig. 17a), yielded an Early Ordovician age of 482 ± 2 Ma (see ***Geochronology***). The second intrusion, named the 'Daley Brook plagiogranite' (Fig. 17b), is a large, oblong-shaped body that intrudes basaltic tuffs of the East Scotch Settlement Formation near the head of Daley Brook.

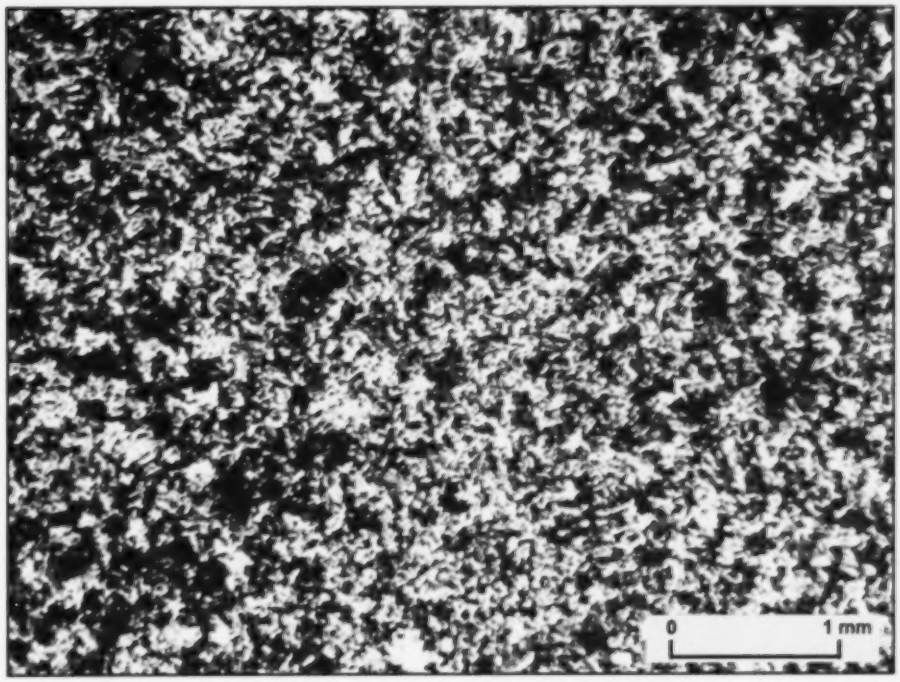

Figure 17a. Photomicrograph of Henderson Settlement plagiogranite composed of fine-grained, equigranular plagioclase (albite) and quartz, with secondary chlorite and Fe–Ti oxides. Photographed under partially crossed polarizers.

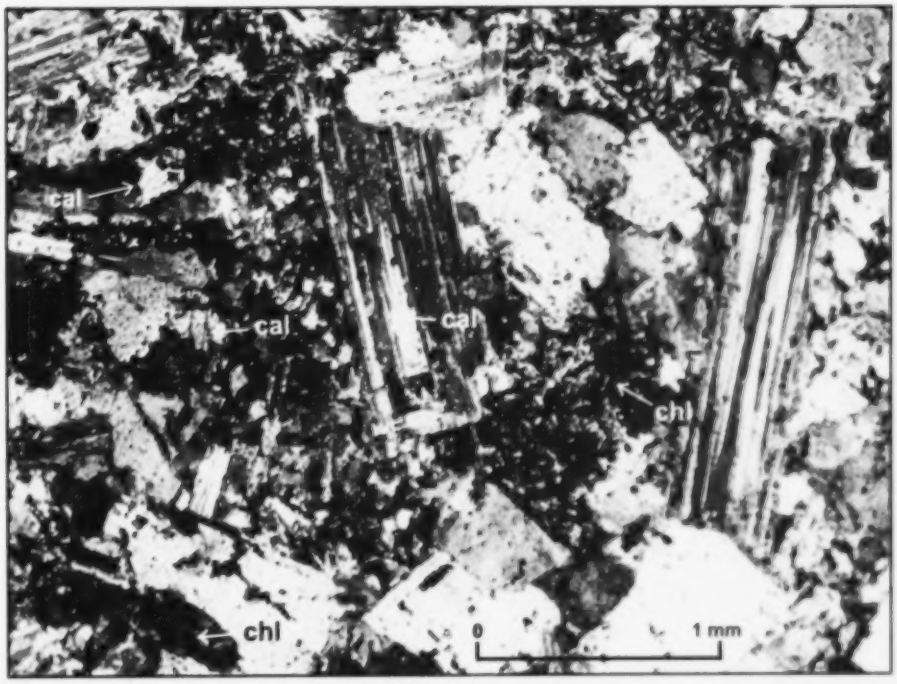

Figure 17b. Photomicrograph of Daley Brook plagiogranite with secondary calcite (cal) and chlorite (chl) partially replacing large albite crystals and plagioclase in the groundmass. Photographed under partially crossed polarizers.

Both intrusions are generally leucocratic, light grey to greyish pink, and consist almost entirely of plagioclase feldspar. The quartz content is varied but generally very low. The Henderson Settlement plagiogranite is fine grained (Fig. 17a) to aphanitic and contains both massive and porphyritic varieties. Porphyritic varieties are composed of plagioclase phenocrysts in a matrix of fine-grained plagioclase laths. The intrusion also exhibits structures in thin section that resemble devitrification textures, suggesting high-level emplacement. The Daley Brook plagiogranite is fine to medium grained, with an equigranular to seriate texture (Fig. 17b), and appears less altered than the Henderson Settlement plagiogranite. Mineral chemistry of constituent plagioclase from the groundmass and phenocrysts in both intrusions indicates that all of the grains analyzed are sodium-rich, consistent with having an albitic composition (D. Hall, pers. comm., 2008).

Stewarton Gabbro

The Ordovician Stewarton Gabbro and other, smaller gabbroic to granitic plugs in the report area are heterogeneous, with compositions ranging from gabbro to granite. Compositionally expanded intrusions are also found on First Run Brook, west of Collina, and on Long Creek in the northernmost part of the map area. Lafontaine (2007) describes "hybrid" intrusions such as potassium feldspar-bearing gabbros from exploration trenches at the Devil Pike Brook gold deposit near The Grant.

The Stewarton Gabbro (Bennett 1965; Venugopal 2003) is the largest intrusion of this type and the largest single map unit in the report area. It is a northeast-trending, rhomboid-shaped body about 3 km wide and 14 km long that extends from Stewarton Corner to Pearsonville (Fig. 3b). It has been referred to as the Stewarton Igneous Complex (Bennett 1965) and the Stewarton Intrusive Complex (McCutcheon and Ruitenberg 1987), but the preferred term, based on the predominant rock type, is the Stewarton Gabbro (e.g., Venugopal 2003). The complex consists of gabbro and anorthositic rocks with varied proportions of granodiorite, quartz diorite, diorite, hybrid rocks, granite, and felsic porphyry. Layering is common in some of the gabbroic units (Venugopal 2003). Quartz monzonite, leucogranite, and feldspar–quartz porphyry typically display cross-cutting relationships with the gabbroic rocks, indicating that the most felsic rocks are the latest intrusive phase (Venugopal 2003).

The felsic rocks in these composite intrusions are distinguished from the rhyolite domes by having lower silica contents. Venugopal (2003) interprets the granodiorite as a product of assimilation between the gabbroic and granitic phases, suggesting a close temporal relationship between mafic and felsic rocks in the complex. He concludes that the Stewarton Gabbro was differentiated and fractionated from a low-potassic tholeiitic basaltic magma that was intruded by a high-level calc-alkaline granitoid intrusion. The intrusion locally exhibits a faint to well-developed foliation parallel with the regional northeast-trending structural fabric; however, it is not penetratively deformed.

The northern boundary of the Stewarton Gabbro is in part faulted against the East Scotch Settlement and Carpenter Brook formations. Contact metamorphic effects are not obvious in

the mafic volcanic rocks of the East Scotch Settlement Formation, but an intrusive contact between the gabbro and sandstone of the Carpenter Brook Formation was observed on East Scotch Settlement Road. Along the southern contact of the gabbro, the Grant Brook Formation is hornfelsed within a broad contact aureole.

The Stewarton Gabbro was previously interpreted as Siluro–Devonian, because the rocks it intrudes were considered to be part of the Silurian Mascarene Group (Bennett 1965; McCutcheon and Ruitenberg 1987; Venugopal 2003). The gabbro was chosen for U–Pb dating because of the Cambrian age subsequently established for the country rocks (this report) and the observation that the gabbro is faulted against all demonstrably Silurian (fossiliferous) strata. The U–Pb dating of pegmatite within the Stewarton Gabbro yielded an Early Ordovician age of 479 ± 2 Ma (see ***Geochronology***).

Bull Moose Hill Porphyry

The Bull Moose Hill porphyry comprises three small feldspar porphyry plugs exposed in the Bull Moose Hill area north of Highway 870 (Fig. 3b). Good exposures occur uphill from the eastern talus slope of Bull Moose Hill and on the east side of Stoney Hill Road where the porphyry intrudes greyish green slate and micaceous sandstone of the Grant Brook Formation.

The porphyry is composed of abundant plagioclase and lesser amphibole phenocrysts in a tan to pinkish groundmass of quartz and feldspar. The plagioclase occurs as large (0.5 cm), pink, subhedral to anhedral glomerocrysts and smaller, greyish to pink, euhedral phenocrysts (Fig. 18). Large anhedral to euhedral amphibole phenocrysts are altered to chlorite and carbonate. Diabase inclusions and xenoliths are very common. The intrusion has an intermediate composition, with a SiO_2 content of just over 67%. The Bull Moose Hill porphyry is lithologically similar to feldspar–quartz porphyry that is considered to be the youngest intrusive phase of the Stewarton Gabbro (Venugopal 2003; his Appendix 4, and his Fig. 4.8). The abundance of diabase xenoliths in the Bull Moose Hill porphyry would seem to support this interpretation.

U–Pb dating of the Bull Moose porphyry yielded a Middle Ordovician age of 467 ± 3 Ma (see ***Geochronology***). If this porphyry is related to the feldspar porphyry in the Stewarton Gabbro, the possibility exists that some of the granitoid rocks in the 479 ± 2 Ma Stewarton Gabbro may not be related to the mafic phases, as suggested by Venugopal (2003).

Silurian–Devonian Intrusions

The vast majority of intrusions in the report area were initially thought to be Late Silurian or Early Devonian; however, only a few of this age are likely present. They include the large stock (the Evandale Granodiorite) on the west side of the Saint John River (Fig. 3a) and a high-level felsite plug that intrudes fossiliferous rocks of the Silurian Henderson Brook Formation near Irish Settlement (Fig. 3b). Lithologically similar felsic intrusions cut the Grant Brook Formation along the entire length of the New River belt. However, preliminary chemical

Figure 18. Abundant large feldspar phenocrysts in the Bull Moose Hill porphyry, Bull Moose Hill. Coin diameter is 1.9 cm.

data for these intrusions show that most of them are unlike the Irish Settlement plug in terms of rare-earth-element profiles (see ***Geochemistry***). Instead, they more closely resemble most of the older felsic rocks in the Annidale belt and therefore are shown as Late Cambrian–Middle Ordovician on Figures 3a and 3b. Gabbro and minor granite that intrude the Long Creek beds to the north of the Annidale belt (Fig. 3b) are also tentatively assigned a Silurian–Devonian age.

A lamprophyre dyke is exposed in a ditch on the west side of Highway 710, just north of the Cameron Road Granite (Fig. 3a). A large lamprophyre boulder (2 m by 2 m) can also be observed on the edge of the clearcut on the south side of Cameron Road. The outcrop in the ditch is deeply weathered and friable, and it contains abundant medium- to coarse-grained, brownish black biotite, potassium feldspar, and white mica (Fig. 19). Segregations and veins of pink feldspar up to 2 cm thick are common. The host rocks are not exposed but are presumably pyritic graphitic black shale of the East Scotch Settlement Formation, which was uncovered by exploration trenches to the east. The lamprophyre occurs in close proximity to several gold occurrences and the Albright Brook Fault—an interesting association, considering the link between shear zone-related gold deposits and lamprophyres (Kerrich and Wyman 1994). Similar lamprophyre dykes are known to intrude Silurian rocks of the Kingsclear Group in the Lake George area of southwestern New Brunswick (Leonard et al. 2006).

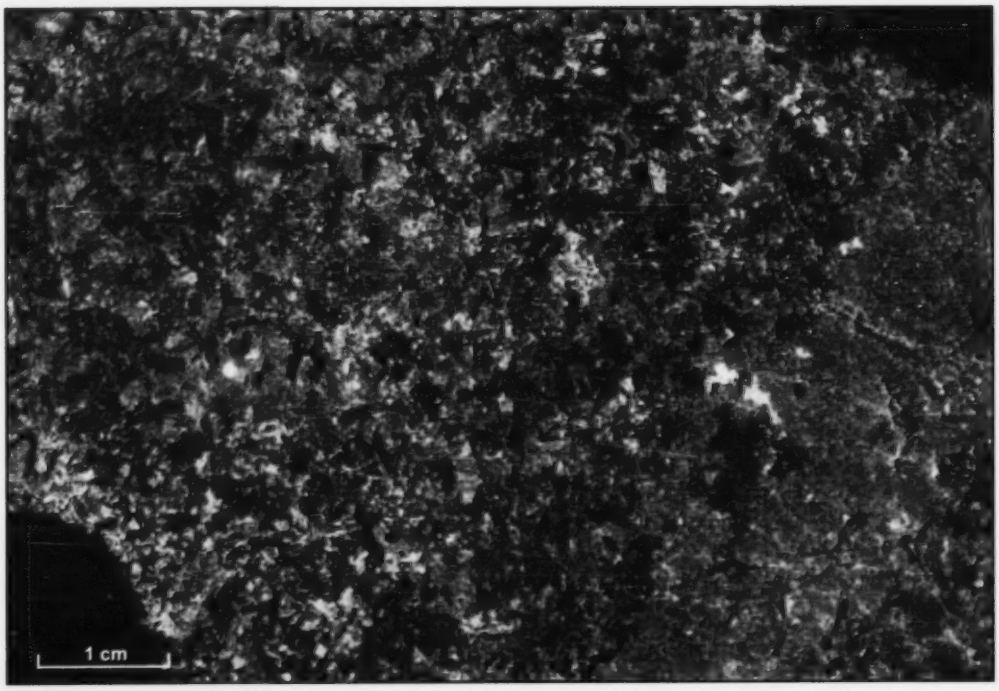

Figure 19. Coarse biotite laths and pink feldspar vein in a slab cut from the lamprophyre dyke on the west side of Highway 710, just north of the Cameron Road Granite (Fig. 3a).

STRUCTURE

As described in part by McLeod et al. (1992) and elaborated on herein, the rocks in the report area exhibit the effects of several episodes of faulting and heterogeneous deformation. The intensity and orientation of these episodes differ considerably between and within mapped units. Due to the multiplicity and complexity of these structural elements, and the intense shearing that commonly obliterates most primary sedimentary features and early structural fabrics, only preliminary observations and interpretations are made below, pending further study.

Faults

The most obvious and common large-scale structural features are steeply southeast-dipping to vertical, east-northeast- to northeast-trending faults and broad (kilometre-scale) shear zones, which are generally parallel to subparallel to the regional northeast-trending, penetrative fabric. Like most of the other similarly oriented minor to major faults in southern New Brunswick, the faults in the report area have undergone a protracted history of movement. The latest movement on these faults is most commonly strike-slip. However, low-angle thrusting, and high-angle reverse and normal movement, have also been documented in the region (e.g., McCutcheon 1981; McCutcheon and Ruitenberg 1987; van Staal and Fyffe 1991; Johnson 2002).

As discussed in detail below, the Taylors Brook Fault and many other major faults in the report area are interpreted as Early Ordovician, low-angle thrusts that were steepened during

later transpressive movement. Also present are younger, northeast- and north- to northwest-trending, vertical to steeply dipping faults that were active well into Carboniferous time. Both the northeast- and northwest-trending faults are commonly defined by shear zones and are associated with economic mineral occurrences (e.g., gold, antimony, and base metal sulphides) in quartz–carbonate vein systems and alteration zones.

Fabrics and Folds

Many of the pre-Silurian units are affected, to a greater or lesser extent, by a single well-developed cleavage. This regional cleavage is particularly prominent in finer grained clastic and tuffaceous lithologies and was formed mostly under lower greenschist metamorphic conditions, with chlorite and/or muscovite–sericite defining the fabric. Some of the more massive rock types, particularly in the Lawson Brook thrust panel, are commonly fractured but not pervasively deformed.

In the western part of the Lawson Brook thrust panel and throughout the Albright Brook–Taylors Brook thrust panel, the regional cleavage generally strikes east-northeast to northeast and dips steeply to moderately to the southeast. A similar cleavage orientation is also present in the western part of the Belleisle Bay Group (i.e., the distal finer grained facies of the Grant Brook Formation). However, farther to the east, it generally is less well developed and shows dip directions ranging from steeply to moderately to the southeast or northwest. Fabric orientations are dominantly east-striking and dip shallowly to moderately to the north in the eastern part of the Lawson Brook thrust panel. Fabrics within schistose rocks in the O'Neill Brook thrust panel are comparatively flat-lying to undulating, with horizontal dips or shallow dips to the northwest and southeast.

The regional cleavage is generally developed subparallel to bedding, but folding directly related to this fabric is rarely observed. At a few localities in the fine-grained sequences within the Albright Brook–Taylors Brook thrust panel, the fabric is axial planar to small (centimetre-scale), close to isoclinal, shallowly plunging, first-generation folds (Fig. 20a). These folds are similar to ones described in the Queen Brook Formation west of the Saint John River (McCutcheon and Ruitenberg 1987). Although bedding and younging directions are typically well preserved in finer grained lithologies in the northwestern part of the Belleisle Bay Group, systematic folding related to cleavage development could not be discerned. In some areas, bedding appears to intersect the northeast-trending, steeply to moderately south-dipping cleavage at random angles. More commonly, bedding is steeply dipping to the southeast or northwest, strikes subparallel to the prominent northeast-trending cleavage, and youngs to the southeast, generally dipping at steeper angles than the fabric. Such relationships are inconsistent with any straightforward folding pattern for these rocks.

The regional fabrics are commonly chaotically refolded within the high-strain zones associated with major faults, particularly in most sedimentary and tuffaceous units of the Albright Brook–Taylors Brook thrust panel. A well-spaced, second-generation fracture cleavage that is axial planar to these folds is frequently developed. For example, in shear zones associated with the

Taylors Brook Fault, a shallow, south-dipping, penetrative cleavage overprints the regional cleavage and is axial planar to shallowly plunging, second-generation mesoscopic folds (Fig. 20b). Similar, shallowly south-dipping, pervasive fabrics locally occur elsewhere within the Albright Brook–Taylors Brook thrust panel, particularly near the Albright Brook Fault in the vicinity of Shannon.

These fabrics are collectively interpreted to be related to north-directed tectonic transport along intra-unit and unit-bounding thrust zones in the Annidale Group (McLeod et al. 1992). Fabric development throughout the Albright Brook–Taylors Brook thrust panel and western part of the Lawson Brook thrust panel is likely a function of this northward-directed thrusting within a progressive thrust front; steeper high-angle reverse faulting would have preceded an episode of shallower dipping thrusting. Similar, but north-dipping second fabrics have been noted in the Long Creek beds, in the eastern part of the Lawson Brook thrust panel, and in the O'Neill Brook schist. These are interpreted to be related to tectonic transport of units along the northern part of the Annidale Group toward the south.

Timing of Faulting and Folding

Penetrative fabrics associated with north-directed thrusting in the Albright Brook–Taylors Brook thrust panel and New River belt developed prior to intrusion of the Early Ordovician Stewarton Gabbro (c. 479 Ma), as intrusive contacts and hornfelsing related to the intrusion clearly cross-cut these structures. A maximum age is indicated by the penetratively deformed Late Cambrian Cameron Road Granite (c. 490 Ma). Similarly oriented fabrics in the western part of the Lawson Brook thrust panel that affect the Lawson Brook Formation (c. 493 Ma) are interpreted to have formed during the same event. These age constraints indicate that the Annidale and Belleisle Bay groups were tectonically interleaved during the Early Ordovician.

In contrast, the timing of southward-directed thrusting associated with tectonic transport of units along the northern part of the Annidale Group noted above is less certain. Any age interpretation hinges on whether the Long Creek beds correlate with the Early Silurian Digdeguash Formation, and if the fabric in both the Long Creek and eastern Lawson Brook units formed at the same time. If the correlation with the Digdeguash Formation is correct, the development of the north-dipping second fabrics in the Long Creek beds took place later, possibly during Siluro–Devonian time. Regional south-directed transport of the Silurian strata of the Fredericton Trough, of which the Digdeguash Formation is part, was demonstrated by Fyffe et al. (1999) and Park and Whitehead (2003). However, none of the above data necessarily precludes the possibility that the fabrics formed in the eastern part of the Lawson Brook thrust panel during an older (Early Ordovician?), south-directed thrusting event coeval with fabric development in that area.

It is not clear whether the flat to shallow, north- and south-dipping second fabrics in the O'Neill Brook schist are associated with northward- or southward-directed thrusting. However, new argon data for metamorphic muscovite in the O'Neill Brook schist indicate that peak

Figure 20a. Small, isoclinal, shallow-plunging first-generation folds in slate of the Carpenter Brook Formation along the upper part of Taylors Brook. Coin diameter is 2.4 cm.

Figure 20b. Tight second-generation folds in fine-grained, greyish green sandstone and siltstone of the Carpenter Brook Formation along the upper part of Taylors Brook. Scale divisions indicate 1 cm.

metamorphism occurred during latest Ordovician time. An age of 444 ± 5 Ma was obtained using the stepwise heating method, which yielded a spectrum with a well-defined plateau over essentially all of the gas released (Table 1; Fig. 21; P. Reynolds, written comm., 2006).

Table 1. Argon data summary for muscovite from the O'Neill Brook schist. Analyses by Peter Reynolds, Dalhousie University, Halifax, Nova Scotia.

T°C	^{39}Ar (mV)	^{39}Ar (%)	Age (Ma) ± 1σ	% ATM	^{36}Ar / ^{40}Ar	^{39}Ar / ^{40}Ar
600	5.7	0.7	422.3 ± 31.86	29.2	0.000987	0.005833
700	33.3	4.1	451.7 ± 6.29	31.3	0.001061	0.005252
750	36.5	4.5	450.8 ± 4.97	6.4	0.000218	0.007175
800	135.8	16.7	441.2 ± 4.14	3.4	0.000117	0.007585
850	192.4	23.7	445.6 ± 3.78	4.1	0.000141	0.007448
900	203.7	25.1	445.4 ± 3.01	2.2	0.000074	0.007603
950	105.2	13	440.8 ± 3.88	0.3	0.000011	0.007838
1000	46.1	5.6	448.5 ± 3.05	2.4	0.000083	0.007526
1050	14.9	1.8	440.1 ± 6.39	2.9	0.000101	0.007641
1100	14.3	1.7	440.9 ± 7.05	5.3	0.000181	0.007439
1200	14	1.7	448.3 ± 8.72	20.9	0.000709	0.006098
1300	4.7	0.5	459.7 ± 26.53	62.4	0.002109	0.002819
1450	2.4	0.3	646.1 ± 98.76	90.2	0.003054	0.000490

Notes: 1. Mean age (800°C–950°C) = 443.8 ± 4.6 Ma (2σ uncertainty, including error in J); J = .002179 ± .0000153.
2. ^{36}Ar / ^{40}Ar and ^{39}Ar / ^{40}Ar are corrected for mass spectrometer discrimination, interfering isotopes and system blanks.
3. mV = arbitrary sensitivity scale.
4. % ATM = per cent atmospheric argon.

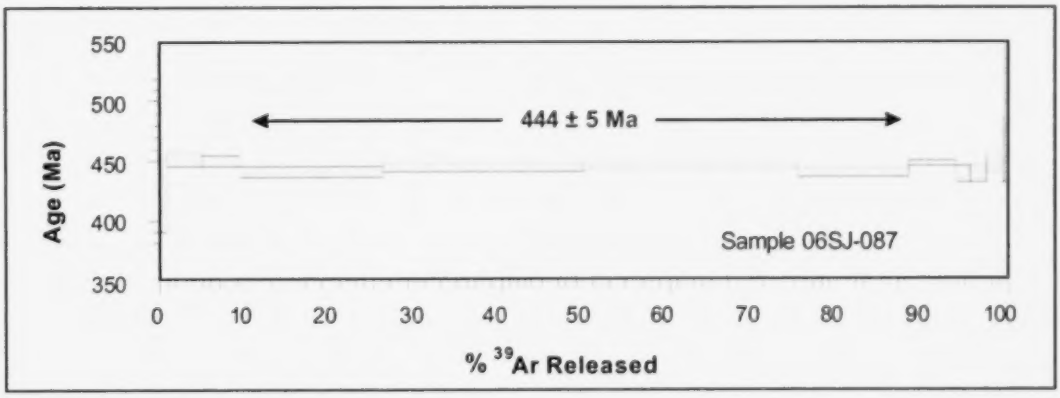

Figure 21. ^{40}Ar/^{39}Ar apparent age spectrum for muscovite concentrate from quartz–muscovite–biotite schist in the O'Neill Brook schist. Analyses and diagrams provided by Peter Reynolds, Dalhousie University, Halifax, Nova Scotia.

The development of a weak penetrative cleavage in the Silurian Henderson Brook Formation, open folding of earlier formed fabric elements in older units, and reactivation along northeast-trending faults are all attributed to Middle Devonian Acadian orogenesis (McCutcheon and Ruitenberg 1987) and subsequent minor crustal readjustment that affected the region.

GEOCHEMISTRY

Sampling and Analytical Methods

A total of 68 samples of mafic and felsic volcanic and plutonic rocks from the report area were analyzed for major, trace, and rare-earth elements (Tables 2 and 3). The rock samples were slabbed, and obvious veining was removed where possible. Major oxide, trace-element, and rare-earth-element (REE) analyses for the majority of samples were analyzed at Activation Laboratories (Ancaster, Ontario) by inductively coupled plasma–mass spectrometry (ICP–MS) using a lithium metaborate–tetraborate fusion. The exceptions were major oxide analyses for samples 01MM, 1600 series, and AN91 series (18 samples in total), which were previously conducted by X-ray fluorescence spectroscopy (XRF) at the Regional Geochemical Centre at St. Mary's University, Nova Scotia. Trace and REE analyses for samples 01MM444-460 were done by XRF at St. Mary's and by ICP–MS at SGS Minerals Services (Lakefield, Ontario), respectively. Archived sample powders for the 1600 and AN91 series samples were re-analyzed for trace elements and REEs by Activation Laboratories by ICP–MS (lithium metaborate–tetraborate fusion) as for the recently collected samples, above.

Mafic Rocks

A total of 23 mafic volcanic samples from the Annidale Group and five samples from the Stewarton Gabbro were analyzed. Major-element mobility due to pervasive alteration and metamorphism is evident on the CaO vs Na_2O diagram of Stillman and Williams (1978), with several samples plotting outside the field of normal basalt (not shown). In some cases, the rocks show extreme CaO and Na_2O depletion or Na_2O enrichment. Carbonitization and/or silicification are common in all of the mafic rocks. Rocks of the East Scotch Settlement Formation locally exhibit intense chromium-rich mica (fuchsite) alteration and serpentinization; consequently, immobile elements such as the high-field-strength elements (HFSE) are used to characterize the volcanic rocks in the Annidale Group.

Mafic rocks in the Annidale Group are mostly subalkaline basalts to basaltic andesites, with a few of the samples displaying andesitic compositions (Fig. 22a). Most samples plot as tholeiites on trace-element diagrams using HFSEs but show considerable scatter into the transitional and calc-alkaline fields on plots using large-ion lithophile elements (Fig. 22b, 22c). On the basis of differences in major and trace-element characteristics, mafic rocks in the Annidale Group are divided into two major types. Type 1 is the largest group; it includes basaltic flows in the East Scotch Settlement Formation and basaltic flows and tuffs in the Lawson Brook Formation. Type 2 rocks consist of an extensive basaltic tuff horizon in the East Scotch Settlement Formation in the vicinity of Spragg Brook and Annidale, but also include one basaltic flow collected from the Lawson Brook Formation in the Marrtown area.

Types 1 mafic rocks are distinguished from Type 2 rocks by having higher overall abundances of Al_2O_3 and TiO_2 and lower abundances of CaO and MgO (Table 2), as well as showing

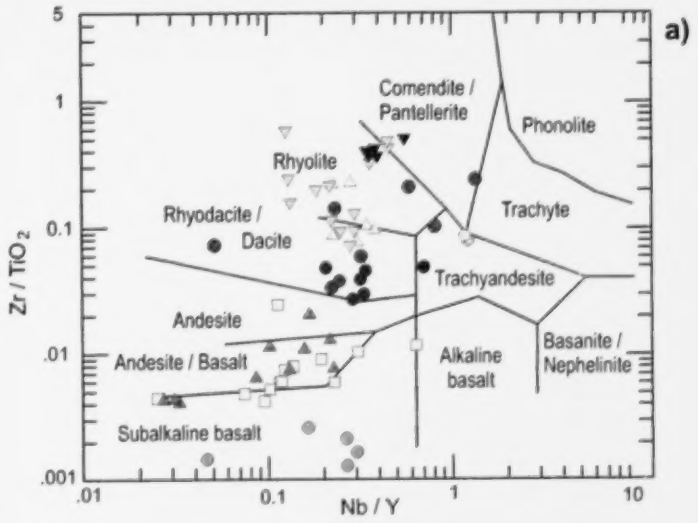

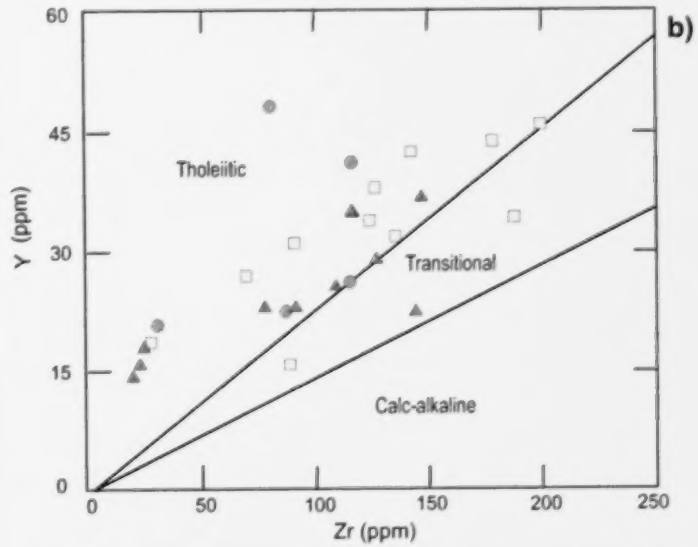

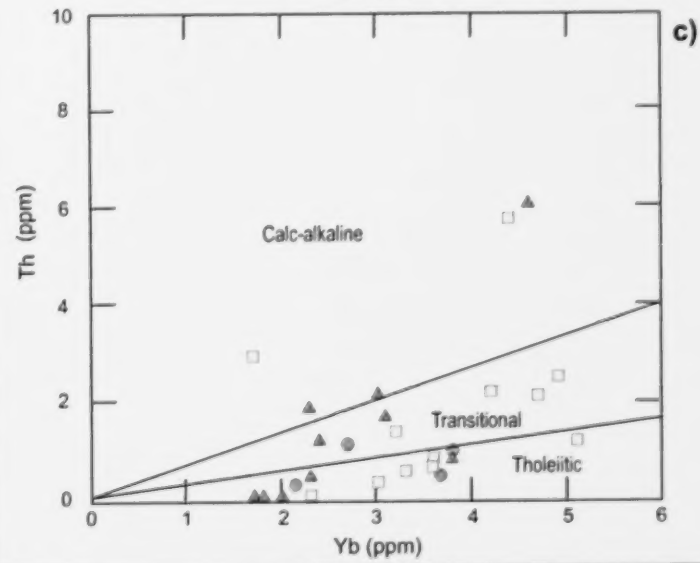

Mafic Volcanic Rocks

- East Scotch Settlement Formation
- Lawson Brook Formation
- Carpenter Brook Formation

Rhyolite Dome Complexes

- London Settlement and Harry Brook suites
- Shannon and Kierstead Mountain suites
- Bald Hill suite

Mafic to Felsic Intrusive Rocks

- Post-Early Silurian felsic intrusion
- Bull Moose Hill porphyry
- Felsic intrusions of uncertain age
- Stewarton Gabbro
- Henderson Settlement plagiogranite
- Daley Brook plagiogranite
- Cameron Road Granite, and granite sheets in the Carpenter Brook Formation

Figure 22. a) Nb/Y vs Zr/TiO_2 diagram for felsic and mafic volcanic rocks of the Annidale Group, and for mafic to felsic intrusions. Fields after Winchester and Floyd (1977).

b) Zr vs Y and c) Yb vs Th variation diagrams for mafic rocks of the Annidale Group, and for the Stewarton Gabbro. Fields defined by Barrett and MacLean (1999).

relatively flat, heavy REE patterns with moderate enrichment in the light REEs (LREEs) on chondrite-normalized plots (Fig. 23a). In contrast, Type 2 mafic rocks are depleted in LREEs, which is reflected in their strong concave-upward REE profile (Fig. 23b). In general, Type 1 rocks in the Lawson Brook Formation tend to have higher overall abundances of REEs than do Type 1 basalts in the East Scotch Settlement Formation (Fig. 23a). Type 2 mafic tuffs in the East Scotch Settlement Formation are further distinguished by having extreme enrichment in Mg (13.7–17.2% MgO) and strong enrichment in Cr (1180–4910 ppm) and Ni (390–880 ppm). The Type 2 basalt sample from the Lawson Brook Formation contains a lower overall abundance of these elements (Table 2), although still higher than in Type 1 mafic rocks. Consequently, all Type 2 samples have high Mg#s that range from 66 to 79 (Table 2) [=100 x mol. MgO / (mol. MgO + mol. FeO_t)], which indicates they have not undergone fractionation.

The Type 1 mafic rocks can be further subdivided into arc-related types and non-arc types. The arc-like basalts generally exhibit varied levels of Nb depletion relative to Th on primitive mantle-normalized spider diagrams (Fig. 23c, 23d), with the most pronounced negative Nb anomalies being in the basaltic andesite flows of the East Scotch Settlement Formation. It is widely accepted that an underabundance of certain HFSEs such as Ta and Nb and overabundance of low-field-strength-elements (LFSE) relative to LREEs are indicative of arc volcanism (e.g., Swinden et al. 1990). All of the East Scotch Settlement Formation shows this pattern except for sample 06SJ68, which is almost identical to the single sample from the Carpenter Brook Formation (Fig. 23e). In contrast with the arc-like rocks, these two samples show enrichment in Nb relative to Th and an overall negative REE trend. Three of the basaltic flows and one basaltic tuff from the Lawson Brook Formation also exhibit non-arc-like characteristics, although they show considerable variations in their REE trends (Fig. 23e). Type 2 mafic rocks are not plotted on the primitive mantle spider diagram, as their Th, Ta and Nb values are all below detection limits.

Virtually all Type 1 mafic rocks plot within the volcanic-arc–subduction-related fields (Fig. 24a, 24b). The Lawson Brook samples tend to plot toward the tholeiitic end of the subduction-related field, whereas the East Scotch Settlement samples plot more toward the calc-alkaline end (Fig. 24a). The LREE-depleted Type 2 rocks plot within the field for normal mid-ocean ridge basalts (N-MORB) on both diagrams. Although LREE depletion can be indicative of N-MORB, the extremely low Ti values in Type 2 rocks of the Annidale Group lie outside the range for mid-ocean-ridge basalts (Wilson 1989). Their very low TiO_2 values are more typical of arc tholeiites and are the reason the Type 2 rocks plot in the arc tholeiite field on the Ti vs V discrimination diagram (Fig. 25). In contrast, most Type 1 samples have Ti:V ratios within the 20 to 50 range, although both types are within the range of back-arc basin basalts. The highly unevolved character and chemical characteristics of Type 2 rocks are generally very similar to LREE-depleted, low-Ti, island-arc tholeiites in the older part of the Wild Bight Group in Newfoundland (MacLachlan and Dunning 1998). Overall, the geochemical signatures for mafic rocks in the Annidale Group are most characteristic of suprasubduction basalts erupted in a rifted arc or back-arc setting (e.g., Pearce 1996).

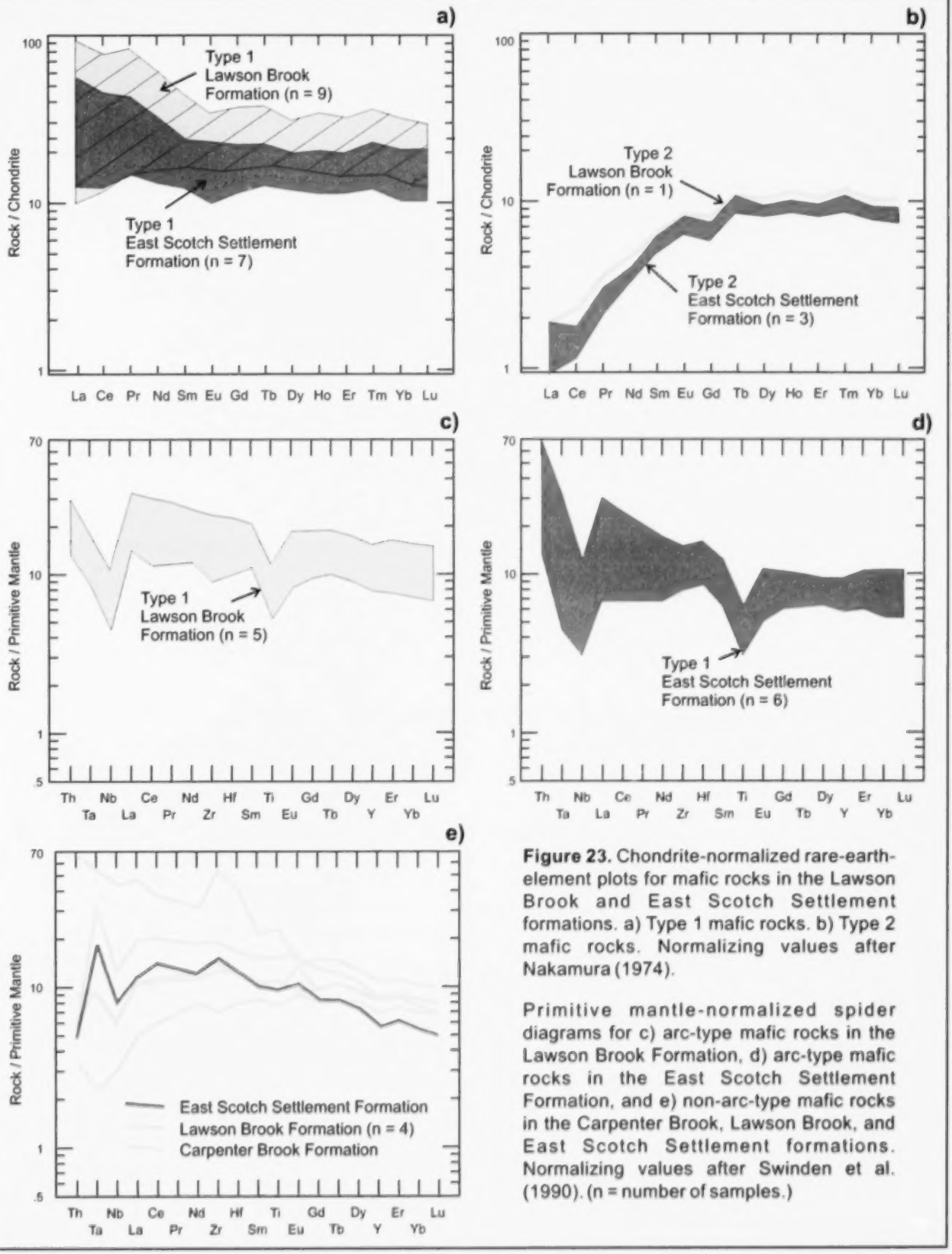

Figure 23. Chondrite-normalized rare-earth-element plots for mafic rocks in the Lawson Brook and East Scotch Settlement formations. a) Type 1 mafic rocks. b) Type 2 mafic rocks. Normalizing values after Nakamura (1974).

Primitive mantle-normalized spider diagrams for c) arc-type mafic rocks in the Lawson Brook Formation, d) arc-type mafic rocks in the East Scotch Settlement Formation, and e) non-arc-type mafic rocks in the Carpenter Brook, Lawson Brook, and East Scotch Settlement formations. Normalizing values after Swinden et al. (1990). (n = number of samples.)

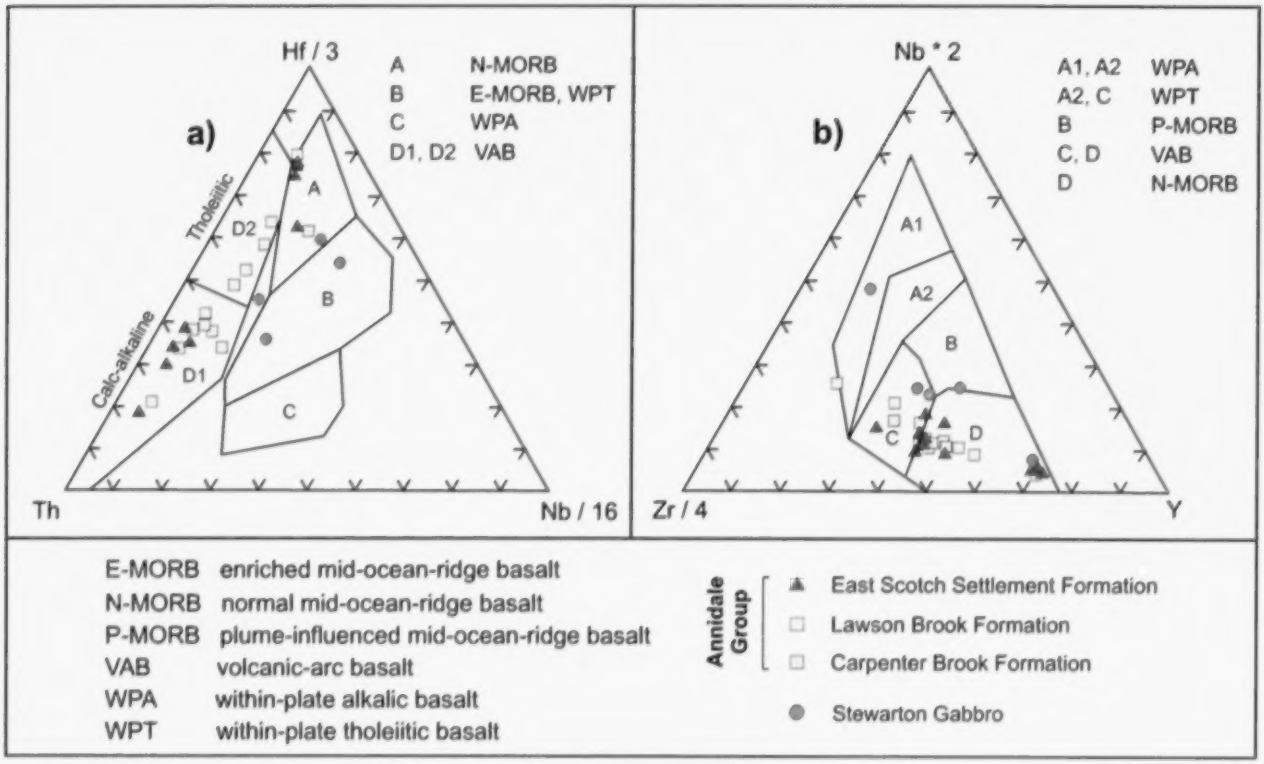

Figure 24. a) Th–Hf–Nb discrimination diagram, fields after Wood (1980). b) Zr–Nb–Y discrimination diagram, fields after Meschede (1986). Both plots are for mafic rocks of the Annidale Group and for the Stewarton Gabbro.

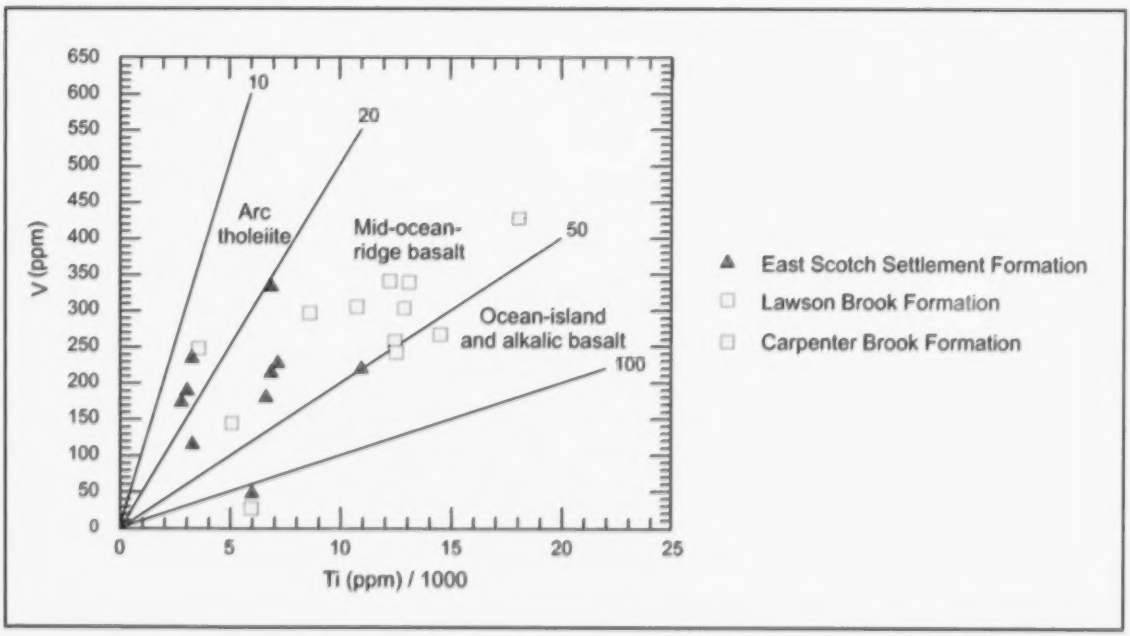

Figure 25. Ti vs V diagram for mafic rocks of the Annidale Group. Fields after Shervais (1982).

The chemistry of the younger Stewarton Gabbro has long been considered 'atypical of average gabbro' because of its low quartz content and high Fe and Ti content (e.g., Bennett 1965; McCutcheon and Ruitenberg 1987). Re-analyses of archived powders from five gabbro samples ranged from 40.1% to 43.3% SiO_2, 17.6% to 23.1% Fe_2O_3, and 2.3% to 7.0% TiO_2 (Table 2c). The gabbros are subalkaline, tholeiitic, and have an average Mg# of about 40. Their anomalously high Ti values cause the samples to plot outside the normal fields on many discrimination diagrams that use this element. On diagrams using HFSE, the Stewarton Gabbro samples show characteristics ranging from normal and enriched MORB to within-plate tholeiites (Fig. 24a, 24b).

Felsic Rocks

The analyzed felsic rocks comprise a compositionally expanded calc-alkaline suite that exhibits a wide range in composition from dacite through to rhyodacite, rhyolite, and peralkaline rhyolite (Fig. 22a). The two plagiogranite intrusions plot in the trachyandesite field because of their high Nb:Y ratios and will be discussed separately. The majority of samples are slightly to moderately peraluminous, having molar proportions of Al_2O_3 that exceed those of ($CaO + Na_2O + K_2O$). A/CNK (molar values) range from 0.91 to 1.7, with only four samples having A/CNK as less than 1 (Table 3). The felsic domes are typically very high in silica, averaging greater than 78% SiO_2 for 16 samples, with some domes having up to 83% SiO_2, due in part to silicification.

Most felsic samples exhibit moderate enrichment in LREEs, and relatively flat to moderately negative-sloping HREE profiles with moderate to strong negative Eu anomalies on chondrite-normalized plots (Fig. 26a–26d). The most prominent negative Eu anomalies are in the c. 493 Ma Lawson Brook Formation, particularly in the Kierstead Mountain suite (Fig. 26b). This is the opposite of what one would expect if declining Eu levels were due to the fractionation of plagioclase over time, as the younger dome complexes tend to have less prominent Eu anomalies, except for one sample in the London Settlement suite (Fig. 26c). This suggests that the felsic domes are not necessarily all related, or alternatively that the undated Kierstead Mountain domes are much younger than the Shannon domes.

The Bald Hill suite is distinguished from other felsic domes in the belt by their extremely high Zr values and overall enrichment in high-field-strength elements (HFSEs) (Table 3). They also have higher absolute abundances of REEs, and a subtle negative overall slope on chondrite-normalized plots (Fig. 26b). Their enrichment in HFSEs is reflected in a trend toward and within the peralkaline rhyolite field on the rock discrimination diagram (Fig. 22a). These chemical characteristics are most similar to the Kierstead Mountain domes, which plot in a similar position on this diagram; however their Zr content is not as high as for the Bald Hill suite (Table 3b). Overall, their extremely high Zr:Nb ratios (>20), moderate to strong negative Eu anomalies, and enrichment of HFSEs and REEs suggest a peralkaline affinity for the Bald Hill suite, which is important in light of its association with gold occurrences in the belt.

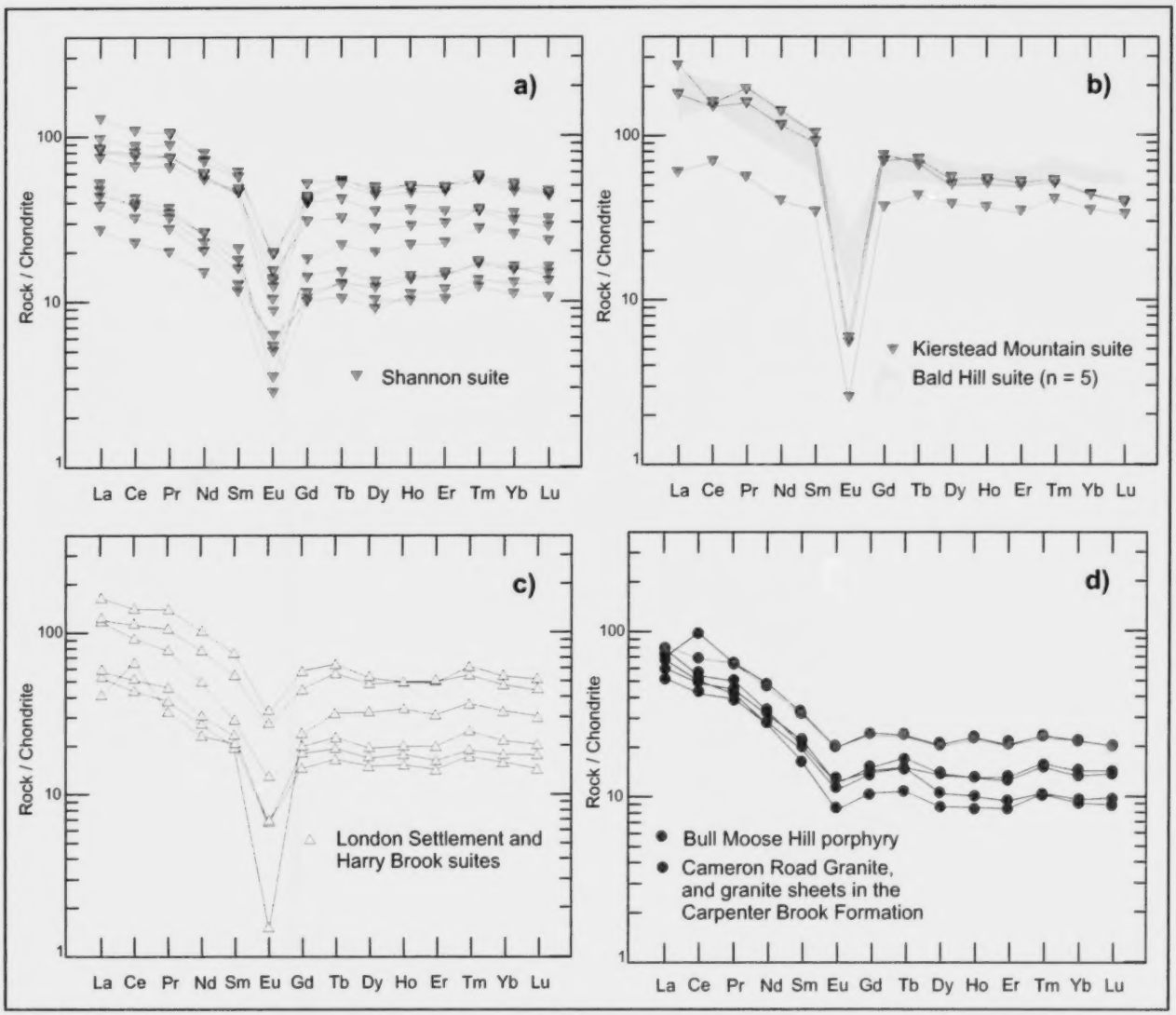

Figure 26. Chondrite-normalized rare-earth-element plots for felsic volcanic rocks of the Annidale Group, and intrusions: a) Shannon suite, b) Kierstead Mountain and Bald Hill suites, c) London Settlement and Harry Brook suites, and d) Bull Moose Hill porphyry, Cameron Road Granite, and granite sheets of the Carpenter Brook Formation. Normalizing values after Nakamura (1974).

Although peralkalinity is not demonstrated by their A/CNK values (Table 3), this is probably due to alkali mobility. Leat et al. (1986) suggest that Zr:Nb ratios higher than 10 are typical of peralkaline rhyolite erupted above subduction zones. The Bald Hill and Kierstead Mountain suites both plot between the ocean-ridge granite (ORG) and within-plate granite (WPG) fields, although still within the range of ORG (Fig. 27a), reflecting their anomalous A-type chemistry. In contrast, the calc-alkaline volcanic rocks of the Annidale Group and related intrusions plot in the volcanic-arc granite/syncollisional granite (VAG/SynCOLG) and ORG fields. The chemical similarities between the Bald Hill and Kierstead Mountain suites may suggest that the latter represent the oldest part of the Lawson Brook Formation and the transition from a rift to a more arc-related setting.

As would be expected, the plagiogranite intrusions are chemically distinct from all other felsic intrusions in the report area. These plagiogranites are albite-rich and hence plot in the trondhjemite field on the ternary normative albite–anorthite–orthoclase (Ab–An–Or) feldspar diagram (Fig. 27b). With their elevated Nb:Y ratios, they fall within the trachyandesite field on the rock discrimination diagram (Fig. 22a). Although the two plagiogranite samples analyzed are petrologically similar, they exhibit diametrically opposed LREE patterns with respect to chondrite (Fig. 27c). The Henderson Settlement plagiogranite is strongly enriched in LREEs, whereas the Daley Brook plagiogranite is strongly depleted in these elements, similar to the Type 2 basalts in the Annidale Group. LREE depletion in granitoid rocks is characteristic of ocean-ridge granites, although the Daley Brook plagiogranite plots near the within-plate-collisional granite boundary on Figure 27a.

The plagiogranites are also distinctive in that they are strongly peraluminous (A/CNK up to 1.6). While peraluminous trondhjemite can be generated by infiltration of sodium-rich metamorphic fluids during alkali metasomatism (e.g., Drummond et al. 1986), the igneous texture observed in thin section rules this out. High-Al_2O_3 trondhjemite can be produced in continental margin paleotectonic settings by melting of crustal and/or mantle sources in suprasubduction zone settings (e.g., Abdel-Fattah and Abdel-Rahman 1990; Nilsen et al. 2007), which is the setting proposed for the Annidale Group.

Felsic intrusions of uncertain age occur mainly in the New River belt. They range in composition from dacite through to peralkaline rhyolite and trachyandesite (Fig. 22a). Although not shown on Figure 26, these intrusions display negative Eu anomalies and have La:Yb ratios ranging from 3.1-7.9 (Table 3e). This is similar to the Late Cambrian–Early Ordovician felsic domes in the Annidale belt, which also display negative Eu anomalies and have La:Yb ratios ranging from 3.8 to 4.9 (Fig. 26a–26c). In contrast, the post-Early Silurian Irish Settlement plug has a La:Yb ratio of 30.3 and no Eu anomaly. Therefore, the felsic intrusions of uncertain age are more likely related to the older period of felsic magmatism in the region and are shown as such on Figures 3a and 3b.

A previous geochemical study suggested that the Annidale Group formed in an extensional, within-plate setting (McLeod et al. 1994); however, the chemical data reported here suggest a more complex magmatic history. The arc signature of the East Scotch Settlement Formation was evident in the earlier study but was difficult to reconcile with the rest of the data. McLeod et al. (1994) proposed that the mixed geochemical signatures could indicate a back-arc setting.

An improved understanding of the internal stratigraphy of the Annidale Group and a more comprehensive set of trace- and rare-earth-element data, as presented in this report, have helped to clarify the tectonic setting. Our data suggest a possible evolution through time from a rift setting for the Carpenter Brook Formation transitional to a back-arc and arc setting for the overlying Lawson Brook and East Scotch Settlement formations, respectively.

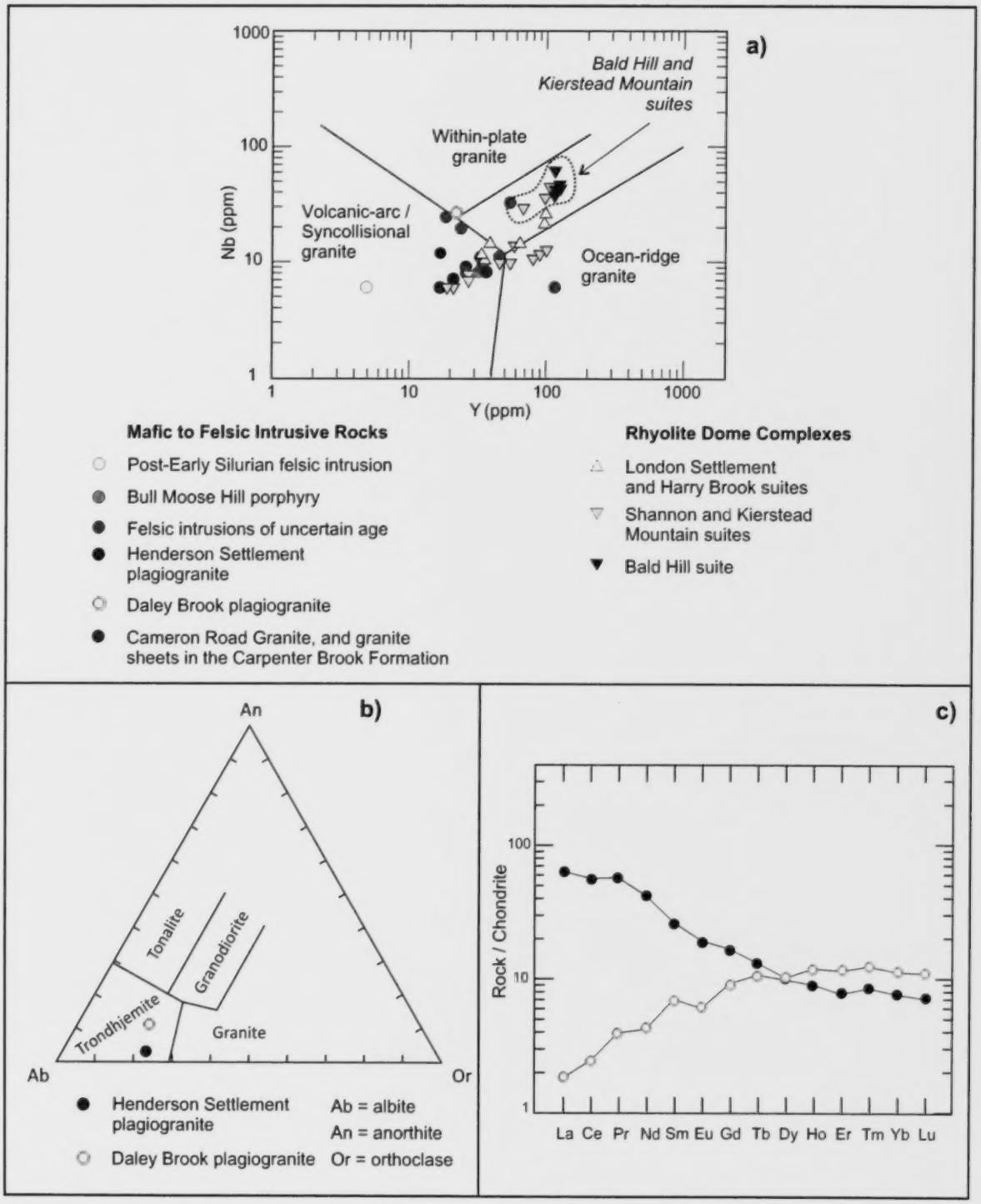

Figure 27. a) Y vs Nb discrimination diagram for felsic volcanic rocks of the Annidale Group, and intrusions. Fields defined by Pearce et al. (1984). b) Plagiogranites plotted on ternary normative Ab–An–Or feldspar diagram of Barker (1979), recalculated to 100%. c) Chondrite-normalized rare-earth-element plot of the two plagiogranites analyzed for the present study. Normalizing values after Nakamura (1974).

Table 2. Whole-rock geochemical analyses for mafic volcanic rocks of the Annidale Group, and for the Stewarton Gabbro.

Table 2a. East Scotch Settlement Formation.

	Type 1 Basaltic Andesite Flows						Type 1 Andesite	Type 2 Basaltic Tuffs		
Sample #	**06SJ42**	**06SJ56**	**06SJ68**	**1601-14**	**1601-103**	**1631-366**	**01MM451**	**06SJ52**	**06SJ64**	**1601-58**
Wt %										
SiO_2	55.43	50.78	45.81	55.4	45.2	57.4	55.14	50.07	47.72	44.19
TiO_2	0.99	1.15	1.84	1.11	1.16	1.19	0.55	0.51	0.48	0.54
Al_2O_3	17.1	15.5	16.13	17.79	17.39	15.14	14.09	9.86	10.66	12.48
Fe_2O_3t	8.24	16.07	10.72	7.61	8.59	10.75	6.73	7.78	8.87	10.04
MnO	0.21	0.3	0.13	0.13	0.13	0.11	0.12	0.18	0.15	0.2
MgO	3.39	7.55	9.15	4.66	3.84	3.7	6.68	14.41	17.22	13.73
CaO	2.97	0.86	5.35	2.14	9.48	3.75	8.20	11.22	6.73	10.97
Na_2O	6.27	0.57	2.56	6.6	4.93	4.29	3.12	1.65	2.31	2.04
K_2O	0.12	1.01	0.17	0.15	0.2	0.08	1.28	1.04	0.01	0.05
P_2O_5	0.22	0.14	0.23	0.22	0.12	0.11	0.22	0.03	0.03	0.03
LOI	4.79	6.07	8.21	4.2	10.1	3.7		2.73	5.66	4.8
Mg#	45	48	63	55	47	41	66	79	79	73
Trace elements (ppm)										
Ba	113	185	201	184	497	224	260	175	8	44
Rb	4	31	5	3	5	<2	31	36	<2	<2
Sr	286	9	153	347	202	144	690	68	26	231
Y	26	37	22	29	23	23	35	15	14	18
Zr	109	147	144	127	77	91	116	22	19	24
Nb	4	8	5	3	2	3	6	<1	<1	<1
Th	1.7	6.1	0.4	2.1	1.2	1.9	0.80	<0.1	<0.1	<0.1
Pb	7	<5	<5	8	<5	6	ND	<5	<5	<5
Ga	15	20	17	16	17	17	16	8	9	11
Zn	80	170	70	60	60	70	36	90	60	50
Cu	<10	<10	<10	50	70	50	85	10	110	30
Ni	<20	50	100	40	40	30	98	880	560	390
V	48	334	221	182	213	223	114	188	175	236
Cr	<20	10	160	50	110	50	124	2000	1180	4910
Hf	3.1	4.5	3.5	3.5	2.4	2.6	NA	0.8	0.7	0.8
Cs	0.9	1	4.2	1.7	0.5	<0.5	NA	0.7	<0.5	0.6
Sc	14	41	34	NA	NA	NA	NA	34	32	NA
Ta	0.3	0.7	0.4	0.2	0.1	0.3	NA	<0.1	<0.1	<0.1
Co	9	27	45	24	25	40	33	60	61	57
U	0.6	2	0.8	0.6	0.3	1.4	0.19	<0.1	<0.1	<0.1
Rare-earth elements (ppm)										
La	9.2	19	7.1	11.3	4.2	10.6	6.8	0.3	0.6	0.5
Ce	24.3	39.6	21.9	25.9	10.8	23.3	19.7	1	1.3	1.5
Pr	3.56	4.91	2.94	3.57	1.64	3.06	3.07	0.24	0.3	0.34
Nd	18	20.5	14.1	16.2	8.3	13.7	15.4	2.1	2.3	2.5
Sm	4.6	4.9	4	4.2	2.5	3.4	4.9	1.1	1	1.2
Eu	1.58	1.74	1.55	1.5	0.76	1.26	1.79	0.49	0.49	0.61
Gd	4.6	5.6	4.4	4.6	3.2	3.7	6.14	2	1.6	2
Tb	0.8	1	0.8	0.9	0.6	0.7	1.07	0.4	0.4	0.5
Dy	4.8	6.8	4.8	5.4	4.2	4.3	6.85	2.9	2.8	3.1
Ho	1	1.4	0.9	1.1	0.8	0.9	1.44	0.6	0.6	0.7
Er	3.1	4.5	2.6	3.2	2.6	2.6	4.21	1.9	1.8	2.1
Tm	0.47	0.69	0.38	0.48	0.38	0.37	0.58	0.29	0.26	0.32
Yb	3.1	4.6	2.3	3	2.4	2.3	3.8	1.8	1.7	2
Lu	0.48	0.7	0.33	0.44	0.36	0.35	0.56	0.26	0.25	0.3

Table 2b. Lawson Brook Formation.

	Type 1 Basaltic to Andesitic Flows							Tuff		Type 2 Flows
Sample #	**03MM10**	**01MM126**	**01MM204**	**06SJ54**	**06SJ67**	**06SJ69**	**01MM205**	**02MM151**	**06SJ38**	**06SJ41**
Wt %										
SiO_2	42.86	45.84	45.91	47.13	61.61	45.64	44.37	51.42	50.34	59.55
TiO_2	1.81	2.05	2.19	2.09	1	2.1	1.44	2.44	4.22	0.6
Al_2O_3	16.83	15.86	16.22	15.47	14.98	14.76	15.4	15.31	18.45	13.66
Fe_2O_3t	11.46	12.12	12.82	14.13	7.89	11.48	11.65	12.08	12.85	9.16
MnO	0.19	0.14	0.21	0.08	0.19	0.26	0.18	0.13	0.16	0.2
MgO	6.41	6.94	5.57	9.43	1.76	7.2	6.92	5.56	2.99	9.02
CaO	13.62	5.07	7.57	0.41	4.36	5.84	11.78	3.28	0.61	10.62
Na_2O	1.19	2.28	3.68	0.12	4.44	3.47	2.69	4.11	0.17	2.89
K_2O	0.05	0.8	0.05	3.94	0.87	0.39	0.06	0.68	4.46	0.36
P_2O_5	0.2	0.19	0.26	0.3	0.45	0.3	0.12	0.4	0.13	0.05
LOI	5.27	8.5	5.5	6.58	2.37	8.61	5	5.03	5.14	3.4
Mg#	53	53	46	57	31	56	54	48	31	66
Trace elements (ppm)										
Ba	16	206	86	320	298	76	18	107	1040	59
Rb	<2	19	<2	36	14	8	<2	5	64	5
Sr	138	182	360	20	228	71	366	101	29	76
Y	32	34	44	42	62	31	27	38	42	19
Zr	135	124	178	142	241	91	69	126	499	27
Nb	4	4	6	5	7	3	2	4	28	<1
Th	0.6	0.8	2.1	1.2	2.7	1.4	0.3	2.2	5.8	<0.1
Pb	<5	<5	<5	7	6	38	<5	5	12	<5
Ga	21	20	22	24	23	20	19	21	34	12
Zn	80	90	100	180	120	110	80	120	120	60
Cu	50	50	10	<10	<10	<10	60	<10	30	170
Ni	110	100	60	<20	<20	50	160	30	30	170
V	307	341	340	258	27	244	297	265	419	249
Cr	280	240	130	<20	<20	110	340	50	<20	440
Hf	3.5	3.4	4.7	4.2	6.7	2.9	2.2	3.7	11.4	0.9
Cs	<0.5	1.4	<0.5	1.3	<0.5	<0.5	<0.5	<0.5	5.5	<0.5
Sc	39	38	43	38	19	40	37	40	42	42
Ta	0.2	0.2	0.4	0.3	0.25	0.2	<0.1	0.3	2.2	<0.1
Co	42	38	44	30	8	35	43	32	47	39
U	0.2	0.3	0.7	0.6	0.7	0.4	<0.1	0.8	1.1	<0.1
Rare-earth elements (ppm)										
La	6.6	6.6	12	10	20.6	8.9	3.2	10.7	29.1	0.6
Ce	18	17.2	31.3	25.9	50	18.4	9.6	28.4	57.3	2
Pr	2.86	2.63	4.61	3.82	7.03	3.05	1.68	4.04	8.94	0.4
Nd	14.3	13.6	22.4	18.8	32.7	14.7	9.5	19.5	38.1	2.9
Sm	4.4	4.2	6.2	5.1	8.9	4.5	3.3	5.6	8.3	1.3
Eu	2.03	1.41	2	1.23	2.89	1.63	1.35	2.17	2.04	0.64
Gd	5.2	5.1	7.4	6.1	10.3	5.2	4.2	6.6	7.8	2.2
Tb	1	1	1.4	1.2	1.9	1	0.8	1.2	1.4	0.5
Dy	6.3	6.2	8.6	7.9	11.7	6.1	5.3	7.7	8.3	3.5
Ho	1.3	1.3	1.7	1.7	2.4	1.2	1.1	1.5	1.6	0.8
Er	3.7	3.9	5.1	5.2	7.3	3.4	3.2	4.5	4.7	2.3
Tm	0.56	0.58	0.75	0.8	1.08	0.5	0.48	0.67	0.69	0.35
Yb	3.6	3.6	4.7	5.1	7	3.2	3	4.2	4.4	2.3
Lu	0.51	0.52	0.69	0.78	1.03	0.46	0.44	0.63	0.63	0.34

Table 2c. Lawson Brook Formation *(cont'd)*, Stewarton Gabbro, and Carpenter Brook Formation.

	Lawson Brook Fm		Stewarton Gabbro					Carpenter Bk Fm
	Gabbro		Gabbro					Basaltic Tuff
Sample #	**06SJ40**	**06SJ46**	**74HB150**	**74HB164**	**74HB166**	**74HB167**	**74HB282**	**06SJ80**
Wt %								
SiO_2	51.32	54.84	40.32	43.31	42.84	43.33	40.08	45.05
TiO_2	2.18	0.85	7.008	3.134	5.26	2.247	6.55	3.02
Al_2O_3	14.87	17.7	10.85	14.89	11.73	14.22	10.96	15.86
Fe_2O_3t	10.23	6.46	19.47	19.76	18.37	17.63	23.12	14.13
MnO	0.17	0.15	0.227	0.393	0.306	0.225	0.303	0.2
MgO	6.25	4.22	7.78	3.28	6.85	6.93	7.01	7.87
CaO	7.03	8.15	11.52	8.15	10.18	11.65	7.34	2.98
Na_2O	4.18	3.43	1.86	3.36	2.32	2.05	2.13	3.14
K_2O	0.47	1.25	0.19	0.38	0.21	0.23	0.56	0.09
P_2O_5	0.34	0.1	0.08	1.14	0.69	0.1	0.21	0.31
LOI	3.32	2.4	0.73	0.67	0.82	1.6	1.77	6.86
Mg#	55	56	44	25	42	44	38	53
Trace elements (ppm)								
Ba	92	127	39	90	47	35	167	56
Rb	12	33	6	7	5	6	18	9
Sr	297	365	197	378	254	292	192	169
Y	47	16	22	48	41	21	26	34
Zr	199	89	86	80	118	31	115	186
Nb	9	5	6	8	11	1	8	8
Th	2.5	2.9	0.3	0.9	0.4	< 0.1	1.1	0.5
Pb	7	5	< 5	9	< 5	< 5	< 5	10
Ga	21	19	20	28	23	22	18	23
Zn	90	60	330	220	270	180	300	110
Cu	60	20	70	30	50	160	30	110
Ni	50	30	< 20	< 20	< 20	< 20	< 20	80
V	302	146	1066	41	624	672	995	428
Cr	170	70	< 20	< 20	< 20	40	< 20	100
Hf	5.5	2.5	2.8	2.3	3.7	1.3	3.8	4.7
Cs	<0.5	0.9	1.6	0.8	< 0.5	< 0.5	2.4	1.5
Sc	44	21	81	48	58	48	71	44
Ta	0.7	0.5	0.8	1.2	1.2	0.4	0.8	0.7
Co	32	23	81	37	59	80	76	54
U	0.7	0.8	< 0.1	0.3	0.1	< 0.1	0.2	0.4
Rare-earth elements (ppm)								
La	15.9	10.8	3	16.8	8.1	2.6	8.8	12.5
Ce	40.9	22.8	9.5	45.8	24.3	7.9	22	32.4
Pr	5.84	2.81	1.87	6.49	4.54	1.59	3.43	4.79
Nd	27.9	12.1	9.8	32.4	22.2	8.6	15.3	22.8
Sm	7.6	2.7	3.1	9.8	6.7	2.8	4	6.2
Eu	2.25	1.12	1.27	4.7	2.89	1.39	1.41	2.4
Gd	8.6	2.8	4	11.2	8.4	3.8	5	7
Tb	1.6	0.5	0.7	1.7	1.4	0.7	0.9	1.2
Dy	9.5	3	4.5	9.3	8.5	4.3	5.5	7.2
Ho	1.9	0.6	0.9	1.8	1.7	0.8	1.1	1.4
Er	5.4	1.8	2.5	5	4.5	2.3	3.2	3.8
Tm	0.79	0.27	0.35	0.67	0.62	0.32	0.45	0.55
Yb	4.9	1.7	2.1	3.8	3.7	1.9	2.7	3.3
Lu	0.74	0.27	0.31	0.52	0.51	0.28	0.39	0.47

Table 3. Whole-rock geochemical analyses for felsic volcanic rocks of the Annidale Group, and felsic–intermediate intrusions.

Table 3a. Lawson Brook Formation.

	Shannon Suite									
Sample #	**06SJ49**	**06SJ53**	**06SJ55**	**06SJ70**	**06SJ71**	**02MM158**	**KT04-55**	**KT04-73**	**KT05-11**	**NB06-04**
Wt %										
SiO_2	83.22	76.98	77.37	76.26	80.67	79.33	80.41	79.64	80.97	78.63
TiO_2	0.04	0.11	0.09	0.05	0.06	0.14	0.18	0.06	0.10	0.11
Al_2O_3	9.61	10.89	10.66	11.75	10.54	10.40	10.16	11.23	9.73	11.73
Fe_2O_3t	0.61	0.56	0.65	1.31	0.65	0.75	0.65	0.74	0.51	1.38
MnO	0.01	0.01	0.02	0.02	0.01	0.01	0.02	ND	ND	0.02
MgO	0.17	0.28	0.40	0.93	0.12	0.12	0.25	0.17	0.02	0.23
CaO	0.06	0.40	1.07	0.05	0.15	0.10	0.21	0.02	0.03	0.16
Na_2O	2.42	0.79	0.20	1.38	3.04	0.58	1.61	3.31	0.76	4.71
K_2O	3.11	7.92	8.25	7.39	4.44	8.07	5.69	3.58	7.29	2.77
P_2O_5	0.02	0.03	0.03	0.02	0.03	0.03	0.05	0.03	0.03	0.02
LOI	0.81	0.75	1.55	0.88	0.47	0.47	0.57	0.71	0.39	0.5
ACNK	1.28	1.03	0.96	1.13	1.03	1.05	1.11	1.2	1.05	1.06
Trace elements (ppm)										
Ba	664	589	325	620	586	544	570	480	464	170
Rb	59	90	62	104	98	66	74	74	58	44
Sr	46	38	28	30	99	19	45	34	15	38
Y	27	19	91	46	27	82	21	102	54	59
Zr	46	98	206	54	55	206	124	314	187	213
Nb	8	6	12	10	7	11	6	13	10	14
Th	6.5	6.6	9.8	8.2	7.1	6.6	6.3	10.6	6.3	8.8
Pb	12	12	10	45	13	<5	12	8	<5	2.5
Ga	9	7	15	12	10	10	10	20	10	21
Zn	<30	<30	<30	<30	<30	<30	<30	<30	<30	15
Cu	<10	<10	<10	<10	<10	<10	<10	<10	<10	20
Ni	<20	<20	<20	<20	<20	<20	<20	<20	<20	<20
V	<5	6	<5	<5	<5	7	8	<5	<5	27
Cr	<20	<20	<20	<20	20	<20	<20	50	80	<20
Hf	2.2	3.1	7.3	2.7	2.4	7.4	3.3	9.8	6.6	6.7
Cs	0.9	0.7	0.9	0.6	<0.5	<0.5	0.5	1.6	<0.5	1.3
Sc	2	3	2	5	3	4	5	2	3	2
Ta	1	0.7	1	1.2	0.8	1	0.5	1.2	1	1.5
Co	<1	<1	<1	<1	<1	<1	1	<1	<1	2
U	2.7	1.3	1.7	1.9	2.1	1.1	1.6	2.3	1.1	1.7
Rare-earth elements (ppm)										
La	8.9	12.7	43.1	14.6	17.8	32.1	16	24.6	27.1	27.1
Ce	19.5	27.3	92.4	33.3	36.2	74.9	32.5	57	65.1	68.2
Pr	2.26	3.17	11.8	3.87	4.11	9.92	3.64	7.35	8.45	8.46
Nd	9.4	12.4	50.9	16	15.6	43.4	14	34.2	36.4	36.1
Sm	2.3	2.5	12.3	4.2	3.5	11.4	3.1	9.6	9.1	9
Eu	0.2	0.43	1.39	0.21	0.41	1.47	0.37	0.9	1.14	0.63
Gd	2.8	2.5	13.6	4.8	3.5	11.6	3.1	11.9	8.6	9.6
Tb	0.6	0.5	2.6	1.1	0.7	2.4	0.6	2.5	1.5	1.9
Dy	4.4	3.2	16.1	7.3	4.7	15	3.5	16.5	9.4	12.1
Ho	0.9	0.7	3.4	1.6	1	3.2	0.7	3.5	2	2.4
Er	3.1	2.4	10.5	5	3.1	10.3	2.3	11	6.6	7
Tm	0.5	0.41	1.59	0.83	0.52	1.65	0.37	1.72	1.08	1.06
Yb	3.4	2.8	10.1	5.5	3.5	10.7	2.4	11.3	7.3	6.6
Lu	0.54	0.45	1.51	0.82	0.5	1.57	0.36	1.67	1.08	0.95

Table 3b. Lawson Brook and Carpenter Brook formations.

	Kierstead Mountain Suite			Bald Hill Suite				
Sample #	**06SJ39**	**06SJ50**	**KT03-06**	**KT-04-19**	**KT-05-07**	**1600-130**	**01MM-455**	**AN91-3-31**
Wt %								
SiO_2	83.22	76.98	77.37	75.15	72.35	75.91	74.06	74.48
TiO_2	0.04	0.11	0.09	0.26	0.24	0.3	0.271	0.3
Al_2O_3	9.61	10.89	10.66	10.96	10.44	11.23	11.19	11.96
Fe_2O_3t	0.61	0.56	0.65	4.42	5.24	4.28	4.52	4.65
MnO	0.01	0.01	0.02	0.12	0.2	0.07	0.121	0.08
MgO	0.17	0.28	0.40	0.3	0.63	2.12	0.91	2.27
CaO	0.06	0.40	1.07	0.02	0.74	0.11	0.13	0.09
Na_2O	2.42	0.79	0.20	2.67	3.48	4.93	2.83	5
K_2O	3.11	7.92	8.25	4.49	3.66	0.16	4.82	0.06
P_2O_5	0.02	0.03	0.03	0.05	0.04	0.02	0.02	0.02
LOI	0.81	0.75	1.55	1.49	2.79	1.6		1.8
ACNK	1.28	1.03	0.96	1.18	0.96	1.32	1.12	1.39
Trace elements (ppm)								
Ba	664	589	325	182	84	47	ND	35
Rb	59	90	62	95	83	3	131	1
Sr	46	38	28	20	38	14	4	29
Y	27	19	91	123	112	114	112	126
Zr	46	98	206	1020	871	914	1242	964
Nb	8	6	12	47	39	41	63	44
Th	6.5	6.6	9.8	17	14.2	16	14.8	16.6
Pb	12	12	10	13	15	2.5	27	2.5
Ga	9	7	15	28	30	30	35	34
Zn	<30	<30	<30	70	110	100	184	100
Cu	<10	<10	<10	10	<10	<10	11	<10
Ni	<20	<20	<20	<20	<20	<20	4	<20
V	<5	6	<5	<5	<5	<5	27	<5
Cr	<20	<20	<20	<20	60	<20	14	<20
Hf	2.2	3.1	7.3	23.9	20.8	23.2	NA	24.8
Cs	0.9	0.7	0.9	1.5	1.4	<0.5	NA	<0.5
Sc	2	3	2	-1	0.5	NA	NA	NA
Ta	1	0.7	1	4.1	3.5	3.9	NA	4.1
Co	<1	<1	<1	<1	<1	<1	8	<1
U	2.7	1.3	1.7	5.7	4.5	4.8	3.45	5.5
Rare-earth elements (ppm)								
La	8.9	12.7	43.1	39.2	62.3	68.9	65.4	80.4
Ce	19.5	27.3	92.4	127	139	154	137	179
Pr	2.26	3.17	11.8	11.4	17.4	19.2	20.3	22.5
Nd	9.4	12.4	50.9	45.7	70.3	77.8	82.5	91
Sm	2.3	2.5	12.3	12.2	16.3	17.4	19.8	20.3
Eu	0.2	0.43	1.39	0.78	0.95	0.98	1.87	1.14
Gd	2.8	2.5	13.6	16.8	16.8	17.2	20.9	19.6
Tb	0.6	0.5	2.6	3.3	3.2	3.4	3.7	3.7
Dy	4.4	3.2	16.1	21	19.5	21	22	23.1
Ho	0.9	0.7	3.4	4.3	3.9	4.2	4.52	4.6
Er	3.1	2.4	10.5	13.4	11.9	12.9	12.8	14.4
Tm	0.5	0.41	1.59	2.1	1.86	1.94	1.89	2.21
Yb	3.4	2.8	10.1	13.3	11.8	12.6	12.4	14
Lu	0.54	0.45	1.51	1.94	1.71	1.91	1.72	2.04

Table 3c. Henderson Settlement and Daley Brook plagiogranites, Cameron Road Granite, and granite sheets in the Carpenter Brook Formation (NA = not analyzed, ND = not detected).

	Henderson Settlement Plagiogranite	Daley Brook Plagiogranite	Cameron Road Granite			Carpenter Brook Formation Granite sheets	
Sample #	**01MM452**	**01MM457**	**01MM449**	**KT05-13**	**NB06-07**	**AN913-39**	**AN913-118**
Wt %							
SiO_2	69.44	65.31	73.84	71.46	72.97	67.02	63.69
TiO_2	0.53	0.71	0.19	0.23	0.25	0.58	0.61
Al_2O_3	15.48	15.07	14.56	13.45	14.52	15.7	17.47
Fe_2O_3t	3.46	5	2.07	2.09	2.01	4.67	4.06
MnO	0.06	0.12	0.03	0.04	0.04	0.07	0.08
MgO	2.8	1.29	0.7	0.71	0.95	3.88	2.18
CaO	0.2	1.51	0.12	2.27	0.11	0.32	1.18
Na_2O	4.35	5.81	1.36	1.45	2.22	4.43	5.91
K_2O	1.84	2.34	6.58	4.25	5.06	1.32	1.09
P_2O_5	0.11	0.18	0.07	0.08	0.09	0.15	0.15
LOI				3.82	1.97	3	3.9
ACNK	1.61	1.01	1.52	1.21	1.56	1.68	
Trace elements (ppm)							
Ba	166	145	550	386	535	71	127
Rb	72	50	151	127	129	47	41
Sr	55	97	16	33	14	42	84
Y	17	21	37	17	21	26	26
Zr	253	512	92	102	99	171	163
Nb	12	26	8	6	7	9	8
Th	3.8	ND	7.3	7.9	8	5.3	4.8
Pb	29	13	59	9	93	2.5	2.5
Ga	19	24	13	13	14	17	17
Zn	76	63	16	<30	30	60	40
Cu	36	207	9	<10	<10	20	<10
Ni	16	7	11	<20	<20	<20	<20
V	68	70	32	23	29	59	67
Cr	15	11	5	30	<20	20	<20
Hf	NA	NA	NA	3.3	3	4.9	4.7
Cs	NA	NA	NA	4.6	3.6	2.2	1.7
Sc	NA	NA	NA	6	6	NA	NA
Ta	NA	NA	NA	0.7	0.8	0.9	0.8
Co	13	11	ND	3	3	10	11
U	0.97	ND	1.7	1.9	1.8	1.5	1.4
Rare-earth elements (ppm)							
La	19.9	0.6	22.4	22.1	25.4	19.5	17.1
Ce	46.4	2.1	82.3	42.5	46.1	41.2	35.8
Pr	6.18	0.45	7.07	4.64	5.52	4.91	4.34
Nd	25.4	2.6	29.8	16.9	20.4	19.3	17.2
Sm	5.1	1.4	6.4	3.3	4.1	4.4	3.9
Eu	1.45	0.45	1.51	0.64	0.94	0.92	0.84
Gd	4.5	2.5	6.6	2.9	3.9	4.1	3.8
Tb	0.6	0.49	1.1	0.5	0.7	0.8	0.7
Dy	3.3	3.4	6.9	3	3.6	4.7	4.6
Ho	0.62	0.82	1.57	0.6	0.7	0.9	0.9
Er	1.74	2.49	4.5	1.9	2.1	2.8	2.9
Tm	0.25	0.36	0.69	0.31	0.31	0.45	0.47
Yb	1.6	2.4	4.7	2.1	2	2.9	3.1
Lu	0.24	0.37	0.68	0.33	0.3	0.46	0.48

Table 3d. London Settlement and Harry Brook suites, and Bull Moose Hill porphyry.

	London Settlement Suite				Harry Brook Suite		Bull Moose Hill Feldspar Porphyry
Sample #	**01MM460**	**NB06-06**	**KT05-06**	**01MM459**	**06SJ043**	**KT05-40**	**06SJ051**
Wt %							
SiO_2	80.15	76.42	76.42	75.76	75.25	79.69	67.58
TiO_2	0.08	0.21	0.15	0.17	0.22	0.21	0.64
Al_2O_3	11.56	13.45	11.94	12.76	11.84	10.85	14.21
Fe_2O_3t	0.38	1.36	1.61	1.74	3.44	1.15	3.91
MnO	0.01	0.01	0.05	0.00	0.02	0.02	0.08
MgO	0.05	0.71	0.21	0.04	1.35	0.29	0.99
CaO	0.04	0.22	0.81	0.49	0.05	0.32	2.82
Na_2O	1.19	7.11	3.57	4.30	4.54	2.58	4.46
K_2O	7.44	0.12	3.52	3.74	1.55	4.75	1.55
P_2O_5	0.03	0.04	0.05	0.05	0.03	0.03	0.2
LOI		0.77	1.65		1.74	0.88	3.67
ACNK	1.14	1.1	1.06	1.06	1.28	1.09	1
Trace elements (ppm)							
Ba	402	106	289	118	170	586	324
Rb	182	3	125	135	23	90	51
Sr	48	127	64	32	39	26	176
Y	35	39	34	64	98	97	35
Zr	62	215	160	161	499	442	240
Nb	11	15	12	15	27	22	9
Th	13.5	16	11.3	15.3	13.1	11.3	7.1
Pb	20	18	17	44	20	10	10
Ga	7	12	14	15	27	15	18
Zn	5	<30	<30	32	120	40	70
Cu	8	10	<10	10	20	<10	<10
Ni	9	<20	<20	9	<20	<20	<20
V	14	6	5	25	7	<5	29
Cr	9	<20	<20	21	<20	<20	<20
Hf	NA	6.7	4.3	NA	14.2	13	6.5
Cs	NA	<5	2.2	NA	1	1.5	2
Sc	NA	4	4	NA	3	3.4	8
Ta	NA	1.6	1.8	NA	2.3	2	0.8
Co	ND	1	<1	ND	<1	<1	5
U	5.04	4	4.7	4.11	3.3	3	1.5
Rare-earth elements (ppm)							
La	19.4	39.7	17.8	12.9	39.5	53.7	25.8
Ce	44.8	79.9	38.3	55.9	97.3	123	54.5
Pr	5.31	8.77	4.38	3.73	12.1	15.6	6.57
Nd	20	31.5	17.3	14.7	49.3	64.8	26.6
Sm	4.8	6	4.1	4.3	11.5	15.6	5.8
Eu	0.54	0.99	0.53	0.12	2.14	2.51	1.56
Gd	4.99	5.5	4.1	6.4	12.3	15.8	5.7
Tb	0.93	1.1	0.8	1.54	2.7	3	1
Dy	5.91	6.8	5.3	11	16.8	18	6.4
Ho	1.28	1.4	1.1	2.44	3.5	3.5	1.3
Er	3.75	4.6	3.3	7.11	11.2	10.91	4.1
Tm	0.58	0.75	0.54	1.10	1.81	1.67	0.64
Yb	4	4.8	3.5	7.3	11.9	10.5	4.2
Lu	0.61	0.71	0.5	1.03	1.75	1.5	0.67

Table 3e. Felsic–intermediate intrusions of uncertain age, and post-Early Silurian intrusion.

	Intrusions of Uncertain Age							Post-Early Silurian Intrusion
Sample #	**01MM-445**	**01MM-453**	**01MM-454**	**01MM-458**	**06SJ-047**	**06SJ-059**	**KT-03-01**	**06SJ-060**
Wt %								
SiO_2	73.15	74.40	78.19	78.36	70.25	77.87	76.11	76.67
TiO_2	0.13	0.14	0.14	0.10	0.58	0.08	0.07	0.05
Al_2O_3	13.63	12.90	12.37	12.11	13.72	12.45	13.73	13.41
Fe_2O_3t	1.69	1.72	2.11	1.12	3.38	1.07	1.13	0.83
MnO	0.06	0.07	0.05	0.01	0.11	0.02	0.12	0.01
MgO	0.21	1.25	0.06	0.15	1.01	0.15	0.23	0.37
CaO	2.46	1.70	0.07	0.02	1.36	0.13	0.39	0.13
Na_2O	5.29	1.26	3.40	5.22	3.35	4.54	1.74	4.45
K_2O	1.65	2.23	3.06	0.70	5.07	3.18	2.98	2.71
P_2O_5	0.07	0.05	0.01	0.02	0.11	0.02	0.03	0.05
LOI	2.70	4.27	1.10	0.79	1.35	0.79	3.33	1.23
Trace elements (ppm)								
Ba	217	270	361	108	365	391	150	328
Rb	90	92	88	45	104	72	179	110
Sr	82	71	17	59	124	24	15	108
Y	118	34	19	55	31.7	45.3	25	5.8
Zr	95	45	322	210	340	117	73	41
Nb	6.0	8.0	26.0	32.0	11	11	20	6
Th	20.1	9.4	9.3	13.2	16.9	10.8	24.1	6.2
Pb	23	33	70	480	12	5	35	8
Ga	15	11	28	19	19	17	22	14
Zn	33	31	372	39	40	15	60	15
Cu	16	12	29	11	10	5	20	5
Ni	8	10	8	8	10	10	10	10
V	20	26	20	13	62	5	25	6
Cr	16	7	18	12	30	20	10	10
Hf	NA	NA	NA	NA	9.4	4.7	3.6	1.7
Cs	NA	NA	NA	NA	1.1	1.8	4.1	2.4
Sc	NA	NA	NA	NA	9	4	5	1
Ta	NA	NA	NA	NA	1.2	1.3	2.2	1
Co	NA	NA	NA	NA	10	2	3	1
U	5.99	2.35	2.72	3.17	3.4	2	5.7	2.5
Rare-earth elements (ppm)								
La	72.5	22.2	6.8	42.1	20.4	27.1	20.6	18.2
Ce	166.0	50.6	16.6	96.2	44.5	61.2	59.4	34.6
Pr	21.40	6.08	2.01	11.80	5.46	7.65	5.50	3.81
Nd	83.90	24.10	7.30	45.70	22.2	30.6	21	13.4
Sm	19.10	5.70	2.00	10.10	5.2	7.4	5.6	2.3
Eu	0.82	0.92	0.31	2.18	1.02	0.7	0.75	0.49
Gd	20.10	5.87	2.26	10.80	5.45	7.34	5.7	1.9
Tb	3.54	1.01	0.41	1.70	0.98	1.28	1	0.24
Dy	21.30	6.07	2.83	10.00	5.69	7.6	5.3	1.11
Ho	4.53	1.25	0.64	2.11	1.23	1.59	1	0.21
Er	13.90	3.94	1.91	6.19	3.93	5.14	2.8	0.63
Tm	2.06	0.59	0.32	0.91	0.59	0.83	0.42	0.09
Yb	13.40	4.10	2.20	6.10	3.8	5.6	2.6	0.6
Lu	1.89	0.63	0.32	0.91	0.56	0.83	0.36	0.09

GEOCHRONOLOGY

Analytical Techniques

The U–Pb analyses (Table 4) were conducted at the Geochronology Laboratory in the Department of Earth Sciences at Memorial University, St. John's, Newfoundland, according to the technique outlined in Sánchez-García et al. (2008). Ages were calculated using the decay constants recommended by Jaffey et al. (1977). The uncertainties on the isotopic ratios were calculated using an unpublished program and are reported at 2σ. Ages are reported as the weighted averages of either the $^{206}Pb/^{238}U$ or $^{207}Pb/^{206}Pb$ ages, calculated using ISOPLOT, and are reported at the 95% confidence level (C.I.).

A total of 14 rock samples, each weighing 25 kg, were collected and sent to Memorial University in 2006–2007. Each sample was washed, then crushed in a jaw crusher and ground to a fine powder. The powder was panned using a Wilfley table to produce 100 ml to 200 ml of heavy mineral concentrate. The concentrate was passed through heavy liquids and a Frantz magnetic separator in a sequence of steps designed to separate minerals according to their density and magnetic susceptibility. The least magnetic high-density fractions contain the high-quality zircon, and it is from these fractions that grains are selected for analyses. Zircon grains are selected according to criteria of morphology and clarity using jewellers' tweezers under a microscope.

Eight of the fourteen samples yielded sufficient high-quality zircon for U–Pb analyses. Figures 28 to 35 show the following for each of the eight samples: a photograph of the zircon population in plane light under the picking microscope, cathodo-luminescence images of the representative grains, and a Concordia diagram. Because so few zircons were recovered from sample NB06-06 (Fig. 29), none were sacrificed for imaging. Those imaged grains, once mounted and polished halfway through, cannot be analyzed by TIMS (U–Pb).

Results

Harry Brook Rhyolite (472 ± 1.7 Ma)

Sample NB06-01 of pink vesicular rhyolite from a subvolcanic dome complex was collected at the extreme northeastern end of the Annidale belt approximately 2 km northwest of the headwaters of Harry Brook (Fig. 3b, geochronology site 4). The outcrop is accessed by a logging road off Dagnino Road on Snider Mountain. This particular sample was chosen because it contained associated gold mineralization.

The sample yielded high-quality euhedral prisms, which show relatively low-contrast growth zoning. Three fractions of four to eight grains were analyzed, giving analyses that are all overlapping and concordant (Fig. 28). An age of 472 ± 1.7 Ma was calculated as the weighted average of the $^{206}Pb/^{238}U$ ages (MSWD = 0.02).

London Settlement Rhyolite (478 ± 2 Ma)

This sample (NB06-06) was of dark grey spherulitic rhyolite from the London Settlement subvolcanic dome complex south of Wickham Road (Fig. 3a, geochronology site 3). The outcrop is accessed by a farm road east of Highway 705.

The sample was chosen to constrain the age of the East Scotch Settlement Formation, which it is thought to intrude. The sample yielded only a small amount of zircon. Three analyses were carried out: Z1 of a single grain, and Z2 and Z3 of two grains each. All are concordant and overlap, but Z1 has a large uncertainty (Fig. 29). The $^{206}Pb/^{238}U$ ages of these three analyses with 2σ uncertainties are as follows: Z1 is 481 ± 6 Ma, Z2 is 477.7 ± 2.5 Ma, and Z3 is 478.2 ± 4 Ma. The weighted average of the three $^{206}Pb/^{238}U$ ages is 478.1 ± 2 Ma.

Cameron Road Granite (490 ± 2.3 Ma)

This sample (NB06-07) was collected from light grey, coarse-grained quartz-eye granite exposed on Cameron Road between Henderson Settlement and Albright Brook (Fig. 3a, geochronology site 5). The sample was selected for two purposes: this granite is the only pervasively deformed intrusion in the Annidale belt, and its age will constrain the age of the Carpenter Brook Formation.

The granite yielded excellent zircon, many as longer prisms that show striking growth zoning (Fig. 30). Three analyses were carried out. The age was calculated as the weighted average of the $^{206}Pb/^{238}U$ ages for analyses Z1 and Z3, as Z2 may have undergone a small amount of lead loss. The calculated age is 489.5 ± 2.25 Ma, which is rounded to 490 ± 2.3 Ma.

Bull Moose Hill Porphyry (467 ± 3 Ma)

Greyish pink feldspar porphyry was sampled (NB06-09) on the southeast slope of Bull Moose Hill northwest of Belleisle Creek (Fig. 3b, geochronology site 8). The porphyry intrudes greyish green and maroon slates and sandstones of the Grant Brook Formation. The sample contains many high-quality zircons with spectacular growth zoning and some patchy, potentially altered domains in some cores (Fig. 31). The best age from data points Z2, Z3, Z4, and Z5 (excluding the least precise Z1) is 467 ± 3 Ma.

Stewarton Gabbro (479 ± 2 Ma)

A sample (NB07-01) of coarse-grained pegmatitic gabbro was collected from the Jack Lake quarry, about 1 km east of the junction of Highway 695 and East Scotch Settlement Road (Fig. 3b, geochronology site 7). The gabbro intrudes the Late Cambrian–Early Ordovician Annidale Group and latest Neoproterozoic–earliest Cambrian Grant Brook Formation of the Belleisle Bay Group.

The gabbro yielded a large amount of coarse angular fragments typical of igneous zircons in gabbro. They are normally interpreted to represent fragments of broken, skeletal zircon that crystallized in the interstices between the major rock-forming silicates. The grains are angular, and some exhibit dramatic zoning under cathodo-luminescence, including sector zoning; one

displays virtually no zoning (Fig. 32). Discounting the most discordant analyses (Z1 and Z2), analyses Z3 to Z7 provide an age of 479 ± 2 Ma as the weighted average of the $^{207}Pb/^{206}Pb$ ages.

Grant Brook Formation (541 ± 3 Ma)

Dark maroon tuffaceous sandstone containing abundant, dark green glassy volcanic fragments was sampled (NB07-02) from an outcrop on Grant Brook about 600 m south of The Grant (Fig. 3a, geochronology site 1). The brook is accessed via the west side of Highway 710.

This sample yielded both rounded zircon (presumed to be detrital) and a smaller number of small 2:1 euhedral prisms. The latter type could represent a single-age igneous population, as the rock was observed to have a tuffaceous component in outcrop. Four analyses of small single euhedral grains were carried out. All analyses overlap on the Concordia diagram (Fig. 33) and have large uncertainties due to the small amounts of lead being measured (6–24 picograms total sample lead). Three analyses range from 539 ± 5 Ma to 544 ± 5 Ma and mutually overlap. The weighted average of these $^{206}Pb/^{238}U$ ages is 541 ± 3 Ma. The fourth analysis has a lower $^{206}Pb/^{238}U$ age, but its $^{207}Pb/^{206}Pb$ age is 548 ± 20 Ma; thus, it might be of the same age but have lost some lead.

Carpenter Brook Formation (<552 ± 2 Ma and >490 ± 2 Ma)

A sample (NB07-03) of quartzose volcaniclastic sandstone containing abundant dark grey volcanic quartz was collected from a clearcut accessed via Cameron Road west of Highway 710 (Fig. 3a, geochronology site 2). The rock has rounded zircon and a low number of small euhedral prisms that display patterns of zoning which appear complicated but igneous. One grain (Fig. 34) has a central part with sector zoning surrounded by outer euhedral growth zones.

Only the small, sharp euhedral prisms were analyzed. The analyses of two single grains and one analysis of two small grains are all concordant within the uncertainties, giving $^{206}Pb/^{238}U$ ages of 616 ± 2 Ma, 552 ± 2 Ma, and 632 ± 5 Ma. These may represent only two ages, because the $^{207}Pb/^{206}Pb$ age of Z1 is 634 Ma with a large uncertainty. One possibility is that Z1 underwent some lead loss along a line such as that shown on Figure 34 (dashed line). The age of the Carpenter Brook volcaniclastic sandstone is constrained by the youngest detrital zircon to be no older than 552 ± 2 Ma and by the age of the cross-cutting Cameron Road Granite to be no younger than 490 ± 2 Ma.

Henderson Settlement Plagiogranite (482 ± 2 Ma)

Grey, medium-grained plagiogranite was sampled (NB07-06) from an outcrop east of Highway 710 near a large beaver pond on Grant Brook (Fig. 3a, geochronology site 6). The granite intrudes grey slate of the Carpenter Brook Formation and was chosen because of its unusual chemistry and associated gold mineralization.

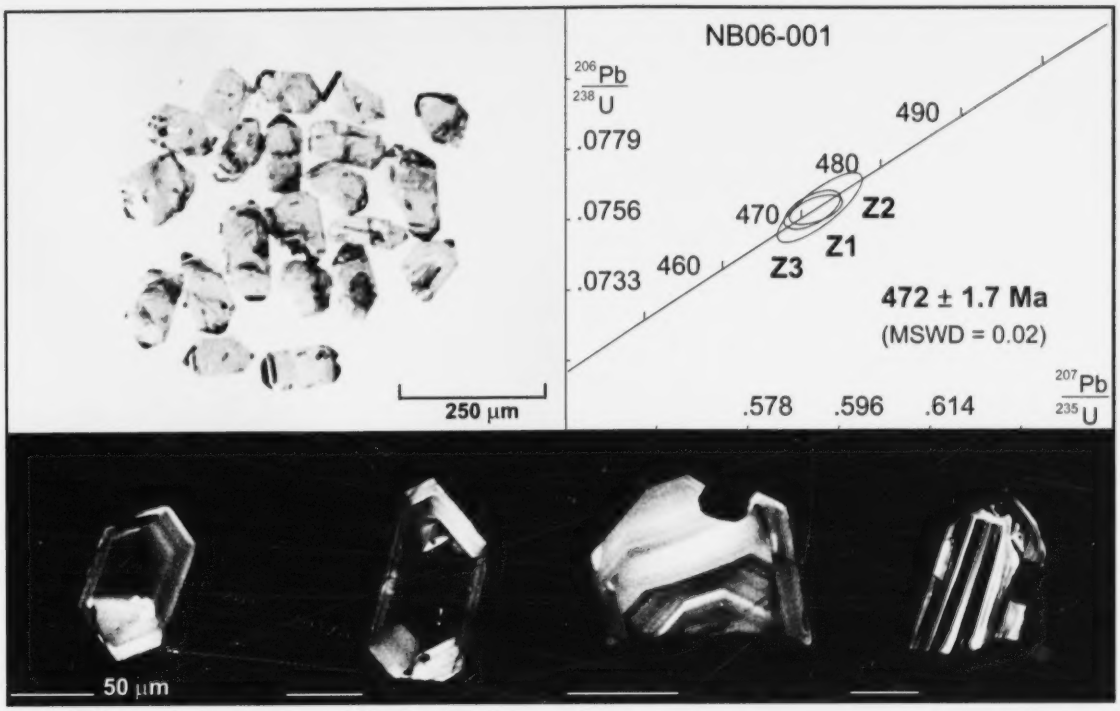

Figure 28. Transmitted light photomicrograph of zircons, Concordia diagram, and cathodo-luminescence images of representative zircon grains: Harry Brook rhyolite.

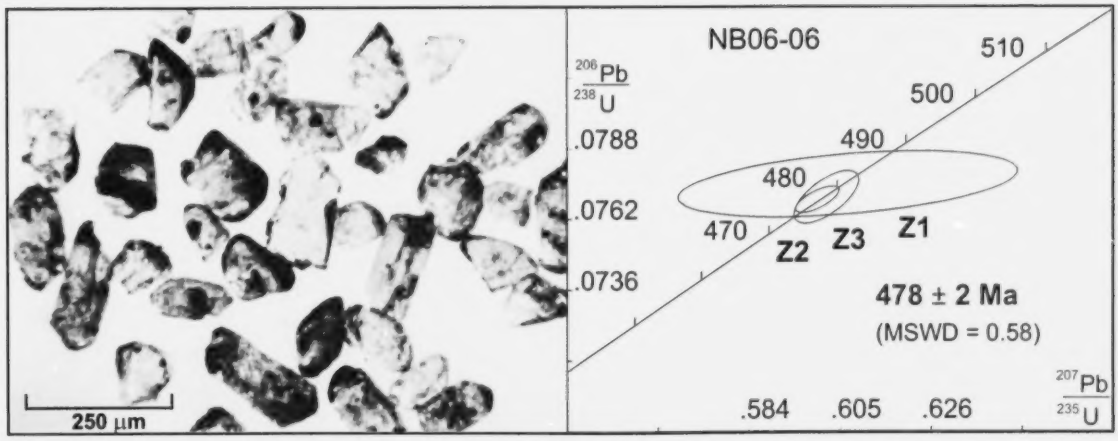

Figure 29. Transmitted light photomicrograph of zircons and Concordia diagram: London Settlement rhyolite.

This sample yielded a large amount of stubby euhedral prisms, many of which have imperfections such as mineral inclusions or internal alteration zones (Fig. 35). They are clearly an igneous population. Each of two concordant analyses of a few clear euhedral prisms (Z1, Z2) is of very high quality; and each independently gives an age of 482 Ma (Fig. 35). The weighted average of the $^{206}Pb/^{238}U$ ages gives 482 ± 2 Ma. A third analysis (Z3) is discordant.

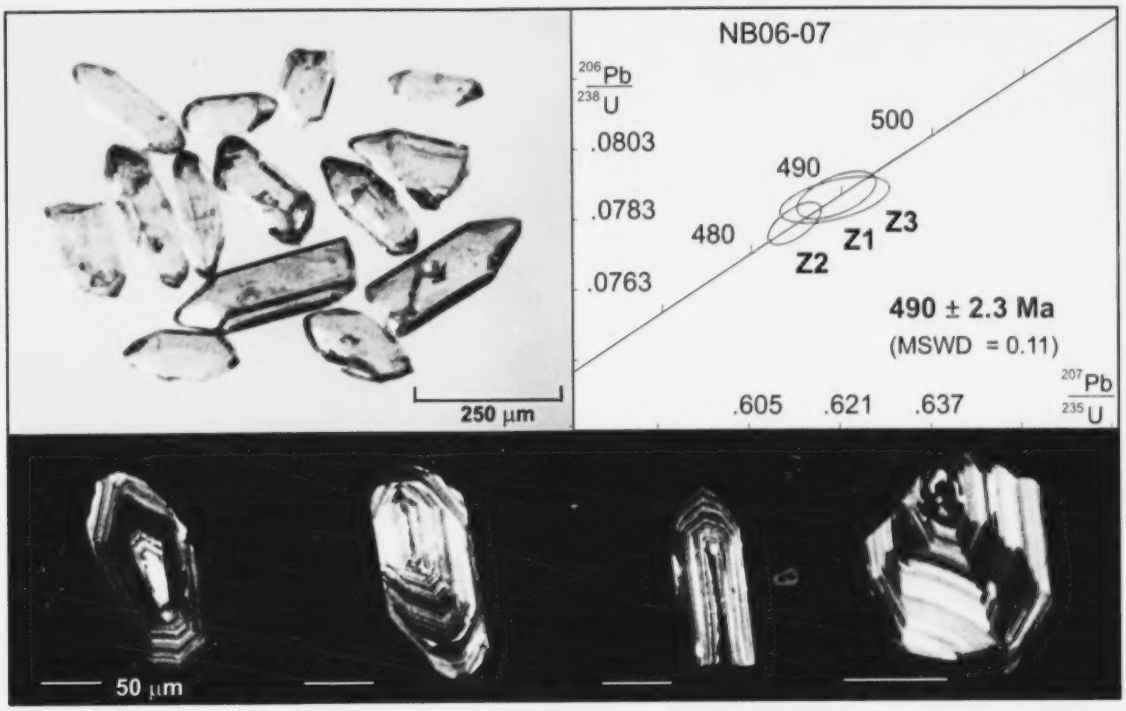

Figure 30. Transmitted light photomicrograph of zircons, Concordia diagram, and cathodo-luminescence images of representative grains: Cameron Road Granite.

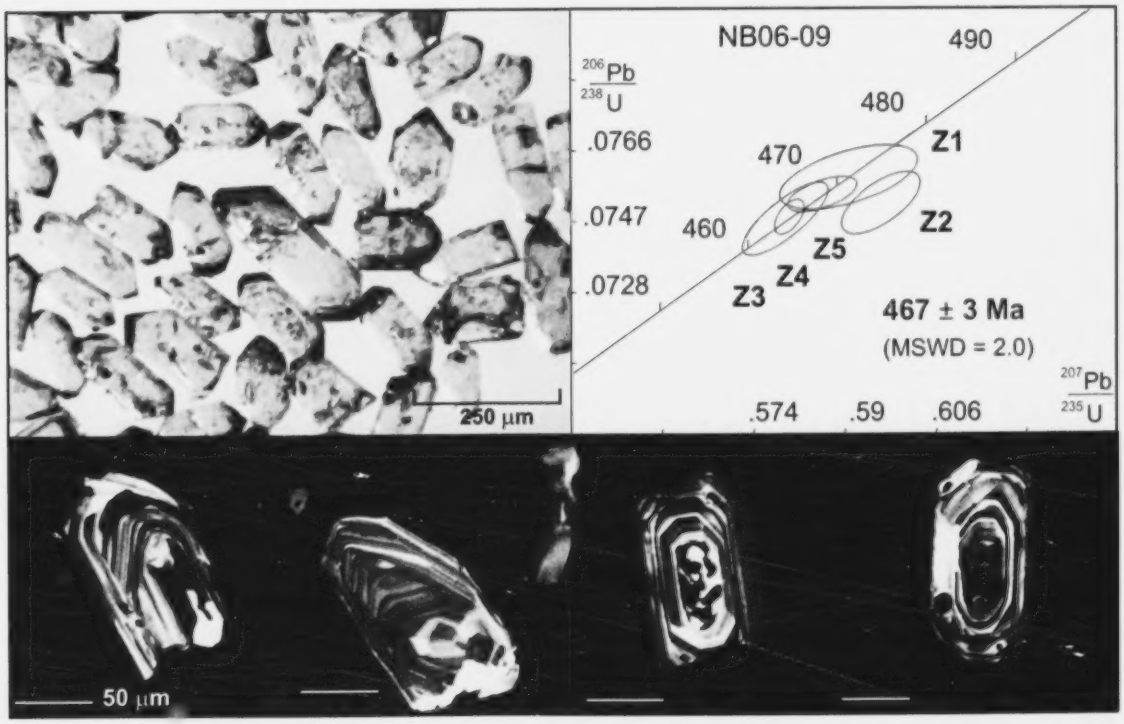

Figure 31. Transmitted light photomicrograph of zircons, Concordia diagram, and cathodo-luminescence images of representative grains: Bull Moose Hill porphyry.

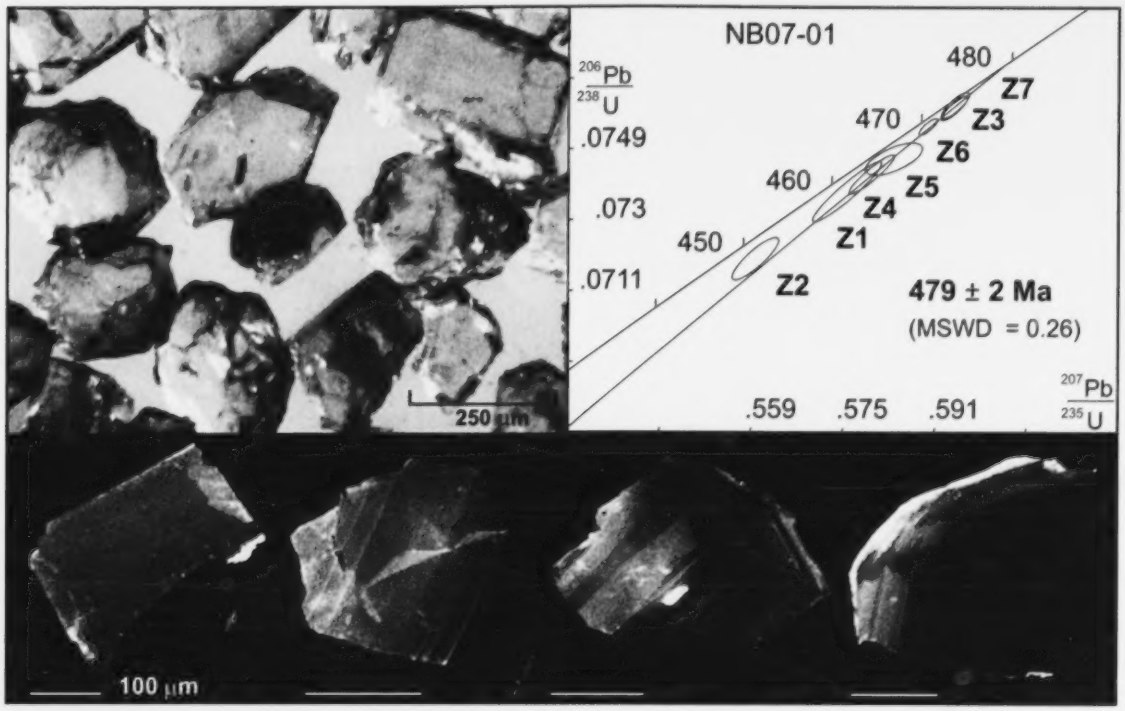

Figure 32. Transmitted light photomicrograph of zircons, Concordia diagram, and cathodo-luminescence images of representative grains: Stewarton Gabbro.

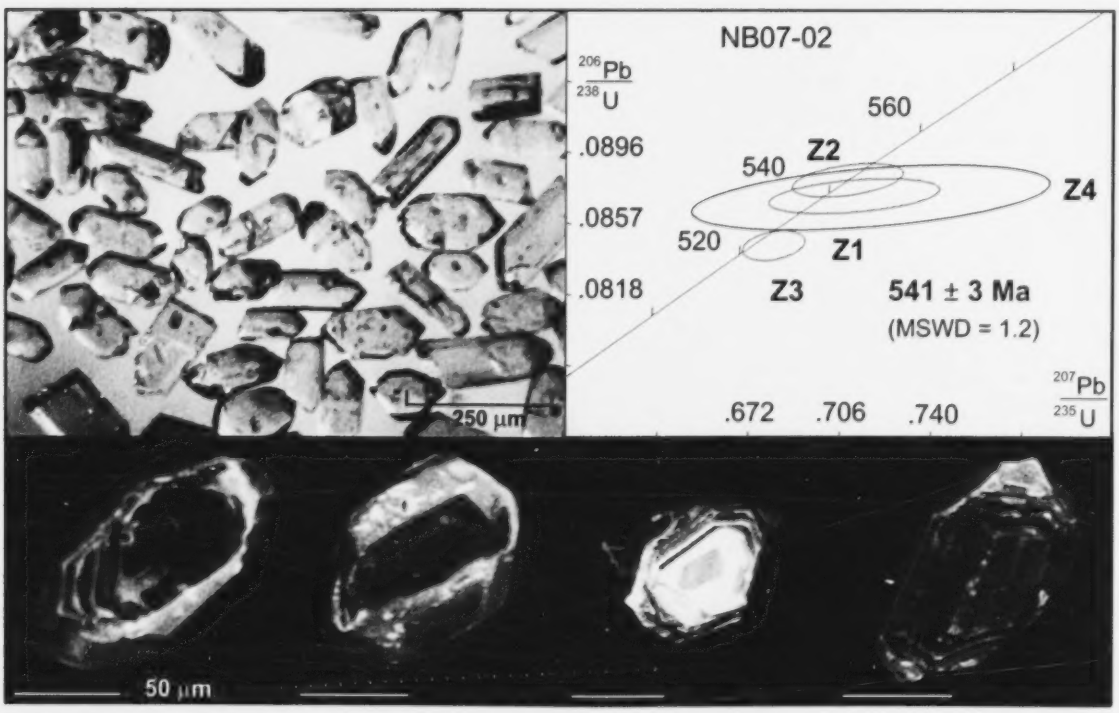

Figure 33. Transmitted light photomicrograph of zircons, Concordia diagram, and cathodo-luminescence images of representative grains: tuffaceous sandstone of the Grant Brook Formation.

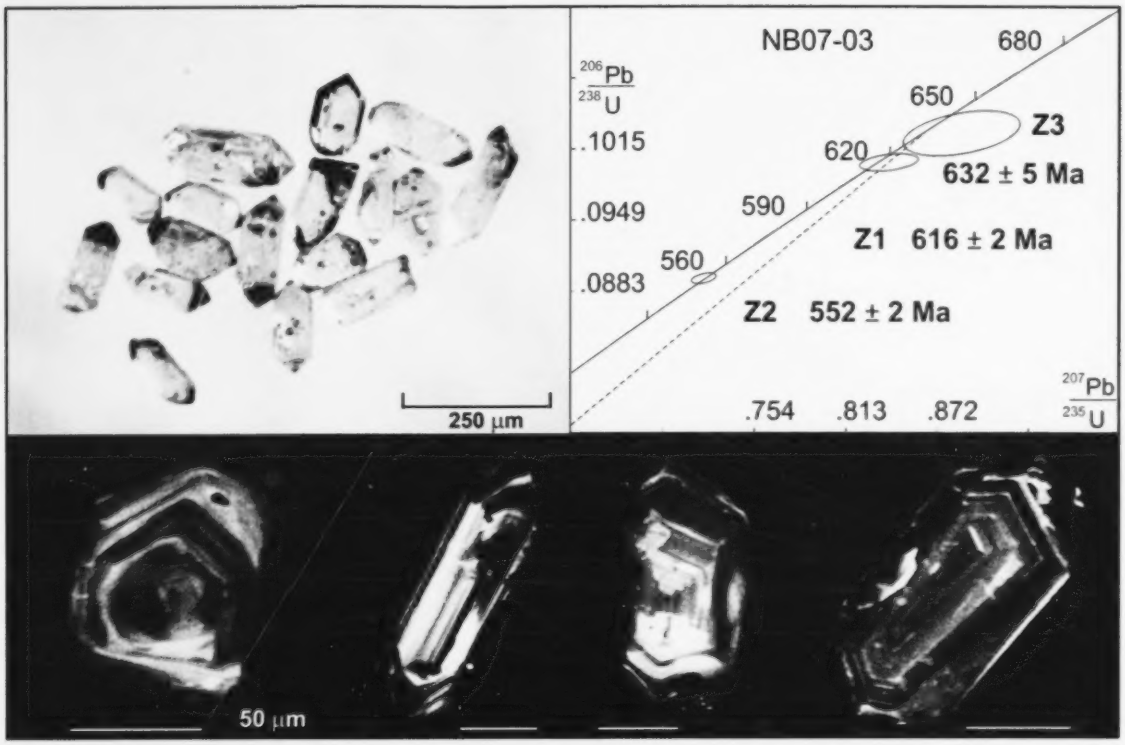

Figure 34. Transmitted light photomicrograph of zircons, Concordia diagram, and cathodo-luminescence images of representative grains: volcaniclastic sandstone of the Carpenter Brook Formation.

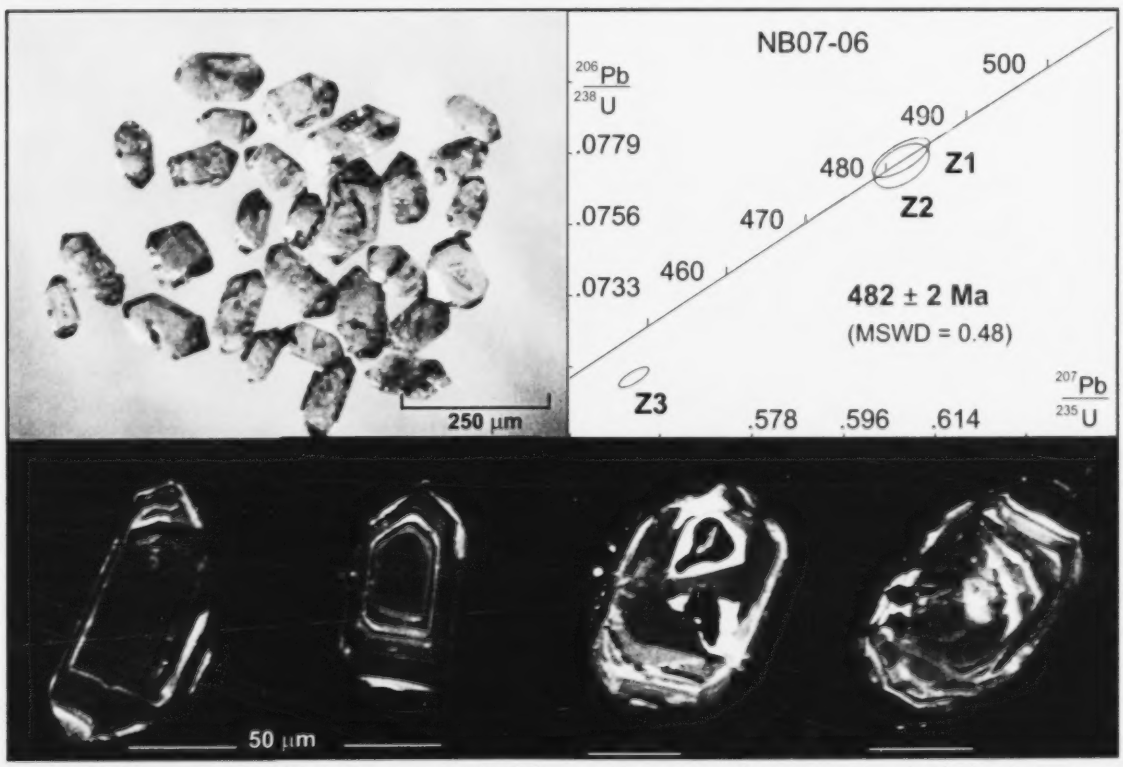

Figure 35. Transmitted light photomicrograph of zircons, Concordia diagram, and cathodo-luminescence images of representative grains: Henderson Settlement plagiogranite.

Table 4. U–Pb isotope composition and ages of all analyzed samples.

Fraction	Char	Wt [1] (mg)	Concentration			Measured		Corrected Atomic Ratios [3]						Age (Ma)		
			U (ppm)	Pb_{rad} [2] (ppm)	$Pb_{tot\ com}$ (pg)	$^{206}Pb/^{204}Pb$	$^{208}Pb/^{206}Pb$	$^{206}Pb/^{238}U$	±	$^{207}Pb/^{235}U$	±	$^{207}Pb/^{206}Pb$	±	$^{206}Pb/^{238}U$	$^{207}Pb/^{235}U$	$^{207}Pb/^{206}Pb$
NB06-001 Harry Brook Rhyolite (20-298215E 5086444N)																
Z-1 (8 grains)	clr, shp 2:1 prm	0.016	71	5.9	5.5	1004	0.2017	0.07592	40	0.5915	42	0.05651	36	472	472	472
Z-2 (5 grains)	clr, shp euh	0.010	119	9.9	8.4	693	0.2084	0.07599	94	0.5923	68	0.05654	42	472	472	473
Z-3 (4 grains)	clr, shp prm	0.008	99	8.1	4.6	843	0.1991	0.07593	52	0.5909	46	0.05644	36	472	471	470
NB06-06 London Settlement Rhyolite (19-729423E 5058884N)																
Z-1 (1 grain)	2:1 prm	0.002	26	2.2	2.4	124	0.2236	0.07748	98	0.6068	320	0.05680	278	481	482	484
Z-2 (2 grains)	lt brn/ amber	0.004	144	12.4	1.6	1792	0.2435	0.07691	40	0.5998	40	0.05656	28	478	477	474
Z-3 (2 grains)	prm	0.003	94	8.0	1.4	962	0.2229	0.07700	78	0.6019	60	0.05669	48	478	478	480
NB-06-07 Cameron Road Granite (20-271535E 5063731N)																
Z-1 (5 grains)	clr, shp euh	0.010	58	5.1	8.1	372	0.2227	0.07883	54	0.6191	78	0.05696	62	489	489	490
Z-2 (9 grains)	clr, shp euh	0.018	76	6.4	8.0	854	0.2120	0.07816	50	0.6120	38	0.05679	30	485	485	483
Z-3 (4 grains)	clr, shp euh	0.008	64	5.6	2.9	879	0.2209	0.07896	56	0.6194	56	0.05689	44	490	489	487
NB06-09 Bull Moose Hill Porphyry (20-285329E 5068123N)																
Z-1 (2 grains)	2:1 shp clr, euh	0.005	51	4.6	1.0	1283	0.3152	0.07587	70	0.5908	98	0.05647	78	471	471	471
Z-2 (10 grains)	clr, shp euh	0.025	79	6.8	26	375	0.2681	0.07518	68	0.5964	56	0.05754	44	467	475	512
Z-3 ((2 grains)	clr shp, euh	0.005	132	11.3	1.3	2333	0.2724	0.07476	80	0.5796	62	0.5623	38	465	464	462
Z-4 (11 grains)	shp, euh prm	0.027	48	4.1	1.4	4482	0.2618	0.07481	38	0.5803	22	0.05626	24	465	465	463
Z-5 (4 grains)	shp, euh prm	0.010	63	5.3	2.9	1035	0.2424	0.07542	38	0.5861	50	0.05636	38	469	468	467
NB07-01 Stewarton Gabbro (20-279180E 5069234N)																
Z-1 (12 grains)	lrg, ang frags	0.036	498	41.6	3.3	24843	0.2589	0.07377	66	0.5757	48	0.05660	16	459	462	476
Z-2 (6 grains)	lrg, clr frags	0.018	336	25.1	4.2	6546	0.1510	0.07196	46	0.5597	34	0.05641	18	448	451	469
Z-3 (5 grains)	lrg, clr ang	0.015	467	35.5	2.4	14030	0.1071	0.07609	28	0.5944	20	0.05666	12	473	474	478
Z-4 (9 grains)	lrg, clr ang	0.027	565	44.4	12	5963	0.1734	0.07424	42	0.5799	32	0.05666	12	462	464	478
Z-5 (4 grains)	lrg, clr ang	0.012	602	52.9	105	338	0.3109	0.07465	36	0.5838	40	0.05672	30	464	467	481
Z-6 (7 grains)	lrg, clr ang	0.014	480	39.9	2.0	15850	0.2207	0.07552	18	0.5897	14	0.5664	8	469	471	477
Z-7 (7 grains)	lrg, clr ang	0.014	494	40.2	1.8	18343	0.1867	0.07602	26	0.5943	20	0.05670	10	472	474	480
NB07-02 Grant Brook Formation – Tuffaceous Sandstone (20-275740E 5060830N)																
Z-1 (1 grain)	2:1 shp prm	0.002	97	9.0	2.5	446	0.1821	0.08722	78	0.7113	260	0.05914	200	539	546	572
Z-2 (1 grain)	2:1 shp euh	0.002	58	5.8	2.0	344	0.2693	0.08809	76	0.7089	168	0.05836	126	544	544	543
Z-3 (1 grain)	2:1 euh prm	0.002	129	12.0	1.7	819	0.2185	0.08449	66	0.6814	94	0.05849	80	523	528	548
Z-4 (1 grain)	2:1 euh prm	0.002	29	2.8	2.0	181	0.2357	0.08713	146	0.7175	546	0.05973	420	539	549	594

Table 4 *(cont'd).*

Fraction	Char	Wt (1) (mg)	Concentration			Measured		Corrected Atomic Ratios (3)						Age (Ma)		
			U (ppm)	Pb^{rad} (2) (ppm)	$Pb^{tot\ com}$ (pg)	$^{206}Pb/^{204}Pb$	$^{208}Pb/^{206}Pb$	$^{206}Pb/^{238}U$	±	$^{207}Pb/^{235}U$	±	$^{207}Pb/^{206}Pb$	±	$^{206}Pb/^{238}U$	$^{207}Pb/^{235}U$	$^{207}Pb/^{206}Pb$
NB07-03 Carpenter Brook Formation (20-272786E 5063593N)																
Z-1 (2 grains)	shp, clr euh	0.004	131	14.3	3.9	861	0.1978	0.10024	66	0.8410	154	0.06085	104	616	620	634
Z-2 (1 grain)	lrg, clr shp, euh	0.002	407	41.9	4.1	1120	0.2789	0.08946	40	0.7216	64	0.05850	46	552	552	549
Z-3 (1 grain)	lrg, clr shp, euh	0.002	136	15.7	1.7	1024	0.2381	0.10295	172	0.8879	308	0.06255	198	632	645	693
NB07-06 Henderson Settlement Plagiogranite (20-273325E 5063512N)																
Z-1 (7 grains)	best clr, prm	0.010	122	10.2	1.9	3153	0.1892	0.07775	52	0.6073	46	0.05665	32	483	482	478
Z-2 (9 grains)	best clr, prm	0.014	193	16.0	4.9	2678	0.1873	0.07748	58	0.6075	44	0.05686	42	481	482	486
Z-3 (14 grains)	clr 2:1 prms	0.021	251	19.6	37.0	650	0.2247	0.07067	26	0.5549	24	0.05695	16	440	448	489

ang	angular	**euh**	euhedral	**med**	medium	**sml**	small	**1, 2**	# of grains in analysis
brn	brown	**frags**	fragments	**prm**	prism	**yel**	yellow		
clr	clear	**lrg**	large	**shp**	sharp	**Z**	zircon		

Notes: (1) Weights of grains were estimated, with potential uncertainties of 25–50% for small samples.
(2) Radiogenic lead.
(3) Atomic ratios corrected for fractionation, spike, laboratory blank of 0.6–2 picograms (pg) common lead, and initial common lead at the age of the sample calculated from the model of Stacey and Kramers (1975), and 0.3 pg U blank. Uncertainties of 2σ are reported after the ratios and refer to the final digits.
All minerals were abraded (Krogh 1982) prior to dissolution.
UTM zone and coordinates of sample sites are in brackets on the title lines (e.g., 20-273325E 5063512N).

TECTONIC IMPLICATIONS

The Annidale and New River belts record a complex late Neoproterozoic and Paleozoic extensional and accretionary tectonic history along the peri-Gondwanan margin of Iapetus. In the northeastern Appalachians, this peri-Gondwanan margin is characterized by the microcontinents of Avalonia and Ganderia (Fig. 1; van Staal et al. 1998; van Staal 2007). In southern New Brunswick, the only undisputed part of Avalonia is the Caledonia belt (Barr and White 1996; Barr et al. 2003b) that contains the classic Early Cambrian–Early Ordovician Avalonian cover sequence (Landing and Westrop 1998).

Neoproterozoic and early Paleozoic rocks in the Brookville, New River, Annidale, and St. Croix belts are considered part of Ganderia (Hibbard et al. 2006). In Newfoundland, Ganderia consists of the Gander Zone and the Exploits Subzone (Fig. 1), each representing different paleogeographic settings marginal to and within the early Paleozoic Iapetus Ocean and adjacent Ganderian microcontinent (van Staal et al. 1998; van Staal 2007; Zagorevski et al. 2007). The Gander Zone is characterized by a distinctive Early Cambrian–Early Ordovician (c. 520–480 Ma) deep-marine sequence deposited on the outer shelf to slope of the Ganderian passive margin (van Staal and Fyffe 1995; van Staal 2007). In contrast, the Exploits Subzone records Cambrian–Middle Ordovician arc systems that developed along

active segments of the Gander margin (van Staal 2007). Remnants of the arc systems extend for more than 1000 km from Maine to Newfoundland. The oldest of these arc systems is the Penobscot arc (van Staal et al. 1998). The Early Cambrian–Early Ordovician (c. 514-486 Ma) rocks of the Penobscot arc and Gander margin were overstepped by a younger Early–Middle Ordovician arc system that comprised the Popelogan–Victoria arc and Tetagouche–Exploits back-arc, which were active between 478 Ma and 454 Ma (van Staal 2007).

A candidate for the oldest volcanic rocks in the Penobscot arc system in New Brunswick is the late Early Cambrian Mosquito Lake Road Formation in the southwestern part of the New River belt (Johnson and McLeod 1996). Rhyolite from the Mosquito Lake Road Formation was dated at 514 ± 2 Ma (Johnson and McLeod 1996; McLeod et al. 2003) and is close in age to the c. 511 Ma Tally Pond Group, the oldest exposed part of the Penobscot arc in Newfoundland (Dunning et al. 1991; Rogers et al. 2006; Zagorevski et al. 2007). Detrital zircon data and stratigraphic relationships indicate that the Mosquito Lake Road sequence was built upon continental crust exposed in the Neoproterozoic–Early Cambrian New River belt (Johnson and McLeod 1996; Fyffe et al. 2009). Similarly, the Tally Pond Group is interpreted to have formed on the c. 563 Ma rocks of the Sandy Brook Group and Cripplebacк Intrusive Suite (Rogers et al. 2006). Basement–cover relationships between the Annidale Group and New River basement are not preserved, but ages of detrital zircons in the Carpenter Brook Formation are compatible with the bipartite division (c. 555 Ma and c. 625 Ma) of Neoproterozoic rocks in the New River belt (Johnson and McLeod 1996; Johnson and Barr 2004).

The evidence presented in this report supports a tectonic model in which the Annidale Group is related to Late Cambrian (c. 497–490 Ma) elements of the Penobscot arc system. In Newfoundland, these rocks are characterized by c. 494 Ma back-arc ophiolites (Dunning and Krogh 1985; Jenner and Swinden 1993) and Early Ordovician arc/back-arc volcanic rocks of the lower Victoria Lake, Wild Bight, and Bay du Nord groups (e.g., MacLachlan et al. 2001). Obduction of Penobscot back-arc crust onto the Gander margin in Newfoundland took place in the Early Ordovician (Colman-Sadd et al. 1992; van Staal et al. 1998; MacLachlan et al. 2001; Zagorevski et al. 2007). In the Annidale belt, Early Ordovician thrusting and juxtaposition of the Late Cambrian (c. 497–490 Ma) arc/back-arc rocks of the Annidale Group against New River basement is constrained by the c. 479 Ma age of the Stewarton Gabbro. The Stewarton Gabbro is nearly identical in age to the Baggs Hill and Partridgeberry Hills granites that stitch the Late Cambrian–Early Ordovician Penobscottian sequences in the Exploits Subzone in Newfoundland (e.g., MacLachlan et al. 2001). Therefore, the timing of thrusting in the Annidale belt was contemporaneous with Penobscottian obduction onto the Gander margin.

Younger intrusive activity in the Annidale and New River belts in Early–Middle Ordovician time (c. 482–467 Ma) is coeval with magmatism associated with the younger Popelogan–Victoria arc and Tetagouche–Exploits back-arc basin in central and northern New Brunswick and Newfoundland. Evidence from northern New Brunswick indicates that blueschist

metamorphism and deformation related to the closure of the Tetagouche–Exploits back-arc basin took place at 447 ± 6 Ma (van Staal et al. 2003), which is remarkably similar to the latest Ordovician–earliest Silurian age (444 ± 5 Ma) for peak metamorphism in the Annidale belt. In the Annidale belt, however, the metamorphism may be more directly related to thrusting and associated tectonic transport of the Fredericton Trough over older rocks to the south (Park and Whitehead 2003).

Despite the foregoing significant correlations, the geographic location of the Annidale and New River belts on the southeastern side of Ganderia differs from that in Newfoundland and requires significant lateral translation and telescoping of inboard and outboard elements within the Appalachian Orogen.

CONCLUSIONS

Some of the key findings of this study are a direct result of the U–Pb dating. Accurate geochronology has allowed us to erect a tentative internal stratigraphy of the Annidale Group and to demonstrate that the Grant Brook Formation is latest Neoproterozoic–earliest Cambrian in age and therefore is part of the Belleisle Bay Group. It has also allowed us to establish that the Annidale and Belleisle Bay groups were affected by a younger period of magmatism that is widespread in the area. Recognition of these two points was of paramount importance to our understanding of the stratigraphy and tectonomagmatic history of the Annidale belt.

The stratigraphy and geochemistry of the Annidale Group suggest that the oldest rocks are mainly epiclastics/volcaniclastic rocks and coeval felsic volcanic/hypabyssal intrusive rocks of the probable Late Cambrian Carpenter Brook Formation and temporally equivalent Bald Hill suite. The Carpenter Brook is intruded by the penetratively deformed Late Cambrian Cameron Road Granite (c. 490 Ma). Rare mafic volcanic rocks in the sequence have non-arc signatures; the rhyolite dome complexes have peralkaline characteristics that suggest a rift environment.

The Carpenter Brook Formation is overlain by the largely bimodal, Late Cambrian (c. 497–493 Ma) Lawson Brook Formation. The latter formation comprises mainly basaltic volcanic rocks and felsic volcanic/dome complexes that exhibit both arc and non-arc signatures, possibly along or near the extensional part of an active continental margin.

The youngest rocks in the Annidale Group are basalt and black shale of the probable Late Cambrian–Early Ordovician East Scotch Settlement Formation. The formation is older than c. 479 Ma, the age of the oldest intrusive unit (the Stewarton Gabbro) that cross-cuts it. The basalts in the sequence have arc geochemical characteristics.

Mafic to felsic intrusions were emplaced into the Annidale and Belleisle groups from c. 482 Ma to c. 467 Ma. They define a younger Early–Middle Ordovician period of magmatism and a possible magmatic hiatus in the Early Ordovician (between c. 490 Ma and 482 Ma). The

c. 479 Ma Stewarton Gabbro intruded deformed and structurally interleaved units in the Annidale Group and its faulted boundary with the Belleisle Bay Group (c. 540 Ma). This constrains the timing of thrusting and juxtaposition of the Annidale Group with New River basement to the Early Ordovician between c. 490 Ma, the youngest known age for the Annidale Group, and c. 479 Ma, the age of the Stewarton Gabbro that stitches their contact.

The age and tectonic history of the Annidale Group is comparable with that of the Penobscot arc/back-arc complex of the Exploits Subzone in Newfoundland. The timing of thrusting and juxtaposition of the Annidale Group and New River basement coincides with the timing of Penobscottian obduction onto the Gander margin in Newfoundland. Younger intrusive activity in the Annidale belt is contemporaneous with magmatism associated with the Victoria–Popelogan arc and Tetagouche–Exploits back-arc complex in the Exploits Subzone in central and northern New Brunswick.

ACKNOWLEDGEMENTS

We thank Rockport Mining Corporation for allowing unlimited access to their drill core, which was tremendously helpful in unravelling the complexities of the Annidale belt. Argon dating by Peter Reynolds at Dalhousie University and SEM analyses by Doug Hall at University of New Brunswick are gratefully acknowledged. Excellent work in the U–Pb laboratory at Memorial University was carried out by Sherri Furey. We also thank the numerous students—in particular, Erin Smith, Keith Seidler and Jennifer Gignac—who provided able assistance during field work.

REFERENCES

Abdel-Fattah, M., and Abdel-Rahman. 1990. Petrogenesis of early orogenic diorites, tonalites and post-orogenic trondhjemites in the Nubian Shield. Journal of Petrology, **31**, p.1285–1312.

Alcock, F.J., and MacKenzie, G.S. 1946. Sussex, Kings and Queens counties, New Brunswick. Geological Survey of Canada, Map 845A (with marginal notes).

Bailey, L.W. 1865. Observations on the Geology of Southern New Brunswick. Queens Printer, Fredericton, New Brunswick, 158 p.

Bailey, L.W., and Matthew, G.F. 1872. Geology of southern New Brunswick. Geological Survey of Canada, Report of Progress for 1870–71, Part 2, p. 13–240.

Barker, F. 1979. Trondhjemite: definition, environment and hypotheses of origin. *In* Trondhjemites, Dacites and Related Rocks. Elsevier Scientific Publishing Company, [New York], Chapter 1, p. 1–11.

Barr, S.M., and White, C.E., 1996, Contrasts in late Precambrian–early Paleozoic tectonothermal history between Avalon composite terrane sensu stricto and other possible peri-Gondwanan terranes in southern New Brunswick and Cape Breton Island, Canada. In Avalonian and Related Peri-Gondwanan Terranes of the Circum-North Atlantic. Edited by R.D. Nance and M.D. Thompson. Geological Society of America, Special Publication, 304, p. 95–108.

Barr, S.M., White, C.E., and Miller, B.V. 2002a. The Kingston terrane, southern New Brunswick, Canada: evidence for an Early Silurian volcanic arc. Geological Society of America, Bulletin, **114**, p. 964–982.

Barr, S., Fyffe, L., King, S., McLaughlin, K., McLeod, M., Miller, B., Thompson, M., and White, C. 2002b. New U–Pb zircon ages, geophysical compilations, and terranes in southern New Brunswick [*abstract*]. 27th Annual Review of Activities, New Brunswick Department of Natural Resources and Energy; Minerals, Policy and Planning Division, Information Circular 2002-1, p. 3–6.

Barr, S.M., White, C.E., and Miller, B.V. 2003b, Age and geochemistry of Late Neoproterozoic and Early Cambrian igneous rocks in southern New Brunswick: similarities and contrasts: Atlantic Geology, **39**, p. 55–73.

Barrett, T.J., and MacLean, W.H. 1999. Volcanic sequences, lithogeochemistry, and hydrothermal alteration in some bimodal volcanic-associated massive sulphide systems. *In* Volcanic-associated massive sulphide deposits: processes and examples in modern and ancient settings. *Edited by* C.T. Barrie and M.D. Hannington. Reviews in Economic Geology, **8**, p. 101–131.

Bartsch, C.J., and Barr, S.M. 2005. Distribution and petrochemistry of Late Neoproterozoic rocks in the southwestern New River Terrane, southern New Brunswick. *In* Geological Investigations in New Brunswick for 2004. *Edited by* G.L. Martin. New Brunswick Department of Natural Resources; Minerals, Policy and Planning Division, Mineral Resource Report 2005-1, p. 1–22.

Bennett, G. 1965. The petrology of the Stewarton igneous complex. Unpublished M.Sc. thesis, University of New Brunswick, Fredericton, New Brunswick, 105 p.

Berti, M., Cuzzani, M.G., Landuzzi, A., Taviani, M., Aharon, P., and Vai, G. B. 1994. Hydrocarbon-derived imprints in olistostromes of the early Serravallian Marnoso-arenacea Formation, Romagna Apennines (northern Italy). Geo-Marine Letters, **14**, p. 192–200.

Colman-Sadd, S.P., Dunning, G.R., and Dec, T. 1992. Dunnage–Gander relationships and Ordovician Orogeny in central Newfoundland: a sedimentary provenance and U–Pb age study. American Journal of Science, **292**, p. 317–355.

Drummond, M.S., Ragland, P.C., and Wesolowski, D. 1986. An example of trondhjemite genesis by means of alkali metasomatism; Rockford Granite, Alabama Appalachians. Contributions to Mineralogy and Petrology, **93**, p. 98–113.

Dunning, G.R., and Krogh, T.E. 1985. Geochronology of ophiolites of the Newfoundland Appalachians. Canadian Journal of Earth Sciences, **22**, p. 1659–1670.

Dunning, G.R., Swinden, H.S., Kean, B.F., Evans, D.T.W., and Jenner, G.A., 1991. A Cambrian island arc in Iapetus: geochronology and geochemistry of the Lake Ambrose volcanic belt, Newfoundland Appalachians. Geological Magazine, **128**, p. 1–17.

Fyffe, L.R. 1995. Fredericton belt. *In* Geology of the Appalachian–Caledonian Orogen in Canada and Greenland. *Edited by* H. Williams. Geological Survey of Canada, Geology of Canada 6, Chapter 6, p. 351–354.

Fyffe and Fricker, 1987. Tectonostratigraphic terrane analysis of New Brunswick. Maritime Sediments and Atlantic Geology, **23**, p. 113–123.

Fyffe, L.R., Pickerill, R.K., and Stringer, P. 1999. Stratigraphy, sedimentology and structure of the Oak Bay and Waweig formations, Mascarene Basin: implications for the paleotectonic evolution of southwestern New Brunswick. Atlantic Geology, **35**, p. 59–84.

Fyffe, L.R., Barr, S.M., Johnson, S.C., McLeod, M.J., McNicoll, V.J., Valverde-Vaquero, P., van Staal, C.R., and White, C.E. 2009. Detrital zircon ages from Neoproterozoic and Early Paleozoic conglomerate and sandstone units of New Brunswick and coastal Maine: implications for the tectonic evolution of Ganderia. Atlantic Geology, **45**, p. 110–144.

Gesner, A. 1841. Third Report of the Geological Survey of the Province of New Brunswick. Henry Chubb, Saint John, New Brunswick, p. 51–59.

Hamilton, J.B. 1961. Geology of Codys, Queens and Kings counties. New Brunswick Department of Natural Resources; Mineral Resources Branch, Geological Notes Series P.M. 59-5 (includes Map Plates 59-7 and 59-7A).

Helmstaedt, H. 1968. Structural analysis of the Beaver Harbour area, Charlotte County, New Brunswick. Unpublished Ph.D. thesis, University of New Brunswick, Fredericton, New Brunswick, 196 p.

Hibbard, J.P., van Staal, C.R., Rankin, D.W., and Williams, H. 2006. Lithotectonic map of the Appalachian Orogen (North), Canada–United States of America. Geological Survey of Canada, Map 02042A.

Jaffey, A.H., Diamond, H., Bentley, W.C., Flynn, K.F., Rokop, D.J., Essling, A.M., and Williams, J., 1977. Half-life of 239Pu by two independent methods. Physical Review, C 16, p. 354–369.

Jenner, G.A., and Swinden, H.S. 1993. The Pipestone Pond Complex, central Newfoundland: complex magmatism in an eastern Dunnage Zone ophiolite. Canadian Journal of Earth Sciences, **30**, p. 434–448.

Johnson, S.C. 2001a. Bedrock geology of the Springfield area (NTS 21H/12f), southern New Brunswick. New Brunswick Department of Natural Resources; Minerals, Policy and Planning Division, Plate 2001-48 (revised 2005).

Johnson, S.C. 2001b. Contrasting geology in the Pocologan River and Long Reach areas: implications for the New River belt and correlations in southern New Brunswick and Maine. Atlantic Geology, **37**, p. 61–79.

Johnson, S.C. 2002. Bedrock geology and mineralization in the Marrtown–Sheba area, southern New Brunswick. *In* Abstracts 2002, 27th Annual Review of Activities. New Brunswick Department of Natural Resources; Minerals, Policy and Planning Division, Information Circular 2002-1, p. 27–28.

Johnson, S.C. 2003. Bedrock geology of the Marrtown area (part of 21H/13), Kings and Queens counties, southern New Brunswick. New Brunswick Department of Natural Resources; Minerals, Policy and Planning Division, Plate 2003-3.

Johnson, S.C. 2005. Discovery of high-grade gold-bearing float in southern New Brunswick. New Brunswick Department of Natural Resources; Minerals, Policy and Planning Division, Plate 2005-55 (with marginal notes).

Johnson, S.C., and Barr, S.M. 2004. New chemical data from Neoproterozoic–Cambrian igneous rocks in the Long Reach area, southern New Brunswick. *In* Geological Investigations in New Brunswick for 2003. *Edited by* G.L. Martin. New Brunswick Department of Natural Resources; Minerals, Policy, and Planning Division, Mineral Resource Report, 2004-4, p. 75–94.

Johnson, S.C., and McLeod, M.J. 1996. The New River belt: a unique segment along the western margin of the Avalon composite terrane, southern New Brunswick. *In* Avalonian and Related Peri-Gondwanan Terranes of the Circum-North Atlantic. *Edited by* R.D. Nance and M.D. Thompson. Geological Society of America, Special Paper, **304**, p. 149–164.

Johnson, S.C., and McLeod, M.J. 2000. Bedrock geology of the Belleisle Bay–Long Reach area, southern New Brunswick. New Brunswick Department of Natural Resources; Minerals, Policy and Planning Division, Plate 2000-36 (revised 2005).

Kerrich, R., and Wyman D.A. 1994. The mesothermal gold–lamprophyre association: significance for an accretionary geodynamic setting, supercontinental cycles and metallogenic processes. Mineralogy and Petrology, **51**, p. 147–172.

Krogh, T.E., 1982. Improved accuracy of U–Pb zircon ages by the creation of more concordant systems using an air abrasion technique. Geochimica et Cosmochimica Acta, **46**, 637–649.

Lafontaine, J. 2007. The Devil Pike Brook gold deposit: an example of an orogenic lode gold deposit in the Canadian Appalachians. Unpublished M.Sc. thesis, University of New Brunswick, Fredericton, New Brunswick, 347 p.

Landing, E., and Westrop, S.R. 1998. Avalon 1997—the Cambrian standard. Third international field conference of the Cambrian chronostratigraphy working group and I.G.C.P. Project 366. New York State Bulletin, **492**, 92 p.

Landing, E., Bowring, S.A., Davidek, K.L., Westrop, S.R., Geyer, G., and Heldmaier, W. 1998. Duration of the Early Cambrian: U–Pb ages of volcanic ashes from Avalon and Gondwana. Canadian Journal of

Earth Sciences, **35**, p. 329–338.

Landing, E., Johnson, S.C., and Geyer, G. 2008. Faunas and Cambrian volcanism on the Avalonian marginal platform, southern New Brunswick. Journal of Paleontology, **82**, p.884–905.

Leonard, P.R.R., Lentz, D.R., and Poujol, M. 2006. Petrolology, geochemistry and U–Pb (zircon) age of the quartz–feldspar porphyry dyke at the Lake George antimony mine, New Brunswick: implications for origin, emplacement process and mineralization. Atlantic Geology, **42**, p. 13–29.

Leat, P.T., Jackson, S.E., Thorpe, R.S., and Stillman, C.J. 1986. Geochemistry of bimodal basalt–subalkaline/peralkaline rhyolite provinces within the Southern British Caledonides. Journal of the Geological Society, **143**, p. 259–273.

Lutes, G.G. 1993. Exploration potential of the Annidale and Shannon rhyolites in southern New Brunswick. *In* Current Research. *Edited by* S.A. Abbott. New Brunswick Department of Natural Resources and Energy; Mineral Resources, Information Circular, 93-1, p. 52–57.

MacKenzie, G.S. 1951. Preliminary map of Hampstead, Queens, Kings and Sunbury counties, New Brunswick. Geological Survey of Canada, Paper 51-19.

MacKenzie, G.S. 1964. Geological map of Hampstead. Geological Survey of Canada, Map 1114A.

MacLachlan, K., and Dunning, G.R. 1998. U–Pb ages and tectonomagmatic relationships of early Ordovician low-Ti tholeiites, boninites and related plutonic rocks in central Newfoundland, Canada. Contributions to Mineralogy and Petrology, **133**, p. 235–258.

MacLachlan, K., O'Brien, B.H., and Dunning, G.R. 2001. Redefinition of the Wild Bight Group, Newfoundland: implications for models of island-arc evolution in the Exploits Subzone. Canadian Journal of Earth Sciences, **38**, p. 889–907.

McCutcheon, S.R. 1981. Revised stratigraphy of the Long Reach area, southern New Brunswick: evidence for major, northwestward-directed Acadian thrusting. Canadian Journal of Earth Sciences, **18**, p. 646–656.

McCutcheon, S.R., and Boucot, A.J. 1984. A new Lower Silurian fossil locality in the northeastern Mascarene–Nerepis Belt, southern New Brunswick. Maritime Sediments and Atlantic Geology, **20**, p. 121–126.

McCutcheon, S.R., and Ruitenberg, A.A. 1987. Geology and mineral deposits, Annidale–Nerepis area, New Brunswick. New Brunswick Department of Natural Resources and Energy; Mineral Resources Division, Memoir 2, 141 p.

McKerrow, W.S., and Ziegler, A.M. 1971. The Lower Silurian paleogeography of New Brunswick and adjacent area. Journal of Geology, **79**, p. 635–646.

McLeod, M.J. 1995. Bedrock geology and metallic mineral occurrences in the Letang Head Harbour Passage area, Charlotte County, New Brunswick. *In* Current Research 1994. *Edited by* S.A.A. Merlini. New Brunswick Department of Natural Resources and Energy; Minerals and Energy Division, Miscellaneous Report 18, p. 141–156.

McLeod, M.J. 1997. Redefinition of the Queen Brook Formation of southern New Brunswick and preliminary geochemistry. *In* Current Research 1996. *Edited by* B.M.W. Carroll. New Brunswick Department of Natural Resources and Energy; Minerals and Energy Division, Mineral Resource Report 97-4, p. 175–190.

McLeod, M.J. 2000. Geology of the Wickham area (NTS 21G/09h), Queens and Kings counties, New Brunswick. New Brunswick Department of Natural Resources; Minerals, Policy and Planning Division, Plate 2000-32 (revised 2005).

McLeod, M.J. 2005. Geology of the Henderson Settlement area (NTS 21H/12e), Queens and Kings counties, New Brunswick. New Brunswick Department of Natural Resources; Minerals, Policy and Planning Division, Plate 2005-50.

McLeod, M.J., Ruitenberg, A.A., and Krogh, T.E. 1992. Geology and U–Pb geochronology of the Annidale Group, southern New Brunswick: Lower Ordovician volcanic and sedimentary rocks formed near the

southeastern margin of Iapetus Ocean. Atlantic Geology, **28**, p. 181–192.

McLeod, M.J., Winchester, J.A., and Ruitenberg, A.A. 1994. Geochemistry of the Annidale Group: implications for the tectonic setting of Lower Ordovician volcanism in southwestern New Brunswick. Atlantic Geology, **30**, p. 87–94.

McLeod, M.J., Johnson, S.C., and Krogh, T.E. 2003. Archived U–Pb (zircon) dates from southern New Brunswick. Atlantic Geology, **39**, p. 209–225.

Meschede, M. 1986. A method of discriminating between different types of mid-ocean ridge and continental tholeiites with the Nb–Zr–Y diagram. Chemical Geology, **56**, p. 207–218.

Nakamura, Y. 1974. Determination of REE, Ba, Fe, Mg, Na and K in carbonaceous and ordinary chondrites. Geochimica et Cosmochimica Acta, **38**, p. 757–775.

Nilsen, O., Corfu, F., and Roberts, D. 2007. Silurian gabbro–dioritie–trondhjemite plutons in the Trondheim nappe complex, Caledonides, Norway: petrology and U–Pb geochronology. Norwegian Journal of Geology, **87**, p. 329–342.

Park, A.F., and Whitehead, J. 2003. Structural transect through Silurian turbidites of the Fredericton Belt southwest of Fredericton, New Brunswick: the role of the Fredericton Fault in late Iapetus convergence. Atlantic Geology, **39**, p. 227–237.

Pearce, J. A. 1996. A user's guide to basalt discrimination diagrams. *In* Trace Element Geochemistry of Volcanic rocks: Applications for Massive Sulphide Exploration. *Edited by* D.A. Wyman. Geological Association of Canada/Mineralogical Association of Canada, Winnipeg, 1996, short course notes, **12**, p. 79–113.

Pearce, J.A., Harris, N.B.W., and Tindle, A.G. 1984. Trace element discrimination diagrams for the tectonic interpretation of granitic rocks, Journal of Petrology, **25**, p. 956–983.

Rogers, N., van Staal, C.R., McNicoll, V., Pollock, J., Zagorevski, A., and Whalen, J. 2006. Neoproterozoic and Cambrian arc magmatism along the eastern margin of the Victoria Lake Supergroup: a remnant of Ganderian basement in central Newfoundland? Precambrian Research, **147**, p. 320–341.

Ruitenberg, A.A., McLeod, M.J., and Krogh, T.E. 1993. Comparative metallogeny of Ordovician volcanic and sedimentary rocks in the Annidale–Shannon (New Brunswick) and Harborside–Blue Hill (Maine) areas: implications of new U–Pb age dates. Exploration and Mining Geology, **2**, p. 355–365.

Sánchez-García, T., Quesada, C., Bellido, F., Dunning, G.R., and González del Tánago, J. 2008. Two-step magma flooding of the upper crust during rifting: the early Paleozoic of the Ossa Morena Zone (SW Iberia). Tectonophysics, **461**, p. 72–90.

Shervais, J.W. 1982. Ti–V plots and the petrogenesis of modern and ophiolitic lavas. Earth and Planetary Science Letters, **57**, p. 101–118.

Stacey, J.S., and Kramers, J.D., 1975. Approximation of terrestrial lead isotope evolution by a two-stage model. Earth Planetary Science Letters, **26**, p. 207–221.

Stillman, C.J., and Williams, C.T. 1978. Geochemistry and tectonic setting of some Upper Ordovician volcanic rocks in east and southeast Ireland. Earth and Planetary Science Letters, **41**, p. 288–310.

Swinden, H.S., Jenner, G.A., Fryer, B.J., Hertogen, J., and Roddick, J.C. 1990. Petrogenesis and paleotectonic history of the Wild Bight Group, an Ordovician rifted island arc in central Newfoundland. Contributions to Mineralogy and Petrology, **105**, p. 219–241.

Tanoli, S.K, and Pickerill, R.K. 1988. Lithostratigraphy of the Cambrian–Lower Ordovician Saint John Group, southern New Brunswick. Canadian Journal of Earth Sciences, **25**, p. 669–690.

Thomas, M.D., and Kiss, F. 2004. Geological Interpretation of the 2004 Marrtown aeromagnetic survey, southeastern New Brunswick. Geological Survey of Canada, Open File Report, 4953.

van Staal, C.R. 2007. Pre-Carboniferous tectonic evolution and metallogeny of the Canadian Appalachians. *In* Mineral Deposits of Canada: A Synthesis of Major Deposit-types, District Metallogeny, the Evolution of Geological Provinces and Exploration Methods. *Edited by* W.D. Goodfellow. Geological Association of Canada, Mineral Deposits Division, Special Publication, **5**, p. 793–818.

van Staal, C.R., and Fyffe, L.R. 1991. Dunnage and Gander zones, New Brunswick: Canadian Appalachian Region. New Brunswick Department of Natural Resources; Minerals, Policy and Planning Division, Geoscience Report 91-2, 39 p.

van Staal, C.R., and Fyffe, L.R. 1995. Gander Zone–New Brunswick. *In* Geology of the Appalachian–Caledonian Orogen in Canada and Greenland, Chapter 3. *Edited by* H. Williams. Geological Survey of Canada, Geology of Canada, **6**, p. 216–223.

van Staal, C.R., Dewey, J.F., MacNiocaill, C., and McKerrow, W.S. 1998. The Cambrian–Silurian tectonic evolution of the northern Appalachians and British Caledonides: history of a complex, west and southwest Pacific-type segment of Iapetus. *In* Lyell, The Past is the Key to the Present. *Edited by* D.J. Blundell and A.C. Scott. Geological Society, London, Special Publication, 1**43**, p. 199–242.

van Staal, C.R., Wilson, R.A., Rogers, N., Fyffe, L.R., Langton, J.P., McCutcheon, S.R., McNicoll, V., and Ravenhurst, C.E. 2003. Geology and tectonic history of the Bathurst Supergroup, Bathurst Mining Camp, and its relationships to coeval rocks in southwestern New Brunswick and adjacent Maine–a synthesis. *In* Massive Sulphide Deposits of the Bathurst Mining Camp, New Brunswick and Northern Maine. *Edited by* W. D. Goodfellow, S.R. McCutcheon, and J.M. Peter. Economic Geology, Monograph 11, p. 37–60.

Venugopal, D.V. 2003. Titanium and phosphate potential of the Stewarton and Lower Coverdale gabbro, southern New Brunswick, Canada. New Brunswick Department of Natural Resources and Energy; Minerals, Policy and Planning Division, Mineral Resource Report 2003-5, 132 p.

Walker, J.D., and Geissman, J.W. 2009 (compilers). Geologic time scale. Geological Society of America, GSA Today, **19**, No. 4/5, p. 60–61.

White, C.E., and Barr, S.M. 1996. Geology of the Brookville terrane, southern New Brunswick, Canada. *In* Avalonian and Related Peri-Gondwanan Terranes of the Circum-North Atlantic. *Edited by* R.D. Nance and M.D. Thompson. Geological Society of America Special Paper 304, p. 95–108.

Wilson, M. 1989. Igneous Petrogenesis: A Global Tectonic Approach. Chapman & Hall, London, United Kingdom.

Winchester, J.A., and Floyd, P.A. 1977. Geochemical discrimination of different magma series and their differentiation products using immobile elements. Chemical Geology, **20**, p. 325–343.

Wood, D.A. 1980. The application of a Th–Hf–Ta diagram to problems of tectonomagmatic classification and to establishing the nature of crustal contamination of basaltic lavas of the British Tertiary volcanic province. Earth and Planetary Science Letters, **50**, p. 11–30.

Zagorevski, A., van Staal, C.R., McNicoll, V., and Rogers, N. 2007. Upper Cambrian to Upper Ordovician peri-Gondwanan Island arc activity in the Victoria Lake Supergroup, Central Newfoundland: tectonic development of the northern Ganderian margin. American Journal of Science, **307**, p. 339–370.

Mineral Resource Report 2009-2

ISBN 978-1-55471-018-8
ISSN 0548-4014

Price $25.00